Palladium-based catalyst for heterogeneous photocatalysis

Ayda Elhage

A thesis submitted to the University of Ottawa
in partial fulfillment of the requirements for the
Doctorate in Philosophy degree in Chemistry

uOttawa

Department of Chemistry and Biomolecular Sciences
Faculty of Science
University of Ottawa

In dedication to

My parents who taught me to believe in myself, to always strive for the best, and even the largest task can be accomplished if it's done one step at a time.

&

My husband, Youssef, and my children, Mohamed & Omar, for their love, endless support and encouragement.

"Hard work is the real key to success. Keep your eyes on the goal, and just keep taking the next step towards completing it. If you aren't sure which way to do something, do it both ways and see which works better."

–John Carmack

"It always seems impossible until it's done"

–Nelson Mandela

Abstract

Over the past decade, heterogeneous photocatalysis have gained lots of interest and attention among the organic chemistry community due to its applicability as an alternative to its homogeneous counterpart. Heterogeneous catalysis offers the advantages of easy separation and reusability of the catalyst. Several studies showed that under optimized conditions, efficient and highly selective catalytic systems could be developed using supported metal/metal oxide nanoparticles. In this dissertation, we summarize the progress in the development of supported palladium nanoparticles for different types of organic reactions.

Palladium-decorated TiO_2 is a moisture, air-tolerant, and versatile catalyst. The direct excitation of Pd nanoparticles selectively isomerized the benzyl-substituted alkenes to phenyl-substituted alkenes (*E*-isomer) with complete conversion over $Pd@TiO_2$ under H_2-free conditions. Likewise, light excited Pd nanoparticles catalyzed Sonogashira coupling, a C-C coupling reaction between different aryl iodides and acetylenes under very mild conditions in short reaction times. On the other hand, UV irradiation of $Pd@TiO_2$ in alcoholic solutions promotes alkenes hydrogenation at room temperature under Argon. Thus, The photocatalytic activity of $Pd@TiO_2$ can be easily tuned by changing the irradiation wavelength. Nevertheless, some of these systems suffer from catalyst deactivation, one of the main challenges faced in heterogeneous catalysis that decreases the reusability potential of the materials. In order to overcome this problem, we developed an innovative method called "*Catalytic Farming*". Our reactivation strategy is based on the crop rotation system used in agriculture. Thus, alternating different catalytic reactions using the same catalyst can reactivate the catalyst surface by restoring its oxidation states and extend the catalyst lifetime along with its selectivity and efficiency. In this work, the rotation strategy is illustrated by Sonogashira coupling –problem reaction that depletes the catalyst– and Ullmann homocoupling – plausible recovery reaction that restores the oxidation state of the catalyst ($Pd@TiO_2$).

The selection of the reactions in this approach is based on mechanistic studies that include the role of the solvent and evaluation of the palladium oxidation state after each reaction.

In a more exploratory analysis, we successfully demonstrated that Pd nanoparticles could be supported in a wide range of materials, including inert ones such as nanodiamonds or glass fibers. The study of the action spectrum shows that direct excitation of the Pd nanoparticles is a requisite for Sonogashira coupling reactions. The main advantages of heterogeneous catalysis compared to its homogeneous counterpart are easy separation and reusability of the catalyst.

Finally in order to facilitate catalyst separation from batch reaction and develop a suitable catalytic system for continuous flow chemistry, we employed glass fibers as catalyst support for a wide variety of thermal and photochemical organic reactions including C-C coupling, dehalogenation and cycloaddition. Different metal/metal oxide nanoparticles, namely Pd, Co, Cu, Au, and Ru were deposited on glass wool and fully characterized. As a proof of concept, Pd decorated glass fibers were employed in heterogeneous flow photocatalysis for Sonogashira coupling and reductive de-halogenation of aryl iodides.

Acknowledgements

I would like to start by expressing my gratitude to my Ph.D. supervisor, Dr. Tito Scaiano. Thank you Tito, for taking a chance on me, and giving me the opportunity to pursue my graduate study in your laboratories. Although, it is quite difficult to remain motivated during the natural ups and downs of a PhD journey, your support and your inspiring stories along with your countless and valuable advice smoother my path. Dr. Scaiano is not only a distinguished scientific, he is also an incredible and an inspiring person. I am very grateful and lucky to have the honour to be one of his students. Dr. Scaiano, thank you for everything.

The Scaiano group is a wonderful environment for research, undergraduate and graduate students along with post docs with wide expertise of different backgrounds, form nanomaterials to physical organic chemistry to biomaterials, constitute the core of the group. Most importantly, huge thank you to our senior research associate, Dr. Anabel Lanterna, for teaching and training me on almost every single instrument in the lab. Your deep knowledge of chemistry, intellect, and passion engraved my daily research and shaped my success. Thank you for your patience in training new graduate student and for all the daily discussions along with the fruitful meetings. Your positive vibes along with your full support made me going and eased my journey. I have learned so much from you! Anabel, you are a great mentor!

Thank you Betty Yakimento, our secretary, and Michel Grenier, our former laser lab technician, for all your hard work to ensure everything runs smoothly in the group. Finally, I'd like to thank my former colleague Nancy Marina for all your chemistry discussions and good times in and outside the lab. I wish all current and former Scaiano group members all the best in their future.

My most sincere gratitude to my parents, Abdo and Hassna, and my siblings, Haissam, Ibrahim, Viviane, Marwan, and Mohamed, for their support and encouragement to follow my dream and earn a doctorate. My parents who taught me to

believe in myself, to always strive for the best, and even the largest task can be accomplished if it's done one step at a time, Without them I would not be where I am today. Wish my dad were still alive to celebrate my accomplishment with us. I am pretty sure, he is looking down at me and he is proud of what I have achieved.

The most interesting part of this journey is having my husband, Youssef, and my twins, Mohamed and Omar, who I have to thank most of all. Their love, endless support and encouragement make this chapter of my life memorable and successful. No words can express how fortunate and grateful I am to have you in my life. Thank You! Merci!

Contribution statement

All of the research presented within this dissertation was conducted under the supervision of Professor Tito Scaiano. The entirety of the work presented in this thesis, would simply not have been possible without the incredible guidance and support of my supervisor Professor Tito Scaiano.

This thesis is based upon five peer-reviewed publications for which I am the leading author. So, while the majority of the experimental work was completed by me personally, I have been fortunate to have had opportunities to collaborate with a number of colleagues during my time in the Scaiano group and visiting professors: Dr. Maria L. Marin −Instituto Universitario Mixto de Tecnología Química (UPV-CSIC), Universitat Politècnica de València, Spain− and Dr. Theodore J Burkey −University of Memphis, Tennesse USA. These amazing people made invaluable contributions to my general training and knowledge of chemistry, and some of our work together resulted in peer-reviewed publications. Cases where I made a direct contribution to the project, but am listed as co-author of the publication, have been noted in the appropriate portion of the List of Publications but have not been discussed in detail in this thesis. In this section, I want to point out some of my own direct contributions to the work that is covered in each body chapter of this thesis, and also to respectfully highlight the intellectual and physical contributions made by each of my collaborators.

Dr. Scaiano and Dr. Anabel Lanterna, whom is former postdoctoral researcher in the Scaiano group, and now senior research associate, provided guidance and suggested several of the experiments, and we regularly engaged in productive discussions, especially regarding the interpretation of all the experimental data.

In my first year as graduate student in Scaiano group, I worked on a project that Dr. Lanterna already started, not presented in this dissertation. It is based on the use of supported gold nanoparticles on TiO_2 (Au@TiO_2) as photocatalysts to photoinduce the

reductive C-C coupling of substituted benzyl bromides. Surface plasmon excitation of supported AuNP in the presence of an amine leads to the C-C coupling at room temperature with good yields in a free-radical mediated reaction. The overall efficiency of the C-C coupling is largely dependent on the nature of the amine used and the light intensity. Dr. Lanterna performed the screening reactions in order to find the optimal conditions, starting from different types of amines, solvents, and catalysts (commercial Au@TiO_2, homemade Au@TiO_2, bared TiO_2, and Au decorated inert support) using the reductive dimerization of 4-nitrobenzyl bromide as a model reaction along with writing the manuscript.. She also proved that the reaction takes place under radical−radical dimerization rather than by a nucleophilic substitution by using a radical-trapping agent (2,2,6,6-tetramethyl-piperidin-1-yl)-oxyl (TEMPO). I was in charge of the reusability test of the photocatalyst for the dimerization of 4-nitrobenzyl bromide under the optimized reaction condition along with the light-intensity effect on the benzyl radical formation. I also performed the reduction of different substituted benzyl bromides using four 530 nm LEDs under the optimized conditions. Quantification was done by ^{1}H-NMR using caffeine as an external standard. In conclusion, AuNP supported on TiO_2 demonstrated good catalytic activity on the reductive dimerization of benzyl bromides. We also confirmed the C-C coupling occurs via radical coupling rather than by nucleophilic substitution (S_N2). It is in fact surprising to see radicals in very low concentrations (usually nanomolar) undergo self-reaction, rather than radical-molecule reactions. For this to occur, the radicals need to have low reactivity, which generally means high resonance stabilization, as is the case for benzylic radicals. Second, solvent with low reactivity such as halogenated solvents is more favourable for that reaction. Low concentrations and modest reactivity for any other free-radical traps are required, and likely the reason why diisopropylehylamine gives better yield than the more reactive triethylamine. It is interesting that these unusual criteria are all met in the current system making radical-radical reactions the preferred process.

My second project as a graduate student, reported in Chapter 2, the photochemical synthesis, characterization of palladium nanoparticles, and application as a photocatalyst in organic transformations namely alkene isomerization and alkene

hydrogenation was largely overseen by Dr. Lanterna, along with Dr. Scaiano himself. Dr. Lanterna provided daily supervision of my experiments, hands-on training, intellectual support, and suggested experiments. Although I performed all experiments personally, this work would not have been possible without the intellectual contributions made by Dr. Lanterna and I credit her with teaching me many of the laboratory, research and writing skills that started me on the right path toward a successful doctoral research program.

I conceived the idea of the heterogeneous catalysis application of supported palladium nanoparticle for Sonogashira coupling reaction. I explored thermal and photochemical routes toward this goal, and optimized the photochemical synthesis of the final nanocomposite material. I tested several candidate systems for catalysis. Although I performed all of the experimental work myself, Dr. Lanterna was involved in training me on everything from product identification and quantification, column chromatography to operating analytical instrument along with analyzing scientific data by manipulating the corresponding software.

The work presented in Chapter 4 on reactions rotation to extend the catalyst lifetime was a result of losing good performance of the catalyst, namely Pd@TiO_2, after the first catalytic cycle for Sonogashira coupling. In order to develop sustainable recovery strategies; Dr. Scaiano, Dr. Lanterna and I proposed a strategy based on a reaction rotation methodology. A method we labeled "*Catalytic Farming"* that is based on rotating the catalytic processes to synthesize alternating target valuable molecules and at the same time reactivate the catalyst surface, thus extending the reusability of the material, and preserving its selectivity and efficiency. This innovative approach to extend the catalyst lifetime is based on the crop rotation system used in agriculture. I performed all of the experimental work myself.

The work presented in Chapter 5 on the use of glass wool as a support for metal nanoparticles for heterogeneous catalysis applications was done in collaboration with my fellow graduate students and postdoctoral fellows to combine our expertise on a variety of research experiments in this project. Dr. Scaiano conceived this idea for

developing of continuous flow heterogeneous photocatalysis system. It started with preliminary tests done by a RISE summer student, Menandro Cruz, starting with glass wool surface functionalization, metal nanoparticles decoration to application in organic transformations. Dr. Maria L. Marin −who was a visiting professor from Spain− performed the reduction of nitrobenzene using ruthenium-decorated glass wool. Dr. Bowen Wang −who is a postdoctoral researcher in our group− performed the photochemical click-chemistry reaction using glass wool supported copper nanoparticles under visible light irradiation. Nancy Marina −who is a former master student− and I performed the light induced reductive dehalogenation of aryl halides using cobalt or palladium decorated glass wool. I performed all the rest of the bench scale photochemistry experiments, as well as the glass wool acid treatment and APTES functionalization prior to metal nanoparticles decoration along with the catalysts characterization.

Finally, the work presented in chapter 6 on the development of continuous flow heterogeneous photocatalysis for Sonogashira coupling and dehalogenation reaction was done in collaboration with Dr. Theodore Burkey, a visiting professor from Tennesse, USA. Dr. Burkey performed the flow reactor setup from polishing the reactor face with sand paper, sealing it with Teflon tape in order to prevent leaking, and to connecting it in a closed loop with Teflon tubing to a reservoir and a Master flex peristaltic pump. I synthesized and characterized all the catalysts used in this study along with reactions mixture preparation and product quantification.

Table of contents

List of publications

Publications Presented in this Thesis

Ayda Elhage, Anabel E. Lanterna*, and Juan C. Scaiano*; Tuneable photocatalytic activity of Palladium-decorated TiO_2: non-hydrogen mediated hydrogenation or isomerization of benzyl-substituted alkenes. ACS Catal. **2017**, 7, 250-255.

Ayda Elhage, Anabel E. Lanterna*, and Juan C. Scaiano*; Light-induced Sonogashira C-C Coupling under Mild Conditions using Supported Palladium Nanoparticles. ACS Sustainable Chem. Eng. **2018**, 6, 1717-1722

Ayda Elhage, Anabel E. Lanterna* and Juan C. Scaiano*; Catalytic farming as green chemistry strategy: rotation of reactions extends catalyst lifetime and performance in Chem. Sci**.**, **2019**, 10, 1419-1425

Ayda Elhage, Bowen Wang, Nancy Marina, M. Luisa Marin, Menandro Cruz, Anabel E. Lanterna* and Juan C. Scaiano*; Glass wool: a novel support for heterogeneous catalysis. Chem. Sci., **2018**, 9, 6844-6852

Ayda Elhage[1], Anabel E. Lanterna[1], Juan C. Scaiano[1]* and Theodore Burkey[2]*; Scalable Strategies for Continuous Flow Heterogeneous Photocatalysis, manuscript submitted

Co-Authored Publications Not Discussed in this Thesis

Ayda Elhage, Amrah Nassim, Paolo Costa, Anabel E. Lanterna* and Juan C. Scaiano*; Photochemical dehalogenation of aryl halides: importance of halogen bonding, manuscript submitted

Ayda Elhage, Juan C. Scaiano and Anabel E. Lanterna; "Dressing up for the occasion: the many faces of titanium dioxide in photocatalysis" in *Photoactive Inorganic Nanoparticles*. ISBN: 9780128145319. eds. J. Pérez-Prieto and M. González-Béjar, Elsevier, 1st edn., **2019**, ch. 4, pp. 73-108.

Anabel E. Lanterna, Ayda Elhage and Juan C. Scaiano*; Heterogeneous photocatalytic C–C coupling: mechanism of plasmon-mediated reductive dimerization of benzyl bromides by supported gold nanoparticles. Catal. Sci. Technol.**, 2015,**5**,** 4336-4340

List of Figures

List of Schemes

List of Tables

List of Abbreviations

[ ]	Concentration
A	Electron acceptor
ACN	Acetonitrile
APTES	(3-Aminopropyl)triethoxysilane
BE	Binding energy
CB	Conduction band
CND	Carbon nanodiamond
D	Electron donor
DABCO	1,4-diazabicyclo[2.2.2]octane
DIPEA	Diisopropylethylamine
DCM	Dichloromethane
DMF	Dimethylformamide
DR	Diffuse reflectance
E_{BG}	Band gap energy
EDG	Electron-donating group
EDS	Energy dispersive X-ray spectroscopy
E_{red}	Reduction potential
E_{ox}	Oxidation potential
EtOAc	Ethyl acetate
EtOH	Ethanol
e^-	Electron

EA	Electron affinity
Equiv.	Equivalent
EWG	Electron-withdrawing group
GC	Gas chromatography
GC-FID	Gas chromatography flame ionization detector
GC-MS	Gas chromatography mass spectrometry
GF	Glass filter
GW	Glass wool
H^+	Proton
h^+	Hole
h	Planck's constant
hν	Light
I-2959	Irgacure 2959
ICP	Inductively coupled plasma
i-Pr_2NEt	N,N-diisopropylethylamine
LED	Light emitting diode
MeO	Methoxy
MeOH	Methanol
MS	Mass spectrometry
NMR	Nuclear magnetic resonance
NGW	Non treated glass wool
ND	Nothing detected
NP	Nanoparticle
ox	oxidation

Ph	Phenyl
ppm	Parts per million
red	reduction
$Ru(bpy)_3^{2+}$	tris(2,2'-bipyridyl)ruthenium(II)
SEM	Scanning electron microscopy
SGW	Silanized glass wool
TEMPO	2,2,6,6-Tetramethyl-1-piperidinyloxyl
TiO_2	Titanium dioxide
TEM	Transmission electron microscopy
TCD	Thermal conductivity detector
THF	Tetrahydrofuran
TLC	Thin layer chromatography
TOF	Turnover frequency
TON	Turnover number
UV	Ultraviolet
VB	Valence band
Vis	Visible
XPS	X-ray photoelectron spectroscopy
ϕ	Quantum yield
λ	Wavelength

1. Introduction

1.1 Opening Remarks

The work presented in this dissertation is centered on the field of heterogeneous photocatalysis. This doctoral thesis comprises a series of five peer-reviewed publications and the associated supporting information, presented in chronological order alongside additional commentary intended to provide further insights and to emphasize the strong ties between chapters. This chapter will focus on introducing the reader to the applications of supported nanomaterials in heterogeneous photocatalysis along with the role of the support and the advantages of using an inexpensive, widely available and easy handled material for heterogeneous catalysis. This is a first step towards an easy way to recover heterogeneous catalysts, and to develop catalysts with great potential for flow chemistry.

Visible-light-mediated photoredox catalysis has emerged as a valuable concept in organic synthesis to induce selective transformations avoiding the undesired photodegradation of organic molecules under UV exposure. The effort to prepare photo-responsive materials is a growing field in heterogeneous catalysis, where it has become one of the most studied approaches for sustainable and alternative routes of chemicals synthesis. Not only benefit from reusability, easy post-reaction separation and limit of product contaminations, also light-induced selective organic transformations contribute to sustainable alternatives. Titanium dioxide (TiO_2) is a well-known semiconductor and its use as a photocatalyst has been widely explored as an alternative heterogeneous photoredox catalyst for the non-reusable expensive homogeneous metal complexes of elements such as Pd, Ru, Pt.[1] TiO_2 particles can be found in three main phases: anatase, rutile, and brukite.[2] TiO_2 is generally sold as TiO_2 P25, which is a mixture of anatase and rutile with a ratio of 3:1 respectively.[3, 4] TiO_2 P25 has demonstrated to be an excellent heterogeneous photocatalyst, due to its chemical stability, nontoxicity and low cost. It has been widely employed in various applications such as photocatalyst for water

and air purification, antimicrobial agent in ceramic, photo electrochemical solar cells, and photocatalyst for many organic reactions.[3, 5]

TiO_2, like all semiconductors, possess a void energy region, which extends from the filled valence band (VB) to the empty conduction band (CB) and it is known as the band gap.[6] As shown in the simplified diagram in Figure 1.1a, upon light excitation of TiO_2 with photons of equal or higher energy than the band gap energy of the material, an electron-hole (e-h) pair (or exciton) is created. Photoexcitation of TiO_2 leads to the promotion of VB electrons into the CB forming e-h pair (e^-_{CB} and h^+_{VB}). The fate of the separated e-h pair can follow several pathways. Figure 1.1a illustrates possible pathways of photogenerated exciton in a semiconductor particle. The "hole" in the VB becomes an excellent electron acceptor after being trapped at the semiconductor surface (h^+_{tr}), while the "electron" now populating the CB and trapped at the surface (e^-_{tr}) is an excellent reducing agent. The probability and the rate of this process depend on both; the respective position of the band edges for the conduction/valence bands and the redox potential levels of the acceptor/donor. The surface e^-_{tr} and h^+_{tr} must be quenched by electron acceptors (e.g. O_2, viologens, etc.) and electron donors (e.g. aliphatic amines, MeOH, THF, etc.) respectively before charge recombination occurs −usually within the nanosecond time scale.[7] Recombination of the photo-generated exciton occurs with the release of heat.

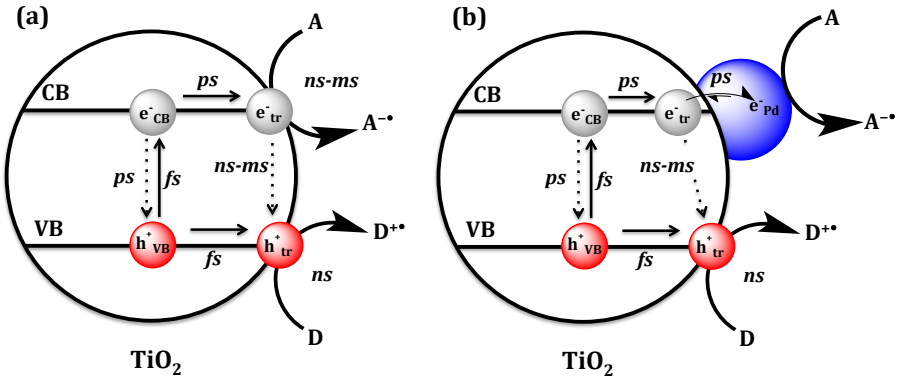

Figure 1.1. The fate of charge carriers generated upon light excitation of semiconductors particles for (a) bare TiO_2 and (b) PdNP-decorated TiO_2, along with the time scales for each event. Legend: CB=conduction band; VB=valence band; A= electron acceptor; D= electron donor; tr= trapped on semiconductor surface.[7, 8, 9]

The main disadvantage of the use of pure nanometric TiO_2 as a photocatalyst is the large band gap (> 3.1eV) of this semiconductor that can only absorb UV light (<400 nm) (Figure S2.2). In order to have a material that can be photo-responsive under visible light irradiation, the band gap of a semiconductor should be higher than 1.6 eV (~700 nm) and less than 3 eV (~400 nm).

Several strategies have been applied to modify the band gap energy including doping, that by creating intrinsic modifications on the TiO_2 crystal lattice (generation of typical defects such as vacancies or surface-related sites) or superficial modifications of TiO_2 surface by adding metal or metal oxide nanoparticles as well as organic dyes (here referred as "decoration"). However, dye molecules decorated on the surface are prone to oxidation by TiO_2, therefore limiting the possibility of catalyst reusability.[8] On the other hand, TiO_2 decorated with metallic nanoparticles is much more robust. Nanomaterials supported on the TiO_2 surface are frequently in the 1-10 nm range. Decorating TiO_2 with metal or metal oxide nanoparticles is a common strategy to increase the lifetime of the charge-separated states in semiconductors, as this provides electronic and spatial barriers to e-h recombination. In addition, decorating TiO_2 with noble transition metals such as Pd or Au shift the absorption profile of the resulting hybrid material to the visible region to create visible light-induced e-h pairs.[10]

Pd nanoparticles can be functionalized onto the TiO_2 surface to act as a sink for the trapped electrons as illustrated in Figure 1.1b. The transfer of the electron from the CB to Pd nanoparticles is energetically favourable. Thus, e-h recombination process slows down. As a consequence, the metal-supported electrons (e^-_{Pd}) are free to induce reduction reactions while the photogenerated holes in the CB have more time to diffuse to the surface and can be quenched by an electron donor. Pd nanoparticles decoration generally results from an electrostatic interaction between the TiO_2 surface and the metal nanoparticles. This resulting material does not show a strong absorption in the visible region compared to the plasmonic Au decorated TiO_2. The light absorption of metal NPs is defined by the optical properties of the free electrons (conduction electrons) and the bound electrons in the filled energy bands. Light absorption through the free electrons

results in localized surface plasmon resonance (LSPR). On the other hand, the light absorption by the bound electrons leads to interband transitions between (n-1) d band and a higher ns band. As a result, a visible light-induced e-h pairs will be generated; hole in the (n-1) d band and excited electrons in a higher energy level ns band. The contribution from LSPR effect and from interband transitions depends on the NP's morphology (size and shape), the metal dielectric function and the light wavelength.[11] Even in the absence of LSPR, Pd nanoparticles exhibit a significant absorption in both visible and UV regions.[11] The photoexcitation of Pd nanoparticles leads to interband transition to afford light excited-electrons (hot electrons). These hot electrons are available at the palladium surface sites, thus enhancing the ability of Pd sites to adsorb and activate reactant molecules. Furthermore, these hot electrons facilitate the photocatalytic organic reactions of the adsorbed molecules at ambient or moderate temperatures.[12, 13] Regardless the underlying mechanism of the reactions driven by energetic electrons of PdNP, there is a dependence of reaction rate on the light intensity. The increase in the number of hot electrons populating high energy levels by increasing the incident light intensity lead to noticeable enhancement in the photocatalytic activity of PdNPs, probably due to the greater number of hot electrons that are transferred to reactants molecules. [11, 13]

In heterogeneous processes, catalyst supports are frequently considered inert and passive, mainly used to restrict the mobility of active catalysts.[14] However, many supports have taken an active and efficient role during the catalytic transformations; this is the case with semiconductors, such as TiO_2. These supports are usually in the form of powders decorated with active metal and/or metal oxides nanostructures. Although, they are easy to recover from reaction mixture, these powder-like materials are not ideal for flow heterogeneous photocatalysis applications. The use of fibrous or filament materials as catalysts support would be a good alternative, as not only they would stay in place and act on flowing solutions, also they would be easy to recover after batch reactions. Glass fibers are fibrous materials made from melted borosilicate glass.[15] Glass fibers are commonly employed for thermal and acoustic insulation or electric insulation fabrics. In chemistry, glass fibers are frequently used as packing materials for gas chromatography

columns or trapping agent for insoluble carbon sources during cells growth.[16] Glass fibers are inexpensive, chemically inert, and available with a variety of surface properties that are easy to modify for better physical and chemical affinity towards catalytic materials. Interestingly, these resulting catalytic active glass fibers could avoid the limitations associated with handling and separation of powders. In 2002, the application of glass fibers in catalysis was reported for oxidation processes that dealt with both gas and liquid phases.[17] Recently, Barelko et al. published a review on advances in the applications of glass fibers in catalysis achieved during the last 15 years where high temperature, or redox harsh conditions are used.[18] Apart from these limited examples in catalysis, no applications yet to organic chemistry were reported, in particular, C-C bond coupling a key reaction in organic synthesis.

The heterogeneous catalytic system presented in this dissertation is based on developing two different types of hybrid materials that are suitable catalysts for different organic transformations under mild conditions:

1- TiO_2 P25 a semiconductor as a support for metal nanoparticles, namely Pd, in the powder form. TiO_2 P25 is a catalytically and light active support.
2- Glass fibres as an inert support decorated with different types of metal nanoparticles.

Palladium-based materials have been studied in a wide range of catalytic applications including hydrogenations, oxidations, and carbon-carbon bond reactions.[19] Palladium is one of the most efficient metals in catalysis.[20] In addition, the high surface-area-to-volume ratio makes nanomaterials highly desirable for use as potential catalysts. In the present work, supported palladium nanoparticles are prepared either by photo-deposition or dark-deposition methods (*vide infra*) and their applications in a wide variety of photochemical transformations were explored. The photo-responsive of palladium-decorated titania ($Pd@TiO_2$), show different reactivity when irradiated with different light sources and thus, the preferred outcome can be tuned by the correct selection of wavelengths to which a single material is exposed. Strategies based on tuning the

excitation sources will stimulate studies using multi-wavelength sources and the discovery of new synthetic routes. However, one of the main challenges in heterogeneous catalysis is to ensure the good performance of the catalyst after the first catalytic cycle. Active catalytic species can be inactivated during the catalytic process leading to lower catalytic efficiency. Throughout this thesis, a distinction will be drawn between catalyst separation and reusability of supported nanomaterials for catalytic applications. Taken together, these works embody the general topic of this dissertation: the design of a versatile, tuneable, multifunctional titanium dioxide supported palladium nanoparticles ($Pd@TiO_2$) for application in heterogeneous catalysis. Chapter 2 and 3 describe the versatility and the tuneable photocatalytic activity of $Pd@TiO_2$ under different light irradiation sources. Thus, production of target valuable molecules can be tuned by the right selection of wavelength; alkene hydrogenation, alkene isomerization or C-C coupling product at room temperature. These specific reactions lead to an innovative approach to extend the catalyst lifetime based on the crop rotation system used in agriculture. Chapter 4 explores the strategy of alternating different catalytic reactions, to reactivate the catalyst surface, thus extending the reusability of $Pd@TiO_2$, and preserving its selectivity and efficiency.[21]

The second part of this dissertation presents our research on the use of glass fibers, glass wool (GW) or / and glass filters (GF), as a support for metal or metal oxides nanoparticles to catalyze number of different reactions under mild conditions. Glass fibers are considered inert and passive support, mainly used to restrict the mobility of active catalyst. Chapter 5 examines the use of glass wool fibers as a support for metal nanoparticles as heterogeneous alternative for fine organic transformations, where more complex and interesting systems can be developed from here. In this context, palladium nanomaterials decorated glass fibers, present an opportunity to develop highly active, easily separable, and reusable heterogeneous catalysts for continuous flow photocatalysis for cross-coupling reactions presented in Chapter 6.

1.2 Synopsis

The body of this thesis will begin with the report of the photochemical synthesis of Pd@TiO_2 and how its photocatalytic activity can be tuned in favour of solvent-mediated hydrogenation or isomerization of benzyl substituted alkenes under H_2-free conditions simply by changing the irradiation wavelength (Chapter 2). PdNP were synthesized by reduction of Pd^{2+} under UVA irradiation in the presence of TiO_2 as illustrated in Scheme 2.1. Characterization of this new material, labeled Pd@TiO_2, showed they have ~2% Pd loading. PdNP are spherical with average size of 1.6 ± 0.9 nm, and present broad absorption in the visible region (400-700 nm). Chapter 2 describes how a water and air tolerant Pd@TiO_2 catalyst shows dual switchable catalytic activities changing from hydrogenation to isomerization on-demand, by minor variations of the reaction conditions. Benzyl-substituted alkenes are selectively isomerized to phenyl-substituted alkenes (E-isomer) with complete conversion over Pd@TiO_2 under H_2-free conditions. The reaction can be thermally induced under air or driven by visible light irradiation at room temperature under Argon (Table 2.1 and Table 2.3). UV irradiation in methanol as solvent leads to efficient hydrogenation (Table 2.2 and Table 2.4). Hence, the ability of Pd@TiO_2 to photo-assist the hydrogenation of alkenes upon UV excitation (<400 nm) can be switched to isomerization simply by using visible light (>400 nm) or thermal heating (solvent boiling point), without addition of H_2 (Scheme 1.2a). In both cases, TiO_2 is catalytically and optically active support. The use of TiO_2 support results in multifunctional nanocomposites, where possible synergistic interactions could lead to higher effectiveness in heterogeneous catalysis of alkene isomerization and hydrogenation (Scheme 2.4). The catalytic hydrogenation of alkenes is one of the most significant addition reactions and widely used in the food industry where, for example H_2 molecules are added to unsaturated vegetable oils and fats. This catalytic process requires the presence of metal catalyst such as Nickel, palladium, platinum or rhodium at high temperature under pressure and hydrogen source.[22] In addition, H_2 is flammable and difficult to handle. The catalytic transfer hydrogenation appears to be an alternative approach that is based on the use of sustainable hydrogen source with excellent stability and easy handling capability. The catalytic transfer

hydrogenation is the addition of H_2 to unsaturated organic compounds (olefins, aldehydes/ketones, nitroarenes) using a safe hydrogen donor such as methanol, isopropanol, hydrazine, sodium borohydride and formic acid other than gaseous H_2.[23] In the present work, Pd@TiO_2 exhibited high catalytic efficiency for the photocatalytic transfer hydrogenation of alkenes under mild conditions with methanol as hydrogen donor. For simplicity the transfer hydrogenation of alkenes presented in this work will be named photocatalytic hydrogenation of alkenes. The photocatalytic hydrogenation of alkenes to alkanes presented in Chapter 2 can be promoted in the absence of H_2 by just using alcoholic suspensions and Pd@TiO_2. Upon UV irradiation, Pd@TiO_2 contributes to solvent oxidation and in situ formation of H_2 (Figure 2.1). Pd-based catalysts are known to perform deuterium labeling in the presence of H_2 by H-D exchange. Chapter 2 describes how the switchable catalytic activities of the Pd@TiO_2 from hydrogenation to isomerization on-demand under mild conditions, is used for selective deuterium incorporation using deuterated solvents. Here H/D exchange is used as a mechanistic tool as shown in Scheme 2.2 and Scheme 2.3, but with clear potential for isotope substitution applications.

The cross-coupling C-C bond formation, namely Sonogashira reaction, can also easily be photocatalyzed by Pd@TiO_2 (Chapter 3). The direct excitation of the PdNPs catalyzes the C-C coupling between aryl iodides and alkynes under very mild conditions in short reaction times (Scheme 3.1). The catalyst is air and moisture tolerant and can be supported in a wide range of materials, including inert ones such as nanodiamonds (Table 3.1) or glass fibers (Chapter 5 and chapter 6). In the case of Pd@TiO_2, the rates of the thermally induced reactions were about 4.7 mM/h at 42°C (the same temperature as reached under light illumination) compare to 7.5 mM/h of the photoinduced Sonogashira coupling. Study of the action spectrum (Figure 3.1) demonstrates that direct excitation of the PdNP is required to yield the desired product. The action spectrum is the plot of the apparent quantum yield (AQY) of the reaction versus the wavelength of the incident light where the same number of photons is delivered to each sample.[9] The AQY of a photochemical transformation is determined by the ratio of reaction rate to the

absorbed light intensity at given wavelength per volume and time ($I_{a,}$ photon flux).[24] The measurement of I_a is easy in homogeneous systems while in heterogeneous system the light can be not only absorbed, it can be also scattered and/or reflected by the suspended particles in the reaction mixture. To overcome this problem in heterogeneous photocatalysis the AQY is calculated by replacing the absorbed photon flux by the incident photon flux (the number of photons arriving at the sample).[24] In the case of Pd@TiO_2 visible excitation works well, while UVA (368 nm) is ineffective for Sonogashira coupling due to TiO_2 shielding of the Pd absorption and leading to different outcome (Scheme 1.2b). The catalyst can be reused a couple of times, but when it loses activity it can be reactivated via different approaches (Figure 2.2 and Table 3.5). The advantages of heterogeneous systems over their homogeneous counterparts are related to the ease of separation and reusability of the materials. However, the deactivation of heterogeneous catalysts after first catalytic cycles is an omnipresent problem.

The research presented in Chapter 4 carries forward the concept of heterogeneous catalyst recovery and reusability, by incorporating sustainable recovery strategies, based on alternating different photocatalytic reactions. The reaction rotation methodology is an innovative approach based on the crop rotation system used in agriculture. Chapter 4 describes in details a method we labeled "Catalytic Farming" that was employed to reactivate the Pd@TiO_2 catalyst surface by restoring its oxidation state, thus extending its life time, and preserving its selectivity and efficiency. To increase the product yield farmers ensure that the nutrients leached by one crop can be absorbed or restored by the following one in the next growing season. In catalysis, the rotation strategy was illustrated by Sonogashira coupling –problem reaction that depletes the catalyst – and Ullmann homocoupling –plausible recovery reaction that restore the oxidation state of the catalyst– as illustrated in Figure 4.1. The selection of reactions in this approach are based on previous mechanistic studies that include the role of the solvent and evaluation of the palladium oxidation state after each reaction (Figure 4.2). The ability to reuse catalysts is consistent with the principles of green chemistry, which encourages the use of sustainable practices.[25] Rotating the catalytic processes by using the same catalyst to synthesize alternating target molecules achieves these goals.

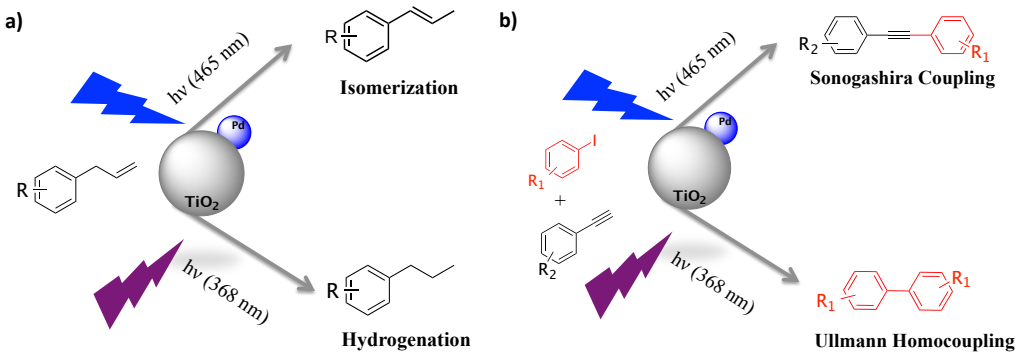

Scheme 1.2. Tunable photocatalytic activity of Pd@TiO_2 catalyst under different light sources. a) Switching from hydrogenation to isomerization of benzyl-substituted alkenes in alcoholic suspension by changing the irradiation wavelength. b) Visible light-induced Sonogashira coupling in alcoholic suspension and UV light-induced Ullmann homocoupling in THF suspension of Pd@TiO_2.

As mentioned above, developing active, selective and efficient heterogeneous catalytic systems are of major interest for a sustainable future due to minimal product contamination, easy-post reaction separation, and reusability of catalysts. In heterogeneous processes, catalyst supports are usually in the form of powders decorated with active metal and/or metal oxides nanostructures. Although, they are easy to recover from reaction mixture, these supports are not ideal for flow chemistry applications. With this in mind, Chapter 5 and Chapter 6 explore the possibility of using fibrous material as catalyst supports with excellent potential of flow photochemistry applications.[26] Glass fibers are inexpensive, available with a variety of surface properties, easy to modify in order to provide physical or chemical affinity towards many catalytic materials. Glass fibers are considered inert and passive support, mainly used to restrict the mobility of active catalyst. Thus, functionalized glass fibers open the opportunity to develop economical heterogeneous catalysts. Chapter 5 presents our efforts to develop an inexpensive, manageable and widely available material, GW, which can act as catalyst support for a number of different reactions under mild conditions. The performance of two types of GW, silanized and non-silanized, upon surface modifications prior to metal or metal oxides deposition were studied in representative classic catalytic processes. Different metal and metal oxide nanoparticles, namely Pd, Co, Au, Cu and Ru, were

derivatized on GW and used as heterogeneous catalysts for a variety of thermal and photochemical reactions, such as, reductive de-halogenation of aryl halides, reductions of nitrobenzene, Csp^3-Csp^3 couplings (C-C coupling of p-nitrobenzyl bromide), N-C heterocycloadditions (click chemistry) and Csp-Csp^2 couplings (Sonogashira couplings) as illustrated in Scheme 5.1. Notice that the use of these materials facilitates the catalyst separation from the reaction vessel, and thus a regular pair of tweezers can be used to remove the catalyst as shown in Figure 5.1 The characterization of new materials by scanning electron microscopy (SEM), energy-dispersive X-ray spectroscopy (EDX), diffuse reflectance (DR), inductive coupled plasma (ICP-OES), and X-ray photoelectron spectroscopy (XPS) along with their impact on selectivity, efficiency and reusability toward the development of commercial heterogeneous photocatalysts are discussed. Additionally, Chapter 6 describes the use of glass fibers as catalyst support for continuous flow heterogeneous photocatalysis of two test reactions: Sonogashira C-C coupling and dehalogenation of aryl iodides. Our approach is based on using robust and mechanically stable catalysts with excellent light transmission properties.

REFERENCES

1. N. Hoffmann, Photocatalysis with TiO_2 Applied to Organic Synthesis, Aust. J. Chem., 2015, 68, 1621-1639; J. Zoller, D. C. Fabry and M. Rueping, Unexpected Dual Role of Titanium Dioxide in the Visible Light Heterogeneous Catalyzed C-H Arylation of Heteroarenes, ACS Catal., 2015, 5, 3900-3904.
2. V. Aravindan, Y. S. Lee, R. Yazami and S. Madhavi, TiO_2 polymorphs in 'rocking-chair' Li-ion batteries, Mater. Today., 2015, 18, 345-351.
3. T. Luttrell, S. Halpegamage, J. Tao, A. Kramer, E. Sutter and M. Batzill, Why is anatase a better photocatalyst than rutile?Model studies on epitaxial TiO_2 films, Sci. Rep., 2014, 4, 4043-4047.
4. T. Ohno, K. Sarukawa, K. Tokieda and M. Matsumura, Morphology of a TiO_2 photocatalyst (Degussa, P-25) consisting of anatase and rutile crystalline phases, J. Catal., 2001, 203, 82-86.
5. M. R. Hoffmann, S. T. Martin, W. Y. Choi and D. W. Bahnemann, Environmental Applications of Semiconductor Photocatalysis, Chem. Rev., 1995, 95, 69-96; A. Fujishima, X. T. Zhang and D. A. Tryk, TiO_2 photocatalysis and related surface phenomena, Surf. Sci. Rep., 2008, 63, 515-582; M. A. Fox and M. T. Dulay, Heterogeneous Photocatalysis, Chem. Rev., 1993, 93, 341-357.
6. A. L. Linsebigler, G. Q. Lu and J. T. Yates, Photocatalysis on TiO_2 Surfaces - Principles, Mechanisms, and Selected Results, Chem. Rev., 1995, 95, 735-758; A. Mills and S. LeHunte, An overview of semiconductor photocatalysis, J. Photoch. Photobio. A, 1997, 108, 1-35.

7. S. T. Martin, H. Herrmann, W. Choi and M. R. Hoffmann, Time-resolved microwave conductivity. Part 1—TiO_2 photoreactivity and size quantization, J. Chem. Soc. Faraday Trans., 1994, 90, 3315-3322.
8. J. Schneider, M. Matsuoka, M. Takeuchi, J. Zhang, Y. Horiuchi, M. Anpo and D. W. Bahnemann, Understanding TiO_2 photocatalysis: mechanisms and materials, Chem. Rev., 2014, 114, 9919-9986.
9. S. P. Pitre, T. P. Yoon and J. C. Scaiano, Titanium dioxide visible light photocatalysis: surface association enables photocatalysis with visible light irradiation, Chem. Commun., 2017, 53, 4335-4338.
10. A. Elhage, A. E. Lanterna and J. C. Scaiano, Light-Induced Sonogashira C-C Coupling under Mild Conditions Using Supported Palladium Nanoparticles, ACS Sustain. Chem. Eng., 2018, 6, 1717-1722; A. Elhage, A. E. Lanterna and J. C. Scaiano, Tunable Photocatalytic Activity of Palladium-Decorated TiO_2: Non-Hydrogen-Mediated Hydrogenation or Isomerization of Benzyl-Substituted Alkenes, ACS Catal., 2017, 7, 250-255; A. E. Lanterna, A. Elhage and J. C. Scaiano, Heterogeneous photocatalytic C-C coupling: mechanism of plasmon-mediated reductive dimerization of benzyl bromides by supported gold nanoparticles, Catal. Sci. Technol., 2015, 5, 4336-4340; B. Wang, J. Durantini, J. Nie, A. E. Lanterna and J. C. Scaiano, Heterogeneous Photocatalytic Click Chemistry, J. Am. Chem. Soc., 2016, 138, 13127-13130; N. Marina, A. E. Lanterna and J. C. Scaiano, Expanding the Color Space in the Two-Color Heterogeneous Photocatalysis of Ullmann C-C Coupling Reactions, ACS Catal., 2018, 8, 7593-7597.
11. E. J. Xiayan Wu, Sarina Sarina and Huai Yong Zhu, Direct photocatalysis of supported metal nanostructures for organic synthesis, J. Phys. D: Appl. Phys., 2017, 50, 283001-283027.
12. S. Sarina, H. Y. Zhu, Q. Xiao, E. Jaatinen, J. Jia, Y. Huang, Z. Zheng and H. Wu, Viable photocatalysts under solar-spectrum irradiation: nonplasmonic metal nanoparticles, Angew. Chem. Int. Ed., 2014, 53, 2935-2940; S. Sarina, H. Y. Zhu, E. Jaatinen, Q. Xiao, H. W. Liu, J. F. Jia, C. Chen and J. Zhao, Enhancing Catalytic Performance of Palladium in Gold and Palladium Alloy Nanoparticles for Organic Synthesis Reactions through Visible Light Irradiation at Ambient Temperatures, J. Am. Chem. Soc., 2013, 135, 5793-5801.
13. S. Sarina, E. Jaatinen, Q. Xiao, Y. M. Huang, P. Christopher, J. C. Zhao and H. Y. Zhu, Photon Energy Threshold in Direct Photocatalysis with Metal Nanoparticles: Key Evidence from the Action Spectrum of the Reaction, J. Phys. Chem. Lett., 2017, 8, 2526-2534.
14. R. Schlçgl, Heterogeneous Catalysis, Angew. Chem. Int. Ed., 2015, 54, 3465 – 3520.
15. A. Ibrahimbegovic, J. B. Colliat, M. Hautefeuille, D. Brancherie and S. Melnyk, Probability Based Size Effect Representation for Failure in Civil Engineering Structures Built of Heterogeneous Materials, Comput. Meth. Appl. Sci., 2011, 22, 291-313.
16. J. G. Gardner and D. H. Keating, Genetic and functional genomic approaches for the study of plant cell wall degradation in Cellvibrio japonicus, Methods Enzymol., 2012, 510, 331-347.
17. Y. Matatov-Meytal and M. Sheintuch, Catalytic fibers and cloths, Appl. Catal. A-Gen., 2002, 231, 1-16.
18. V. V. Barelko, M. V. Kuznetsov, V. G. Dorokhov and I. Parkin, Glass-Fiber Woven Catalysts as Alternative Catalytic Materials for Various Industries. A Review, Russ. J. Phys. Chem. B, 2017, 11, 606-617.
19. N. Semagina, A. Renken and L. Kiwi-Minsker, Palladium nanoparticle size effect in 1-hexyne selective hydrogenation, J. Phys. Chem. C, 2007, 111, 13933-13937; Z. Hou, N.

Theyssen, A. Brinkmann and W. Leitner, Biphasic aerobic oxidation of alcohols catalyzed by poly(ethylene glycol)-stabilized palladium nanoparticles in supercritical carbon dioxide, Angew. Chem. Int. Ed., 2005, 44, 1346-1349; R. Narayanan and M. A. El-Sayed, Effect of Catalysis on the Stability of Metallic Nanoparticles: Suzuki Reaction Catalyzed by PVP-Palladium Nanoparticles, J. Am. Chem. Soc., 2003, 125, 8340-8347.

20. A. T. Bell, The Impact of Nanoscience on Heterogeneous Catalysis, Science, 2003, 299, 1688-1691.
21. A. Elhage, A. E. Lanterna and J. C. Scaiano, Catalytic farming: reaction rotation extends catalyst performance, Chem. Sci., 2019, 10, 1419-1425.
22. D. Wang and D. Astruc, The Golden Age of Transfer Hydrogenation, Chem. Rev., 2015, 115, 6621-6686.
23. X. Z. Jie Li, Ning-Zhao Shang, Cheng Feng, Shu-Tao Gao and and C. Wang, Nitrogen-enriched porous carbon supported Pd-nanoparticles as an efficient catalyst for the transfer hydrogenation of alkenes, New J.Chem., 2018, 42, 16823-16828; Z. S. Qureshi, P. B. Sarawade, M. Albert, V. D'Elia, M. N. Hedhili, K. Kohler and J. M. Basset, Palladium Nanoparticles Supported on Fibrous-Structured Silica Nanospheres (KCC-1): An Efficient and Selective Catalyst for the Transfer Hydrogenation of Alkenes, Chemcatchem., 2015, 7, 635-642; K. Ganjehyan, B. Nişancı, M. Sevim, A. Daştan and Ö. Metin, Monodisperse CuPt alloy nanoparticles assembled on reduced graphene oxide as catalysts in the transfer hydrogenation of various functional organic groups, Appl. Organometal. Chem., 2019, 33, e4863.
24. H. Kisch, On the Problem of Comparing Rates or Apparent Quantum Yields in Heterogeneous Photocatalysis, Angew. Chem. Int. Ed., 2010, 49, 9588 – 9589.
25. P. Anastas and N. Eghbali, Green chemistry: principles and practice, Chem. Soc. Rev., 2010, 39, 301-312.
26. A. Elhage, B. Wang, N. Marina, M. L. Marin, M. Cruz, A. E. Lanterna and J. C. Scaiano, Glass wool: a novel support for heterogeneous catalysis, Chem. Sci., 2018, 9, 6844-6852.

2. Tuneable Photocatalytic Activity of Palladium-Decorated TiO_2: Non-Hydrogen-Mediated Hydrogenation or Isomerization of Benzene-Substituted Alkenes

2.1 Preamble to chapter 2

The following chapter describes the development of a published synthetic protocol and material characterization of Pd@TiO_2, along with its application in heterogeneous catalysis for two different organics transformations: alkene isomerization and alkene hydrogenation. The photo-responsive Pd@TiO_2 can have different reactivity when irradiated with different light sources and thus, the preferred outcome can be tuned by the correct selection of wavelengths. Strategies based on tuning the excitation sources will stimulate studies using multi-wavelength sources and the discovery of new synthetic routes

The original motivation for this line of research was to expand the scope of a tested photochemical method for the preparation of hybrid materials based on titanium dioxide decorated with noble metal or metal oxide nanoparticles, then their applications as an alternative heterogeneous photoredox catalyst to the homogenous metal complexes catalysts. The resulting hybrid materials, Pd@TiO_2, absorb light in the visible region, which can be suitable catalysts for different organic transformation under mild conditions. Isomerisation of benzyl-substituted alkenes can be thermally induced or driven by visible light irradiation over Pd@TiO_2 to selectively afford the *trans*-isomer product. On the other hand, UV irradiation in methanol as a solvent leads to complete alkene hydrogenation in a short reaction time. To our delight, the new hybrid catalyst is not only versatile and selective, it is also air and moisture tolerant and its reactivity can be tuned by the correct selection of wavelengths to which the material is exposed. Pd@TiO_2 is used for selective deuterium incorporation using deuterated solvents under H_2 free conditions; here H/D exchange is used as a mechanistic tool but with clear potential for isotope substitution applications. These features intensified the impact of

this work, which has been selected by the Editorial Board of Synfacts for its important insights.

2.2 Postprint Version of Manuscript

First published in: ACS Catal. **2017**, 7, 250-255

ABSTRACT

Palladium-decorated TiO_2 is a moisture and air-tolerant versatile catalyst. Its photocatalytic activity can be tuned in favour of hydrogenation or isomerization of benzyl-substituted alkenes simply by changing the irradiation wavelength. Benzyl-substituted alkenes are selectively isomerized to phenyl-substituted alkenes (*E*-isomer) with complete conversion over Pd@TiO_2 under H_2-free conditions. The reaction can be thermally induced under air or driven by visible light irradiation at room temperature under Ar. UV irradiation in methanol solvent leads to efficient hydrogenation. The fine-tunability of the catalyst can also be used for selective deuterium incorporation using deuterated solvents; here H/D exchange is used as a mechanistic tool but with clear potential for isotope substitution applications.

INTRODUCTION

Alkene isomerisation reactions have often been encountered as undesired side-reactions during asymmetric catalytic hydrogenation[1] or metathesis reactions,[2] that have the potential to compromise enantioselectivity and promote the formation of by-products. However, the deliberate and controlled isomerisation of a pre-existing alkene bond can afford positional and geometric isomers that are difficult to prepare using conventional methods. Established methods for carrying out these transformations include: treatment of an easily prepared alkene substrate with radicals[3], boranes[4], halogens,[5] and strong acids[6]. However, there are many disadvantages associated with these methods due to functional group incompatibility with the harsh reaction conditions that are often required for isomerisation to occur. Photochemical methods have been

applied to the (E)/(Z)-isomerisation of alkenes,[7] but the success of this approach is substrate dependent, with mixtures of products controlled by the photostationary state often being produced.[8] The use of transition-metal-based catalysts offers several advantages over these more conventional methods, such as functional group tolerance, mild reaction conditions, product selectivity, and reliability.[1, 9] From an industrial perspective, catalytic processes are more desirable than those using stoichiometric reagents, as product separation is greatly simplified, particularly if heterogeneous catalysts are used. This is especially advantageous for the synthesis of pharmaceutical compounds intended for human consumption, which must adhere to strict purity requirements.[10] The allyl phenyl ether group is important in the perfumery and food industries, where *t*-anethole and *i*-eugenol have high industrial demand as intermediates for the synthesis of various perfumery chemicals, pharmaceutical compounds, and beverages. *t*-Anethole is a naturally occurring product, extracted from anise and fennel oils, with variable proportion of its *cis* isomer as an impurity. However the increasing industrial demand has made it necessary to develop alternative synthetic routes for *t*-anethole, the only valuable product due to the toxicity of its *cis* isomer. From an academic point of view, several methodologies have been reported to isomerize the estragole to anethole either catalyzed by metal complexes of Pd, Ru and Rh,[11] or carried out over catalysts belonging to the hydrotalcite family.[12] Most of the selective bond isomerization of estragole studies has been done using homogeneous catalysis under a nitrogen atmosphere to maintain the catalyst stability. Nevertheless they are not commercially viable due to the high synthetic costs.

The use of supported PdNPs has been explored in the last few years because of their potential to replace Pd complexes as catalysts.[13] Imamura et al. have developed a solvent-mediated hydrogenation of alkenes using the photocatalytic ability of TiO_2 combined with the well-known H-Pd surface interaction.[14] On the other hand, Zhu and Shon have recently presented a mechanism for hydrogenation/isomerization reactions in the presence of H_2 on PdNP surface.[15] Here we present a water- and air- tolerant PdNP-decorated TiO_2 (Pd@TiO_2) catalyst that shows dual switchable catalytic activities changing from hydrogenation to isomerization on-demand, by minor variations of the

reaction conditions. Thus, the ability of Pd@TiO_2 to photoassist the hydrogenation of alkenes upon UV excitation can be switched to lead to isomerization simply by using visible light or thermal heating, without addition of H_2. Like the hydrogenation reaction, the photo-induced isomerization is also performed under Argon, whilst the thermally induced reaction is air tolerant. The photocatalyst can be reused several times with excellent performance (*vide infra*). Both conditions selectively lead to the *trans* reaction product. The selective isomerization of estragole to *t*-anethole has been studied using *i*-propanol and methanol as solvents and reducing agents under both reflux and visible light irradiation, respectively. Furthermore, mechanistic studies demonstrate the reaction is solvent-mediated allowing selective deuterium incorporation. The scope of the catalytic activity has been explored with a group of valuable industrial compounds, including *i*-eugenol.

RESULTS AND DISCUSSION

PdNPs were synthesized by reduction of Pd^{2+} under UVA irradiation in the presence of TiO_2[16] (~ 25 nm particle size, band gap energy ~3.2 eV[17]), Scheme 2.1. The major advantage of this synthetic route is that it does not require an organic ligand/reductant that could arrest particle growth; it also maximizes the available nanoparticle surface. Pd@TiO_2 were characterized by inductively coupled plasma optical emission spectrometry (ICP-OES), transmission electron microscopy (TEM) and X-ray photoelectron spectroscopy (XPS) to determine the total Pd loading, the particle size and the oxidation state of the Pd species, respectively. The synthesis described in the Supporting Information (SI, page 30) leads to 2 % Pd loading with average particle size of (1.6 ± 0.9) nm (Scheme 2.1 and Figure S2.1). The XPS analysis of the binding energies of Pd was calculated on the basis of the binding energy (284.8 eV) of C 1s and using reference values from the literature.[18] A high-resolution scan over the range 327-347 eV reveals several peaks associated to different Pd species present in the sample (Figure S2.6). Two pairs of doublet signals can be recognized after deconvolution: a double of a Pd ($3d_{5/2}$) peak at around 334.7 eV and a Pd ($3d_{3/2}$) peak at around 339.9 eV

which can be assigned to Pd(0);[19] the second pair located in a higher region (337.2 and 342.3 eV) in comparison with the Pd(0) indicates the presence of PdO.[20]

The direct, selective, and non-hydrogen mediated isomerization of benzyl-substituted alkenes over Pd@TiO_2 catalyst was studied for the synthesis of *t*-anethole using estragole. Table 2.1 summarizes the conditions screened for the optimization of the thermally induced isomerization of estragole under air.

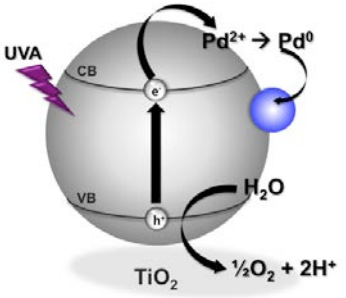

Scheme 2.1. Proposed mechanism for the photochemical synthesis of supported PdNP

The best conditions were found when estragole was mixed together with Pd@TiO_2 catalyst in *i*-propanol and refluxed for 24 h. Changing the catalyst support for a known inert material such as crystal nanodiamonds (CND), the yield of the reaction decreases dramatically (*cf.* entries i-iii and iv-vii in Table 2.1). These results show that the role of TiO_2 is much more than simply anchoring the PdNP. Additionally, the reaction is highly favoured in alcohols, although small conversion and lower selectivity has been found using non-protic solvents (Table 2.1, entries viii-ix). These two conditions might be explained because of the reduction of PdO over TiO_2 by secondary alcohols, which is favoured at high temperature.[18] Control reactions in the presence of TiO_2 or in the absence of catalyst were also performed.

Considering that upon UV light irradiation Pd@TiO_2 can catalyze the hydrogenation of alkenes[14] (tested here for estragole (Table 2.2, entry vi)), and that it has an important absorption in the visible region, probably due to the presence of Pd or PdO NPs (See Figure S2.2); the same reaction was tested upon visible irradiation at room temperature. Unexpectedly, only isomerization products are found after 4 h of

irradiation, as can be noticed in Table 2.2, entry i. The reaction works well in methanol and goes to completion in 24 h (with traces of hydrogenation product, probably due to some UV light contamination on the LED emission, see Figure S2.3 in the supporting information) under Ar atmosphere.

The temperature of the mixture rises up to ca. 50 ºC upon excitation at 465 nm. Notice that the total irradiance used under visible light is about 3 times higher compared to UV light (*vide infra*). Neither the hydrogenation nor the isomerization work under air, suggesting that a reducing environment is required for both reactions.

Table 2.1: Effect of solvents and catalyst supports on the thermal isomerization of estragole

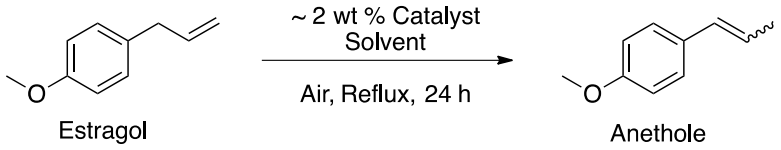

Estragol Anethole

	Solvent	Catalyst	% Conv	% A Yield
i	*i*-propanol	Pd@CND	20	18 (≥90)
ii	Toluene	Pd@CND	35	32 (71)
iii	Acetonitrile	Pd@CND	ND	ND
iv	*i*-propanol	Pd@TiO_2	100	>99 (>90)
v	*i*-propanol[b]	Pd@TiO_2	ND	ND
vi	methanol[a]	Pd@TiO_2	70	69 (86)
vii	methanol[b]	Pd@TiO_2	11	6 (>90)
viii	Toluene	Pd@TiO_2	45	33 (60)
ix	acetonitrile	Pd@TiO_2	15	8 (53)
x	*i*-propanol	--	ND	ND
xi	*i*-propanol	TiO_2	ND	ND

[a]Conversion yields drop to ca. 39% in deuterated methanol. [b]Reaction time: 6h. Solvent boiling point: *i*-propanol = 85 °C, Acetonitrile = 85 °C, Toluene = 111 °C, Methanol = 65 °C. % Yields and conversions were calculated by GC-FID and/or ^{1}H NMR using *t*-butylbenzene and dimethyl sulfone as external standards, respectively. Percent A Yield corresponds to the total isomerization products; values between brackets show the selectivity towards the trans isomer. No hydrogenation products have been detected under these conditions. Similar yields were found under an inert atmosphere.

Different catalyst concentrations were tested for both isomerization and hydrogenation (Table S2.1 in the supporting information). Overall, different products can be obtained under essentially the same conditions, simply by switching the excitation wavelength. Further, when TiO_2 is replaced by CND (with same NPs size distribution, *cf.* Figure S2.1 c and d in the supporting information), the isomerization products are also formed, albeit in lower yields. However, for Pd@CND, hydrogenation products could not be detected, even upon 368 nm irradiation. Finally, comparing the isomerization yields obtained after conventional heating (entry vii, Table 2.1), microwave irradiation (entry x, Table 2.2) and light irradiation (entry i, Table 2.2) there is clear evidence that the catalytic activity of the Pd@TiO_2 is dominated by a photoinduced process even if a minor thermal contribution may be involved in the isomerization process. This is reminiscent of what has been recently described for Pt NPs (<10 nm) that can indeed absorb visible light when embed on SiO_2 supports resulting from enhanced near field of resonant scattering modes.[21]

Table 2.2: Effect of irradiation light and atmosphere on the photocatalytic isomerization of estragole at room temperature

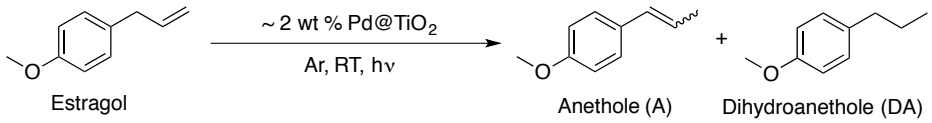

Estragol Anethole (A) Dihydroanethole (DA)

	Time (h)	hν (nm)	Solvent	% Conv	% DA	% A
i	4	465	methanol	48	ND	48 (75)
ii	24	465[a]	methanol	100	7	93 (86)
iii	24	465	*i*-propanol	58	ND	58 (81)
iv	24	465[b]	methanol	55	ND	55 (80)
v	24	465[d]	methanol	0	ND	ND
vi	4	368	*i*-propanol	100	100	ND
vii	24	368[c]	methanol	0	ND	ND
viii	24	465[d]	methanol	33	ND	33 (73)
ix	4	368[d]	methanol	15	ND	15 (53)
x	4	MW[e]	methanol	0	ND	ND
xi	24	465	toluene	25	ND	22 (82)
xii	24	465	toluene-d_8	26	ND	21 (81)

[a]Conversion yields drops to ca. 56 % in deuterated methanol [b]Catalyst two months old. [c]Under air. [d]Pd@CND. [e]55 ºC and 20 bars. % Yields and conversions were calculated by GC-FID and/or 1H NMR using *t*-butylbenzene and dimethyl sulfone as external standards, respectively. Irradiance 10,035 mWm^{-2} using 465 nm LED and 4,865 mWm^{-2} using 368 nm LED. Percent A Yield corresponds to the total isomerization products; values between brackets show the selectivity towards the *trans* isomer.

Although the determination of the quantum yield (QY) of heterogeneous catalysts is well known to be complex[22] we decided to measure the 'apparent' QY (AQY) of the isomerization reaction. Uneven absorption of the photon flux is expected due to minor changes in the nature and light scattering of the suspension, therefore in the QY calculation the absorbed photon flux was replaced by the incident photon flux. The latter was determined using $Ru(bpy)_3Cl_2$ as the actinometer.[23] Considering 4 h of reaction, the AQY was found ~0.29 % and ~0.53 % when 10 mg and 15 mg of catalyst were used, respectively.

Pd-based catalysts are also known to perform deuterium incorporation in the presence of H_2 by H-D exchange.[24] Here we evaluated the deuterium incorporation in order to gain insight the mechanism of the thermally and light-induced isomerization and to evaluate its potential synthetic value. Yields about 40 % isomerization (no double bond reduction) were found after refluxing the reaction mixture for 24 h in CD_3OD, in contrast to the ca. 70 % found using regular methanol (cf. entry vi, Table 2.1). This isotopic effect hints to an important role of the solvent during the rate-limiting step of the reaction. ^1H NMR spectra were recorded showing ~21% of deuterium incorporation in position a (Scheme 2.2) exclusively (D_1). The same experiment was carried out upon 465 nm irradiation as per conditions in Table 2.2, entry ii. Although a great isotopic effect was found using methanol-d_4 (vide infra), minimal deuterium incorporation was detected by integration of the ^1H NMR signals.

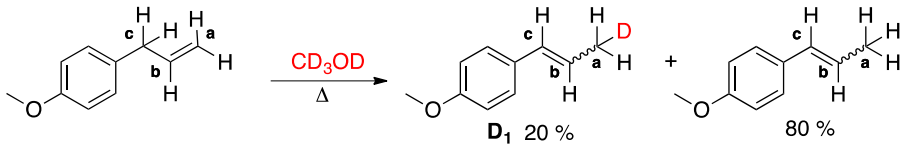

Scheme 2.2. Deuterium incorporation for isomerization upon reflux in CD_3OD.

UV irradiation (4 h) in CD_3OD led to full reduction of the double bond. ^1H and ^2H NMR show deuteration in positions a, b and c with 0.75, 0.72 and 0.56 D incorporation, respectively (See Figure S2.4). Deuteration in position c demonstrates the

photocatalytic hydrogenation process occurs concurrently with isomerization. Thus, the deuterated products (D_2 and D_3) could be obtained by isomerization of estragole to anethole as proposed in Scheme 2.3, followed by deuterium incorporation (path a) or by direct reaction of estragole (path b). Although, no generation of estragole was detected when anethole is submitted to 368 nm irradiation for 4 h, additional experiments in deuterated solvent show also deuteration in positions a, b and c. This reinforces the idea that isomerization can also take place upon UV irradiation, but these products cannot be detected before they inexorably go to full hydrogenation process in the time range studied here, see SI (Figure S2.4 C and Table S2.2).

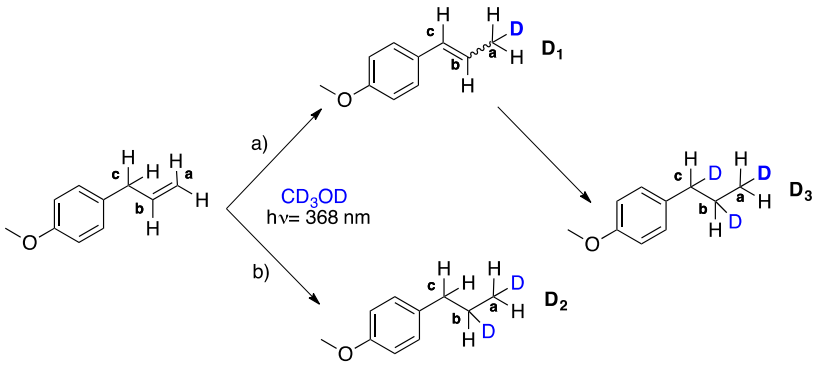

Scheme 2.3. Deuterium incorporation for hydrogenation under 368 nm irradiation in CD_3OD.

Zhu and Shon have recently suggested that the hydrogenation/isomerization reactions in the presence of H_2 on PdNP surface must occur through a mono-σ bonded Pd-alkyl intermediate followed by β-hydride elimination as they previously proposed.[15] When there is no H_2 present, a π-allyl Pd hydride mechanism is suggested. Figure 2.1 shows the analysis of the gas phase of the Pd@TiO_2 catalyst suspended in methanol under Ar atmosphere upon irradiation at 368 nm or 465 nm. As expected, a large amount of H_2 can be identified upon UV irradiation (Scheme S2.2) but no generation of H_2 was detected when the catalyst was exposed to blue light (465 nm). The presence of H_2 suggests the mechanism involved in the hydrogenation reaction, although run at almost the same conditions as the isomerization, might be different. We show here that either under heating or visible light irradiation, benzyl alkenes can be isomerized without

addition of H_2, but through a solvent-dependant reaction. Thus, although small deuterium incorporation was found under both conditions, the reaction yields are reduced to a half in methanol-d_4, suggesting a significant isotopic effect on the isomerization itself. When the same experiments were performed in toluene-d_8 no isotopic effect was found (Table 2.2, entries xi and xii). We believe the solvent might be involved in the decomplexation step of the reaction, when the π-bonded Pd-allyl intermediate has to be released from the Pd surface to lead to products (Scheme 2.4 A). This process might be critical to obtain high yields when the reactions are performed in alcohols. Also, it is known that alcohols can decompose on Pd and PdO surfaces, releasing CO, a good reducing agent for PdO,[18] which would account for the differences found between MeOH and *i*-propanol.[25] As the sample is heated or illuminated with visible light, the decomposition of the alcohol can reduce the surface of the PdNP[18] and promote isomerization. The use of deuterated alcohols can decrease the rate of this process and all the concomitant surface processes (i.e., isomerization). The major implication of this mechanism is that the formation of π-allyl Pd-hydride does not require H_2 gas to proceed. This is simply explained because the Pd−H adduct is generated from the oxidative addition of Pd to the C−H bond α to the alkene group to produce a π-allyl metal-hydride intermediate (Scheme 2.4 A). On the other hand, as reported by Imamura et al., 368 nm excitation of Pd@TiO_2 composites in methanol generates H_2 by alcohol oxidation on the TiO_2 surface (Scheme 2.4B and S2.1D). The Pd-alkyl mechanism shown in Scheme 2.4 B requires the presence of the Pd−H species for the catalytic reaction to occur. Our results show that H_2 can be generated in-situ by the oxidation of methanol to methanal on the TiO_2 surface. Thus, in the absence of TiO_2, (i.e., when CND is used as catalyst support), only isomerization products can be found upon 368 nm irradiation, simply because no H_2 is generated on the inert diamond surface. Scheme 2.4 summarizes mechanistically the four situations encountered in this work, that is, thermal isomerization under air, photochemical isomerization with visible light under Ar, photochemical hydrogenation and hydrogen generation (a process that also occurs in the absence of substrate) both under UV light and Ar. In order to facilitate

visualizing the various situations, Scheme S2.1 in the Supporting information presents each case as a separate panel.

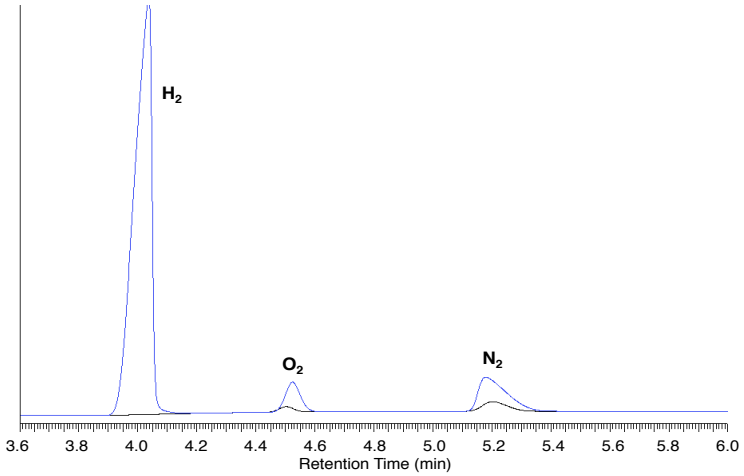

Figure 2.1. Gas chromatogram using Thermal Conductivity Detection (TCD). Gas phase of the Pd@TiO_2 in methanol upon 465 nm irradiation (black) and 368 nm irradiation (blue).

The scope of the isomerization reaction studied with different allyl benzyl derivate under thermally or light-induced catalysis is summarized in Tables 2.3 and 2.4, respectively. Table 2.3 shows that the photocatalytic isomerization of benzyl alkenes generally works better than the thermally induced reaction. There are however, some exceptions where only thermal catalysis can drive to isomerization in less than 48 h (cf. entries iv and vi in table 2.3 and table 2.4). The selectivity of the reaction towards the *trans* product was excellent in both cases. Linear alkenes and cyclic dienes were also tested for these reactions but the volatility of both, the reagents and the products, made the analysis of the reaction progress very difficult.

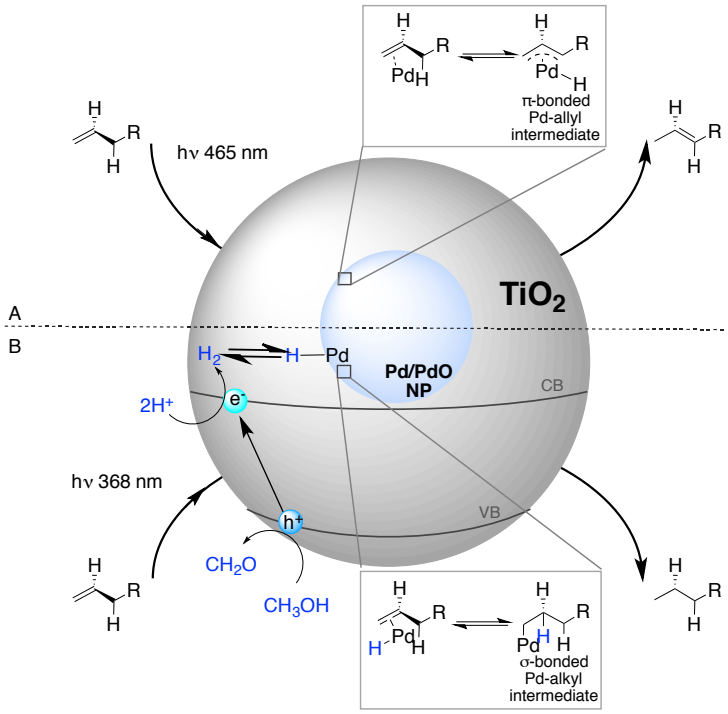

Scheme 2.4. A. Isomerization of alkenes upon irradiation at 465 nm. The formation of the π-allyl Pd-hydride adducts on the Pd surface does not require the presence of H_2 gas. **B.** σ-alkyl Pd hydride adduct can be formed on the Pd surface activated upon H_2 generation by UV light excitation. Notice in this cartoon the size of the particles has been exaggerated to show easily the process on the Pd surface, but they are not on scale. The grey boxes magnify the surface phenomena.

Pd@TiO_2 catalyst was tested for potential reuse in the direct, selective and non-hydrogen mediated isomerization of estragole under thermally and photo-induced catalysis, by performing the reaction at least three times (Figure 2.2). The reaction was scaled up to facilitate catalyst recovery and reuse. While the thermal catalytic activity decreases after the first cycle and becomes negligible by the third use; the photocatalytic activity of Pd@TiO_2 remains quite reasonable after four catalytic cycles (see SI for more details). We believe that under these conditions (methanol and an argon atmosphere) Pd is reduced in situ to lead to essentially the same behaviour as the fresh samples. Interestingly, even a sample aged for two months under air still shows 50% of its 'fresh' activity (see Table 2.2, entry iv).

Table 2.3. Thermal isomerization of different allyl benzyl derivatives catalyzed by Pd@TiO2 after 24 h reflux in *i*-propanol.

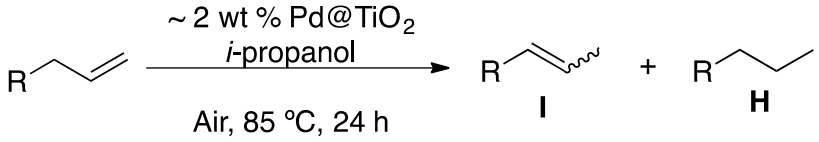

	R	% Conv	% I Yield	% Selectivity *trans*
i	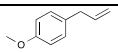	100 (100*)	100 (93)	93 (86)
ii	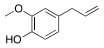	66 (72)	66 (72)	73 (86)
iii	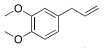	55 (69)	55 (69)	76 (61)
iv		45 (11)	45 (11)	77 (100)
v	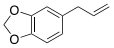	30 (59)	30 (59)	80 (88)
vi		15 (NR)	13 (--)	60 (--)
vii	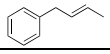	NR (NR)	--	--

*7% yield of product H. NR: No reaction. ND: No detectable. % Yields and conversions were calculated by GC-FID and/or ^{1}H NMR using *t*-butylbenzene and dimethylsulfone as external standards, respectively. Values in brackets correspond to the % yields obtained under irradiation as per conditions in Table 2.4 after 24 h.

Table 2.4. Light induced isomerization of different allyl benzyl derivatives catalyzed by $Pd@TiO_2$

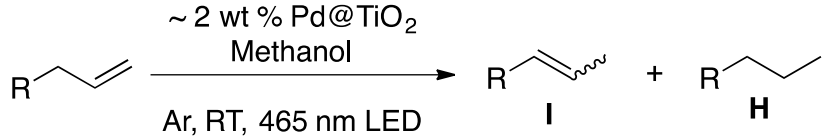

		Time	% Conv	% Yield	
				I	H
i	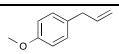	24 h	100	93 (86)	7
ii	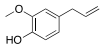	42 h	100	90 (87)	10
iii	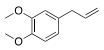	30 h	100	100 (92)	--
iv		48 h	24	24 (71)	--
v	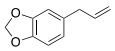	48 h	100	100 (92)	--
vi		48 h	ND	traces	--
vii	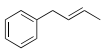	48 h	ND	traces	--

% yields and conversions were calculated by GC-FID and/or ^{1}H NMR using *t*-butylbenzene and dimethylsulfone as external standards, respectively. Values between brackets correspond to the % selective yield towards *trans* isomer

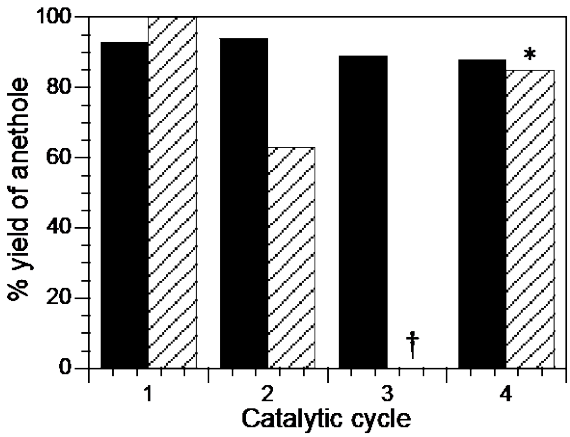

Figure 2.2. Catalyst reusability test upon 465 nm LED irradiation (solid bar) or dark conditions at 85 ºC (lined bar), using the same conditions as in table 2.3. †No conversion detected. *After catalyst recovery treatment with I-2959.

Storing the catalyst under air as well as its use might lead to partial oxidation of PdNPs as was confirmed by XPS (Figure S2.7). The shifting of the Pd 3d peaks with the aging of the catalyst to higher binding energy indicates that Pd can be slowly oxidized to Pd^{2+}. Significant loss of the catalytic activity occurs after multiple uses, as shown in Figure 2.2 for the thermal isomerization at 85 ºC. In order to reactivate the used catalyst, three different reduction treatments detailed in the Supporting Information were performed: 1) heating treatment in *i*-propanol;[18] 2) H_2 treatment; and 3) photochemical treatment using Irgacure-2959 (I-2959), a photoinitiator well-known for the generation of reducing ketyl radicals.[26] Even when the three recovery methods seem to generate more reduced Pd species (Figure S2.7); surprisingly, only I-2959 treatment fully recovers the thermally induced catalytic activity of Pd@TiO_2.

CONCLUSIONS

The tunability of the Pd@TiO_2 catalyst was demonstrated for the isomerization/hydrogenation of benzyl-substituted alkenes. The hybrid composite is known to drive hydrogenation of alkenes under UV light irradiation by generation of H_2 upon methanol oxidation. However, minor changes on the reaction conditions can drive the reaction to totally different but controllable products. It has been demonstrated that the isomerization of benzyl alkenes could be performed over Pd@TiO_2 in methanol by both, thermally and visible light induced catalysis, the latter by working under an inert atmosphere. The proposed isomerization mechanism suggests a π-allyl Pd-hydride intermediate that can be formed in the absence of H_2 and mediated by solvent participation. Multiple deuterium incorporations can be achieved managing different labelling position by slightly modifying the reaction conditions. The reusability of the catalyst is very good when used under light exposure. Although its catalytic activity is reduced after use in thermal catalysis, the catalyst can be easily reactivated by UVA irradiation in presence of the benzoin I-2959.

REFERENCES

1. K. Borszeky, T. Mallat and A. Baiker, Palladium-catalysed enantioselective hydrogenation of alkenoic acids. Role of isomerization, Catal. Lett., 1999, 59, 95-97.
2. S. H. Hong, D. P. Sanders, C. W. Lee and R. H. Grubbs, Prevention of undesirable isomerization during olefin metathesis, J. Am. Chem. Soc., 2005, 127, 17160-17161; C. S. Higman, A. E. Lanterna, M. L. Marin, J. C. Scaiano and D. E. Fogg, Catalyst Decomposition during Olefin Metathesis Yields Isomerization-Active Ruthenium Nanoparticles, Chemcatchem., 2016, 8, 2446-2449.
3. Y. Ichinose, K. Nozaki, K. Wakamatsu, K. Oshima and K. Utimoto, Et_3B Induced Stereoselective Radical-Addition of Ph_3GeH to Acetylenes and Its Application to Isomerization of Olefins, Tetrahedron Lett., 1987, 28, 3709-3712.
4. H. C. Brown and M. V. Bhatt, Organoboranes .4. Displacement Reaction with Organoboranes Derived from Hydroboration of Branched-Chain Olefins . A Contrathermodynamic Isomerization of Olefins, J. Am. Chem. Soc., 1966, 88, 1440-&.
5. T. T. Ling, E. Poupon, E. J. Rueden, S. H. Kim and E. A. Theodorakis, Unified synthesis of quinone sesquiterpenes based on a radical decarboxylation and quinone addition reaction, J. Am. Chem. Soc., 2002, 124, 12261-12267.
6. A. J. Hubert and Reimling.H, Acid-Catalyzed Isomerization of Substituted Indenes - Attempted Synthesis of Indenylacetone from Prop-2-Ynylindene, J. Chem. Soc. C, 1969, 944-950.
7. K. Hashimoto, Y. Masuda and H. Kominami, Photocatalytic Isomerization of 1-Butene over Palladium-Loaded Titanium(IV) Oxide Particles: Lewis Acid-like Features of the Photocatalyst, ACS Catal., 2013, 3, 1349-1355.
8. N. J. Turro, V. Ramamurthy and J. C. Scaiano, Modern molecular photochemistry of organic molecules, University Science Books, United States of America, 2010.
9. E. Larionov, H. Li and C. Mazet, Well-defined transition metal hydrides in catalytic isomerizations, Chem. Commun., 2014, 50, 9816-9826; S. K. Sharma, V. K. Srivastava and R. V. Jasra, Selective double bond isomerization of allyl phenyl ethers catalyzed by ruthenium metal complexes, J. Mol. Catal. A-Chem., 2006, 245, 200-209; K. Borszeky, T. Mallat and A. Baiker, Diastereoselective hydrogenation at indenols: Evidence for sterically and electronically unfavorable adsorption on palladium, J. Catal., 1999, 188, 413-416; K. Borszeky, T. Mallat and A. Baiker, Asymmetric hydrogenation of indene carboxylic acids: stereochemistry of hydrogen addition, Tetrahedron-Asymmetry., 1999, 10, 4781-4789; K. Borszeky, T. Burgi, Z. Zhaohui, T. Mallat and A. Baiker, Enantioselective hydrogenation of alpha, beta-unsaturated carboxylic acids over cinchonidine modified palladium: Nature of modifier-reactant interaction, J. Catal., 1999, 187, 160-166.
10. I. W. Davies, L. Matty, D. L. Hughes and P. J. Reider, Are heterogeneous catalysts precursors to homogeneous catalysts?, J. Am. Chem. Soc., 2001, 123, 10139-10140.
11. S. K. Sharma, V. K. Srivastava, P. H. Pandya and R. V. Jasra, Solvent-free isomerization of methyl chavicol to trans-anethole using transition metal complexes as catalysts, Catal. Commun., 2005, 6, 205-209; B. Lastra-Barreira and P. Crochet, Ruthenium-catalyzed estragole isomerization: high trans-selective formation of anethole, Green. Chem., 2010, 12, 1311-1314.
12. D. Kishore and S. Kannan, Catalytic isomerization of estragole to anethole over hydrotalcites and HT-like compounds, J. Mol. Catal. A-Chem., 2006, 244, 83-92.
13. F. M. McKenna, R. P. K. Wells and J. A. Anderson, Enhanced selectivity in acetylene hydrogenation by ligand modified Pd/TiO_2 catalysts, Chem. Commun., 2011, 47, 2351-

2353; F. M. McKenna and J. A. Anderson, Selectivity enhancement in acetylene hydrogenation over diphenyl sulphide-modified Pd/TiO_2 catalysts, J. Catal., 2011, 281, 231-240; J. Seth, C. N. Kona, S. Das and B. L. V. Prasad, A simple method for the preparation of ultra-small palladium nanoparticles and their utilization for the hydrogenation of terminal alkyne groups to alkanes, Nanoscale., 2015, 7, 872-876.

14. K. Imamura, Y. Okubo, T. Ito, A. Tanaka, K. Hashimoto and H. Kominami, Photocatalytic Hydrogenation of Alkenes to Alkanes in Alcoholic Suspensions of Palladium-loaded Titanium(IV) Oxide without the Use of Hydrogen Gas, RSC Adv., 2014, 4, 19883-19886.
15. E. Sadeghmoghaddam, H. Gu and Y.-S. Shon, Pd Nanoparticle-Catalyzed Isomerization vs Hydrogenation of Allyl Alcohol: Solvent-Dependent Regioselectivity, ACS Catal., 2012, 2, 1838-1845; D. J. Gavia, M. S. Maung and Y. S. Shon, Water-Soluble Pd Nanoparticles Synthesized from omega-Carboxyl-S-Alkanethiosulfate Ligand Precursors as Unimolecular Micelle Catalysts, ACS Appl. Mater. Inter., 2013, 5, 12432-12440.
16. D. C. Yang, W. Feng, G. J. Wu, L. D. Li and N. J. Guan, Nitrate hydrogenation on Pd-Cu/TiO_2 catalyst prepared by photo-deposition, Catal. Today, 2011, 175, 356-361.
17. A. L. Linsebigler, G. Q. Lu and J. T. Yates, Photocatalysis on TiO_2 Surfaces - Principles, Mechanisms, and Selected Results, Chem. Rev., 1995, 95, 735-758.
18. A. Jurgensen, N. Heutz, H. Raschke, K. Merz and R. Hergenroder, Behavior of Supported Palladium Oxide Nanoparticles under Reaction Conditions, Studied with near Ambient Pressure XPS, Anal. Chem., 2015, 87, 7848-7856.
19. K. Noack, H. Zbinden and R. Schlögl, Identification of the state of palladium in various hydrogenation catalysts by XPS, Catal. Lett., 1990, 4, 145-155.
20. M. P. Casaletto, A. Longo, A. Martorana, A. Prestianni and A. M. Venezia, XPS study of supported gold catalysts: the role of Au0 and Au+δ species as active sites, Surf. Interface Anal., 2006, 38, 215-218; A. M. Venezia, G. Pantaleo, A. Longo, G. Di Carlo, M. P. Casaletto, F. L. Liotta and G. Deganello, Relationship between Structure and CO Oxidation Activity of Ceria-Supported Gold Catalysts, J. Phys. Chem. B, 2005, 109, 2821-2827.
21. N. Zhang, C. Han, Y. J. Xu, J. J. Foley, D. T. Zhang, J. Codrington, S. K. Gray and Y. G. Sun, Near-field dielectric scattering promotes optical absorption by platinum nanoparticles, Nat. Photonics., 2016, 10, 473-483.
22. H. Kisch, On the Problem of Comparing Rates or Apparent Quantum Yields in Heterogeneous Photocatalysis, Angew. Chem. Int. Ed., 2010, 49, 9588-9589.
23. S. P. Pitre, C. D. McTiernan, W. Vine, R. DiPucchio, M. Grenier and J. C. Scaiano, Visible-Light Actinometry and Intermittent Illumination as Convenient Tools to Study $Ru(bpy)_3Cl_2$ Mediated Photoredox Transformations, Sci. Rep., 2015, 5, 16397.
24. N. Modutlwa, T. Maegawa, Y. Monguchi and H. Sajiki, Synthesis of deuterium-labelled drugs by hydrogen-deuterium (H-D) exchange using heterogeneous catalysis, J. Labelled Compd. Rad., 2010, 53, 686-692; T. Kurita, K. Hattori, S. Seki, M. Mizumoto, F. Aoki, Y. Yamada, K. Ikawa, T. Maegawa, Y. Monguchi and H. Sajiki, Efficient and convenient heterogeneous palladium-catalyzed regioselective deuteration at the benzylic position, Chem. Eur. J., 2008, 14, 664-673; T. Maegawa, N. Ito, K. Oono, Y. Monguchi and H. Sajiki, Bimetallic Palladium-Platinum-on-Carbon-Catalyzed H-D Exchange Reaction: Synergistic Effect on Multiple Deuterium Incorporation, Synthesis-Stuttgart., 2009, 2674-2678.
25. Z. H. N. Al-Azri, W. T. Chen, A. Chan, V. Jovic, T. Ina, H. Idriss and G. I. N. Waterhouse, The roles of metal co-catalysts and reaction media in photocatalytic

hydrogen production: Performance evaluation of M/TiO_2 photocatalysts (M = Pd, Pt, Au) in different alcohol-water mixtures, J. Catal., 2015, 329, 355-367.

26. K. L. McGilvray, M. R. Decan, D. S. Wang and J. C. Scaiano, Facile photochemical synthesis of unprotected aqueous gold nanoparticles, J. Am. Chem. Soc., 2006, 128, 15980-15981.

2.3 Postprint Version of Supporting Information

EXPERIMENTAL

Reagents

Unless otherwise specified, all chemicals were purchased from Sigma-Aldrich or Fisher Scientific and used without further purification. Titanium dioxide (TiO_2-P25) was a gift from Evonik Degussa.

INSTRUMENTATION

Transmission electron microscopy (TEM) images were collected on a JEM-2100F FETEM (JEOL) operating at 200 kV. X-ray photoelectron spectroscopy (XPS) was recorded using Kratos analytical model Axis Ultra DLD, using monochromatic aluminum Ka X-rays at 140 W. XPS data was analyzed using CasaXPS software, Version 2.3.15 and all fittings obtained using a Gaussian 30% Laurentian and a Shirley baseline. The proportion of Pd in the catalysts was determined by Inductively Coupled Plasma Emission Spectrometry (ICP-EOS), using an Agilent Vista Pro ICP Emission Spectrometer. Approximately 10 mg portions were accurately weighed in triplicate and digested with aqua regia. Solutions were further diluted and measured by ICP-ES. The Pd 340.458 emission line was used for quantification. Diffuse reflectance measurements were carried out in VARIAN Cary 100 UV-VIS Spectrophotometer coupled with an integrating sphere accessory. Microwave irradiation was performed using a Biotage Initiator Eight microwave reactor and Biotage microwave vials.

UV irradiation used for catalyst synthesis was performed in a Luzchem photoreactor equipped with UVA bulbs (typically operated with 14 bulbs, corresponding to ~75 W/m^2 with ~ 4% spectral contamination). Light-emitting diodes (LEDs) of 10 W

from LedEngin were used for the photocatalytic hydrogenation/isomerization in the UV (centered at 368 nm) and visible region (centered at 465 nm) working at 700 mA.

Hydrogen detection was carried out in a Perkin Elmer, Claurus Gas Chromatograph couple to Thermal Conductivity Detector (TCD) using Argon as a carrier gas. Quantification was carried out in a Perkin Elmer, Claurus Gas Chromatograph coupled to a Flame Ionization Detector (FID) and a DB-5 column (30 m length, 0.320 mm diameter, 0.25 μm film) using Helium as a carrier gas and *t*-Butyl benzene as external standard. GC-MS analyses were performed on an Agilent 6890-N Gas Chromatograph with an Agilent 5973 mass selective detector calibrated with acetophenone. All ^{1}H NMR spectra were recorded on a Bruker AVANCE 400 spectrometer expressing the chemical shifts in ppm relative to the H-signal of the internal tetramethylsilane (TMS) and using $SO_2(CH_3)_2$ as the external standard. ^{2}H NMR spectra were acquired on a Bruker AVANCE 300 spectrometer using the deuterated chloroform as external standard for calibration.

Catalyst preparation

Palladium nanoparticles supported on TiO_2 (Pd@TiO_2) were prepared by photodeposition of PdNP onto TiO_2 (P25). In brief, TiO_2 (500 mg) and $PdCl_2$ (22 mg, for 2% Pd@TiO_2, w/w%) were dispersed in 200 mL of Milli-Q water, sonicated for 15 minutes and irradiated in a Luzchem photoreactor equipped with 14 UVA bulbs for 8 hours with vigorous stirring. The brownish slurry was centrifuged and washed with Milli-Q water at least five times to remove unreacted $PdCl_2$ and dried in a desiccator overnight under vacuum. The resulting dark gray powder was characterized by TEM, XPS, ICP-EOS and DRS. The catalyst was kept under argon for assuring reliable activity. All reactions were performed with material at most 3 weeks old.

PdNP supported on crystal nanodiamonds (Pd@CND) were prepared by photodeposition of PdNPs onto Fenton treated CND. The Fenton reaction has been used to purify commercial CND by the selective mineralization of the soot.[1] In brief, 100 mg of treated CND and $PdCl_2$ (4 mg, for 2% Pd@CND, w/w%) were mixed in 40 mL of Milli-Q water and stirred for 10 minutes at room temperature. Next, 12 mg of the

benzoin Irgacure-2959^{TM} (I-2959) in 10 mL of EtOH 99% were added as a photo-initiator. The resulting mixture was irradiated for 1 hour in a Luzchem photoreactor equipped with 14 UVA bulbs. The gray slurry was cleaned using the same procedure explained above for Pd@TiO_2.

Sample preparation for isomerization of estragole

Thermal-induced isomerization under conventional heating: 20 mg of 2% Pd@TiO_2 (2.4 mol% Pd) were dispersed in 8 mL of *i*-propanol by sonication *ca.* for 5 min in a clean round bottom flask, then 25 µL (0.16 mmol) of reactant were added. The reaction mixture was heated up to 85 ºC (solvent boiling point) under air with continuous stirring for 24 hours. The progress of the reaction was monitored by GC-MS. The solid catalyst was separated either by filtration or by centrifugation and crude product was obtained after solvent evaporation. Quantification was done either by ^{1}H-NMR or by GC-FID.

Control experiments were carried out using estragole as starting material. The same procedure was followed to run the reaction under air, in the presence and in the absence of pure TiO_2 (P25).

Thermal-induced isomerization using Microwave irradiation: 15 mg of 2% Pd@TiO_2 (1.8 mol% Pd) were dispersed in 4 mL of methanol in a clean MW tube, then 20 µL (0.14 mmol) of reactant were added. The reaction mixture was purged with argon for 15 min then submitted to 4 h MW irradiation at 55 ºC and maximum pressure set up to 20 bars. Quantification was performed by GC-FID.

Light-induced isomerization or hydrogenation: 15 mg of 2% Pd@TiO_2 (1.8 mol% Pd) were dispersed in 4 mL of methanol in a clean cuvette, then 20 µL (0.14 mmol) of reactant were added. The reaction mixture was purged with argon for 15 min then irradiated with 368 nm LED for 4 hours for the photocatalytic hydrogenation. As for the photocatalytic isomerization, the reaction mixture was irradiated with 465 nm LED with continuous stirring for 24 hours at room temperature. The progress of the reaction was monitored by GC-MS. The solid catalyst was separated either by filtration or by centrifugation and crude product was obtained after solvent evaporation.

Quantification was done either by ^{1}H-NMR or by GC-FID. Control experiments were carried out as mentioned above.

Table S2.1 shows the different catalyst concentration evaluated after 4 h of isomerization or hydrogenation reaction. Notice that hydrogenation reaction strongly depends on the light irradiance, as some isomerization products might be expected by lowering the light intensity. These side products could be fully hydrogenated by simply increasing either the intensity of the light or the exposure time.

Catalyst Recyclability

Pd@TiO_2 catalyst was tested for potential reusability in the direct, selective and non-hydrogen mediated isomerization of estragole for both thermal and light-induced catalysis using the conditions explain above within at least three reusability cycles. The reaction was scaled up to facilitate catalyst recovery and reuse. The samples were placed in a 15 mL centrifuge tube, and centrifuged at 2500 rpm for 10 min to recover, wash and reuse the catalyst.

Catalyst Recovery

The catalyst used was recovered from the reaction mixture and then treated by one of the three following procedures:

1) Heat treatment in *i*-propanol: The recovered catalyst was suspended in 8 mL of 99% i-propanol in a clean round bottom flask. The mixture was heated up to 78 ºC (solvent boiling point) under air with continuous stirring overnight. Primary alcohol was used due to its ability to be decomposed via decarbonylation on Pd and PdO surfaces[2] releasing CO, a good reducing agent for PdO.[3] The resulting material was separated as mentioned above.

2) H_2 treatment: the catalyst was re-suspended in 8 mL of i-propanol in a clean round bottom flask. The resulting mixture was purged with H_2 at room temperature for one hour with stirring. The resulting gray slurry was treated as mentioned above.

3) Photochemical treatment: the catalyst was re-suspended in 10 mL of Milli-Q water, then 10 mL of EtOH 99% and 20 mg of benzoin Irgacure-2959^{TM} (I-2959) as a photo-initiator were added. The resulting mixture was irradiated for 5 hours with UVA at room temperature with vigorous stirring. The gray slurry was centrifuged and washed with Milli-Q water at least four times then dried in the desiccator overnight under vacuum.

Apparent quantum yield (AQY)

The AQY (Φ_{ap}) was calculated using equation (1)

$$\Phi_{ap} = \frac{\text{moles consumed (or produced)/time(s)}}{\text{moles of incident photons/time(s)}} \qquad (1)$$

The amount of incident photons was determined by using $Ru(bpy)_3Cl_2$ (QY = 0.019) as actinometer.[4] Thus, the well-known singlet oxygen chemistry employing the oxidation of 1,9-diphenylanthracene (DPA) to its corresponding endoperoxide was followed by UV-Vis spectroscopy. Briefly, the absorption spectra of a typical actinometry experiment was performed with $Ru(bpy)_3Cl_2$ (0.1635 mM) and DPA (0.10 mM) in acetonitrile and irradiated with a 465 nm LED for 10 second .

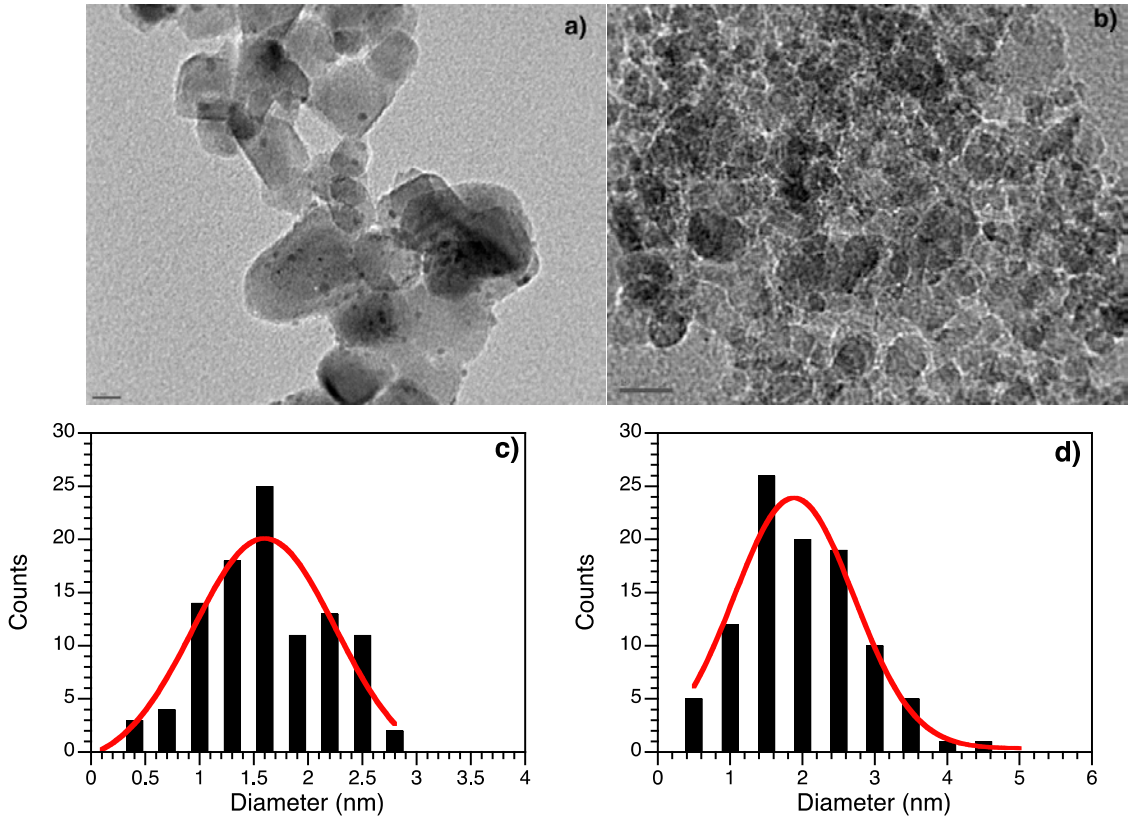

Figure S2.1. TEM image of Pd nanoparticles synthesized over a) TiO_2 and b) CND (scale bar 10 nm). Particle distribution of c) Pd@TiO_2, average diameter: (1.6 ± 0.9) nm; and d) Pd@CND, average diameter: (2 ± 1) nm.

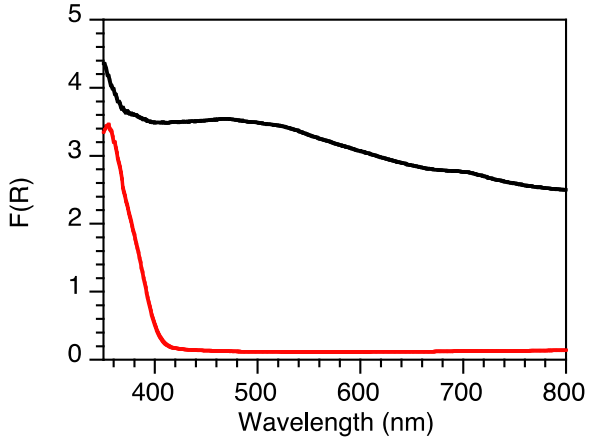

Figure S2.2. Diffuse reflectance spectra of pristine TiO_2 (red) and Pd@TiO_2 (black).

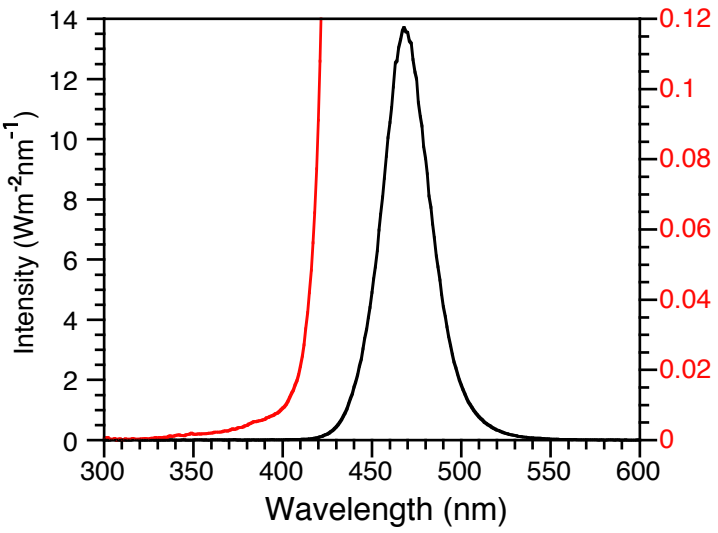

Figure S2.3. Emission spectrum of 465 nm LED. Zoom in the UV region (red) shows 0.12 % of UV contamination below 400 nm.

Table S2.1. Isomerization and hydrogenation yields obtained at different catalyst concentrations.

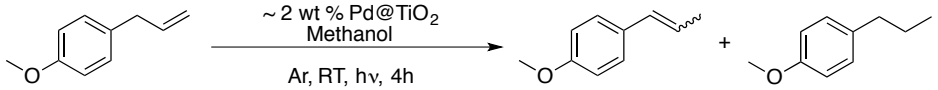

Estragol — Anethole (A) — Dihydroanethole (DA)

Entry	Catalyst (mg)	hν (nm)	% Conv	% A	% DA
i	5	465[a]	0	0	ND
ii	10	465[a]	21	21	ND
iii	15	465[a]	45	45	ND
iv	5	368[b]	44	23	21
v	10	368[b]	63	32	30
vi	15	368[b]	100	71	29
vii	15	368 [b, c]	100	100	0

[a]10,035 mWm^{-2}. [b] 3,831 mWm^{-2}. [c] 7 h

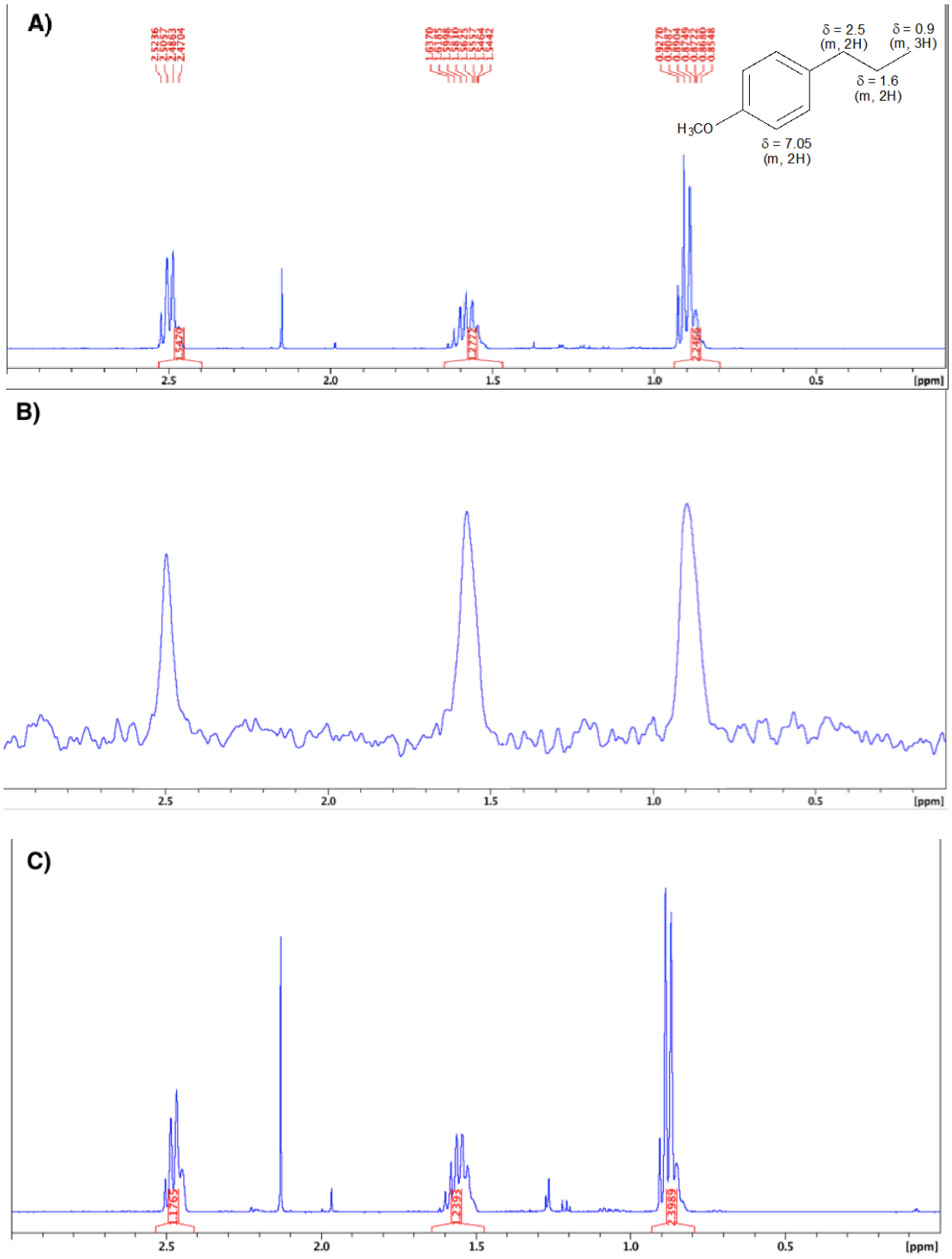

Figure S2.4. Aliphatic region of NMR spectra after hydrogenation under 368 nm irradiation for 4h of: Estragole (A) ^{1}H NMR (400 MHz, CD_3OD), (B) ^{2}H NMR (300 MHz, CD_3OD), and Anethole (C) ^{1}H NMR (400 MHz, CD_3OD). Integrations in the ^{1}H NMR spectra were calibrated to the aromatic signal at 7.05 ppm, 2H.

Additional deuterium incorporation experiments

Multiple-deuterium incorporation is favoured whether the reaction mixture is subjected to heat or visible irradiation for 24 h prior UV light irradiation. Thereby, isomerization run under reflux (ca. 39 % conversion) and followed by full reduction upon UV light irradiation would rise to multiple-deuterium incorporation as shown in Table 2.1. Integration analysis of the ^{1}H NMR spectrum shows 1.24 D, 0.75 D and 0.56 D deuterium incorporation in positions a, b and c, respectively (Figure S2.5 A and B). Surprisingly, pre-isomerization under 465 nm irradiation (*ca.* 55 % conversion) dramatically increases the deuterium incorporation showing 2.09 D, 1.34 D and 1.18 D in positions a, b and c, respectively (Figure S2.5 C and D). This method has shown the best conditions for multiple deuterium incorporation. The results suggest that pre-activation of the surface, as found with the thermal-treatment, is more important under light. The multiple deuterium incorporation suggests both pre-treatments, thermally and light-induced, can also activate the palladium surface promoting deuteration.

Table S2.2. Pd@TiO_2 catalyzed hydrogenation/deuteration of estragole or *t*-anethole

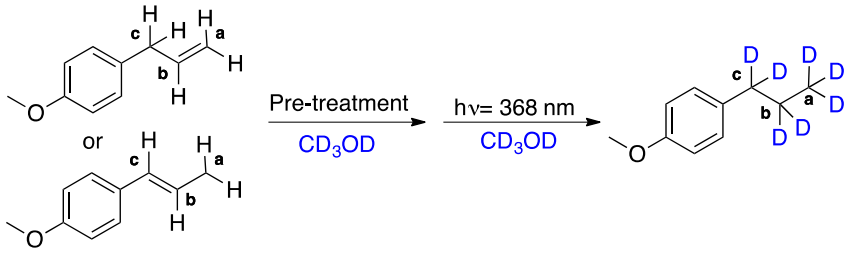

Entry	Reactant	Pre-treatment	D content (H integral loss*) a	b	c
i	Estragole	--	0.75	0.72	0.56
ii	Estragole	Thermal isomerization	1.24	0.75	0.56
iii	Estragole	Photo isomerization (465 nm)	2.09	1.34	1.18
iv	*t*-Anethole	--	0.60	0.76	0.82

*Number of D at the labeled position.

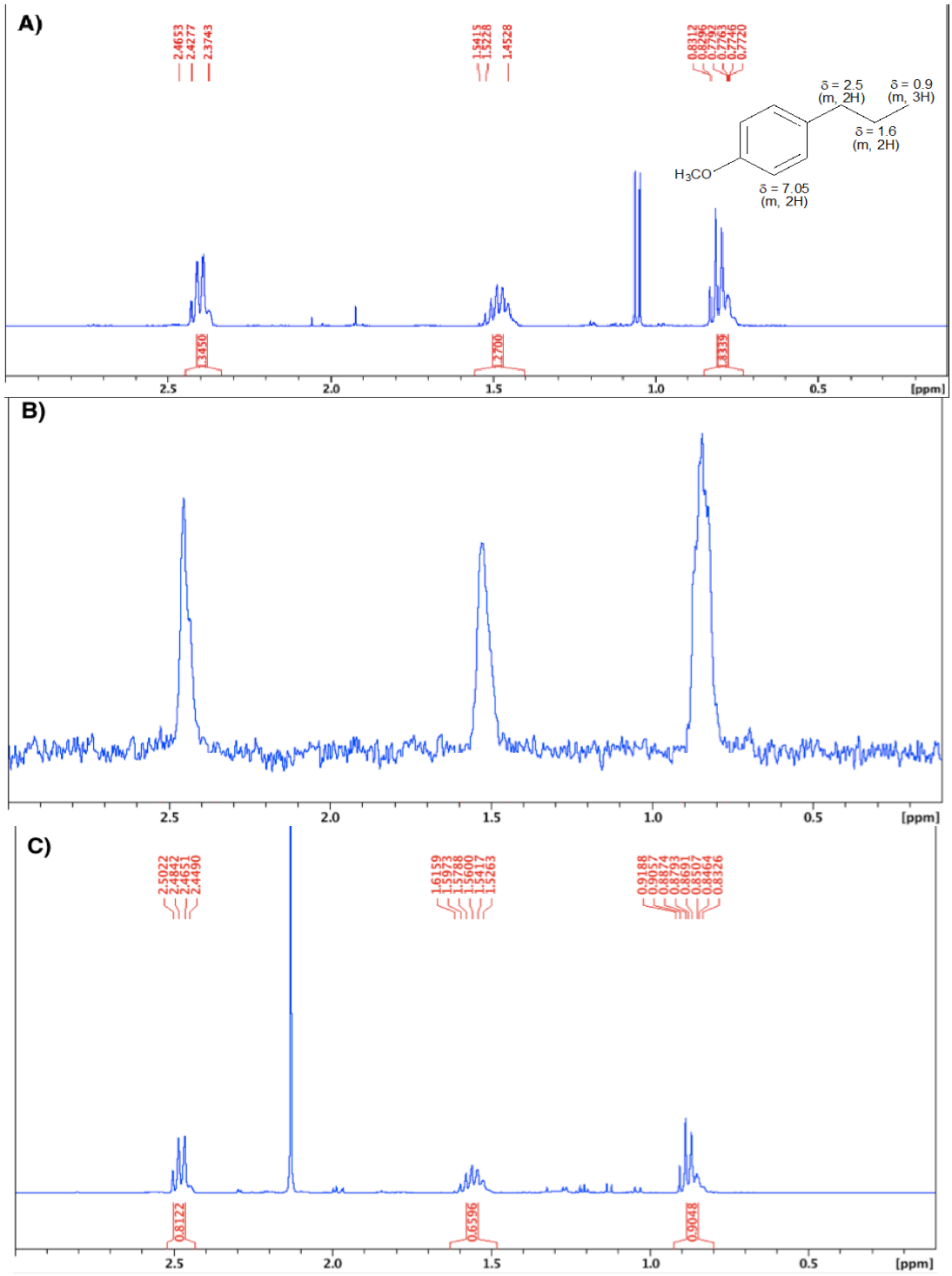

Figure S2.5. Aliphatic region of NMR spectra for the hydrogenation of estragol under 368 nm irradiation for 4h. Pre-heating treatment for 24 h (A) ^{1}H NMR (400 MHz, CD_3OD), and (B) ^{2}H NMR (300 MHz, CD_3OD). Pre-irradiation treatment at 465 nm for 24 h (C) ^{1}H NMR (400 MHz, CD_3OD). Integrations in the ^{1}H NMR spectra were calibrated to the aromatic signal at 7.05 ppm, 2H.

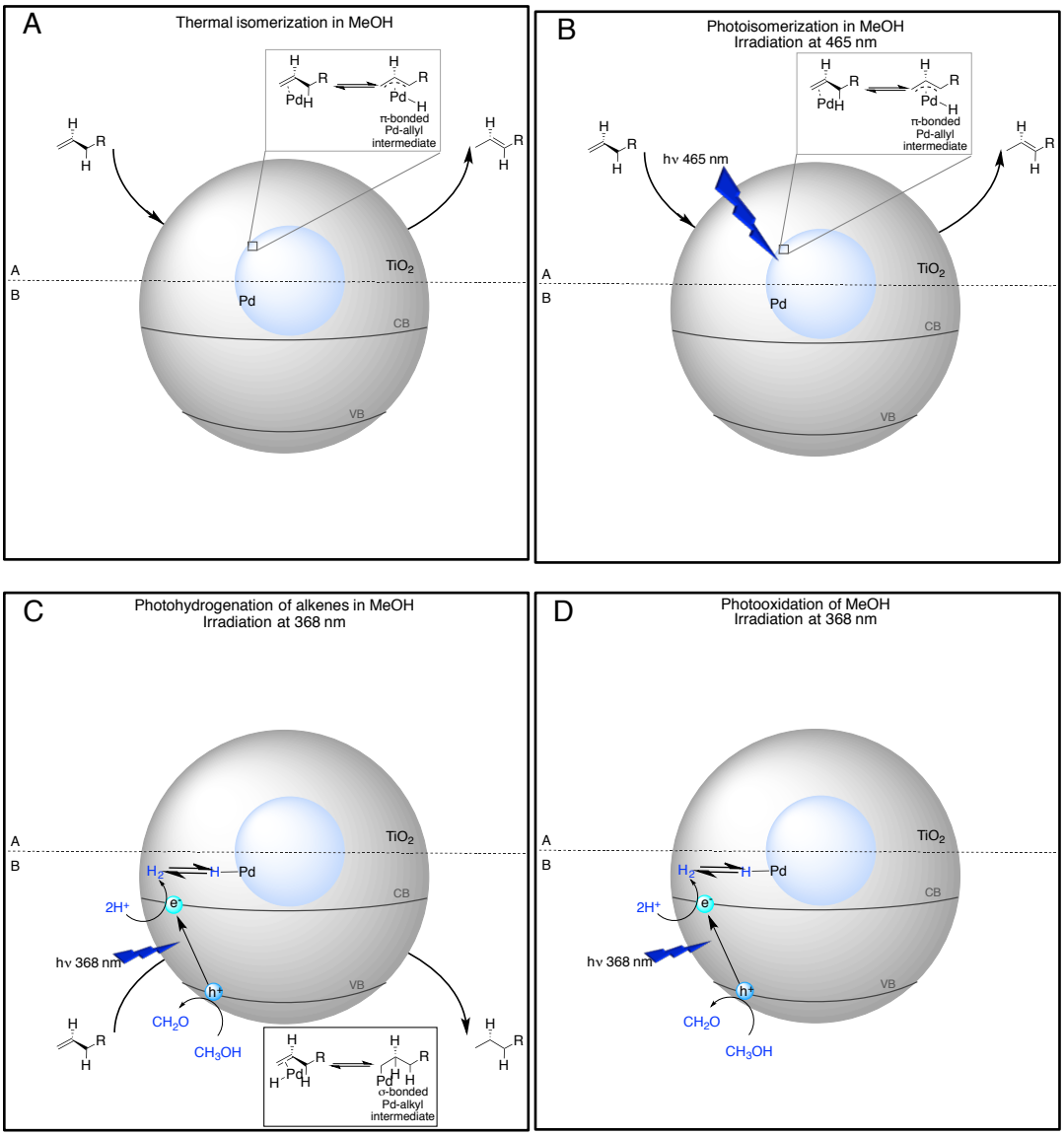

Scheme S2.1. A subset of the 4 situations summarized in Scheme 2.4 in the main text: A corresponds to thermal isomerization under air, B to photoisomerization at 465 nm under argon, C to the 365 nm photohydrogenation of alkenes and D to the generation of hydrogen from methanol in the absence of alkene.

$$CH_3OH + h\nu \longrightarrow CH_2{=}O + 2\,H^+ + 2\,e^- (H_2)$$

Scheme S2.2. Photoxidation of Methanol upon UV light excitation of TiO_2[5]

Table S2.3. Catalyst reusability test upon thermal conditions under air

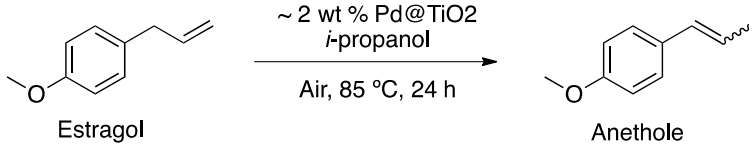

Catalytic cycle	% Conversion	% Yield trans	% Yield cis	% Selectivity
1	100	93	7	93
2	63	58	5	92
3	ND	ND	ND	---
Recovered[a]	85	75	10	88

% Yields and conversions were calculated by GC-FID using *t*-butylbenzene as external standard. [a]I-2959 treatment.

Table S2.4. Catalyst reusability test upon visible light irradiation under argon

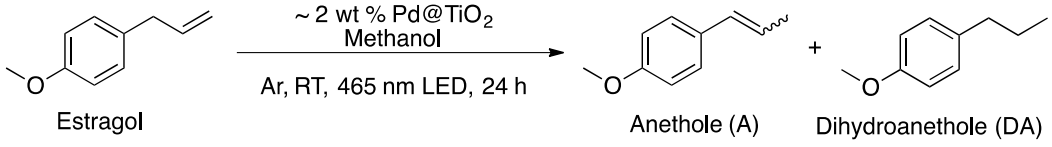

Catalytic cycle	% Conversion	% DA Yield	% A Yield trans	% A Yield cis	% Selectivity
1	100	7	80	13	86
2	100	6	80	14	85
3	100	11	79	10	89
4	100	12	79	9	90

% Yields and conversions were calculated by GC-FID using t-butylbenzene as external standard.

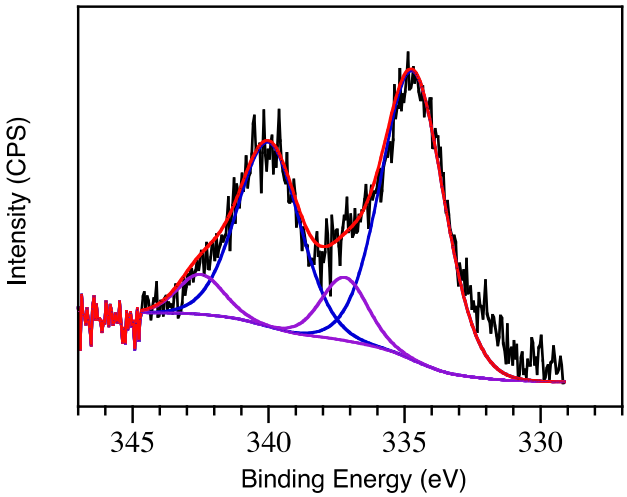

Figure S2.6. Deconvoluted Pd 3d HR-XPS spectra for Pd@TiO_2 catalyst. The curve fitting of the Pd 3d core-level spectrum is performed by using two spin-orbit split Pd $3d_{5/2}$ and Pd $3d_{3/2}$ components, separated by ~5.2 eV.

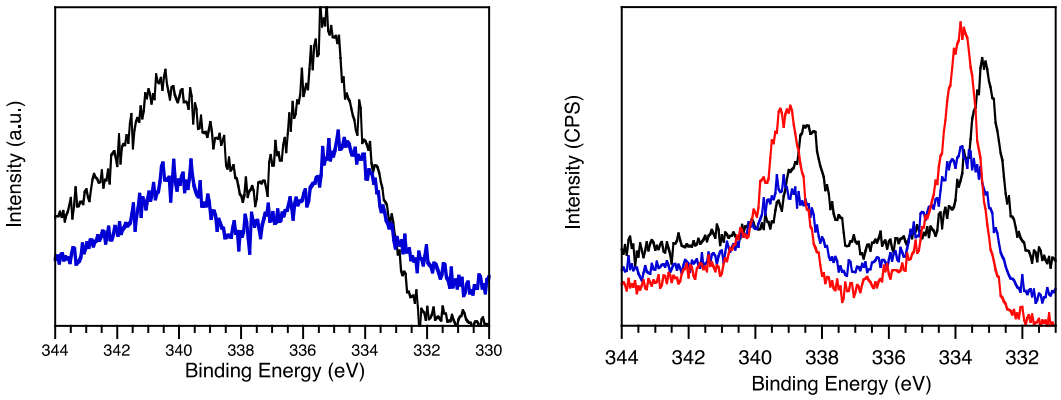

Figure S2.7. Pd 3d HR-XPS spectra for Pd@TiO_2 catalyst Left: fresh (blue) and two month old (black). Right: Catalyst treated by H_2 (black), heat (blue) and I-2959 (red). Shift of Pd 3d peaks to lower binding energies correspond to the formation of more Pd reduced species.

REFERENCES

1. R. Martín, P. C. Heydorn, M. Alvaro and H. Garcia, General Strategy for High-Density Covalent Functionalization of Diamond Nanoparticles Using Fenton Chemistry, Chem. Mater., 2009, 21, 4505-4514.
2. J. L. Davis and M. A. Barteau, The Influence of Oxygen on the Selectivity of Alcohol Conversion on the Pd(111) Surface, Surf. Sci., 1988, 197, 123-152.
3. V. A. Bondzie, P. H. Kleban and D. J. Dwyer, Kinetics of PdO formation and CO reduction on Pd(110), Surf. Sci., 2000, 465, 266-276; K. Shimizu, Y. Kamiya, K. Osaki, H. Yoshida and A. Satsuma, The average Pd oxidation state in Pd/SiO_2 quantified by L-3-edge XANES analysis and its effects on catalytic activity for CO oxidation, Catal. Sci. Technol., 2012, 2, 767-772.
4. S. P. Pitre, C. D. McTiernan, W. Vine, R. DiPucchio, M. Grenier and J. C. Scaiano, Visible-Light Actinometry and Intermittent Illumination as Convenient Tools to Study $Ru(bpy)_3Cl_2$ Mediated Photoredox Transformations, Sci. Rep., 2015, 5, 16397.
5. J. Schneider, M. Matsuoka, M. Takeuchi, J. L. Zhang, Y. Horiuchi, M. Anpo and D. W. Bahnemann, Understanding TiO_2 Photocatalysis: Mechanisms and Materials, Chem. Rev., 2014, 114, 9919-9986.

This manuscript has been adapted from ACS Cata. **2017**, 7, 1, 250-255 with permission, from the American Chemical Society. Small changes to the original manuscript provide consistent formatting and clarity with respect to the overall thesis.

2.4 Accompaniment to Chapter 2

This article, beyond being my first peer-reviewed publication as primary contributing author, describes my first independently led research project as a graduate student. In addition to achieving our goal of exploring the tuneable photocatalytic activity of palladium decorated TiO_2 for valuable target molecules by selecting the proper wavelength irradiation, another valuable outcome of this project was that it required training on various laboratory instruments, photochemical approaches and in material synthesis and characterization.

Visible light irradiation significantly enhances the intrinsic catalytic performance of non-plasmonic transition metals nanoparticles such as Pd nanopartciles (PdNP) by exciting the interband electrons. Upon light excitation, the conduction electrons of the PdNP gain the energy of the incident light. These hot electrons are available at the palladium surface sites, thus enhancing the ability of Pd sites to adsorb and activate reactant molecules. Furthermore, these light excited electrons facilitate the photocatalytic organic reactions of the adsorbed molecules at ambient or moderate temperatures. The diffuse reflectance of the catalyst, Pd@TiO_2, show broad absorption in the visible region, which means any selection of wavelength in the visible spectrum (between 400-700 nm) could excite the PdNP, and thus afford the desired product. The use of blue light (centered at 465 nm) was selected to excite Pd@TiO_2 due to its highest energy, and the results published are discussed in the following chapters (Chapter 3 and 4).

3. Light-Induced Sonogashira C−C Coupling under Mild Conditions Using Supported Palladium Nanoparticles

3.1 Preamble to Chapter 3

The following chapter describes the application of Pd@TiO_2 in heterogeneous catalysis for cross coupling C-C bond formation, namely Sonogashira reaction. Here we show that direct excitation of PdNPs can selectively catalyze the C-C coupling between aryl iodides and terminal alkynes under very mild conditions in a short reaction time. The original motivation for this line of research was to expand the scope of the catalytic application of supported PdNP in organic synthesis under visible light irradiation. Many organics transformations, like C-C coupling, carried out over homogeneous Pd catalysts require high temperature to achieve high yields. Although homogenous catalysts have shown good catalytic activity, they have several drawbacks such as difficult post-reaction separation, air and water sensitivity, and non-reusability. In this respect, the use of supported PdNPs has been explored in the last few years because of their potential to replace Pd complexes as catalysts. Our own interests have centered on photo-induced reactions, trying to use very mild conditions that avoid potential reagent or product decomposition and help retain the integrity of the catalysts themselves.

An emerging field in catalysis, the PdNPs can successfully be supported on a wide range of material, namely titanium dioxide (TiO_2), carbon nanodiamond (CND) or niobium oxide (Nb_2O_5), and demonstrates great photocatalytic efficiency toward the desired product under ligand-free environment. Study of the action spectrum shows that direct excitation of PdNP is required to yield the desired product, while the excitation of the support is ineffective for Sonogashira coupling.

3.2 Postprint Version of Manuscript

First published in: ACS Sustainable Chem. Eng. **2018**, 6, 1717−1722.

ABSTRACT

The Sonogashira reaction can easily be photocatalyzed by supported palladium nanoparticles. Herein, we demonstrate that the direct excitation of the PdNPs can catalyze the C-C coupling between different aryl iodides and acetylenes under very mild conditions in short reaction times. The catalyst is air- and moisture-tolerant and can be supported in a wide range of materials, including inert ones such as nanodiamonds. Study of the action spectrum demonstrates that direct excitation of the PdNPs is required, and in the case of Pd@TiO_2, for example, visible excitation works well whereas UVA (368 nm) is ineffective due to TiO_2 shielding of the Pd absorption. The catalyst can be reused a couple of times, but when it loses activity it can be readily reactivated via a simple reductive photochemical strategy.

INTRODUCTION

C-C coupling reactions are among the most important strategies in synthetic organic chemistry. The idea of constructing complex molecular architectures from suitable tailored building blocks has been explored for decades. Palladium (Pd) catalyzed cross-coupling reactions comprise one of the most efficient methods for the construction of C-C, C-N and C-O bonds.[1, 2] These cross-coupling methodologies have revolutionized synthetic organic chemistry, having found widespread use in organic synthesis and material science, and playing an important role in pharmaceutical, agrochemical and fine chemical industries.[3] Metal-catalyzed Sonogashira coupling reactions lead to the formation of new C-C bonds and they are now the most important method for preparing aryl alkynes and conjugated enynes, which are key precursors in the synthesis of natural products, pharmaceuticals, and organic molecular materials.[4] Pd complexes constitute the most commonly used catalysts; however, opinion remains divided with regard to the identity of the catalytically active species, specifically whether they are the soluble metal complexes introduced or the surfaces of metallic

shown outstanding activity,[6] homogeneous catalysts have several drawbacks such as post reaction separation of the product from the catalyst, non-reusability, air and water sensitivity.[7] The search for heterogeneous, reusable and efficient catalysts to replace the homogeneous ones promises practical solutions to many problems in catalysis. Gonzalez-Arellano et al. reported the use of a gold-ceria nanomaterial as a heterogeneous catalyst for this reaction, where Au(I) seems to be the catalytically active species, although Au(0) and Au(III) were the predominant components of the solid catalyst.[8] Sagadevan et al. reported the use of CuCl for photo-induced Sonogashira C-C coupling at room temperature.[9] However, the use of Cu halides is sensitive to air leading to formation of homo-coupling products (Glaser coupling)[10]. Additionally, the deficiency as well as the excess of copper intake raises some environmental and health concerns.[11] Therefore, remarkable efforts have been dedicated to develop Sonogashira cross-coupling procedures in the absence of copper additives, so-called copper-free Sonogashira coupling.[2, 12]

In this respect, the use of supported palladium nanoparticles (PdNPs) has been explored in the past few years because of their potential to replace Pd complexes as catalysts.[13] We recently showed that Pd-based nanomaterials can be used as heterogeneous catalysts for alkene isomerization/hydrogenation reactions.[14] A Pd-on-silica catalyst has been shown to catalyse the Sonogashira coupling under reflux (for example ethanol, but not methanol) or under microwave heating at temperatures up to 150°C.[15]

Our own interests have centered on photoinitiated reactions, trying to use very mild conditions that avoid potential reagent or product decomposition and help retain the integrity of the catalysts themselves. Further, with a view at potential imaging applications, the ability of light to provide temporal and spatial control is a very desirable feature. Today's advanced and inexpensive light-emitting diode (LED) technologies allow reactions to be initiated under very mild conditions and with at least 10 times less power consumption that typical laboratory microwave ovens. Further, knowledge of the absorption spectra of reagents and products allows the selection of

narrowband LED illuminators at benign wavelengths that prevent the photodegradation of organics.

Here we demonstrate the use of supported PdNPs on different materials that can successfully catalyze Sonogashira C-C couplings under visible light irradiation at room temperature. The successful use of different materials as catalyst supports, namely titanium dioxide (TiO_2), carbon nanodiamond (CND) or niobium oxide (Nb_2O_5), demonstrates the versatility of the photocatalytic activity of PdNP to work in ligand-free environments, an emerging field in catalysis. To the best of our knowledge, this is the first time that PdNP-decorated TiO_2 (Pd@TiO_2), CND (Pd@CND) or Nb_2O_5 (Pd@Nb_2O_5) have been used as catalysts for the Sonogashira C-C couplings of different phenylacetylene and aryl iodides (Scheme 3.1), although we note the catalyst also works under thermal conditions. Both sets of conditions selectively lead to the cross-coupling product without incorporation of ligands.

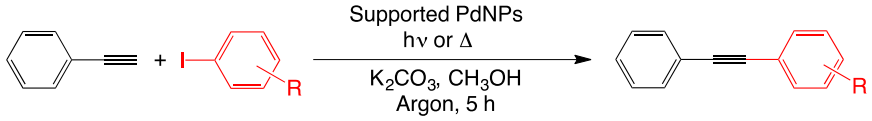

Scheme 3.1. Sonogashira C-C coupling catalyzed by supported PdNPs under mild conditions.

The selection of TiO_2 as a support is known to affect tandem reactions in which the change of the irradiation source can give different outcomes.[14] Therefore, we also examined the action spectrum to determine which spectral region drives the photocatalytic reaction. This photochemical mechanistic tool demonstrates that, in this system, the catalytic process is centered exclusively on the Pd nanoparticles and that the support is essentially inactive, except in the case of Nb_2O_5 where abundant acid sites may cause a small rate reduction.

RESULTS AND DISCUSSION

The use of PdNP-decorated materials (TiO_2, CND and Nb_2O_5) was explored for the selective cross-coupling of iodobenzene and phenylacetelyne under both reflux and visible light irradiation. The Sonogashira reaction was investigated under conventional heating (thermal conditions) using methanol as solvent under air or Ar atmosphere. The results summarized in Table 3.1 show that both Pd and heating are needed for the

reaction to proceed (entries i-iv). Although previous report suggest that higher temperatures are needed,[15] here we show that methanol boiling point (65 ºC) is sufficient for the reaction to proceed. The efficiency of the catalyst with different supports changes slightly, with TiO_2 as the most promising one. Although the reaction works best under argon, it is reasonably air-tolerant.

Table 3.1. Different experimental conditions tested for the thermal-induced Sonogashira C-C coupling using Pd-decorated materials.

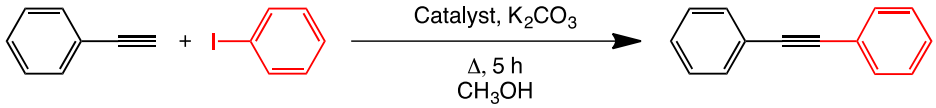

	Catalyst	Conditions	% Conversion	% Yield[a]
i	none	65 ºC, Ar	0	ND
ii	TiO_2	65 ºC, Air	0	ND
iii	Pd@TiO_2	RT, Ar	0 (57)	0[b] (50)
iv	Pd@TiO_2	65 ºC, Air	66	47[c]
v	Pd@TiO_2	65 ºC, Ar	>99	82[c]
vi	Pd@CND	65 ºC, Air	71	35[c]
vii	Pd@Nb_2O_5	65 ºC, Air	75	24[c]

Reactions conditions: 1 eq. of Iodobenzene, 1.3 eq. of Phenylacetylene, 2 eq. of K_2CO_3, 4 mL methanol, 15 mg catalyst. [a]Yields were determined by GC-FID using *t*-butylbenzene as an external standard. [b]Under dark conditions, values between brackets were run at 42 ºC. [c]Traces of alkyne homo-coupling were found.

The Sonogashira coupling was also evaluated under different conditions upon visible light irradiation (465 nm LED), as summarized in Table 3.2. Thus, the photocatalytic reaction only proceeds when Pd-decorated materials are irradiated with visible light (465 nm LED). Further, the reaction is dependent on the presence of PdNP to selectively favour the C-C sp-sp^2 heterocoupling (Table 3.2, entries i-v). The role of the base was also evaluated, and the best conditions were found when the aryl iodide and the phenylacetylene were mixed together with Pd@TiO_2 catalyst (Pd-loading ~1.3 wt%) with 2 equiv of K_2CO_3 using methanol as solvent and irradiated for 5 h under argon atmosphere (Table 3.2, entry v-ix and Figure S3.1). It is known that K_2CO_3 in MeOH can generate a stronger base, methoxide,[16] and this might explain why other bases such as TEA (Table 3.2, entry iv) cannot perform as well. When the catalyst

support was changed to a known inert and rather transparent material such as crystal nanodiamonds (CND, Pd-loading ~1.7 wt% by ICP-OES), the yield of the reaction remained the same (cf. entries v and x, Table 3.2). The use of niobium oxide as a support considerably drops the yield of the reaction (Table 3.2, entry xi), presumably due to interaction of the base with the acid sites on the surface of the support.[17] Accordingly, the material has slightly low Pd-loading (0.7 wt% by ICP-OES) comparing with TiO_2 or CND, although all materials were prepared under the same conditions. In addition, TEM images show that the particle size (~ 3 nm) was slightly larger than those found in the other two supports (Figure S3.3). Interestingly, the photoinitiated cross-coupling reaction also showed air tolerance, although more time was needed to achieve complete conversion (Table 3.2, entry ix). Additional experiments run in different solvents (Table S3.2) show the reaction is highly favoured in polar protic solvents (e.g. methanol), possibly due to the K_2CO_3 solubility,[16] although small conversion and lower selectivity were found using non-protic polar solvents (i.e. THF, ACN). The reaction is also moisture tolerant (Table 3.2, entry viii). The intensity of the irradiation also affects the product yield (Table 3.2, entry vi) suggesting a photochemical process involved in the reaction (vide infra). The optimum amount of catalyst was determined ~1.5 mol% as shown in Figure S3.2. In comparison to the performance of thermally induced reactions, the better performance of photoexcited Pd@CND is clear (*cf.* Table 3.1 entry vi and Table 3.2 entry x). In the case of $Pd@TiO_2$, the rates of the thermally and photoinduced reactions were determined to compare their relative efficiencies. For this, the reaction was performed in dark conditions at 42°C (the same temperature as reached under light illumination) and under illumination (conditions in entry v, Table 3.2), and the rates of the reaction were about 4.7 mM/h and 7.5 mM/h, respectively. Finally, other metal nanoparticles (Cu, Au) were tested under the same reaction conditions using 465 nm LED and 532 nm LED as irradiation sources respectively (Table 3.2, entries xii-xv). The Cu-based catalyst resulted in the formation of the alkyne homocoupling product[10] and only moderate yields of the desired product. Decomposition of the catalyst within the time of reaction was also detected in the case of copper. Although there are reports on the excellent performance of AuNPs towards Sonogashira couplings,[8, 18] commercial

Au@TiO_2 was found to lead to negligible conversion under the very mild conditions used in our system.

Table 3.2. Different experimental conditions tested for the light-induced Sonogashira C-C coupling using Pd-decorated materials.

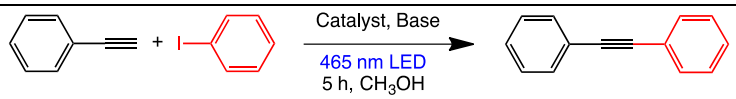

	Catalyst	Base	Atm	% Conversion	% Yield[a]
i	none	K_2CO_3	Ar	0	ND
ii	TiO_2	K_2CO_3	Ar	0	ND
iii	Pd@TiO_2	none	Ar	0	ND
iv	Pd@TiO_2	TEA	Ar	38 (53)	30 (40)
v	Pd@TiO_2	K_2CO_3	Ar	>99	80-86
vi[b]	Pd@TiO_2	K_2CO_3	Ar	70	34
vii[c]	Pd@TiO_2	K_2CO_3	Ar	37	35
viii[d]	Pd@TiO_2	K_2CO_3	Ar	100	68
ix	Pd@TiO_2	K_2CO_3	Air	54(>99)	52 (80)
x	Pd@CND	K_2CO_3	Ar	>99	78
xi	Pd@Nb_2O_5	K_2CO_3	Ar	53	36
xii	Cu@TiO_2	K_2CO_3	Air	>99	38[e]
xiii	Cu@TiO_2	K_2CO_3	Ar	>99	30[e]
xiv	Au@TiO_2	K_2CO_3	Air	0	ND[f]
xv	Au@TiO_2	K_2CO_3	Ar	0	ND[f]

Values between brackets correspond to 24 h of reaction. Reactions conditions: 1 eq. of Iodobenzene, 1.3 eq. of Phenylacetylene, 2 eq. of base, 4 mL methanol, 15 mg catalyst. Irradiation: 465 nm LED set at 1 W/cm^2. [a]Yields were determined by GC-FID using *t*-butylbenzene as an external standard. [b]Irradiation at 0.2 W/cm^2. [c]1 eq. of K_2CO_3. [d]Solvent= 9:1 CH_3OH:H_2O. [e]Alkyne homo-coupling was found as the major product, catalyst decomposition was also detected. [f]Irradiation source: four 532 nm LEDs each of them working at 0.56 Wcm^{-2} . No conversion detected under conventional heating conditions.

It is important to highlight that homocoupling products from the aryl iodide reagents were not detected under the conditions studied. Indeed, no coupling products were detected if only one of the reagents is subjected to the reaction conditions (Table S3.3), which further confirms the selectivity of this catalyst towards cross-coupling reaction. Additionally, the alkyne product shows strong stability under the reaction conditions, despite the well-known reductive properties of the catalyst under light.[14, 19]

Interestingly, phenylacetylene can undergo deuterium incorporation under these conditions when the reaction is run in deuterated methanol. This clearly indicates that the H-Pd surface interaction is strong enough to deprotonate the alkyne and form the corresponding carbanion, a strong base able to act as a nucleophile, or in the absence of substrate, to trap the deuterium (D)[20] (Scheme 3.2).

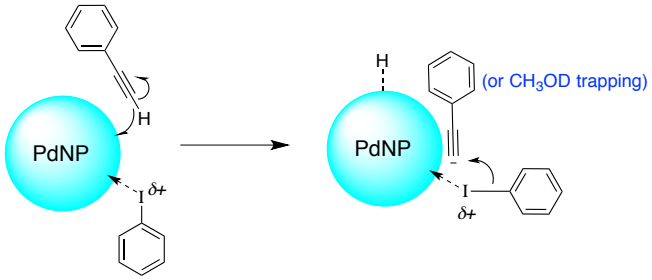

Scheme 3.2. Proposed mechanism for Sonogashira coupling or phenylacetylene deuteration in the absence of aryl iodides and in the presence of CD_3OD.

To investigate further the photocatalytic activity of this material, the action spectrum of the Pd@TiO_2 photocatalyst was measured. This technique is widely used in photobiology and was recently introduced by us in an example of heterogeneous photocatalysis.[21] An action spectrum can be described as a plot of the apparent quantum yield (AQY) of the reaction versus the wavelength of the incident photons when the same number of einsteins of energy is delivered to the sample.[21] An action spectrum can help differentiate if the photoreaction is simply the consequence of a lowering of the semiconductor band gap or due to the absorption band of Pd@TiO_2 that extends to longer wavelengths (ca. 740 nm in this case). Thus, if the mechanism involves direct Pd excitation (sometimes referred to as direct photocatalysis),[21] the action spectrum will simply resemble the absorption profile of the photocatalyst. Then, the action spectrum can be obtained by plotting the AQY (ν_0/ϕ) versus the wavelength of incident photons (see calculations in SI). As can be seen in Figure 3.1, the catalytic performance in the visible region overlaps with the diffuse reflectance spectrum of the Pd@TiO_2 catalyst, suggesting the light-induced Sonogashira coupling involves the direct excitation of PdNPs. Additionally, the dependence on the irradiation intensity was evaluated by using a 465 nm LED (Table S3.4). As expected, we found that the rate of the cross-coupling

reaction is proportional to the light intensity (Figure S3.10). This is in agreement with reported photocatalytic mechanism of nonplasmonic metallic nanoparticles, where the intensity and the light wavelength can interfere with the photothermal product yields.[22] Interestingly, the photonic efficiency of the reaction suddenly drops to zero when irradiation below 400 nm is used. This can be readily rationalized by the fact that the light absorption efficiency of TiO_2 increases below 400 nm effectively, shielding the PdNP from light absorption and therefore the generated local heat is not localized at the Pd centers. However, when Pd@CND was used similar catalytic efficiencies were found using both UV light or blue light (Table 3.3). This further confirms the idea of TiO_2 role as a simple support that can be easily replaced by inert materials such as CND.

Table 3.3. Comparison of the use of CND and TiO_2 as supports and their catalytic performance upon excitation using different irradiation wavelengths.

	Catalyst	λ (nm)	% Conversion	% Yield
i	Pd@CND	465	100	78
ii	Pd@CND	368	100	80
iii	Pd@TiO_2	465	100	82
iv	Pd@TiO_2	368	100	18*

Conditions: 4 h irradiation at 1 Wcm^{-2}. *Mixture of by-products includes around 35 % of stilbene.

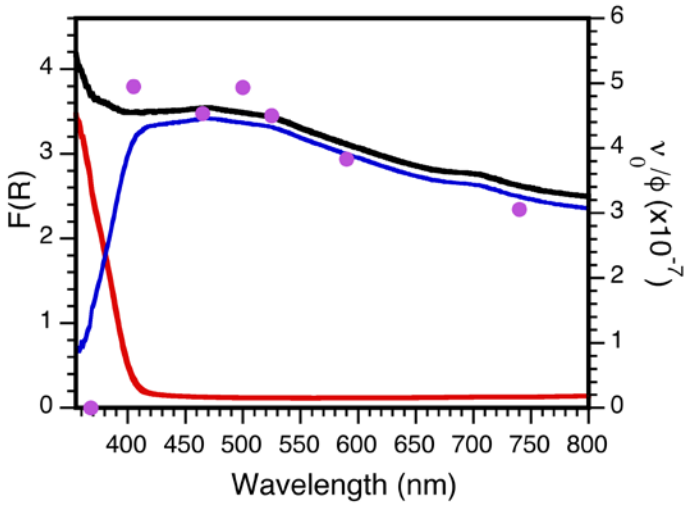

Figure 3.1. Comparison of the acquired action spectrum (pink dots) and the diffuse reflectance spectra of the TiO_2 (red), the Pd@TiO_2 (black), and the difference spectrum (blue). Conditions: 2 hours of irradiation, irradiance of 0.19 W cm^{-2} (See SI). Notice that the action spectrum was performed under different irradiance conditions comparing to the reaction studied in table 3.2, and therefore, it does not correspond to the AQY of the reaction (*vide infra*).

The scope of the catalytic activity was explored with a diverse group of aryl iodides and alkynes, as shown in Table 3.4. Notice that for *para*-substituted aryl iodides, both electron withdrawing- and electron-donating groups show excellent yields (AQY ~0.14 %). As expected, the ortho-substituted analogues exhibit lower yields in the same reaction time (AQY ~0.06 %). The reaction can be also used with an aliphatic alkyne (5-chloro-1-pentyne) affording a >99 % yield of the cross coupling product in 5 h under visible light irradiation. In contrast, no cross coupling product were detected in the cases where an alkyl iodide was employed (Table 3.4, entries xiv-xv).

Table 3.4. Scope of the reaction using different substituted aryl iodides and phenyl alkyne and 1.5 wt % Pd@TiO_2.

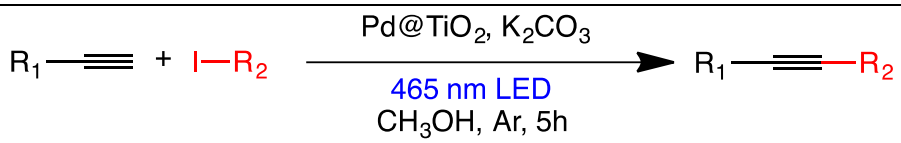

	R_1	R_2	% Conversion[a]	% Yield[b]
i	Ph-	p-CO_2CH_3 -Ph-	>99	92[c]
ii	Ph-	p-OCH_3-Ph-	>99	99[c]
iii	Ph-	o-OCH_3-Ph-	60(80)	60(80)[c]
iv	Ph-	p-NH_2-Ph-	>99	99
v	Ph-	p-NO_2-Ph-	>99	99[c]
vi	Ph-	o-CH_3-Ph-	48 (80)	43[c](67)
vii	Ph-	o-NH_2-Ph-	50(60)	44[c](52)
viii	Ph-	p-CF_3-Ph-	>99	99[c]
ix	Ph-	Ph-	>99	82
x	*p*-NH_2-Ph-	Ph-	>99	99
xi	*p*-OCH_3-Ph-	Ph-	>99	99
xii	o-NH_2-Ph-	Ph-	55(59)	39[c] (50)
xiii	*p*-CH_3-Ph-	Ph-	>99	>99
xiv	Ph-	Ph$(CH_2)_2CH_2$-	>99	ND[d]
xv	Cl$(CH_2)_2CH_2$-	Ph$(CH_2)_2CH_2$-	>99	ND[d]
xvi	Cl$(CH_2)_2CH_2$-	Ph-	>99	>99

[a]Irradiation: 465 nm LED set at 1 W/cm^2 . [b]Yields were determined by GC-FID using *t*-butylbenzene as an external standard. Values within parentheses correspond to 24 h of reaction. [c]Isolated yields. C-C coupling product not detected, complete conversion toward (3-methoxypropyl)-benzene after 24 h of reaction.

The photocatalyst can be reused twice with good performance (Table 3.5). The catalytic activity drops down drastically after the second cycle, but both ICP-OES analyses of the reaction mixtures and filtration tests (see details in SI) show no Pd-leaching from the catalyst. (XPS) studies suggested accumulation of alkyne hydrogenation products on the surface as the likely cause for poisoning (Figure S3.5). In order to restore the catalytic activity, an easy recovery phototreatment[14] using I-2959 and UVA light can be performed (See SI). Further analysis of the material before and after reaction indicated an increase in the particle size and changes on the oxidation state of Pd species. Such effects can be reversed by phototreatment with I-2959 (Figures S3.4 and S3.5), recovering the catalytic activity of the material.

Table 3.5. Catalyst reusability for the reaction under conditions described in Table 3.4, entry iii.

	Cycle	Conversion (%)	Yield (%)
i	1	100	99
ii	2	75	75
iii	3	<5	Traces
iv	4[a]	100	78

[a]After catalyst recovery treatment with I-2959.

CONCLUSIONS

We demonstrated that supported PdNPs can act as photocatalysts for Sonogashira coupling independently of the material chosen as a support. Mild conditions, good tolerance for air and moisture, and spatial and temporal control are some of the advantages that can be highlighted for this material. Interestingly, the catalyst can perform as well under regular thermal conditions as under photocatalytic conditions. In Particular, Pd@TiO_2 drives the Sonogashira reaction within short reaction times (usually 5 h) with unprecedented yields under mild conditions. The performance of the photocatalyst matches very well the absorption profile of the supported PdNP.

REFERENCES

1. X. Li, J. Zhang, X. Zhao, Y. Zhao, F. Li, T. Li and D. Wang, Trace amount Pd(ppm)-catalyzed Sonogashira, Heck and Suzuki cross-coupling reactions based on synergistic interaction with an asymmetric conjugated pyridinespirofluorene, Nanoscale., 2014, 6, 6473-6477; H. Veisi and N. Morakabati, Palladium nanoparticles supported on modified single-walled carbon nanotubes: a heterogeneous and reusable catalyst in the Ullmann-type N-arylation of imidazoles and indoles, New. J. Chem., 2015, 39, 2901-2907; S. Gowrisankar, A. G. Sergeev, P. Anbarasan, A. Spannenberg, H. Neumann and M. Beller, A General and Efficient Catalyst for Palladium-Catalyzed C-O Coupling Reactions of Aryl Halides with Primary Alcohols, J. Am. Chem. Soc., 2010, 132, 11592-11598.
2. M. Cui, H. Wu, J. Jian, H. Wang, C. Liu, S. Daniel and Z. Zeng, Palladium-catalyzed Sonogashira coupling of amides: access to ynones via C-N bond cleavage, Chem. Commun., 2016, 52, 12076-12079.
3. A. O. King and N. Yasuda, in Organometallics in Process Chemistry, Springer Berlin Heidelberg, 2004, pp. 205-245.
4. R. Chinchilla and C. Najera, The Sonogashira reaction: a booming methodology in synthetic organic chemistry, Chem. Rev., 2007, 107, 874-922.
5. R. Cano, A. F. Schmidt and G. P. McGlacken, Direct arylation and heterogeneous catalysis; ever the twain shall meet, Chem. Sci., 2015, 6, 5338-5346.
6. A. L. Stein, F. N. Bilheri and G. Zeni, Application of organoselenides in the Suzuki, Negishi, Sonogashira and Kumada cross-coupling reactions, Chem. Commun., 2015, 51, 15522-15525; Y. N. Kotovshchikov, G. V. Latyshev, N. V. Lukashev and I. P. Beletskaya, Alkynylation of steroids via Pd-free Sonogashira coupling, Org. Biomol. Chem., 2015, 13, 5542-5555; S. Kim, J. Rojas-Martin and F. D. Toste, Visible light-mediated gold-catalysed carbon(sp(2))-carbon(sp) cross-coupling, Chem. Sci., 2016, 7, 85-88.
7. D. J. Cole-Hamilton, Homogeneous catalysis--new approaches to catalyst separation, recovery, and recycling, Science, 2003, 299, 1702-1706.
8. C. Gonzalez-Arellano, A. Abad, A. Corma, H. Garcia, M. Iglesias and F. Sanchez, Catalysis by gold(I) and gold(III): a parallelism between homo- and heterogeneous catalysts for copper-free Sonogashira cross-coupling reactions, Angew. Chem. Int. Ed., 2007, 46, 1536-1538.
9. A. Sagadevan and K. C. Hwang, Photo-Induced Sonogashira C-C Coupling Reaction Catalyzed by Simple Copper(I) Chloride Salt at Room Temperature, Adv. Synth. Catal., 2012, 354, 3421-3427.
10. K. Balaraman and V. Kesavan, Efficient Copper(II) Acetate Catalyzed Homo- and Heterocoupling of Terminal Alkynes at Ambient Conditions, Synthesis, 2010, 3461-3466.
11. B. R. Stern, Essentiality and Toxicity in Copper Health Risk Assessment: Overview, Update and Regulatory Considerations, J. Toxicol. Environ. Health., 2010, 73, 114-127.
12. D. Mery, K. Heuze and D. Astruc, A very efficient, copper-free palladium catalyst for the Sonogashira reaction with aryl halides, Chem. Commun., 2003, 1934-1935; K. Heuze, D. Mery, D. Gauss and D. Astruc, Copper-free, recoverable dendritic Pd catalysts for the Sonogashira reaction, Chem. Commun., 2003, 2274-2275; R. Zhang, G. Lyu, D. Y. Li, P. N. Liu and N. Lin, Template-controlled Sonogashira cross-coupling reactions on a Au(111) surface, Chem. Commun., 2017, 53, 1731-1734; X. Pu, H. Li and T. J. Colacot, Heck alkynylation (copper-free Sonogashira coupling) of aryl and heteroaryl chlorides, using Pd complexes of t-Bu_2(p-$NMe_2C_6H_4$)P: understanding the

structure-activity relationships and copper effects, J. Org. Chem., 2013, 78, 568-581; N. Li, R. K. Lim, S. Edwardraja and Q. Lin, Copper-free Sonogashira cross-coupling for functionalization of alkyne-encoded proteins in aqueous medium and in bacterial cells, J. Am. Chem. Soc., 2011, 133, 15316-15319.

13. F. M. McKenna, R. P. K. Wells and J. A. Anderson, Enhanced selectivity in acetylene hydrogenation by ligand modified Pd/TiO_2 catalysts, Chem. Commun., 2011, 47, 2351-2353; F. M. McKenna and J. A. Anderson, Selectivity enhancement in acetylene hydrogenation over diphenyl sulphide-modified Pd/TiO_2 catalysts, J. Catal., 2011, 281, 231-240; J. Seth, C. N. Kona, S. Das and B. L. V. Prasad, A simple method for the preparation of ultra-small palladium nanoparticles and their utilization for the hydrogenation of terminal alkyne groups to alkanes, Nanoscale., 2015, 7, 872-876; C. M. Granadeiro, L. S. Nogueira, D. Juliao, F. Mirante, D. Ananias, S. S. Balula and L. Cunha-Silva, Influence of a porous MOF support on the catalytic performance of Eu-polyoxometalate based materials: desulfurization of a model diesel, Catal. Sci. Technol., 2016, 6, 1515-1522; V. Kozell, M. McLaughlin, G. Strappaveccia, S. Santoro, L. A. Bivona, C. Aprile, M. Gruttadauria and L. Vaccaro, Sustainable Approach to Waste-Minimized Sonogashira Cross-Coupling Reaction Based on Recoverable/Reusable Heterogeneous Catalytic/Base System and Acetonitrile Azeotrope, ACS Sustain. Chem. Eng., 2016, 4, 7209-7216; B. Wang, X. N. Guo, G. Q. Jin and X. Y. Guo, Visible-light-enhanced photocatalytic Sonogashira reaction over silicon carbide supported Pd nanoparticles, Catal. Commun., 2017, 98, 81-84.
14. A. Elhage, A. E. Lanterna and J. C. Scaiano, Tunable Photocatalytic Activity of Palladium-Decorated TiO2: Non Hydrogen -Mediated Hydrogenation or Isomerization of Benzyl Substituted Alkenes, ACS Catal., 2017, 7, 250-255.
15. R. Ciriminna, V. Pandarus, G. Gingras, F. Beland, P. D. Cara and M. Pagliaro, Heterogeneous Sonogashira Coupling over Nanostructured SiliaCat Pd(0), ACS Sustain. Chem. Eng., 2013, 1, 57-61.
16. A. Y. Platonov, A. N. Evdokimov, A. V. Kurzin and H. D. Maiyorova, Solubility of potassium carbonate and potassium hydrocarbonate in methanol, J. Chem. Eng. Data., 2002, 47, 1175-1176.
17. S. Impellizzeri, S. Simoncelli, C. Fasciani, M. L. Marin, G. L. Hallett-Tapley, G. K. Hodgson and J. C. Scaiano, Mechanistic insights into the Nb_2O_5 and niobium phosphate catalyzed in situ condensation of a fluorescent halochromic assembly, Catal. Sci. Technol., 2015, 5, 169-175.
18. A. Corma, R. Juarez, M. Boronat, F. Sanchez, M. Iglesias and H. Garcia, Gold catalyzes the Sonogashira coupling reaction without the requirement of palladium impurities, Chem. Commun., 2011, 47, 1446-1448.
19. K. Imamura, Y. Okubo, T. Ito, A. Tanaka, K. Hashimoto and H. Kominami, Photocatalytic Hydrogenation of Alkenes to Alkanes in Alcoholic Suspensions of Palladium-loaded Titanium(IV) Oxide without the Use of Hydrogen Gas, RSC Adv., 2014, 4, 19883-19886.
20. B. Chatterjee and C. Gunanathan, The ruthenium-catalysed selective synthesis of mono-deuterated terminal alkynes, Chem. Commun., 2016, 52, 4509-4512.
21. S. P. Pitre, T. P. Yoon and J. C. Scaiano, Titanium dioxide visible light photocatalysis: surface association enables photocatalysis with visible light irradiation, Chem. Commun., 2017, 53, 4335-4338.
22. S. Sarina, H. Y. Zhu, Q. Xiao, E. Jaatinen, J. F. Jia, Y. M. Huang, Z. F. Zheng and H. S. Wu, Viable Photocatalysts under Solar-Spectrum Irradiation: Nonplasmonic Metal Nanoparticles, Angew. Chem. Int. Ed., 2014, 53, 2935-2940.

3.3 Postprint Version of the Supporting Information

MATERIALS AND INSTRUMENTATION

Unless otherwise specified, all chemicals were purchased from Sigma-Aldrich or Fisher Scientific and used without further purification. Titanium dioxide (TiO_2-P25) was purchase from Univar Canada.

Transmission electron microscopy (TEM) images were collected on a JEM-2100F FETEM (JEOL) operating at 200 kV. X-ray photoelectron spectroscopy (XPS) was recorded using Kratos analytical model Axis Ultra DLD, using monochromatic aluminum Ka X-rays at 140 W. XPS data was analyzed using CasaXPS software, Version 2.3.15 and all fittings obtained using a Gaussian 30% Laurentian and a Shirley baseline. The proportion of Pd in the catalysts was determined by Inductively Coupled Plasma Optical Emission Spectrometry (ICP-OES), using an Agilent Vista Pro ICP Emission Spectrometer. Approximately 10 mg portions were accurately weighed in triplicate and digested with aqua regia. Solutions were further diluted and measured by ICP-OES. The Pd 340.458 emission line was used for quantification. Diffuse reflectance (DR) measurements were carried out in VARIAN Cary 100 UV-VIS Spectrophotometer coupled with an integrating sphere accessory.

UV irradiation used for catalyst synthesis was performed in a Luzchem photoreactor equipped with UVA bulbs (typically operated with 14 bulbs, corresponding to ~0.029 W/cm^2 (left: 0.025 right: 0.020) with ~ 4% spectral contamination). Light-emitting diodes (LEDs) of 10 W from LedEngin were used for the photocatalytic Sonogashira coupling in the visible region (centered at 465 nm) working at 1 W/cm^2.

Quantification was carried out in a Perkin Elmer, Claurus Gas Chromatograph coupled to a Flame Ionization Detector (FID) and a DB-5 column (30 m length, 0.320 mm diameter, 0.25 μm film) using Helium as a carrier gas and t-Butyl benzene as external standard. GC-MS analyses were performed on an Agilent 6890-N Gas Chromatograph with an Agilent 5973 mass selective detector calibrated with acetophenone. All ^{1}H NMR and the ^{13}C NMR spectra were recorded on a Bruker

AVANCE 400 spectrometer expressing the chemical shifts in ppm relative to the H-signal of the tetramethylsilane (TMS) and to the C-signal of the deuterated chloroform as internal standard, respectively.

Chromatography: Flash column chromatography was performed using 230-400 mesh silica gel. Preparatory thin layer chromatography (PTLC) was performed using 1000 μm thick glass baked TLC plates.

Experimental procedures

Catalyst preparation: Palladium nanoparticles supported on TiO_2 ($Pd@TiO_2$), crystal nanodiamonds (Pd@CND) or Nb_2O_5 ($Pd@Nb_2O_5$) were prepared by photodeposition of PdNP as previously described.[1] The resulting dark gray powders were characterized by TEM, XPS, ICP-EOS and DR. Preparation of $Cu@TiO_2$ was performed as previously reported.[2] Characterization of $Cu@TiO_2$ and $Au@TiO_2$ were also performed as reported in our previous publications.[2, 3]

Sonogashira C-C coupling:

Thermal-induced Sonogashira C-C coupling under conventional heating: 15 mg of $Pd@TiO_2$ (or Pd@CND or $Pd@Nb_2O_5$) were dispersed in 4 mL of methanol by sonication ca. for 5 min in a clean round bottom flask, then 14 μL of Iodobenzene 1eq. (0.12 mmol), 18 μL of Phenylacetylene 1.3 eq. (0.16 mmol) and 33 mg of K_2CO_3 as a base 2 eq. (0.24 mmol), were added. The reaction mixture was purged with argon then heated up to 65 ºC (solvent boiling point) under argon with continuous stirring for 5 hours. The solid catalyst was separated either by filtration or by centrifugation and crude product was obtained after solvent evaporation. Quantification was done either by GC-FID or ^1H NMR. The same procedure was followed to run the reaction under air. Control experiments were carried out using both reagents with 2 eq. of base as starting material.

Visible light-induced Sonogashira C-C coupling: 15 mg of $Pd@TiO_2$ (or Pd@CND or $Pd@Nb_2O_5$) were dispersed in 4 mL of methanol in a 10 mL clean quartz tube, then 14 μL of Iodobenzene (1 eq., 0.12 mmol), 18 μL of Phenylacetylene (1.3 eq.,

0.16 mmol) and 33 mg of K_2CO_3 (2 eq., 0.24 mmol), were added. The reaction mixture was purged with argon for 15 min then irradiated with 465 nm LED light source set up at 1W/cm^2 for 5 hours. As for the control reaction with Au@TiO_2, the reaction mixture was irradiated with a liquid-cooled 532 nm LED apparatus previously described[3] with continuous stirring for 5 hours at room temperature under argon or under air atmosphere. The solid catalyst was separated either by filtration or by centrifugation and crude product was obtained after solvent evaporation. Quantification was done by GC-FID. Control experiments were carried out as mentioned above.

General procedure for isolation of cross-coupling products:

The solid catalyst was separated by centrifugation and the resulting supernatant was concentrated using a rotovap to afford dry reaction mixture. Ethyl acetate (25 mL) was added to dissolve organic compounds; the resulting mixture was washed with H_2O (4x, 25 mL) to get rid of K_2CO_3 and of water-soluble products. The organic layer was dried over anhydrous $MgSO_4$, then concentrated using a rotovap to yield the crude product. Purification of the crude was done by column chromatography (hexanes:ethylacetate).

Catalyst Recyclability: The reusability of the Pd@TiO_2 catalyst was tested for the light-induced direct, selective cross coupling reaction under the conditions described above. The reaction was scaled up to facilitate catalyst recovery and reuse. The catalyst was recovered after each reaction by centrifugation (2500 rpm for 10 min), washing and drying.

Catalyst Recovery: The used catalyst was recovered from the reaction mixture and then treated by Photochemical treatment: the catalyst was re-suspended in 10 mL of Milli-Q water, then 10 mL of EtOH 99% and 20 mg of benzoin Irgacure-2959^{TM} (I-2959) as a photo-initiator were added. The resulting mixture was irradiated for 3 hours with UVA at room temperature with vigorous stirring. The gray slurry was cleaned using the same procedure explained above for the UVA treatment.

Leaching test: In order to examine if any Pd-species leached into the solution are responsible for the photocatalytic activity, we examined the activity of the solution after

separation of the solid catalyst. For this, the visible light-induced Sonogashira C-C coupling was run using the optimized conditions as reported in table 3.2, entry v. Briefly, 15 mg of Pd@TiO_2 were dispersed in 4 mL of methanol in a 10 mL test tube, then 14 µL of Iodobenzene (1 eq., 0.12 mmol), 18 µL of Phenylacetylene (1.3 eq., 0.16 mmol) and 33 mg of K_2CO_3 (2 eq., 0.24 mmol), were added. The reaction mixture was purged with Argon for 15 min then irradiated with 465 nm LED light source set up at 1W/cm^2 for 1 hour. The solid catalyst was separated by centrifugation and 3 mL of supernatant were transferred to a test tube, purged with Argon and irradiated with 465nm LED for another 4 hours. Aliquots were taken every two hours. Quantification was done either by GC-FID.

Action spectrum

The action spectrum was performed using the conditions described in a previous publication.[4] The energy of a photon at each wavelength is defined as equations 1 and 2, where h is Plank's constant (6.626 x 10^{-34} J.s or $W.s^2$), c is the speed of light (2.998 x10^8 m/s), and λ is the wavelength of the light source in nm.

$$E_{photon} = \frac{hc}{\lambda} \tag{1}$$

$$E_{photon}(in\ kcal\ mol^{-1}) = \frac{28{,}600}{\lambda(in\ nm)} \tag{2}$$

From this relationship, the number of photons arriving at the sample can be determined from the irradiance. Dividing this value by Avogadro's number gives the photon flux, or the moles of photons arriving at the sample per unit time, resulting in equation 3.

$$\phi = \frac{\lambda(19\ W\ m^{-2})}{h\ c\ 6.022\ 10^{23} mol^{-1}} \tag{3}$$

The photon flux was calculated for each LED used, and the initial rate (v_0) was corrected by the photon flux for each experiment to obtain the apparent quantum yield (v_0/ϕ), as shown in Table S3.1.

Table S3.1. Experimental and calculated data for the construction of an action spectrum

λ (nm)	Yield (%)	ν_0 (10^{-7} mol/min)	φ (mol/m^{2}min)	ν_0 / φ (10^{-7})
368	0	0	0.36	0
405	19	1.9	0.39	4.95
465	21	2.1	0.45	4.53
500	24	2.4	0.49	4.93
525	23	2.3	0.51	4.50
590	22	2.2	0.57	3.83
740	22	2.2	0.72	3.05

Reaction conditions: 1 eq. Iodobenzene, 1.3 eq. Phenylacetylene, 2 eq. K_2CO_3, 4 mL methanol, 15 mg Pd@TiO_2. Argon atmosphere. Irradiation time: 2 h. Irradiance: 0.1907 W/cm^2. Yields were determined by GC-FID using *t*-butylbenzene as an external standard

Table S3.2. Different solvents tested for the photocatalytic Sonogashira C-C coupling using Pd@TiO_2

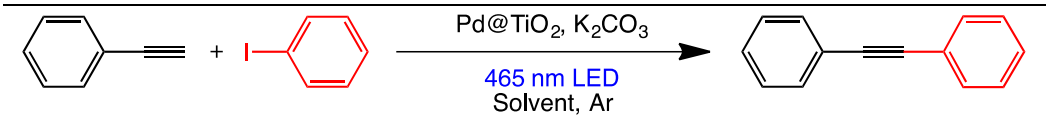

Entry	Solvent	Solvent polarity	Time (h)	% Conversion	% Yield[a]
i	Methanol (CH_3OH)	0.791	5	100	84
ii			24	100	80
iii	Acetonitrile (CH_3CN)	0.46	5	43	27
iv			24	52	31
v	Tetrahydrofuran (THF)	0.207	5	32	ND[b]
vi			24	35	ND
vii	Toluene ($PhCH_3$)	0.099	5	0	ND
viii			24	0	ND

Reactions conditions: 1 eq. of Iodobenzene, 1.3 eq. of Phenylacetylene, 2 eq. of K_2CO_3, 4 mL solvent, 15 mg catalyst. Irradiation: 465 nm LED set at 1 W/cm^2. [a]Yields were determined by GC-FID using *t*-butylbenzene as an external standard. [b] no homo-coupling by-products detected.

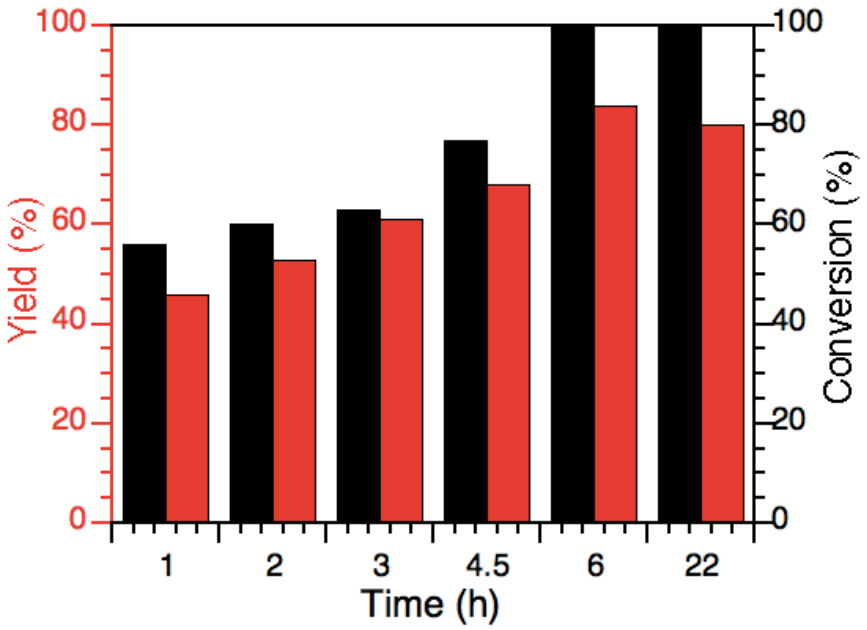

Figure S3.1. Photocatalytic Sonogashira C-C coupling versus time. Conditions as per table 3.2, entry v.

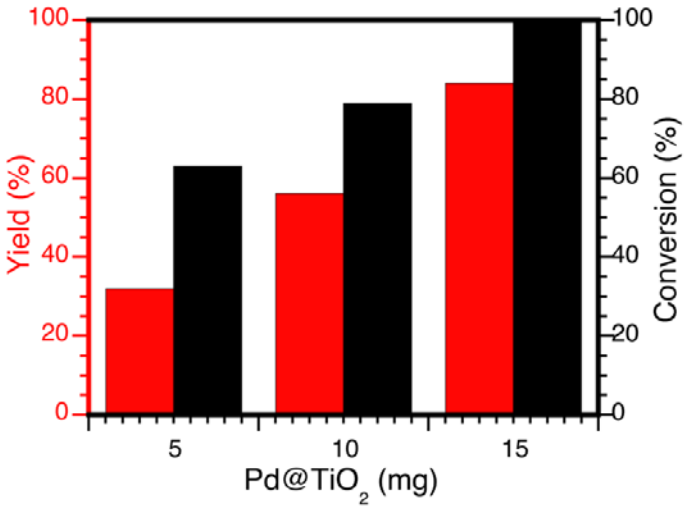

Figure S3.2. Photocatalytic Sonogashira C-C coupling using Pd@TiO_2 different amounts of catalyst. Reaction conditions as per Table S3.2, entry i. Notice that Pd@TiO_2 contains ~1.3 % of Pd; thus, 5 mg, 10 mg and 15 mg of catalyst are equivalent to 0.5, 1.0 and 1.5 mol % of Pd.

Table S3.3. Stability of reagents and product under the photocatalytic reaction conditions.

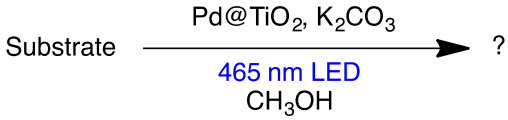

Entry	Substrate	Atmosphere	Time (h)	Decomposition
				% Conv
i	Phenylacetylene	Ar	5	ND
ii	Phenylacetylene	Ar	5	100[a]
iii	Iodobenzene	Ar	5	ND
iv	Diphenylacetylene	Ar	5	ND
v	Diphenylacetylene	Ar	24	14[b]

[a]CD3OD, 100% yield of deuterated phenylacetylene. [b]Traces of *t*-stilbene and *c*-stilbene detected.

Table S3.4. Photocatalytic Sonogashira C-C coupling under different light intensity.

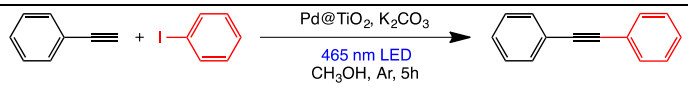

Entry	Light intensity (W/cm^2)	% Conversion	% Yield[a]
i	1	100	82
ii	0.8	72	55
iii	0.4	50	29
iv	0.2	48	22

Reactions conditions: 1 eq. of Iodobenzene, 1.3 eq. of Phenylacetylene, 2 eq. of K_2CO_3, 4 mL solvent, 15 mg Pd@TiO_2. [a]Yields were determined by GC-FID using *t*-butylbenzene as an external standard.

Table S3.5. Scope of light induced Sonogashira coupling using alkyl iodide, aliphatic alkyne as starting material and 1.5 wt % Pd@TiO_2.

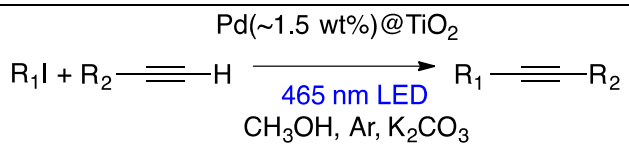

Entry	Substrate 1 R_1I	Substrate 2 R_2—≡—H	Time (h)	% Yield[a]
i	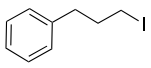 1-iodo-3-phenyl propane	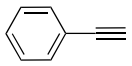 Phenylacetylene	24	ND
ii	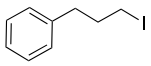 1-iodo-3-phenyl propane	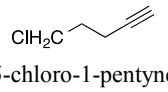 5-chloro-1-pentyne	24	ND
iii	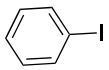 Iodobenzene	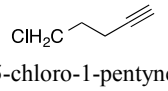 5-chloro-1-pentyne	5	>99

Reactions conditions: 1 eq. of Iodocompound, 1.3 eq. of Alkyne, 2 eq. of K_2CO_3, 4 mL solvent, 15 mg Pd@TiO_2. Reaction was followed by GC-FID. [a]Yields were determined by H NMR. ND: nothing detected.

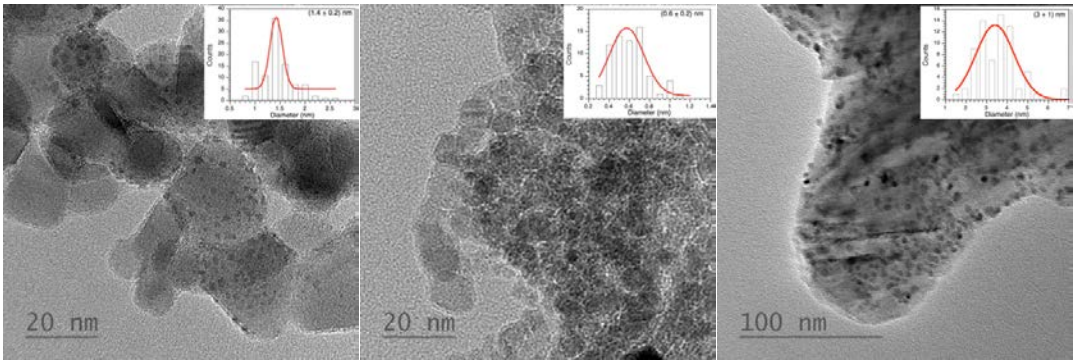

Figure S3.3. TEM images and particle size distribution of Pd@TiO_2, Pd@CND and Pd@Nb_2O_5.

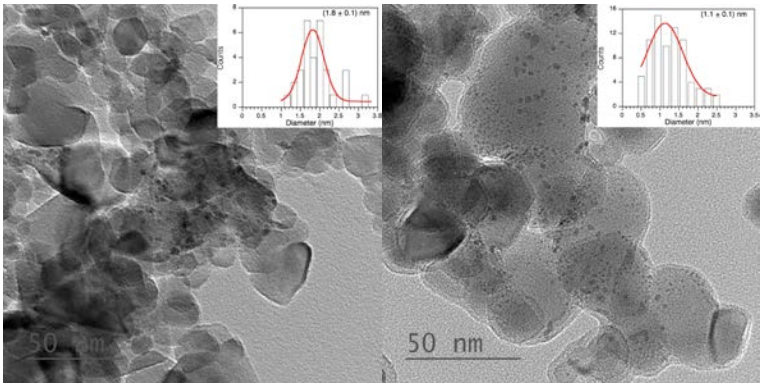

Figure S3.4. TEM image and particle size distribution of used Pd@TiO_2 before *(left*, ~1.8 nm) and after (*right,* ~1.1 nm) the recovery treatment. Scale bars: 50 nm.

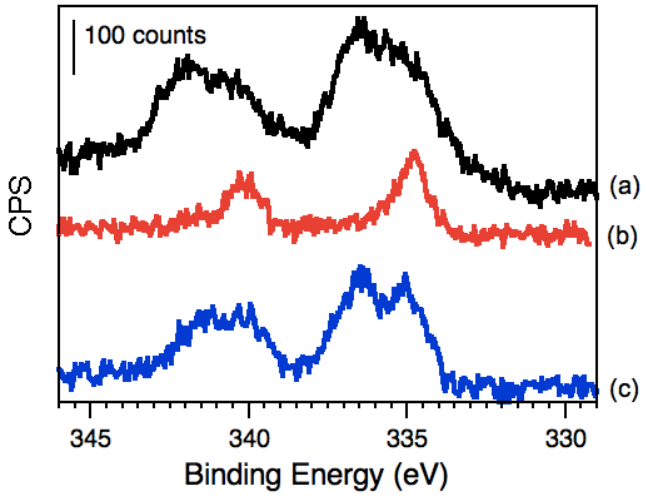

Figure S3.5. Pd 3d HR-XPS spectra of Pd@TiO_2 before use (a), after use (b) and after treatment with I-2959 (c).

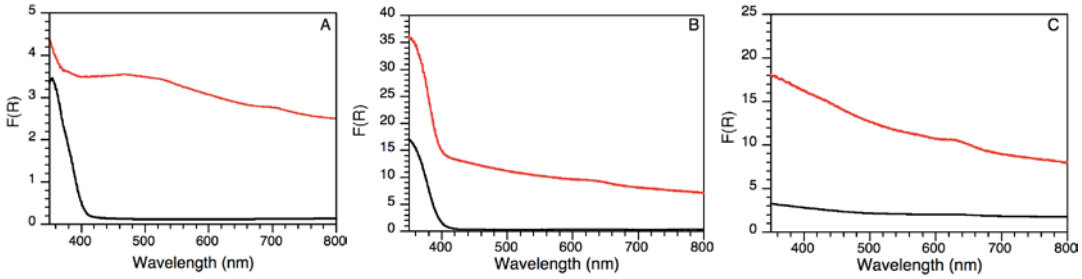

Figure S3.6. Diffuse reflectance spectra of A) pristine TiO_2 (black) and Pd@TiO_2 (red), B) pristine Nb_2O_5 (black) and Pd@Nb_2O_5 (red), C) CND (black) and Pd@CND (red).

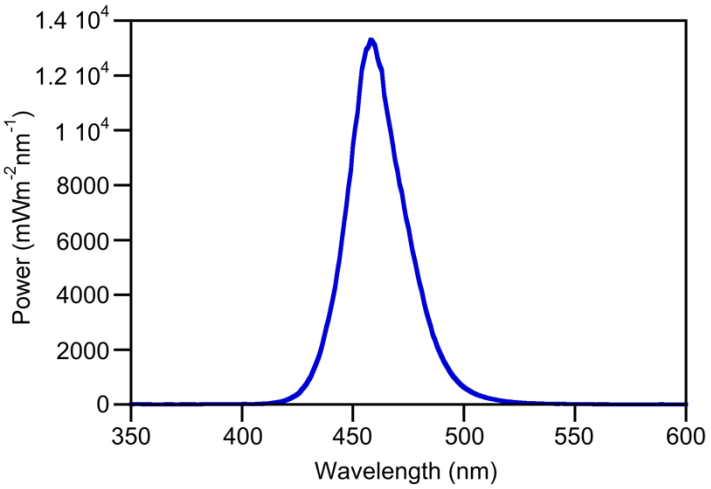

Figure S3.7. Emission spectrum for the 10 W 465 nm LED utilized for the photocatalytic Sonogashira coupling reaction.

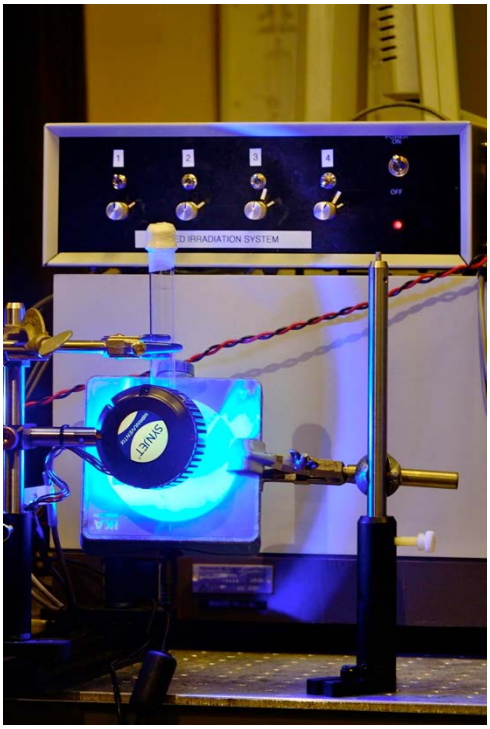

Figure S3.8. Picture of LED set up used for the photocatalytic Sonogashira reactions.

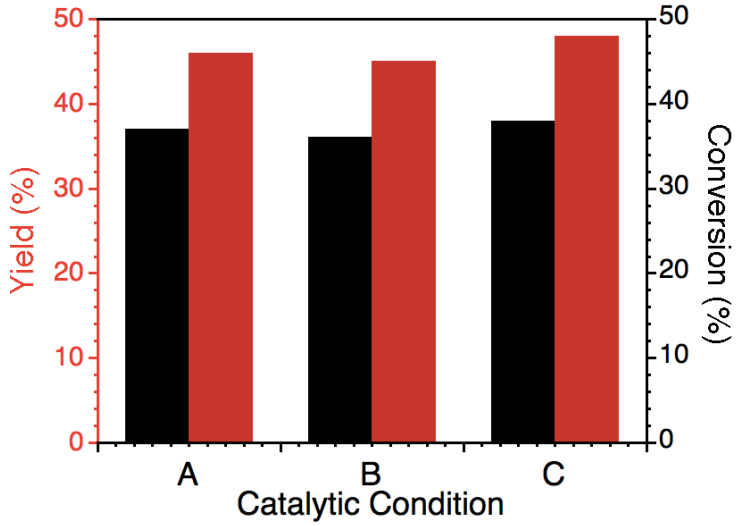

Figure S3.9. Metal leaching test: Photocatalytic Sonogashira C-C coupling using Pd@TiO_2 after (A) 1 h of irradiation under reaction conditions described in Table 3.2, entry v; and then separation of the supernatant and irradiation for (B) 2h and (C) 4h.

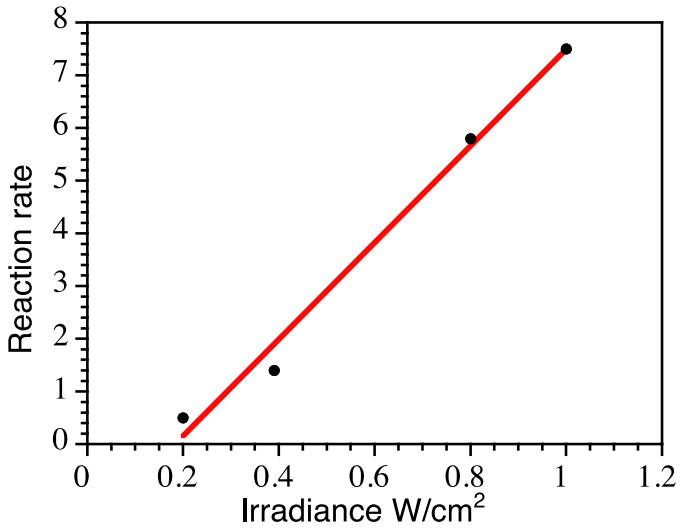

Figure S3.10. Reaction rate vs. four different light intensity at 465nm for the photocatalytic Sonogashira reactions.

REFERENCES

1. A. Elhage, A. E. Lanterna and J. C. Scaiano, Tunable Photocatalytic Activity of Palladium-Decorated TiO2: Non Hydrogen -Mediated Hydrogenation or Isomerization of Benzyl Substituted Alkenes, ACS Catal., 2017, 7, 250-255.
2. B. Wang, J. Durantini, J. Nie, A. E. Lanterna and J. C. Scaiano, Heterogeneous Photocatalytic Click Chemistry, J. Am. Chem. Soc., 2016, 138, 13127-13130.
3. A. E. Lanterna, A. Elhage and J. C. Scaiano, Heterogeneous photocatalytic C-C coupling: mechanism of plasmon-mediated reductive dimerization of benzyl bromides by supported gold nanoparticles, Catal. Sci. Technol., 2015, 5, 4336-4340.
4. S. P. Pitre, T. P. Yoon and J. C. Scaiano, Titanium dioxide visible light photocatalysis: surface association enables photocatalysis with visible light irradiation, Chem. Commun., 2017, 53, 4335-4338.

^{1}H NMR, ^{13}C NMR and GC-MS data and spectra

Methyl-4-(phenylethynyl)benzoate (table 3.4, entry i)

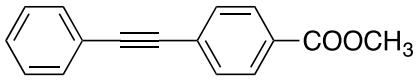

^{1}H NMR (400 MHz, $CDCl_3$): δ 8.02 (d, 2 H), 7.58 (d, 2 H), 7.54 (m, 2 H) 7.36 (m, 3 H), 3.91(s, 3H); ^{13}C NMR (100 MHz, $CDCl_3$): δ166.46, 131.63, 131.4, 129.42, 128.65, 128.33, 122.6, 120.4, 92.25, 89.29, 88.52, 52.12, 29.6; HRMS calculated for $C_{16}H_{12}O_2$: 236.0837, found: m/z= 236.1.

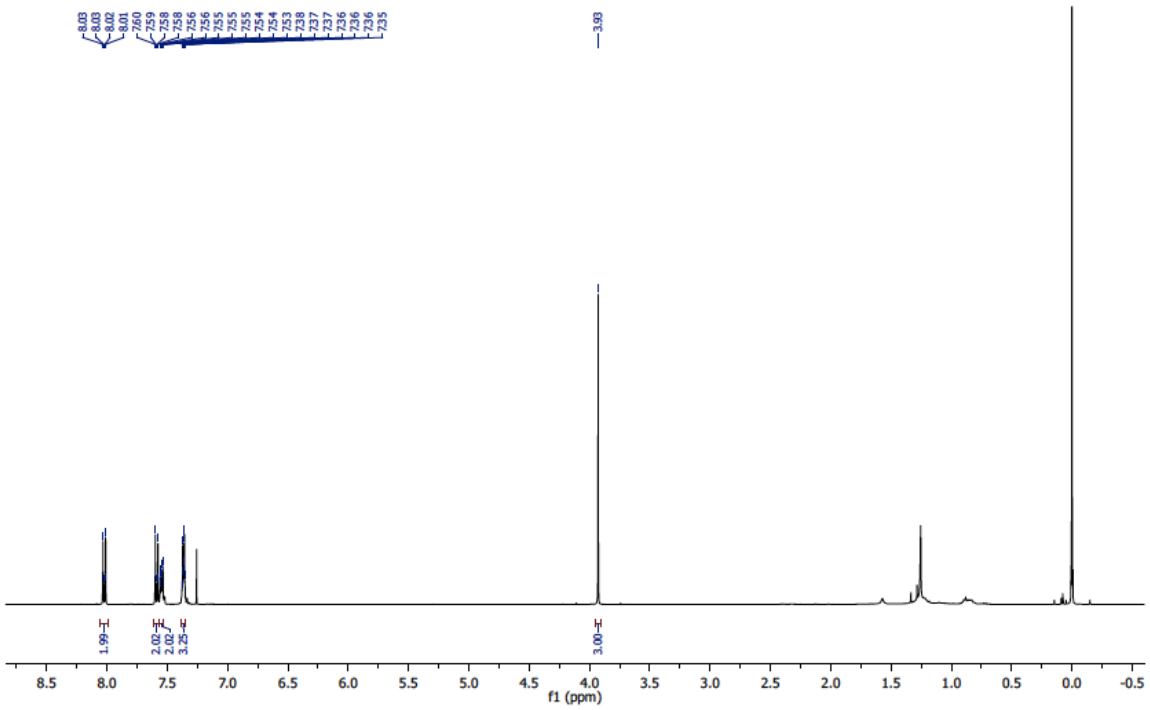

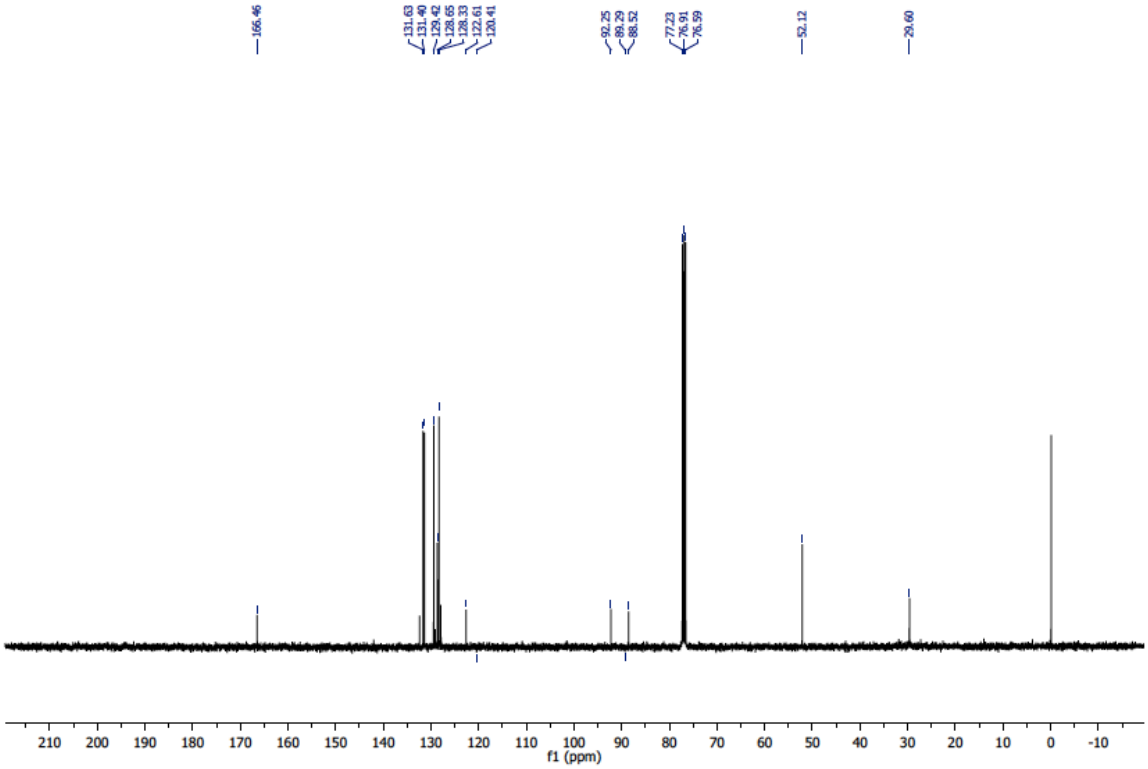
166.46
131.63
131.40
129.42
128.65
128.33
122.61
120.41
92.25
89.29
88.52
77.23
76.91
76.59
52.12
29.60
210 200 190 180 170 160 150 140 130 120 110 100 90 80 70 60 50 40 30 20 10 0 -10
f1 (ppm)

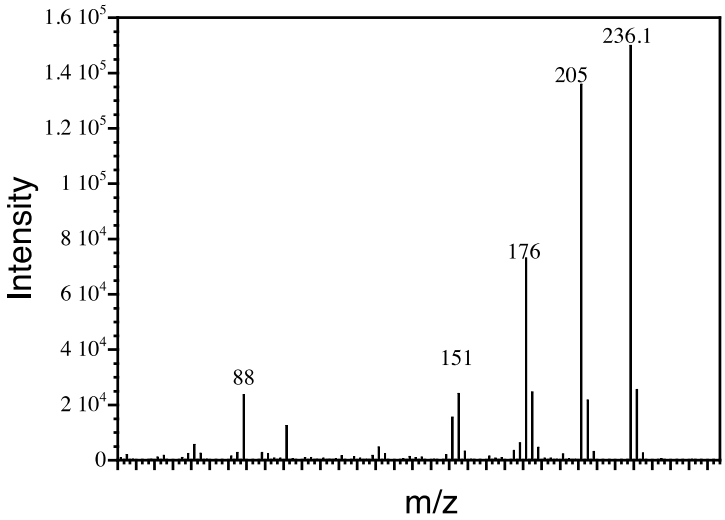
1.6 10^5
1.4 10^5
1.2 10^5
1 10^5
8 10^4
6 10^4
4 10^4
2 10^4
0
Intensity
236.1
205
176
151
88
m/z

1-methoxy-4-(phenylethynyl)benzene (table 3.4, entry ii- xi)

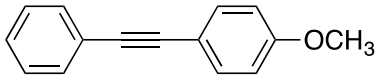

^{1}H NMR (400 MHz, CDCl3): δ 7.51-7.45 (m, 4 H), 7.32-7.30 (m, 3 H), 6.87-6.85 (d, 2 H), 3.81(s, 3 H); ^{13}C NMR (100 MHz, CDCl3): δ 159.76, 133.18, 131.58, 131.58, 128.43, 128.06, 115.53,114.13, 89.51, 88.20, 55.41; HRMS calculated for $C_{15}H_{12}O$: 208.0888, found: m/z=208.1.

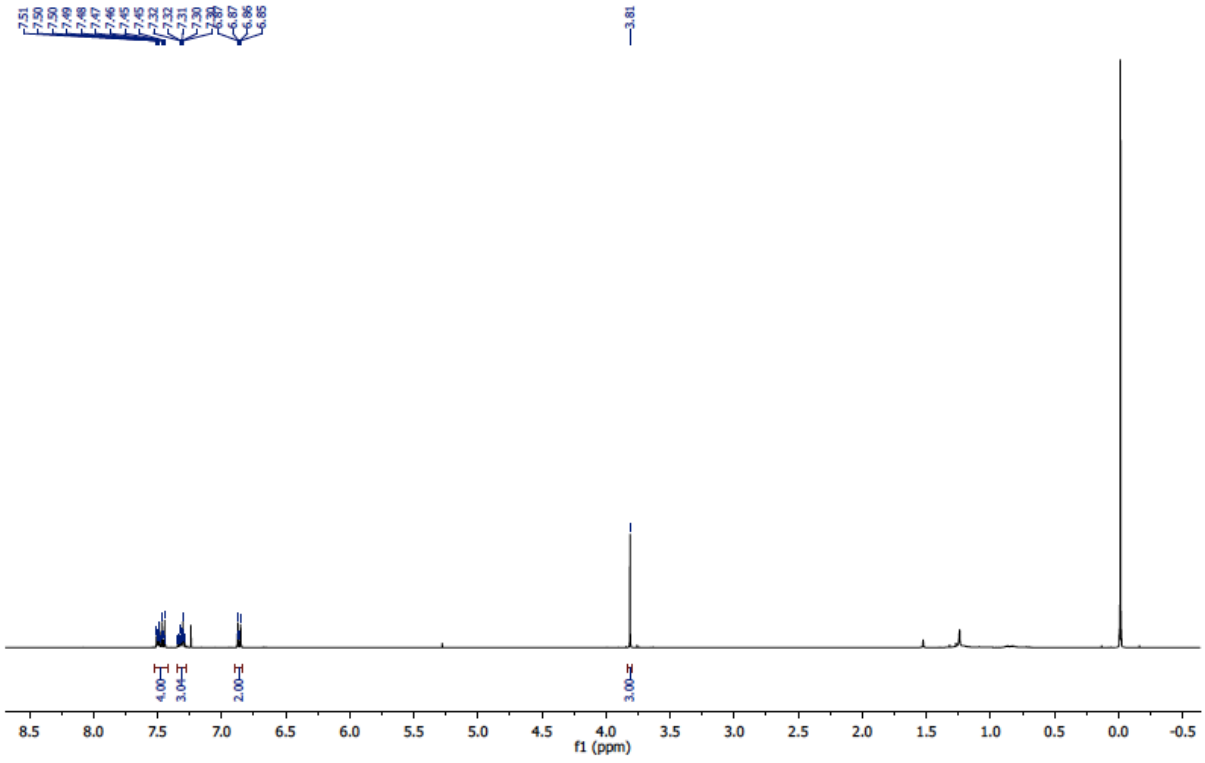

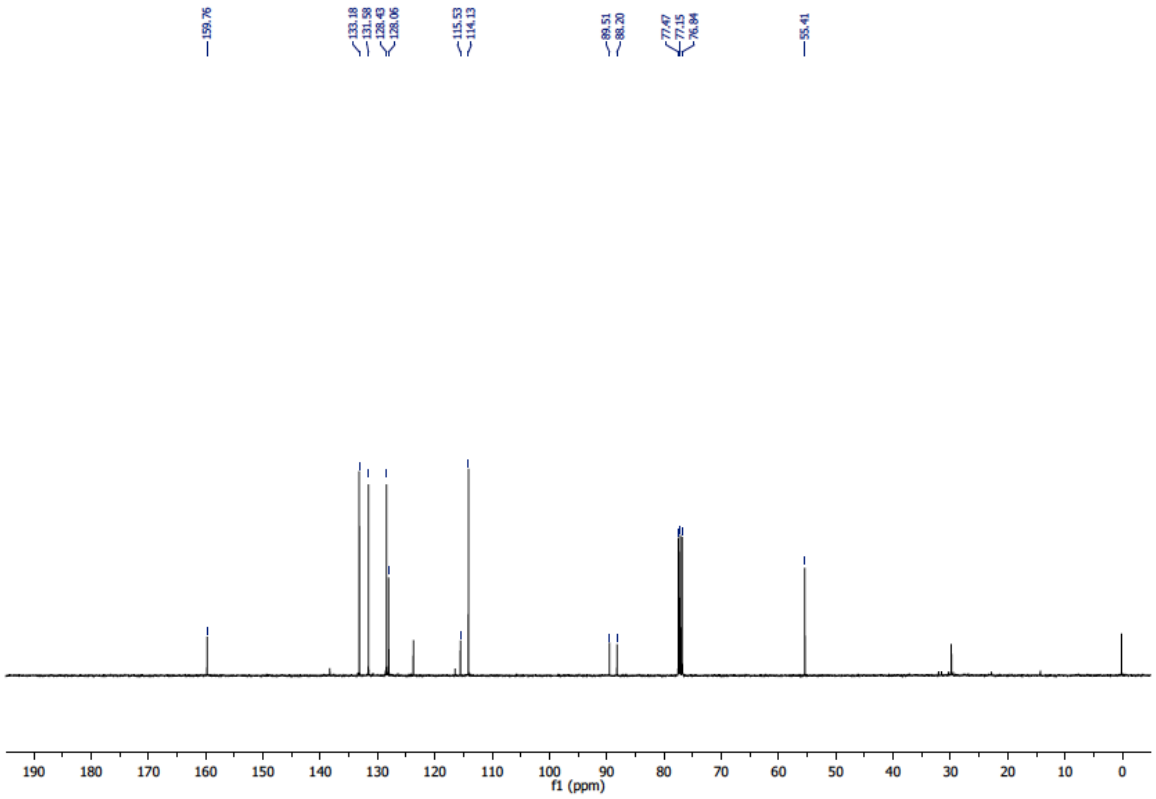
159.76
133.18
131.58
128.43
128.06
115.53
114.13
89.51
88.20
77.47
77.15
76.84
55.41
190 180 170 160 150 140 130 120 110 100 90 80 70 60 50 40 30 20 10 0
f1 (ppm)

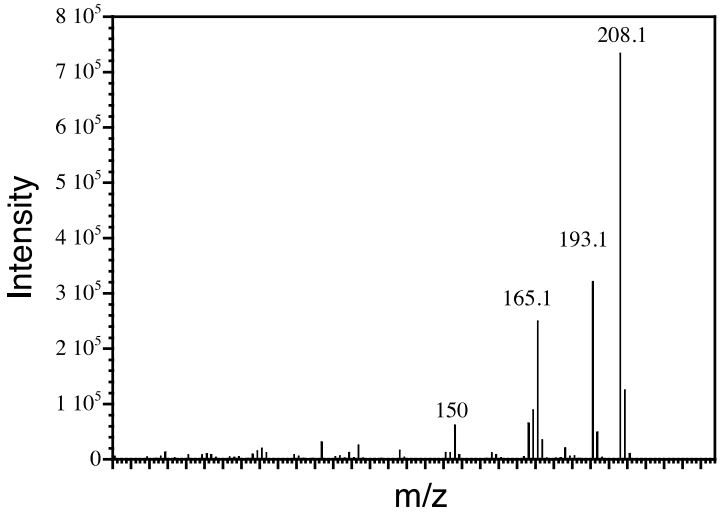
Intensity
m/z
208.1
193.1
165.1
150

1-methoxy-2-(phenylethynyl)benzene (table 3.4, entry iii)

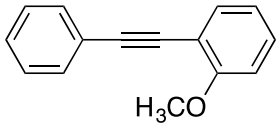

^{1}H NMR (400 MHz, CDCl3): δ 7.57-7.55 (m, 2 H), 7.56-7.54 (d, 1 H), 7.35-7.32 (m,4 H), 6.95-6.89 (m, 2 H), 3.91(s, 3 H); ^{13}C NMR (100 MHz, CDCl3): δ 160.22, 133.86, 131.95, 130.03, 128.51, 128.37, 123.86, 120.77, 112.76, 111.00, 93.70, 90.67, 86.00, 56.12, 29.99; HRMS calculated for $C_{15}H_{12}O$: 208.0888, found: m/z= 208.1.

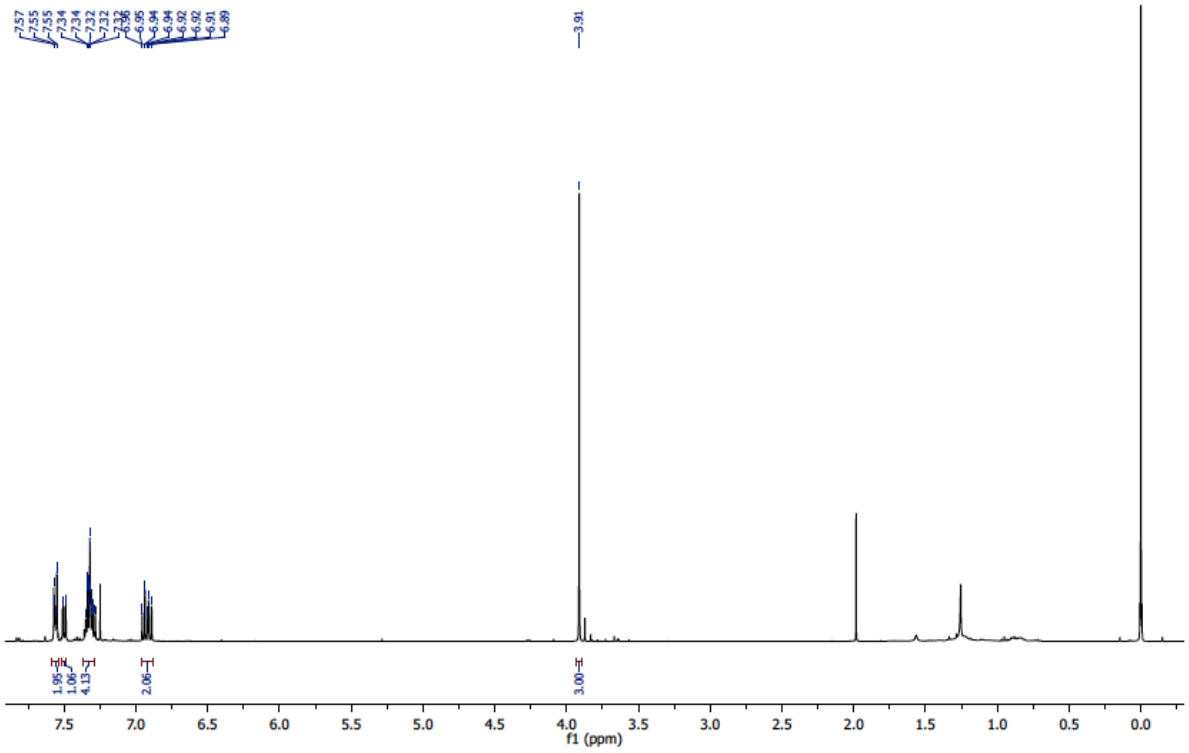

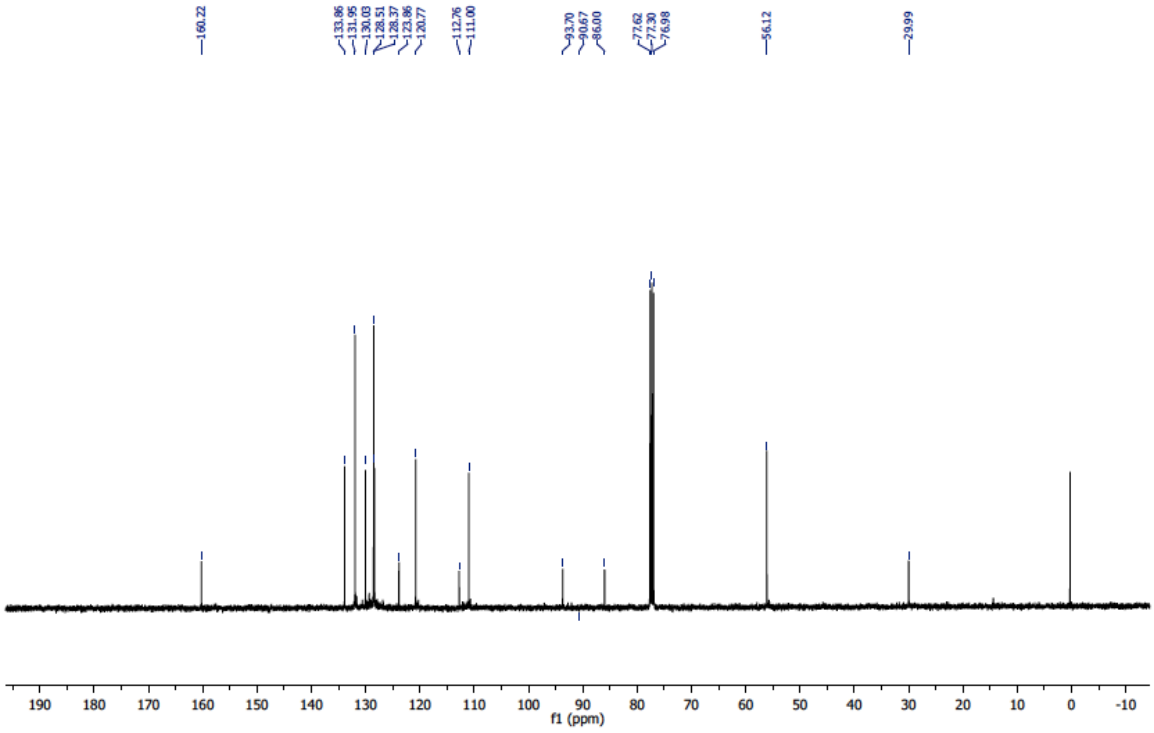
160.22
133.86
131.95
130.03
128.51
128.37
123.86
120.77
112.76
111.00
93.70
90.67
86.00
77.62
77.30
76.98
56.12
29.99
190 180 170 160 150 140 130 120 110 100 90 80 70 60 50 40 30 20 10 0 -10
f1 (ppm)

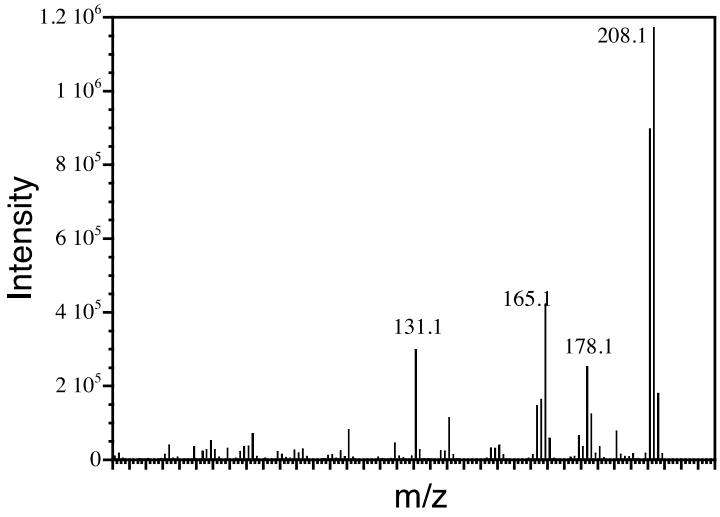
1.2 10^6
1 10^6
8 10^5
6 10^5
4 10^5
2 10^5
0
Intensity
208.1
165.1
131.1
178.1
m/z

4-(phenylethynyl) aniline (table 3.4, entry iv- x)

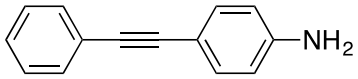

^{1}H NMR (400 MHz, $CDCl_3$): δ 7.50-7.47 (d, 2 H), 7.35-7.30 (m, 5 H), 6.64-6.62 (d, 2 H), 3.81 (s, 2 H); ^{13}C NMR (100 MHz, $CDCl_3$): δ 146.75, 133.08, 131.47, 128.37, 127.76, 125.02, 124.04, 114.86, 112.78, 90.21, 87.44; HRMS calculated for $C_{14}H_{11}N$: 193.0891, found: m/z=193.1

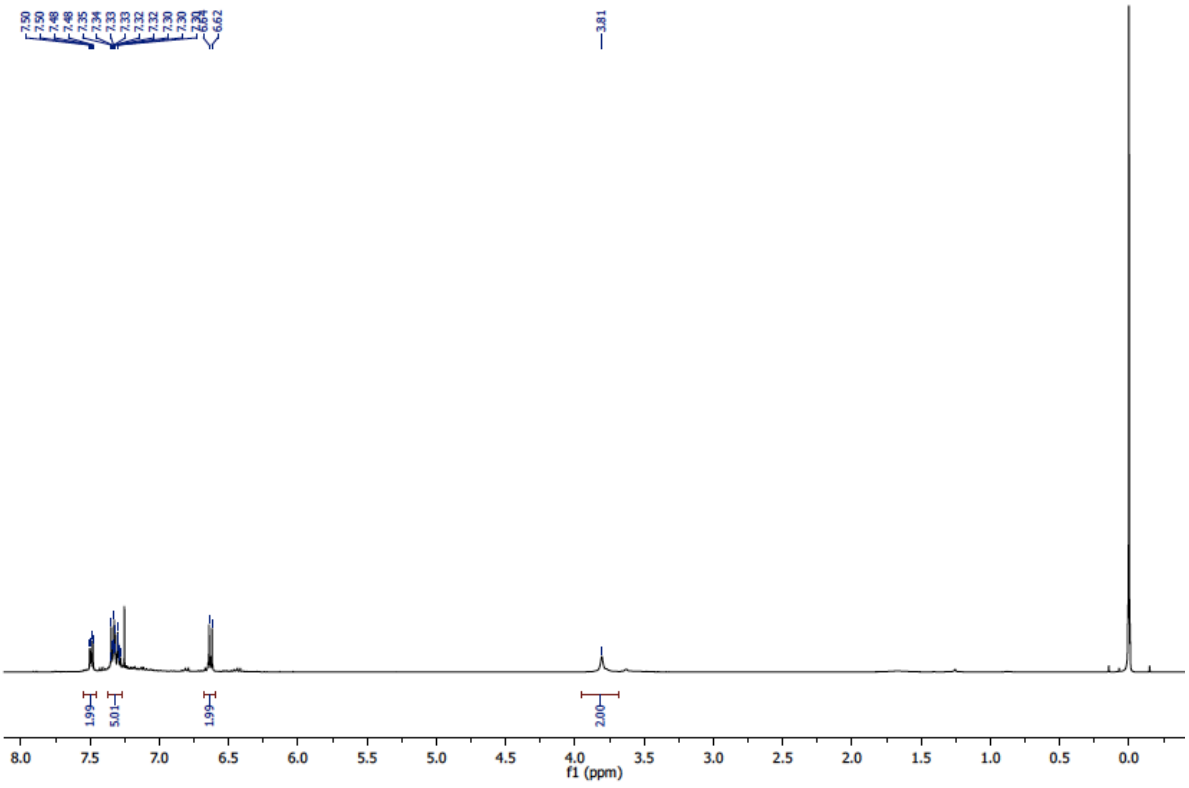

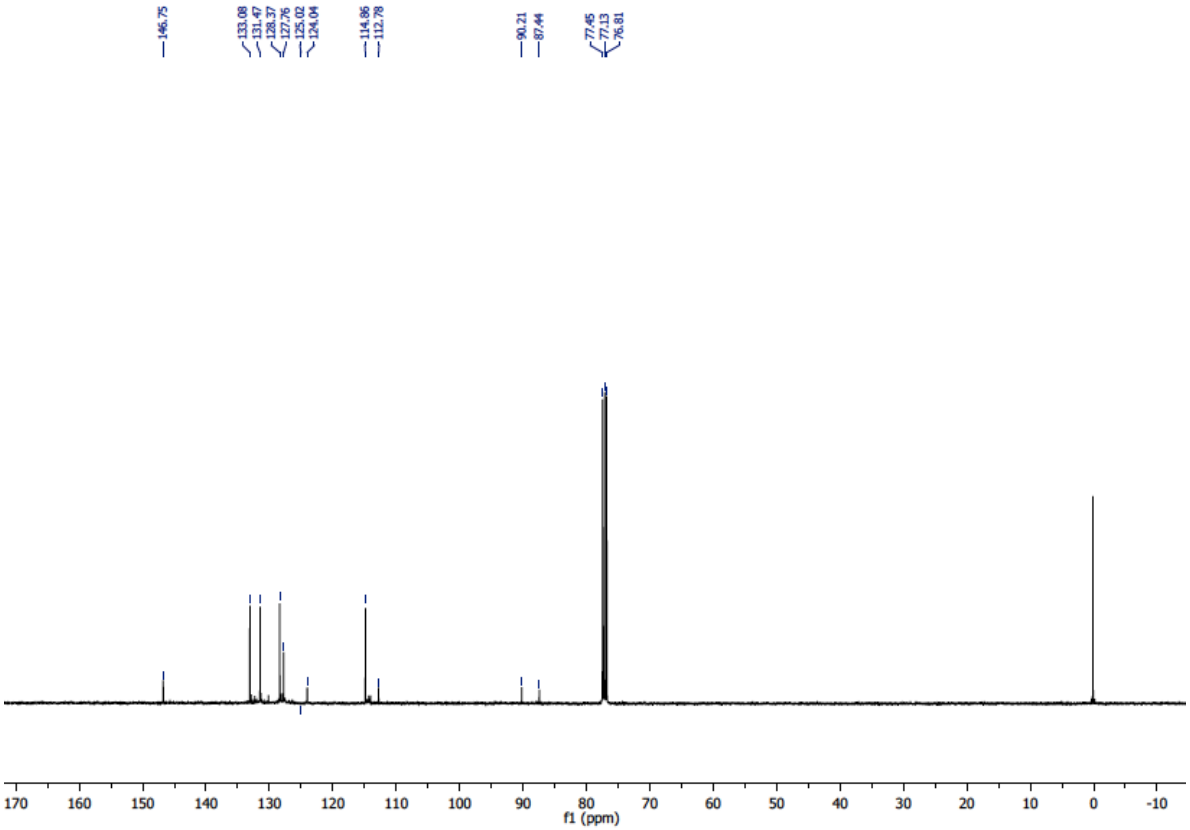
146.75
133.08
131.47
128.37
127.76
125.02
124.04
114.86
112.78
90.21
87.44
77.45
77.13
76.81
170 160 150 140 130 120 110 100 90 80 70 60 50 40 30 20 10 0 -10
f1 (ppm)

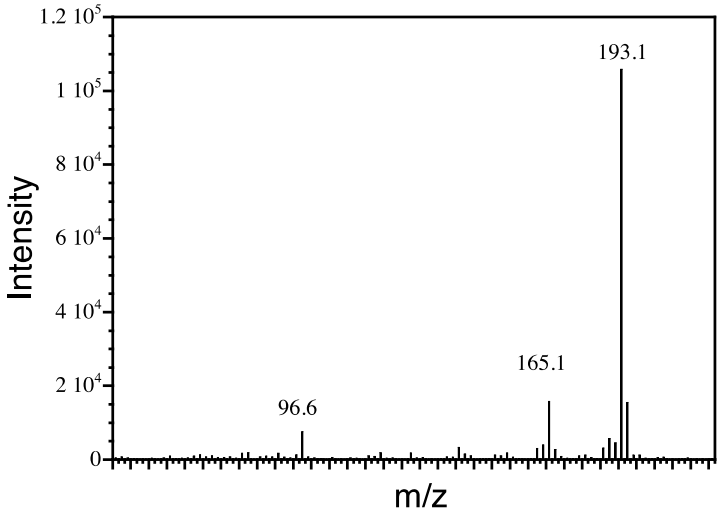
1.2 10^5
1 10^5
8 10^4
6 10^4
4 10^4
2 10^4
0
Intensity
193.1
165.1
96.6
m/z

1-nitro-4-(phenylethynyl)benzene (table 3.4, entry v)

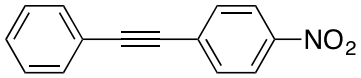

^{1}H NMR (400 MHz, $CDCl_3$): δ 8.24-8.21 (d, 2 H), 7.68-7.66 (d, 2 H), 7.58-7.55 (m, 2H), 7.41-7.39 (m, 3 H); ^{13}C NMR (400 MHz, $CDCl_3$): δ 146.92, 132.19, 131.77, 130.2, 129.2, 128.46, 123.57, 122.53, 122.04, 94.63, 87.5; HRMS calculated for C_{14} H_9NO_2: 223.0633, found: m/z= 223.1.

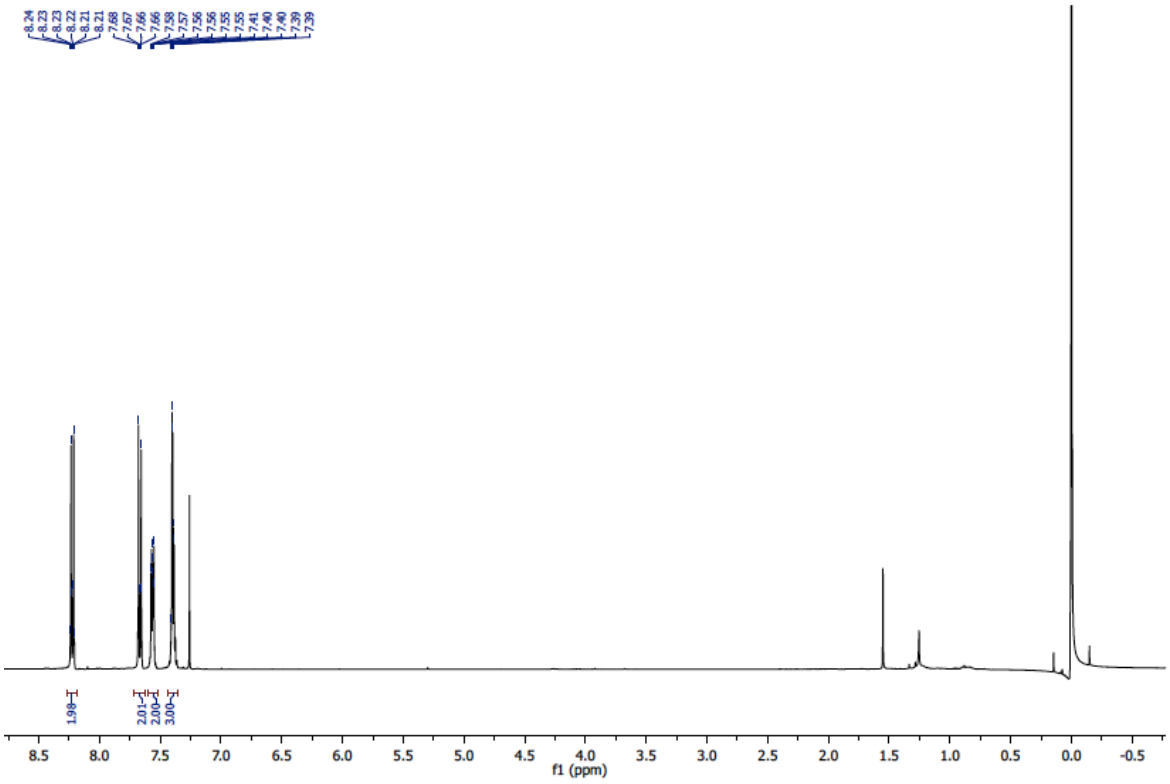

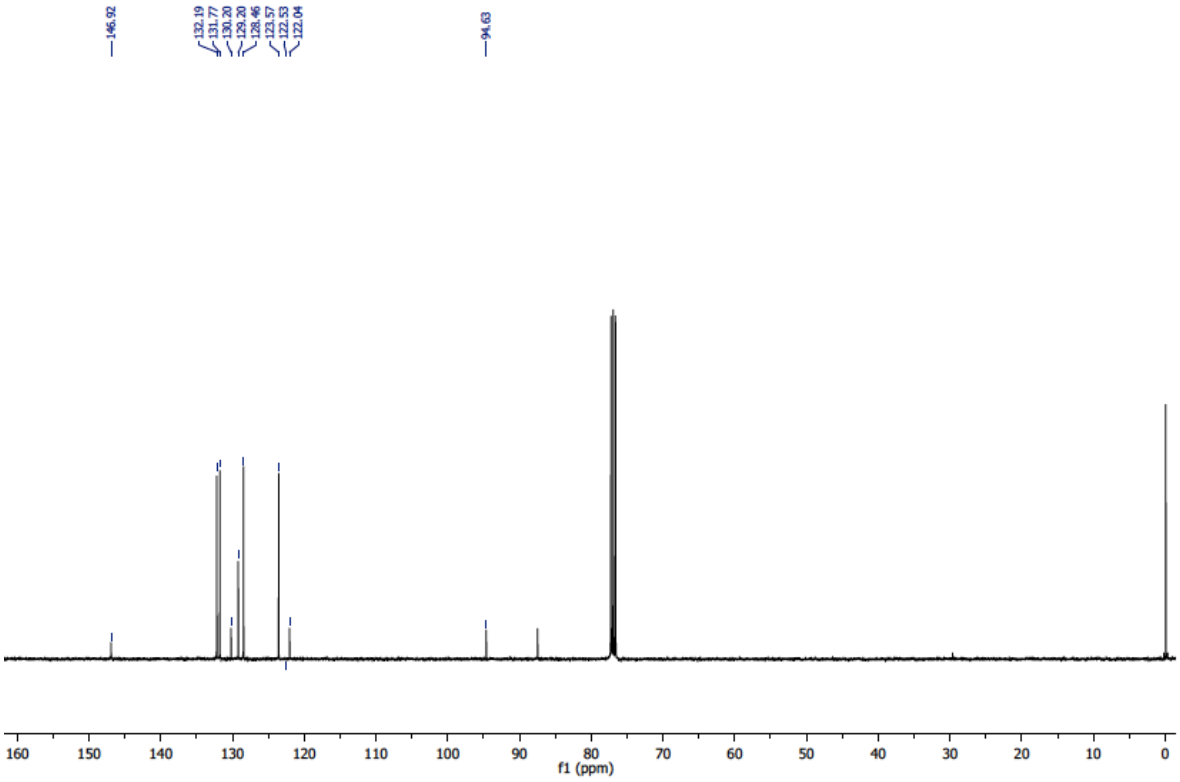
146.92
132.19
131.77
130.20
129.20
128.46
123.57
122.53
122.04
94.63
160
150
140
130
120
110
100
90
80
70
60
50
40
30
20
10
0
f1 (ppm)

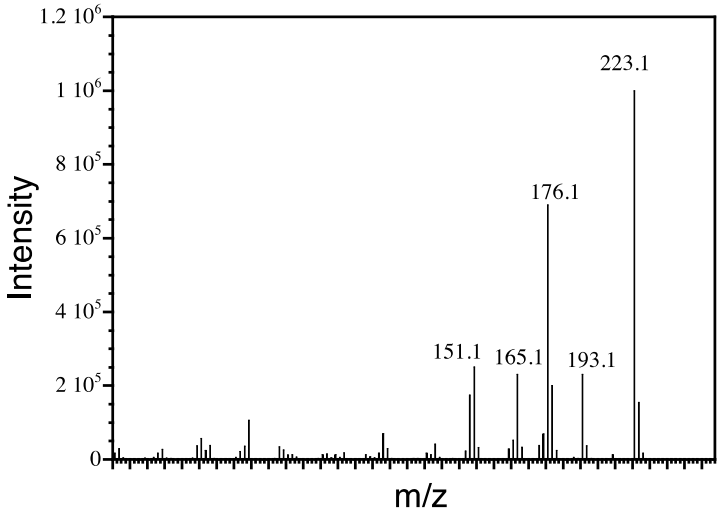
1.2 10^6
1 10^6
8 10^5
6 10^5
4 10^5
2 10^5
0
Intensity
223.1
176.1
151.1
165.1
193.1
m/z

2-(phenylethynyl) aniline (table 3.4, entry vii-xii)

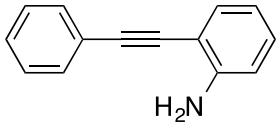

^{1}H NMR (400 MHz, $CDCl_3$): δ 7.53-7.51 (m, 2 H), 7.36-7.33 (m, 4 H), 7.32-7.24 (m, 1H), 6.73-6.69 (d, 2 H), 4.26 (s, 2H); ^{13}C NMR (100 MHz, $CDCl_3$): δ 147.56, 131.94, 131.25, 129.51, 128.16, 127.99, 123.11, 117.77, 114.12, 107.1, 94.47, 85.66; HRMS calculated for $C_{14}H_{11}N$: 193.0891, found: m/z= 193

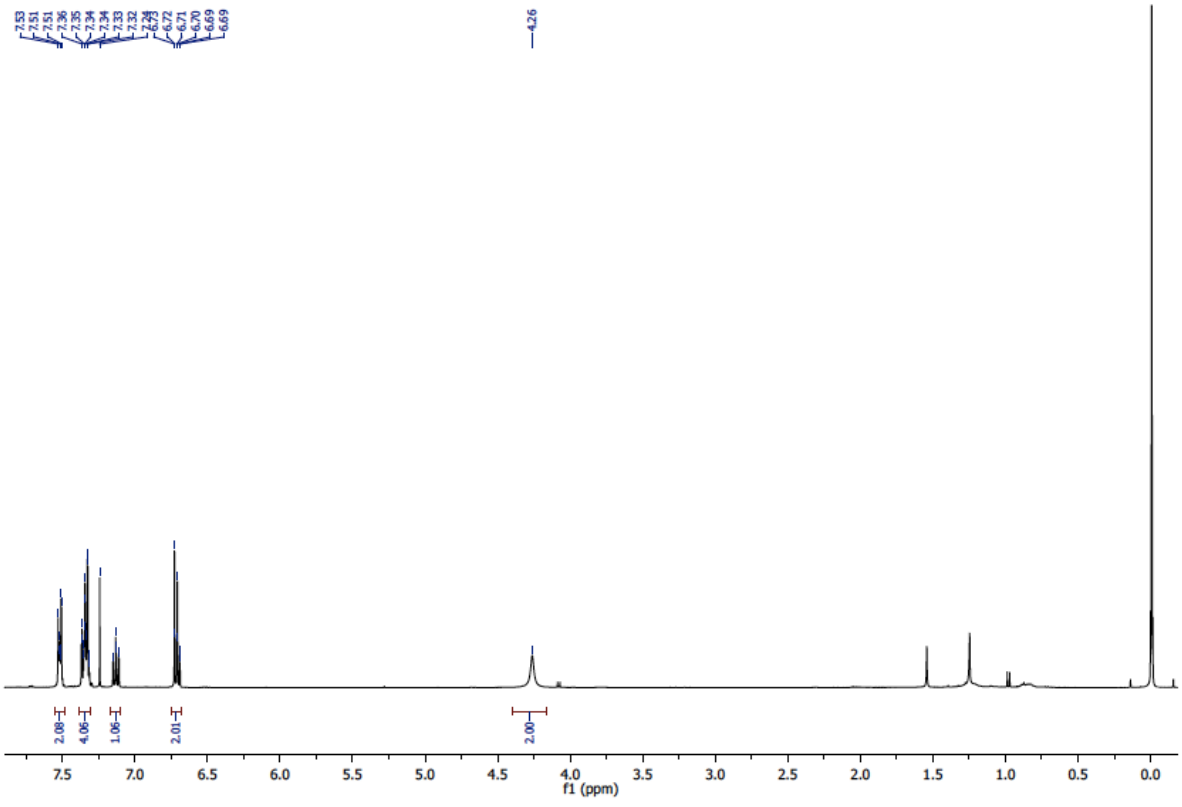

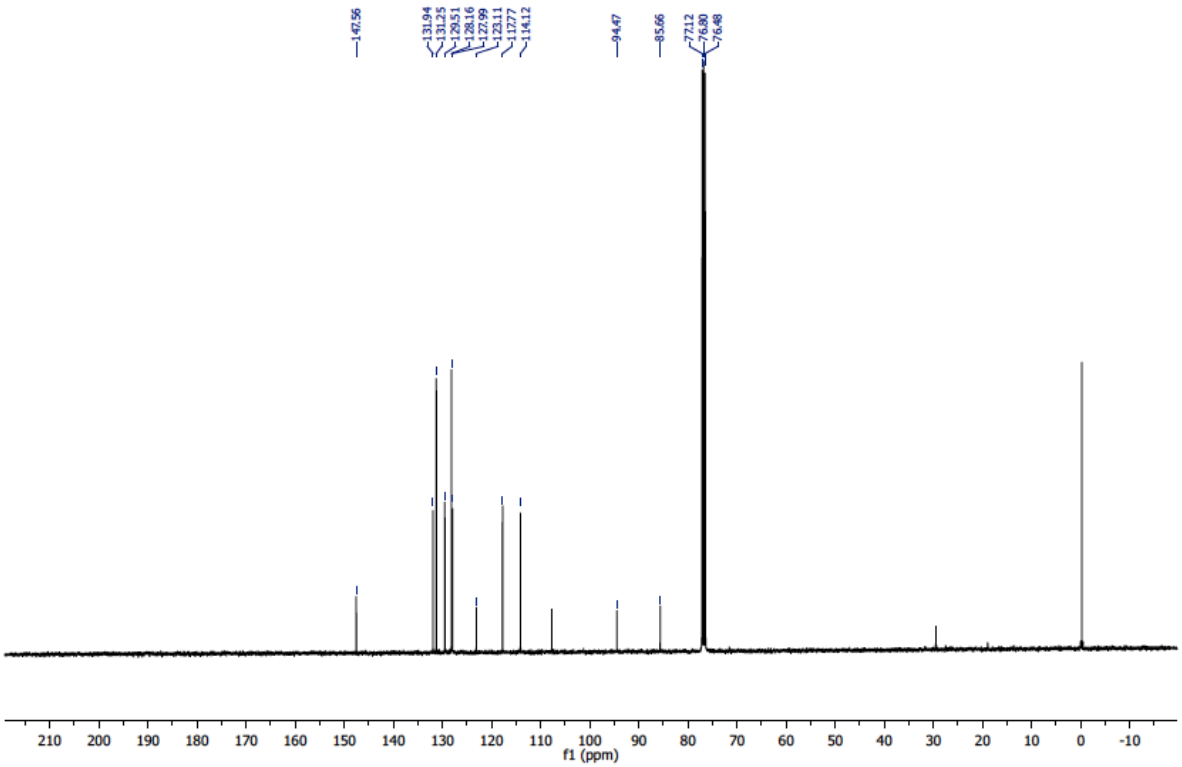
147.56
131.94
131.25
129.51
128.16
127.99
123.11
112.77
114.12
94.47
85.66
77.12
76.80
76.48
210 200 190 180 170 160 150 140 130 120 110 100 90 80 70 60 50 40 30 20 10 0 -10
f1 (ppm)

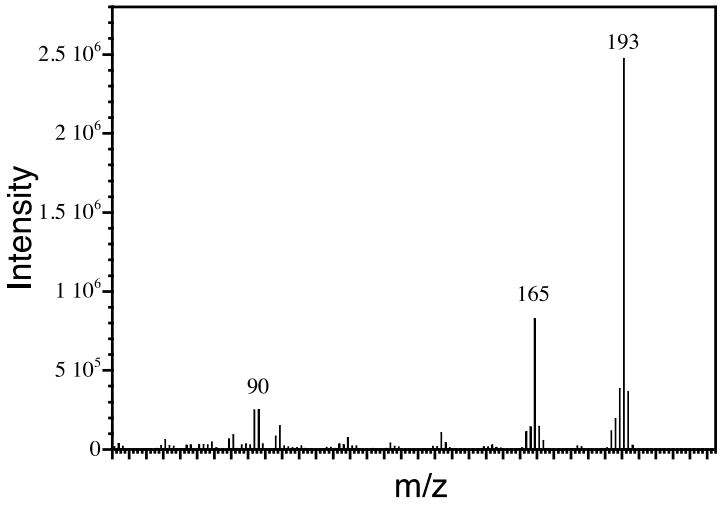
Intensity
2.5 10^6
2 10^6
1.5 10^6
1 10^6
5 10^5
0
193
165
90
m/z

1-methyl-2-(phenylethynyl)benzene (table 3.4, entry vi)

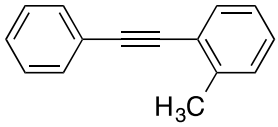

^{1}H NMR (400 MHz, $CDCl_3$): δ 7.56-7.54(m, 2 H), 7.52-7.50 (d, 1 H), 7.36-7.35 (m, 3H), 7.25-7.18(d, 2H) 7.17-7.16 (d, 1 H) 2.53 (s, 3 H); ^{13}C NMR (100 MHz, $CDCl_3$): δ 140.09, 131.74, 131.41, 129.36, 128.34, 128.25, 128.19, 128.06, 125.48,123.46, 122.93, 93.23, 88.23, 29.60, 20.64; HRMS calculated for $C_{15}H_{12}$: 192.0939, found: m/z= 192.2

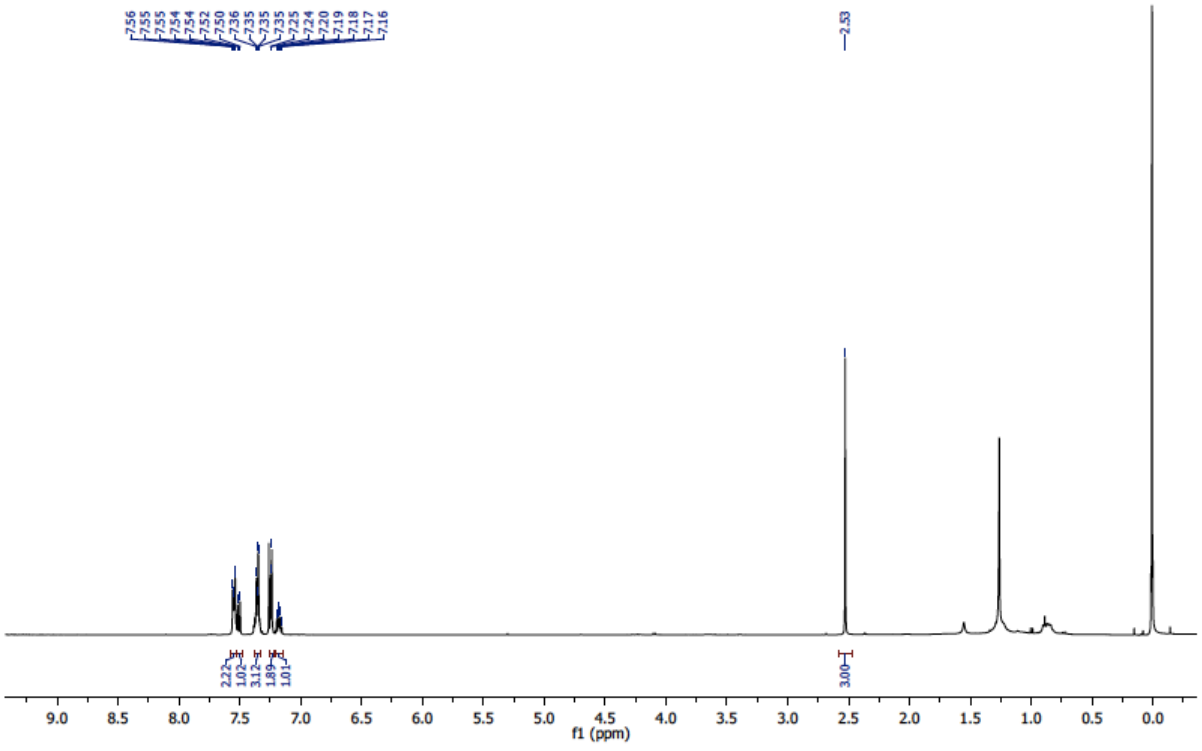

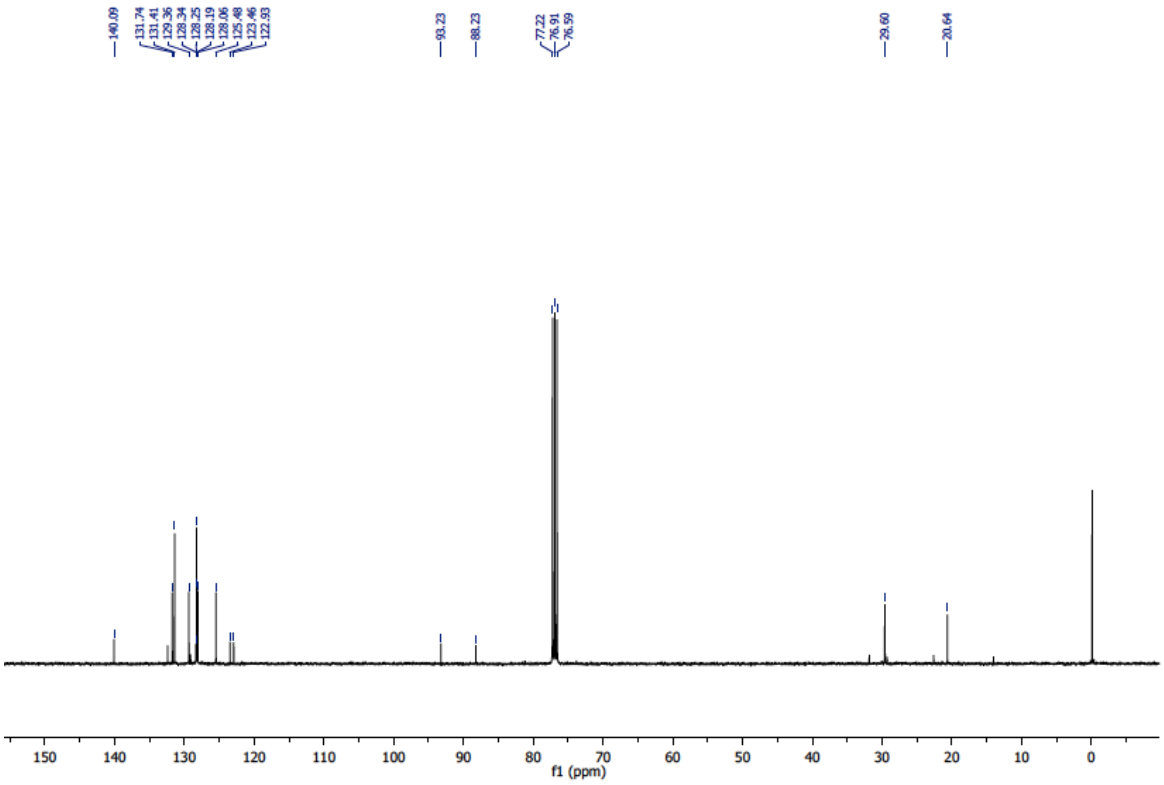
140.09
131.74
131.41
129.36
128.34
128.25
128.19
128.06
125.48
123.46
122.93
93.23
88.23
77.22
76.91
76.59
29.60
20.64
150
140
130
120
110
100
90
80
70
60
50
40
30
20
10
0
f1 (ppm)

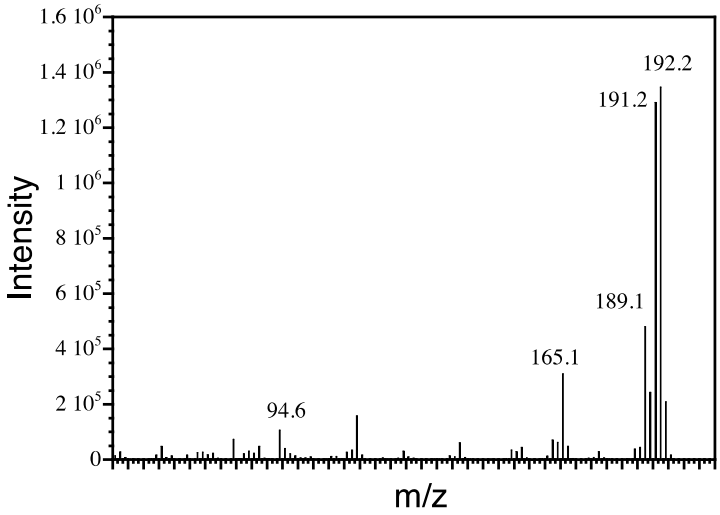
1.6 10^6
1.4 10^6
1.2 10^6
1 10^6
8 10^5
6 10^5
4 10^5
2 10^5
0
Intensity
192.2
191.2
189.1
165.1
94.6
m/z

1-(phenylethynyl)-4-(trifluoromethyl) benzene (table 3.4, entry viii)

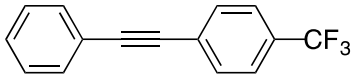

^{1}H NMR (400 MHz, $CDCl_3$): δ 7.62-7.57 (m, 4 H), 7.55-7.52 (m, 2 H), 7.36-7.33 (m, 3H); ^{13}C NMR (100 MHz, $CDCl_3$): δ 131.71, 131.66, 128.74, 128.36, 125.20, 125.16, 122.49, 91.67, 87.88; HRMS calculated for $C_{15}H_9F_3$: 246.0656, found: m/z = 246.1

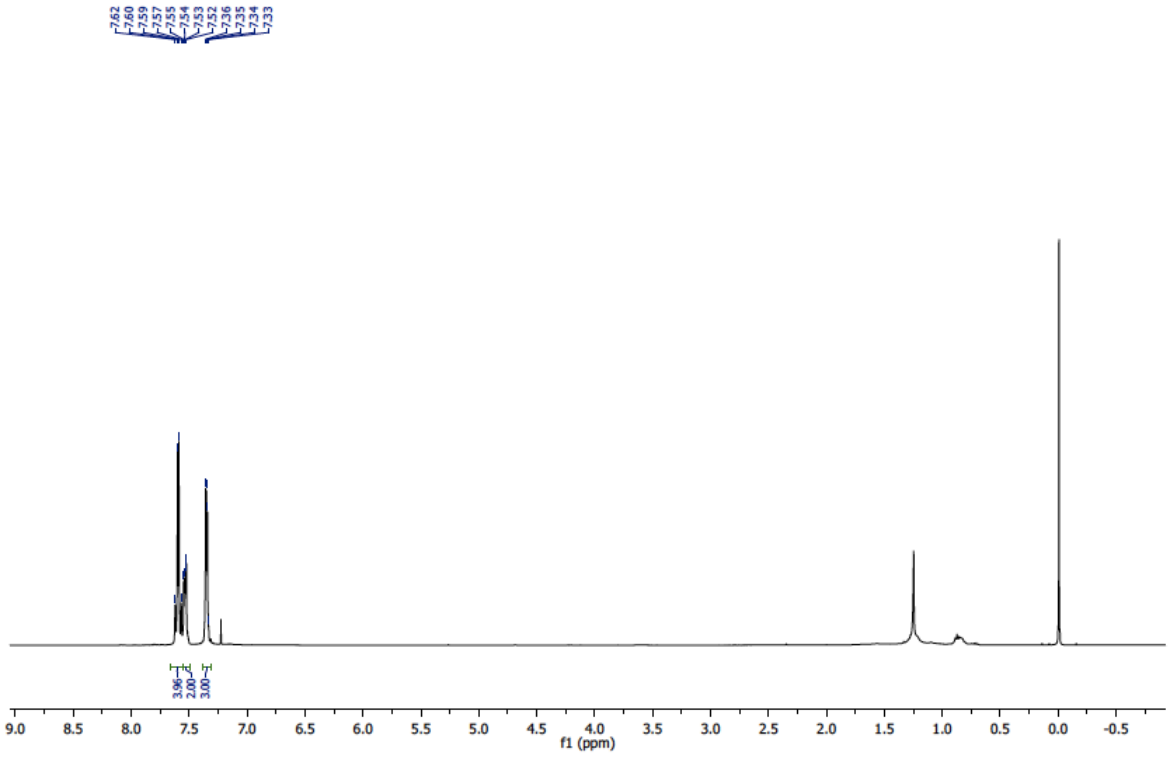

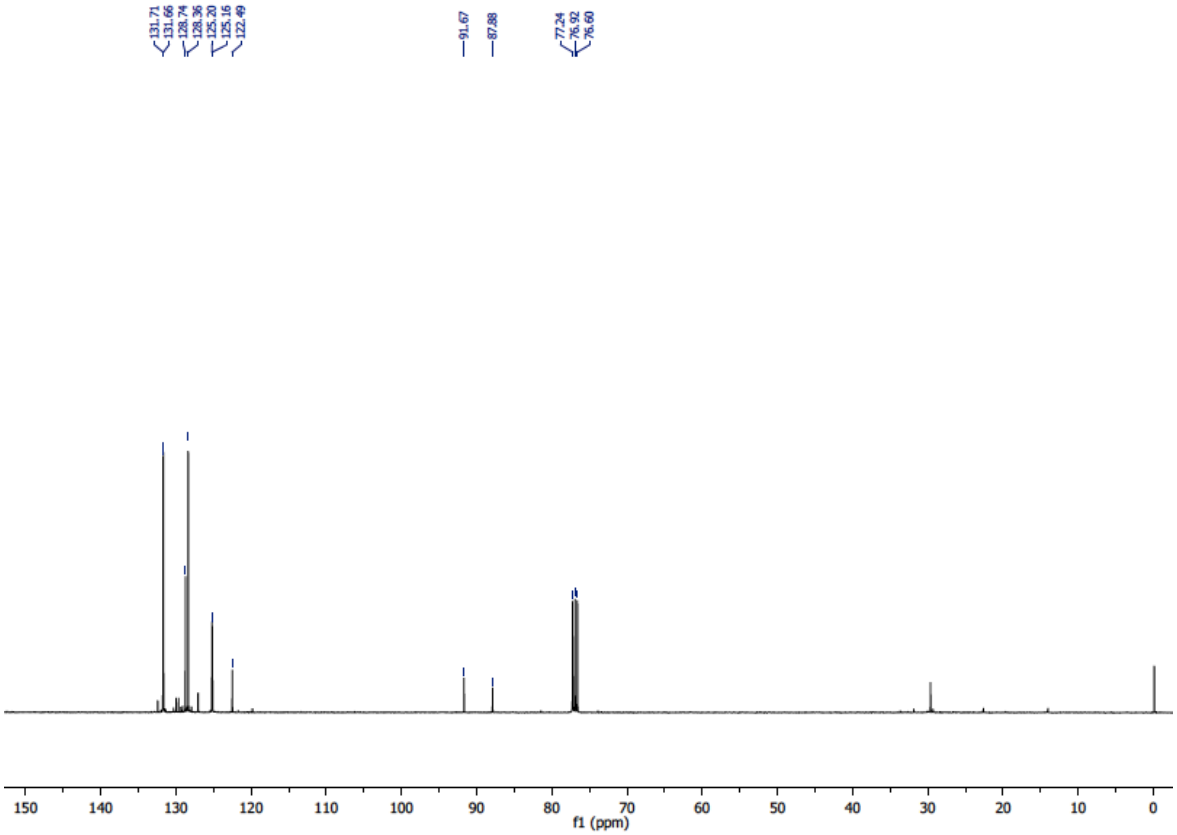
131.71
131.66
128.74
128.36
125.20
125.16
122.49
91.67
87.88
77.24
76.92
76.60
150
140
130
120
110
100
90
80
70
60
50
40
30
20
10
0
f1 (ppm)

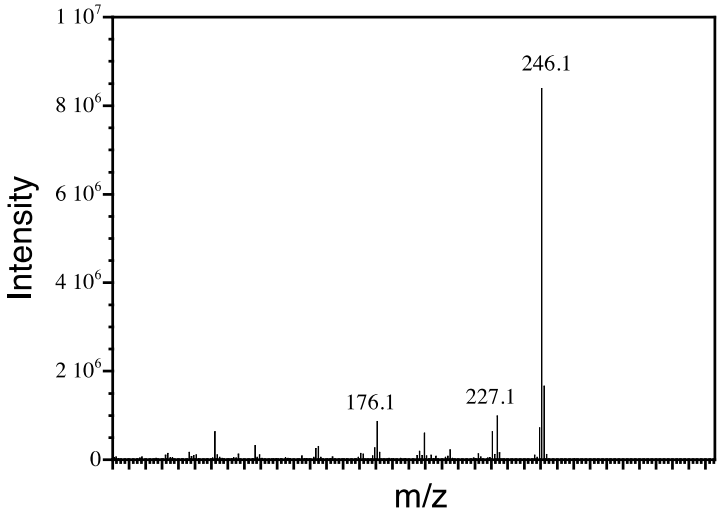
1 10^7
8 10^6
6 10^6
4 10^6
2 10^6
0
Intensity
246.1
176.1
227.1
m/z

Diphenylacetylene (table 3.4, entry ix)

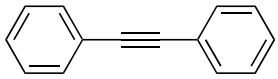

^{1}H NMR (400 MHz, $CDCl_3$): δ 7.55-7.52 (m, 4 H), 7.35-7.24 (m, 6 H); ^{13}C NMR (100 MHz, $CDCl_3$): δ 131.62, 128.35, 128.26, 123.29, 89.37; HRMS calculated for $C_{14}H_{10}$: 178.0783, found: m/z = 178.1.

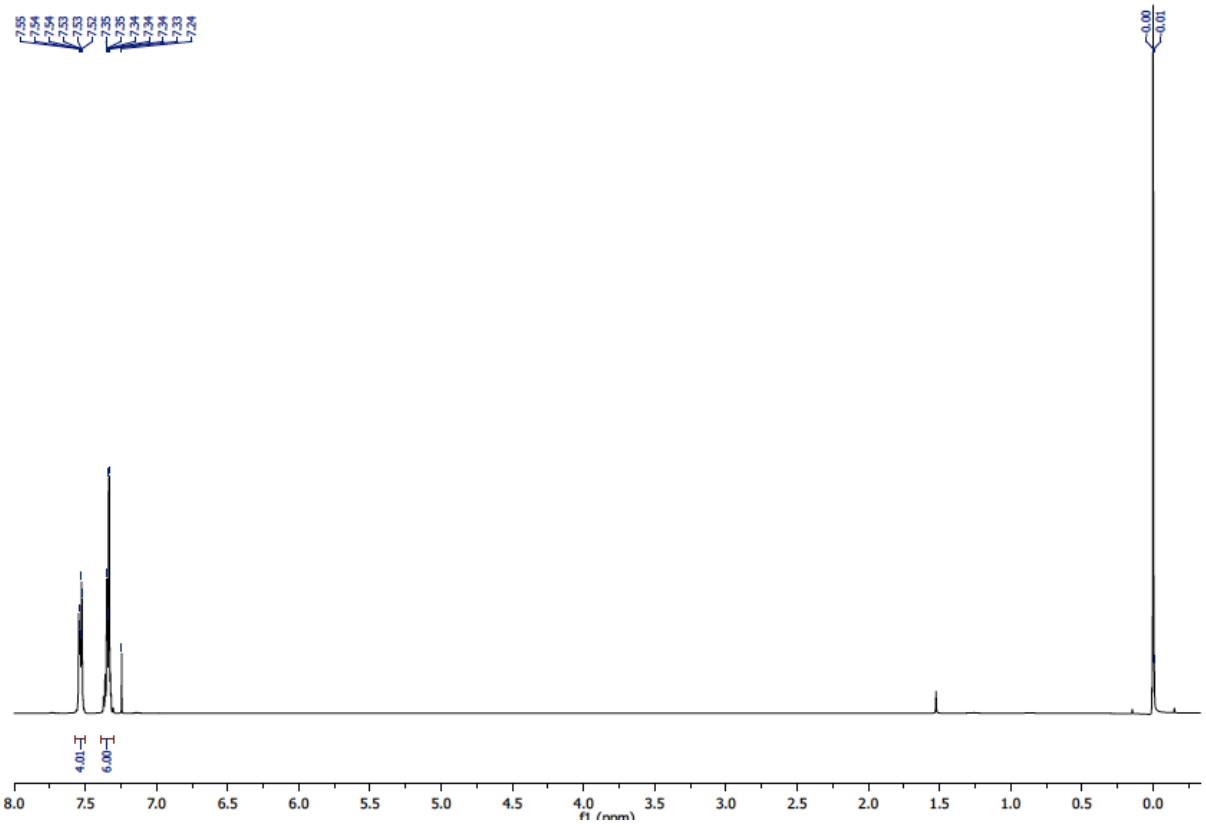

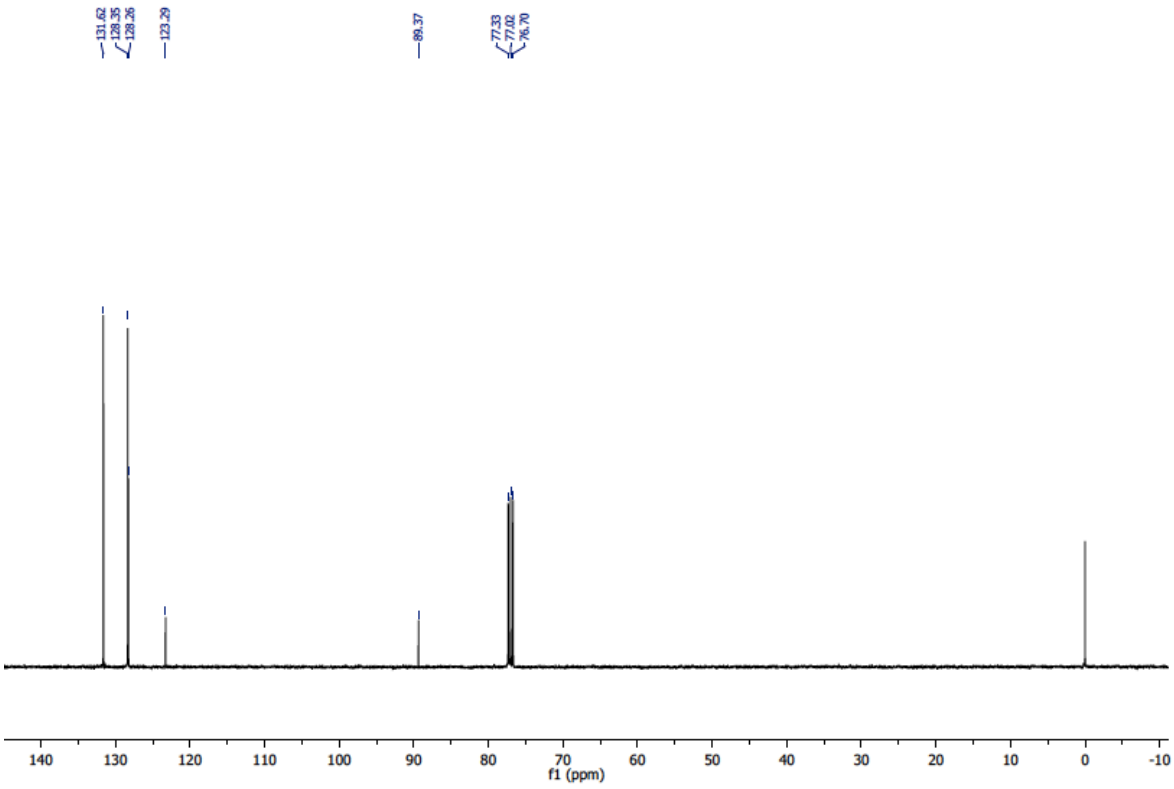
131.62
128.35
128.26
123.29
89.37
77.33
77.02
76.70
140
130
120
110
100
90
80
70
60
50
40
30
20
10
0
-10
f1 (ppm)

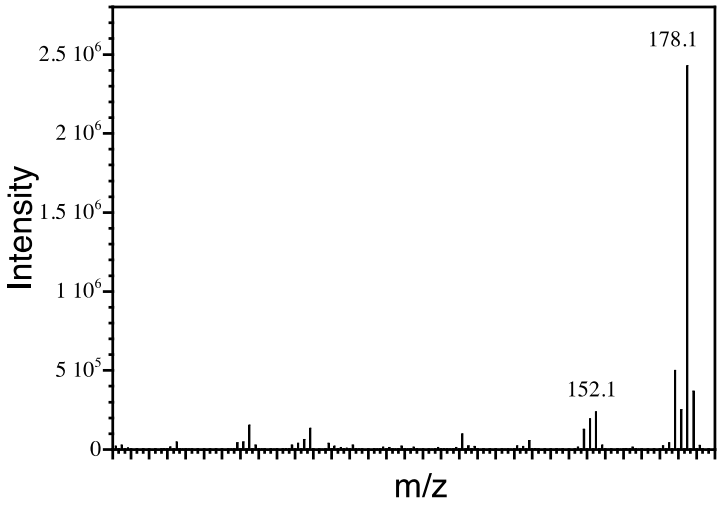
178.1
152.1
Intensity
m/z
2.5 10^6
2 10^6
1.5 10^6
1 10^6
5 10^5
0

1-methyl-4-(phenylethynyl)benzene (table 3.4, entry xiii)

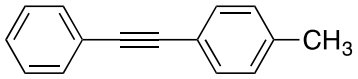

^{1}H NMR (400 MHz, $CDCl_3$): δ 7.54-7.52 (m, 2 H), 7.44-7.42 (d, 2 H), 7.36-7.32 (m, 3H), 7.17-7.15 (d, 2 H) 2.37 (s, 3 H); ^{13}C NMR (100 MHz, $CDCl_3$): δ 138.44, 131.60, 131.56, 130.75, 129.17, 128.97, 128.37, 125.30, 123.54, 121.6, 120.24, 89.61, 88.77, 21.57; HRMS calculated for $C_{15}H_{12}$: 192.0939, found: m/z= 192.1

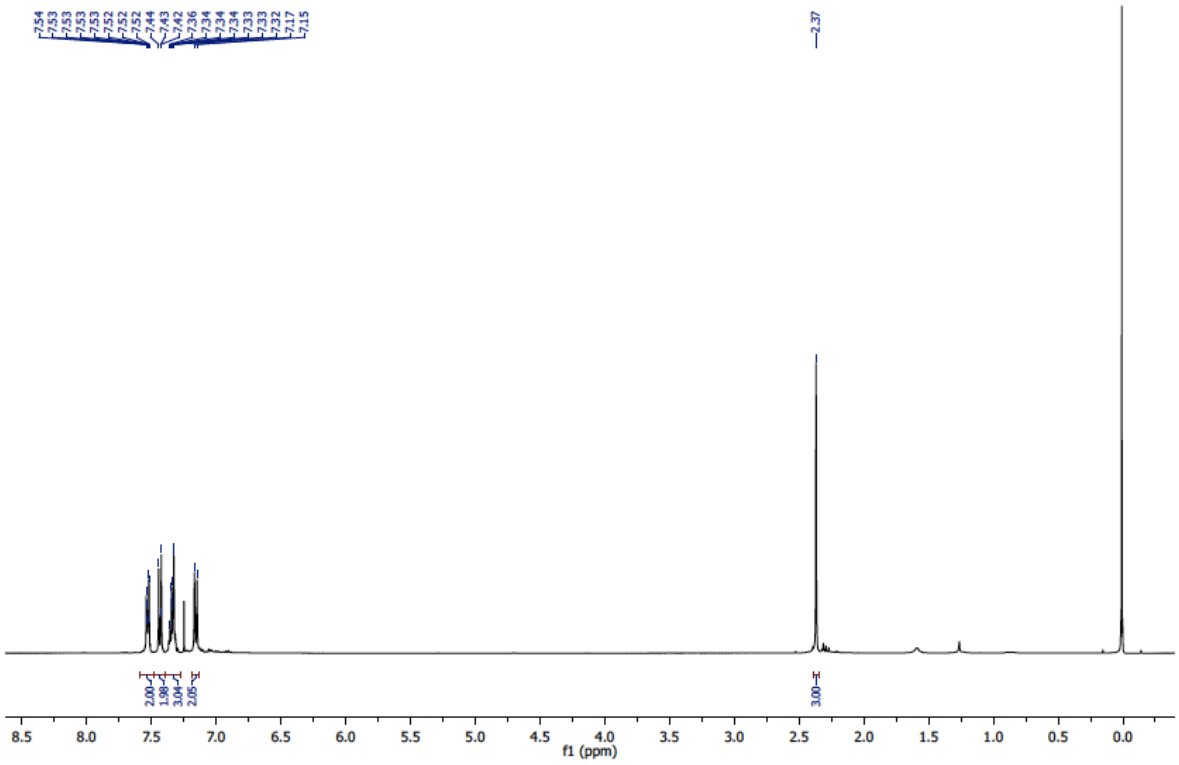

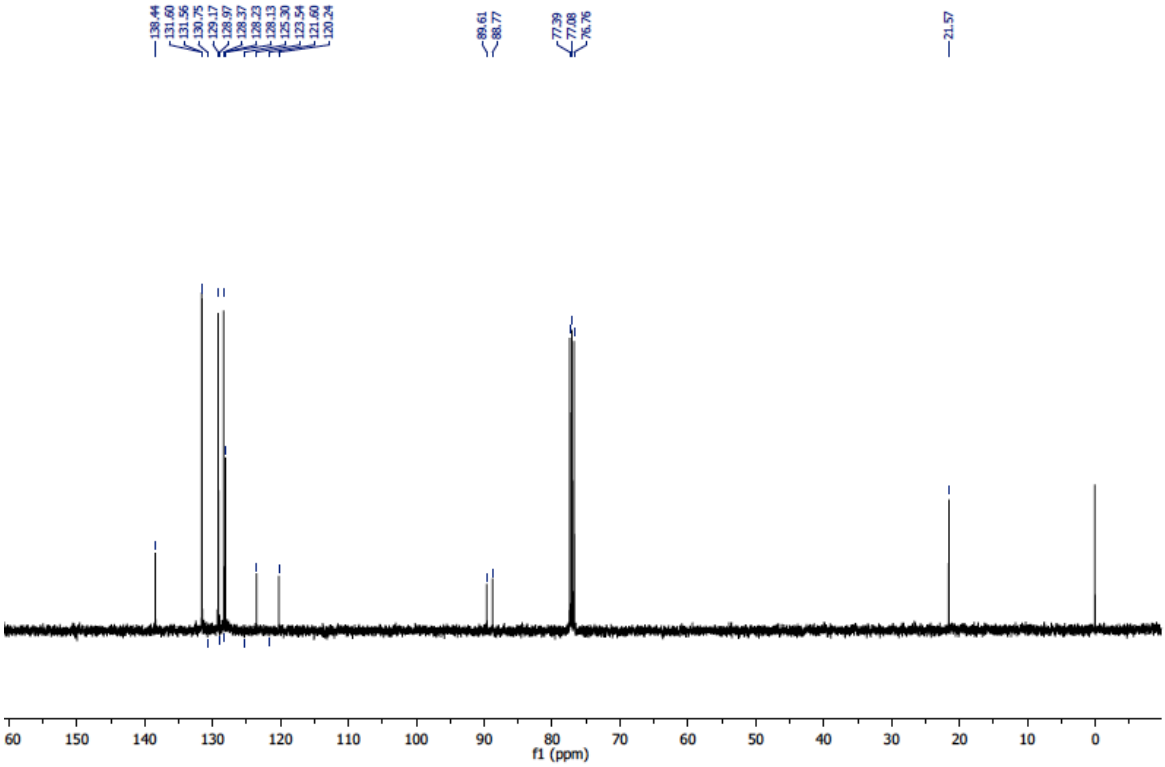
138.44
131.60
131.56
130.75
129.17
128.97
128.37
128.23
128.13
125.30
123.54
121.60
120.24
89.61
88.77
77.39
77.08
76.76
21.57
60
150
140
130
120
110
100
90
80
70
60
50
40
30
20
10
0
f1 (ppm)

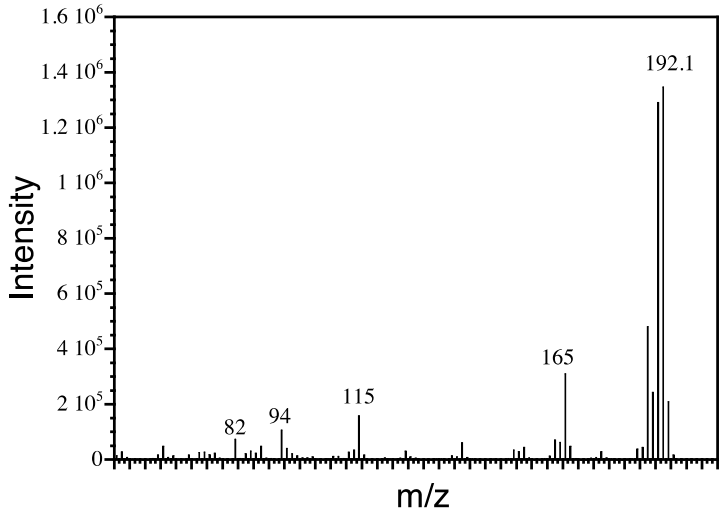
1.6 10^6
1.4 10^6
1.2 10^6
1 10^6
8 10^5
6 10^5
4 10^5
2 10^5
0
Intensity
192.1
165
115
94
82
m/z

5-chloro-1-phenyl-1-pentyne (table 3.4 entry xvi)

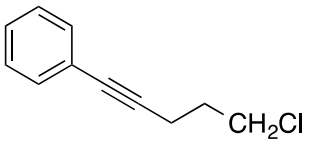

^{1}H NMR (400 MHz, $CDCl_3$): δ 7.41-7.40(m, 2H), 7.34-7.38 (m, 3H), 3.73-3.70 (t, 2H), 2.63-2.59(m, 2H) 2.09-2.03(m, 2H) ^{13}C NMR (100 MHz, $CDCl_3$): δ 131.64, 128.29, 127.84, 123.64, 88.12, 81.58, 43.80, 31.53, 16.93; HRMS calculated for $C_{11}H_{11}Cl$: 178.05, m/z found: 178.05

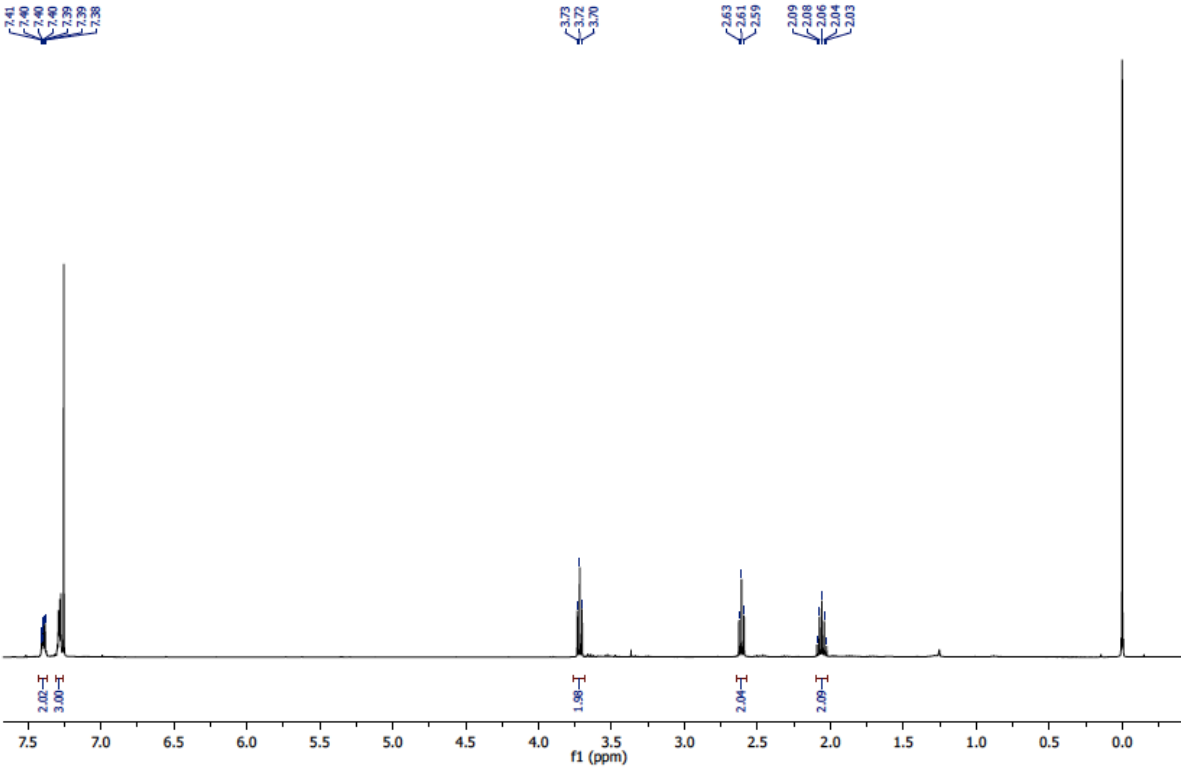

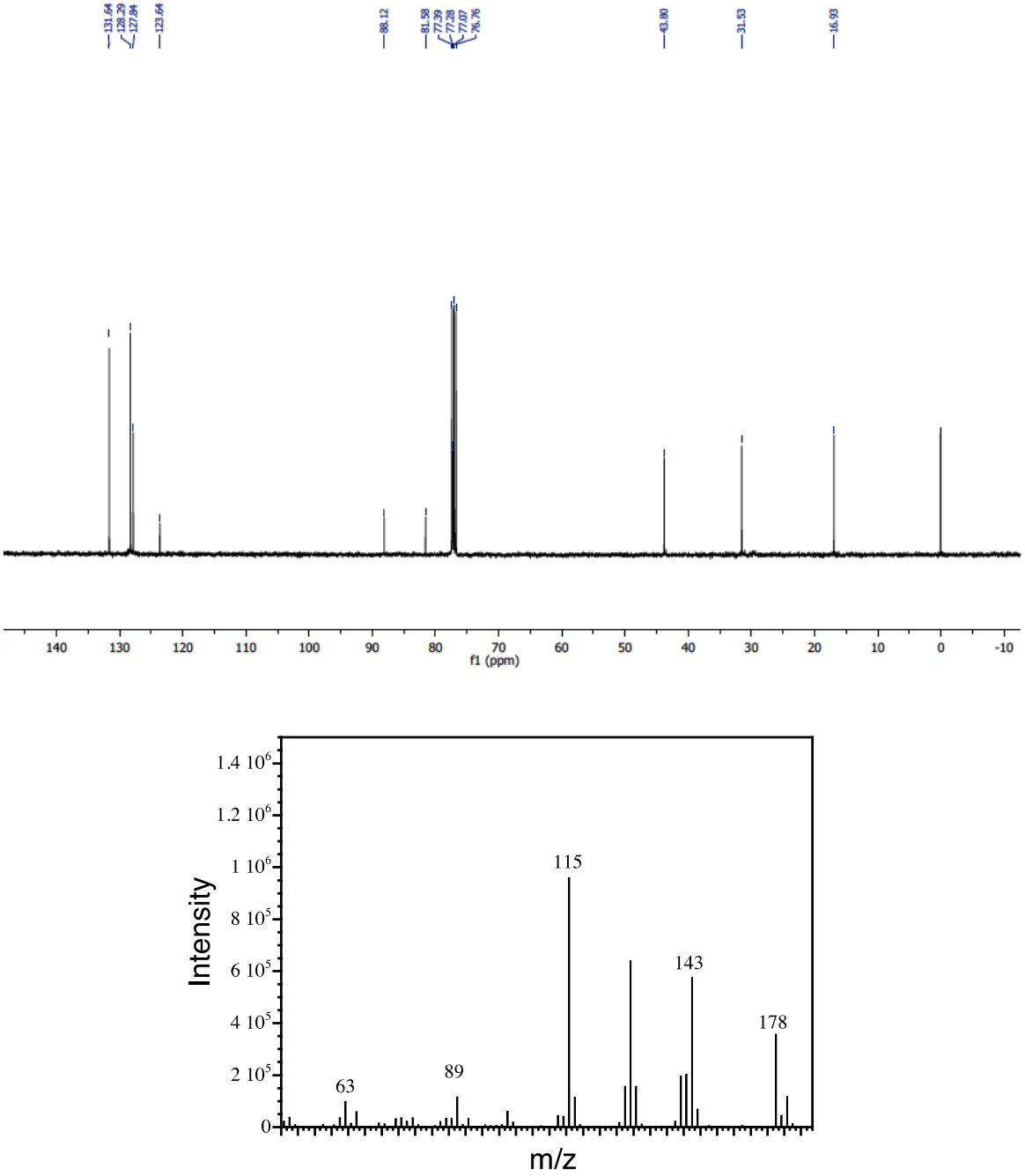

Figure S3.11. ^{1}H NMR (top) ^{13}C NMR (middle) and MS spectra (bottom)

This manuscript has been adapted from ACS Sustainable Chem. Eng. 2018, 6, 1717-1722 with permission, from the American Chemical Society. Small changes to the original manuscript provide consistent formatting and clarity with respect to the overall thesis.

3.4 Accompaniment to Chapter 3

This chapter describes the catalytic application of supported Pd nanoparticles toward Sonogashira coupling under very mild conditions. Study of the action spectrum confirms that direct excitation of PdNP is required to afford the desired product. Further, we found that the rate of the cross-coupling reaction is proportional to the light intensity. Thus, in this case light intensity can interfere with the product yields. This is in agreement with proposed mechanism of non-plasmonic PdNP and that is due to the population of light excited electrons at the Pd surface active sites.

The catalytic activity of Pd@TiO_2 drops down after the second cycle. Although no Pd leaching from the catalyst was detected, XPS studies suggest a change in the oxidation state of the Pd during the reaction. As reported in this Chapter, the poor performance of the catalyst in terms of recyclability can be restored using different reducing processes e.g. I-2959 and UVA light irradiation. Furthermore, mechanistic studies that include the role of the solvent and evaluation of the palladium oxidation state after each organic transformation (presented in Chapter 2 and Chapter 3 along with the study described in Chapter 4) led us to an innovative approach into recovering the photocatalytic activity of Pd@TiO_2. This approach is based on the reaction rotation methodology, explained in details in the next chapter.

4. Catalytic farming: reaction rotation extends catalyst performance

4.1 Preamble to Chapter 4

In the previous study, we demonstrated that Pd@TiO_2 photocatalyze the Sonogashira coupling under mild conditions in a short reaction time. The catalyst can be easily recovered from the reaction mixture by centrifugation while its reusability was limited to two cycles. TEM images did not show any big changes in the PdNP size. Furthermore, the leaching test (filtration test) along with the ICP-OES analyses of both, the reaction mixtures and solid catalysts after three catalytic cycles, confirmed no Pd leaching. Interestingly, XPS analysis showed changes in the oxidation state of the PdNP from one reaction cycle to the next one.

The research presented in this Chapter carries forward the concept of heterogeneous catalyst recovery and reusability, by incorporating sustainable recovery strategies based on alternating different photocatalytic reactions. The reaction rotation methodology is an innovative approach; it is extrapolated from the crop rotation system used in agriculture. This strategy is employed to reactivate the Pd@TiO_2 catalyst surface by restoring its oxidation state, a method that we called "*catalytic farming*". The selection of reactions in this approach is based on mechanistic studies that include the role of the solvent and the evaluation of the PdNP oxidation state after each reaction.

The catalytic farming concept defined the impact of this work by identifying a new sustainable methodology for reactivating the efficiency as well as the selectivity of heterogeneous catalysts. This strategy provided a platform for synthesis of valuable target molecules as a tool in reactivating catalysts. These features intensified the impact of this work –hence its publication in the flagship journal of the Royal Society of Chemistry. Also, the chemistry news magazine −ChemistryWorld− has highlighted it for its important insights.

4.2 Postprint Version of Manuscript

First published in: Chem. Sci., **2019**.10,1419-1425

ABSTRACT

The use of heterogeneous catalysis has key advantages compared to its homogeneous counterpart, such as easy catalyst separation and reusability. However, one of the main challenges is to ensure good performance after the first catalytic cycles. Active catalytic species can be inactivated during the catalytic process leading to reduced catalytic efficiency, and with that loss of the advantages of heterogeneous catalysis. Here we present an innovative approach in order to extend the catalyst lifetime based on the crop rotation system used in agriculture. The catalyst of choice to illustrate this strategy, Pd@TiO_2, is used in alternating different catalytic reactions, which reactivate the catalyst surface, thus extending the reusability of the material, and preserving its selectivity and efficiency. As a proof of concept, different organic reactions were selected and catalyzed by the same catalytic material during target molecule rotation.

INTRODUCTION

The industrial production of fine chemicals has led to the development of a plethora of different catalysts, many based on Pd complexes.[1] Although many industrial applications utilize homogeneous Pd complexes, heterogeneous Pd metal-based systems are finding their place among industrial processes. The advantages of heterogeneous systems over their homogeneous counterparts are related to the ease of separation and reusability of the materials. [2] Further, an increased interest in improved understanding of the catalytic activity of heterogeneous materials, has led to exciting developments in the field.[3] However, the deactivation of heterogeneous catalysts is a ubiquitous problem, yet to be resolved.[4] Particularly in the petroleum industry, many sacrificial oxidative or reductive processes are utilized in order to extend the catalytic activity, and in the

process to decrease the quantities of spent petroleum catalysts. [5] Our contribution deals with smaller scale production, as it may be applicable to pharmaceuticals, fine chemicals and high value added organic synthesis. We have previously reported on Pd-decorated TiO_2,[6, 7, 8] a versatile material that can be used for different organic transformations, showing variable catalyst longevity. In order to develop sustainable recovery strategies, we propose a strategy based on a reaction rotation methodology, a method we label Catalytic Farming due to its resemblance to agricultural practices. [9 10] As it is well-known in agriculture, the continuous use of the same crop can reduce the content of certain nutrients in the soil, thus reducing the soil yield. With crop rotation, farmers ensure that the nutrients leached or restored by one crop can be absorbed by the following one in the next growing season. The same idea can be extrapolated to catalysis: one reaction can deplete the catalyst of certain properties that can be restored by another reaction during the next catalytic cycle. The ability to reuse catalysts is consistent with the principles of green chemistry, which encourages the use of sustainable practices.[11]

RESULTS AND DISCUSSION

In this work, we demonstrate that rotating the catalytic processes to synthesize alternating target molecules achieves these goals. Just as retaining the properties and richness of the soil is key to agriculture, having a robust catalyst able to perform many catalytic cycles is essential for their efficient and prolonged application in organic synthesis.

Our choice of catalyst to illustrate our rotation strategy is palladium nanoparticles (~1.3 nm, 2 wt%) deposited on nanometric TiO_2 (Pd@TiO_2), predominantly in its anatase form, a catalyst that we have utilized for several organic transformations,[6, 7, 8] including C-C coupling reactions (Ullmann homo-coupling and Sonogashira coupling).[6, 7] These are among the examples we use to illustrate the catalytic farming concept, along with alkene isomerization (or hydrogenation)[8] also described in this contribution (Scheme 4.1). We based our reaction selection on previous mechanistic studies that include the role of the solvent and evaluation of the catalyst after each reaction. Thus, while catalytic Sonogashira reaction deteriorates rapidly with

usage –problem reaction–; catalytic Ullmann reaction shows great catalyst recyclability –plausible recovery reaction; as illustrated in Figure 4.1. Note that we use the word 'deterioration' rather than the more conventional 'poisoning'; the latter suggests contamination by some unwanted material, while deterioration seems a broader description, perhaps more suitable in this case where the results suggest that changes in the oxidation state of palladium (*vide infra*) may be behind the reduced catalyst performance.

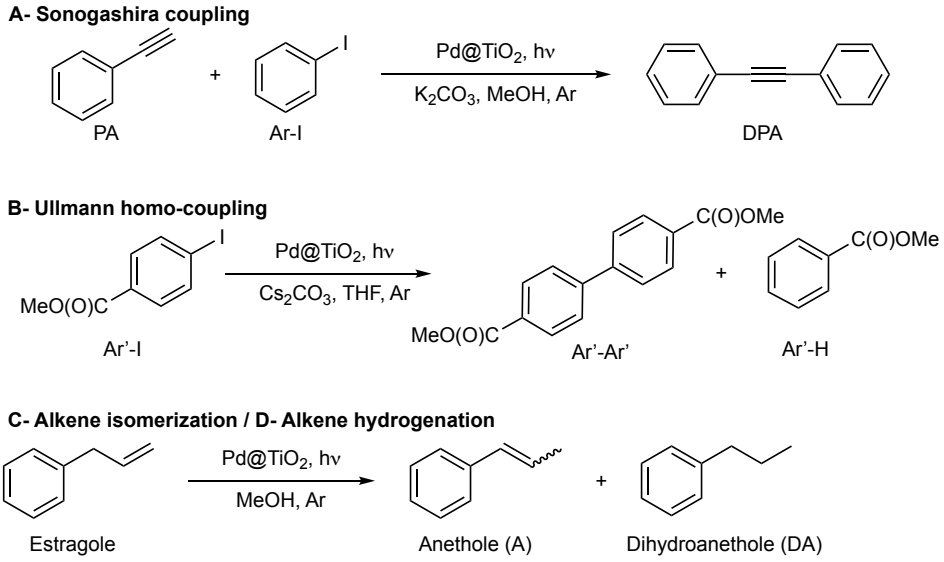

Scheme 4.1. Reactions used to demonstrate the catalytic farming concept. A- Sonogashira coupling is catalyzed by supported PdNP upon visible light irradiation in methanol (MeOH) and Ar atmosphere in the presence of base (K_2CO_3). B- Ullmann homo-coupling of methyl 4-iodobenzoate (Ar'-I) proceeds under UV-Vis light irradiation in the presence of catalyst ($Pd@TiO_2$) and base (Cs_2CO_3) utilizing tetrahydrofuran (THF) as solvent and Ar atmosphere. C- Alkene isomerization[8] of estragole can be carried out upon blue light irradiation of a methanolic suspension of $Pd@TiO_2$ under argon atmosphere. D. Alkene hydrogenation of estragole can be performed under the isomerization conditions by switching the light to UV light.

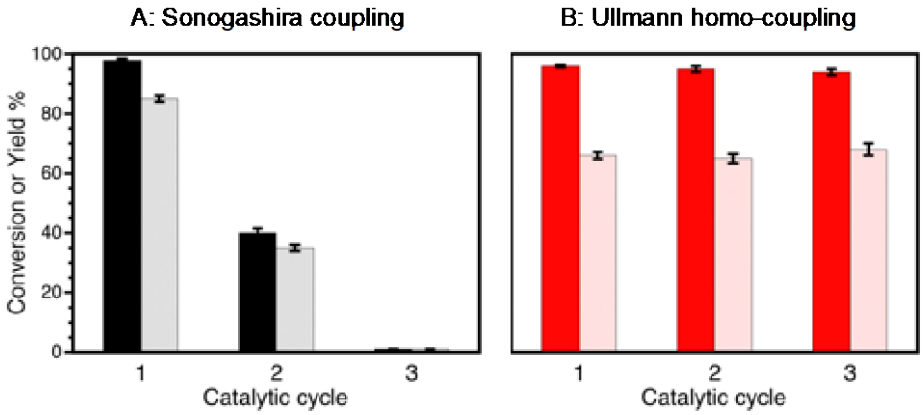

Figure 4.1. Conversions (dark bars) and yields (light bars) obtained after several catalytic cycles of reactions A and B in Scheme 1. While reaction A experiences a dramatic efficiency drop, reaction B can be catalysed with excellent conversions and yields for several catalytic cycles. Reaction conditions: A- Sonogashira coupling upon 450 nm irradiation at 2.7 W cm^{-2}, B- Ullmann homo-coupling upon 368 nm and 465 nm irradiation at 0.3 and 1.6 W cm^{-2}, respectively.

Inspired by the crop rotation process utilized in agriculture, we realized the importance of understanding the reaction mechanism as well as the properties of the catalytic material used. Mechanistically the reactions of Scheme 4.1 involve electron-hole charge separation when irradiated in the UVA region and direct excitation of the Pd nanoparticles when visible light is used (Scheme 4.2). Further details appear in earlier publications.[6, 7, 8] It is important to highlight that the solvents used for each reaction play an important role on the activity and reusability of this catalyst, actively participating in the reaction mechanism.

A closer look to Sonogashira reaction has shown[7] that the decreased catalytic performance indicated in reaction A (Scheme 4.1) is not due to the leaching of Pd species from Pd@TiO_2; in fact, ICP measurements revealed that >97% of the Pd is retained by the catalyst after three reaction cycles. Further, the reaction supernatant shows no catalytic activity after separation from the solid catalyst, reinforcing the heterogeneous nature of the reaction.[7] Material characterization showed that particle size is not altered during the catalytic processes.

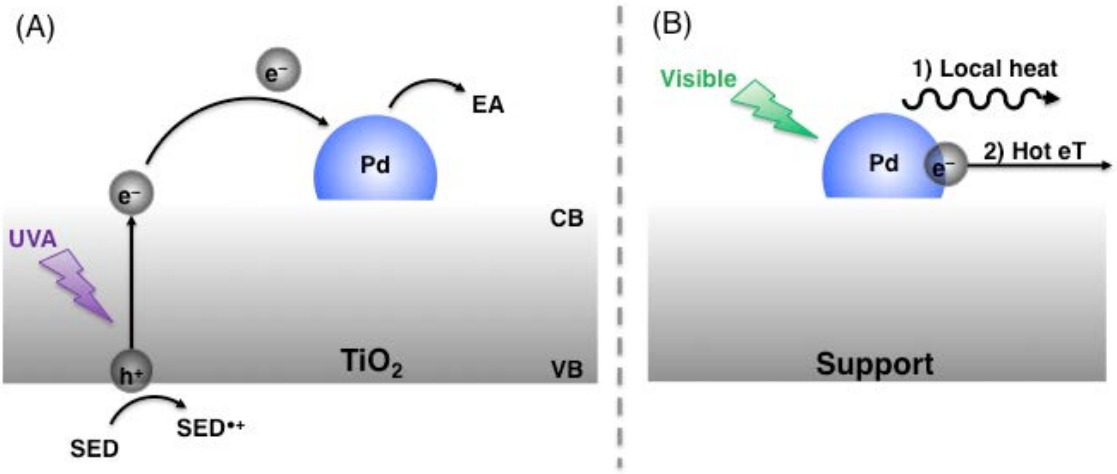

Scheme 4.2. Suggested mechanisms under UVA (A) or visible (B) irradiation. (A) Upon UVA excitation an electron is pumped from the valence band (VB) into the conduction band (CB) of the semiconductor (TiO_2). The electron can be trapped by the Pd nanoparticle attached to the surface slowing down the electron-hole recombination kinetics. Therefore, electron acceptor reagents (EA) can react more easily on the catalyst surface whereas a sacrificial electron donor (SED), frequently the solvent, quenches the hole. (B) Under visible light excitation, the generation of hot electrons on the Pd surface can photocatalyze reactions through (1) local heat generation or (2) hot electron transfer (eT), [12] the latter being the accepted mechanism for this type of non-plasmonic nanoparticles.

With all this in mind, we decided to perform XPS analyses of the materials. One can observe that the HR-XPS spectrum of Pd changes after the first cycle of Sonogashira reaction. These changes, illustrated in Figure 4.2A and 4.2B are consistent with changes in the oxidation state of Pd on the catalyst surface. For instance, XPS analysis of the fresh catalyst suggests the presence of PdO,[8] with a small contribution of more reduced palladium species. In contrast, more reduced Pd species are found after the first use of the catalyst for the Sonogashira reaction. This change accompanies the loss of activity after the first catalytic cycle. Interestingly, after performing the Ullmann reaction there is less contribution of the reduced Pd species, with less dramatic changes comparing to the fresh material (Figure 4.2C), consistent with the great reusability for this reaction. To our surprise, photochemical treatment with THF –the solvent used during Ullmann coupling– restores the oxidation state of Pd to almost the same as in the fresh material, Figure 4.2D. This is in agreement with our previous studies over thermal alkene isomerizations[8] utilizing the same catalyst, where we reported the oxidation of Pd

species during the catalytic reaction. We then described photocatalytic treatments performed over used Pd@TiO_2 catalyst with complete recovery of the catalyst efficiency.[7, 8] Thus, oxidation changes of the Pd surface provide a plausible rationalization for catalyst deterioration, reductive treatments –such as irradiation in the presence of a reductive benzoin photoinitiator (I-2959)– completely recovered the catalytic activity.[8]

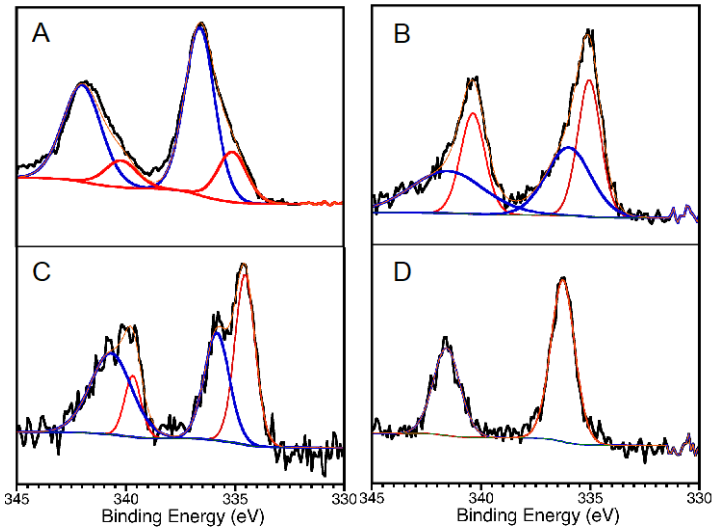

Figure 4.2. Pd 3d HR-XPS spectra for Pd@TiO_2 catalyst. A) Fresh catalyst: Pd 3d core-level spectrum deconvoluted by using two spin-orbit split Pd $3d_{5/2}$ and Pd $3d_{3/2}$ components centred at 336.6 eV and 342.0 eV and separated by ~5.4 eV; attributed to PdO.[8] Small contribution of more reduced palladium species are also found on the material (components at 335.1 eV and 340.2 eV). B) Catalyst after Sonogashira reaction: high contribution of more reduced species (spin-orbit components at 335.0 (336.0) eV and 340.4 (341.5) eV). C) Catalyst after Ullmann reaction: similar contribution of both oxidized and less oxidized species. D) Catalyst after Sonogashira reaction and post-treatment with THF: oxidation state of Pd restored to almost the same as in the fresh material (336.1 and 341.5 eV).

Considering these observations, we designed a series of different reaction rotations where one would expect the most efficient reactions (Ullmann C-C coupling) would help to improve the efficiencies of the poor ones (Sonogashira C-C coupling). After screening the reaction-rotation conditions –similar to what happens in agriculture– we found the right combination of reactions. Accordingly, rotation with Ullmann reaction remarkably improves the efficiency of the catalyst towards Sonogashira

coupling (Figure 4.3), with up to 80 % yield (1 h) after 6 catalytic cycles, Supplementary Table S4.1. Clearly the Ullmann reaction assists in maintaining the catalyst performance in the Sonogashira reaction. In the same series of experiments (see Supplementary Table S4.2) we show that it is not essential to always alternate the reactions, and that two of the same kind can be performed in sequence.

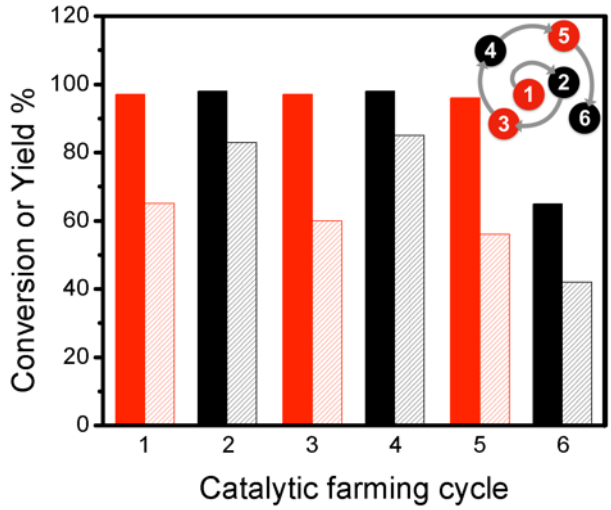

Figure 4.3. Conversions (dark bars) and yields (light bars) for catalytic farming of Pd@TiO_2 by rotation between Sonogashira coupling (black) upon 450 nm irradiation at 2.7 W cm^{-2} for 30 min and Ullmann homo-coupling (red) upon 368 nm and 465 nm irradiation at 0.3 and 1.6 W cm^{-2} for 1 h. Compare to Fig. 1A-B. The spiral at the top-right corner helps us visualize the sequence of reactions with the number representing the reaction sequence, and the colour the type of reaction. Similar spirals are included in other figures.

We were also able to establish that the catalytic farming strategy can be further expanded to additional reactions. Thus, reactions, such as alkene isomerization or hydrogenation, Scheme 4.1,[8] can contribute to the catalytic farming strategy while retaining catalyst performance. Accordingly, reaction C (or D) when run independently can be catalyzed with excellent conversions and yields for several catalytic cycles (Figure 4.4).

The addition of the isomerization reaction serves to illustrate the robustness of the reaction rotation strategy. While alkene isomerization does not restore the catalytic activity toward Sonogashira reaction, its inclusion in the catalytic farming process does not alter the performance of Sonogashira C-C coupling (Figure 4.5). In the cases of

Figure 4.5 it is clear that the Ullmann reaction plays an important role in extending the catalyst lifetime.

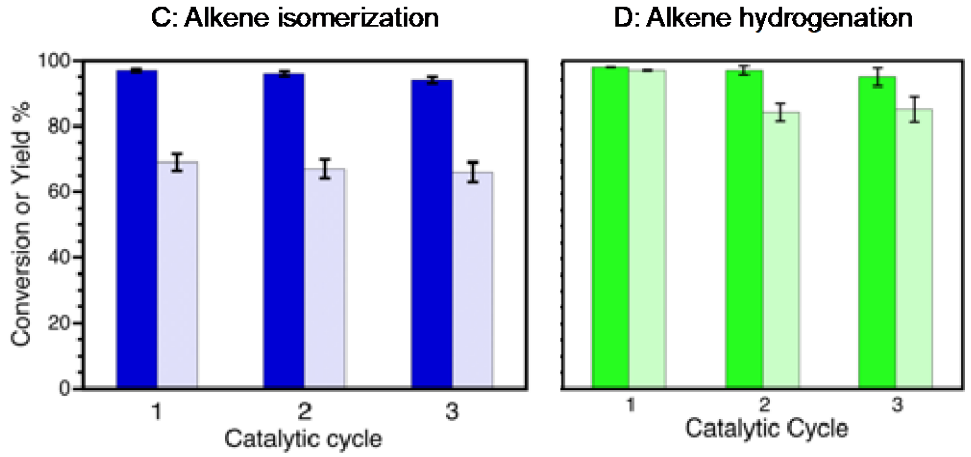

Figure. 4.4. Conversions (dark bars) and yields (light bars) obtained after several catalytic cycles of (C) alkene isomerization upon 450 nm irradiation at 2.7 W cm^{-2} and (D) alkene hydrogenation upon 368 nm irradiation at 0.3 W cm^{-2}. Notice that each catalytic cycle implies catalyst separation –cleaning cycles– before reusability test.

As already noted, alkene isomerization deactivates the catalyst towards Sonogashira coupling, Figure 4.5A, whereas Sonogashira coupling partially retains the catalyst activity towards alkene isomerization. Hence, in the crop rotation analogy, Sonogashira coupling cannot follow isomerization. Likewise, the alkene isomerization is drastically decreased if used as an in-between reaction (Figure 4.5 B), however this reaction does not affect the performance of Ullmann as a subsequent reaction (Figure 4.5 C). Further, Sonogashira coupling shows excellent reactivity in catalytic cycles 4^{th} and 5^{th} with excellent TON numbers (2,037 and 2,011 TON per Pd NP, respectively –See Supplementary Table S4.3–). Notice that the rotation outcome also depends on the irradiation conditions; hence, when using lower irradiation intensities, Sonogashira coupling is only partially deactivated by the alkene isomerization reaction (See Supplementary Table S4.4). Similar results are found when using alkene hydrogenation reaction (See Supplementary Table S4.5). Notice that under these conditions after 6 catalytic cycles, the Ullmann reaction no longer serves as a "catalyst recovery

treatment" and only THF treatment (vide infra) partially restores the Sonogashira reaction (See Supplementary Table S4.6).

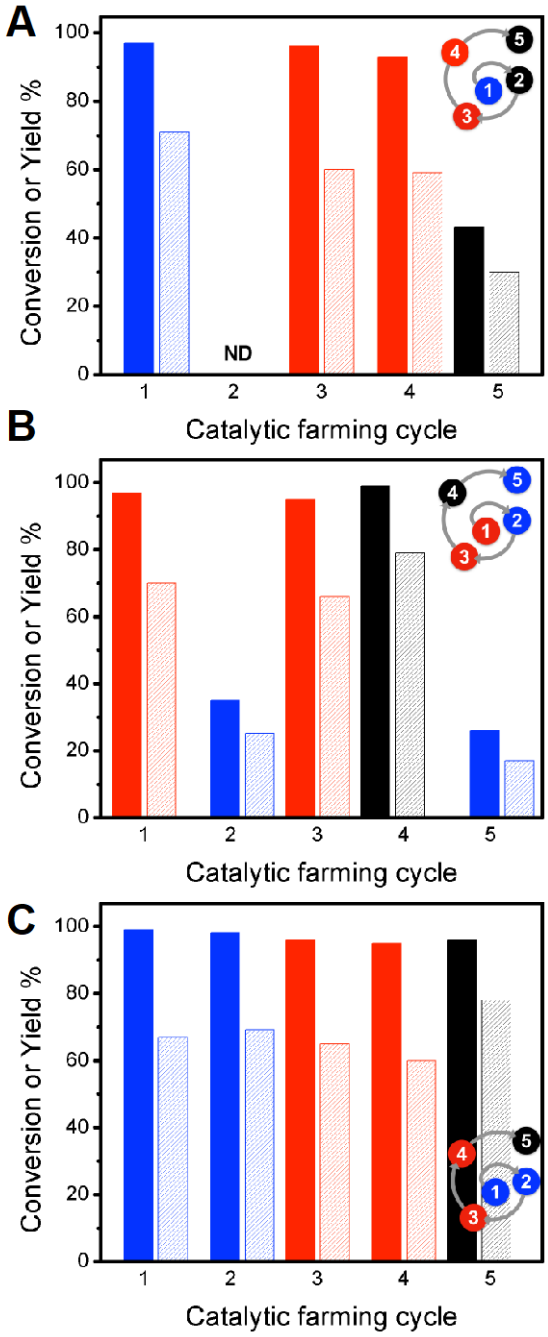

Figure 4.5. Conversions (dark bars) and yields (light bars) for catalytic farming of Pd@TiO_2 by rotation of three different reactions: Alkene isomerization (blue), Ullmann homo-coupling (red) and Sonogashira coupling (black). Alternating reactions rotations show different performance for each reaction. See Supplementary Table S4.3.

Table 4.1. Improvement of the catalytic activity of Pd@TiO_2 toward Sonogashira coupling after different reactions rotation.

Rotation	Cycle	% Yield	Rotation	Cycle	% Yield
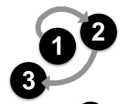	2	39	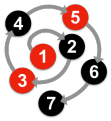	7	62
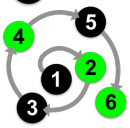	5	21	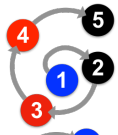	5	30
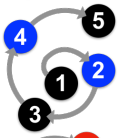	5	25	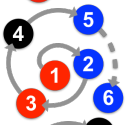	4	79
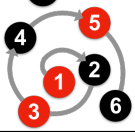	6	80	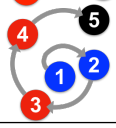	5	79

Alternating reactions rotations show different performance for each reaction. Sonogashira coupling (black), Ullmann homo-coupling (red), Alkene isomerization (blue) and alkene hydrogenation (green). See Experimental Section for reactions conditions.

A summary of the improvements achieved toward Sonogashira coupling using this reaction rotation strategy can be found in in Table 4.1. The concept of reaction rotation represents a paradigm shift in heterogeneous catalysis by bringing catalyst reuse and recovery in the area of fine chemicals much closer to the principles of green chemistry. In our case, the Ullmann reaction seems to play a critical role in retaining catalyst performance. However, if the Ullmann reaction does not result in desirable or value-added products, then it could be perceived as a sacrificial reaction with potential financial and environmental costs. This brings us back to the practices of organic farming, where similar scenarios can be encountered. In agriculture in some cycles of crop rotation, a "cover crop" is cultivated with the sole objective of protecting and enriching the soil; a typical example is clover.[13] Similar practices can be implemented in catalytic farming, for example Pd@TiO_2 can be irradiated with UVA-blue light in THF, converting some of the THF to dihydrofuran and hydrogen and in the process restoring the catalyst (Figure 4.6); clearly the same is achieved with the Ullmann reaction (Scheme 4.1). The choice between Ullmann chemistry or a recovery treatment (the

"cover crop" in agriculture) would ultimately be made on the basis of market demands and business practicality, parameters that should be considered on a case-by-case basis. Thus, there is no need of a sacrificial cycle if one step in the rotation offers limited or no benefit.

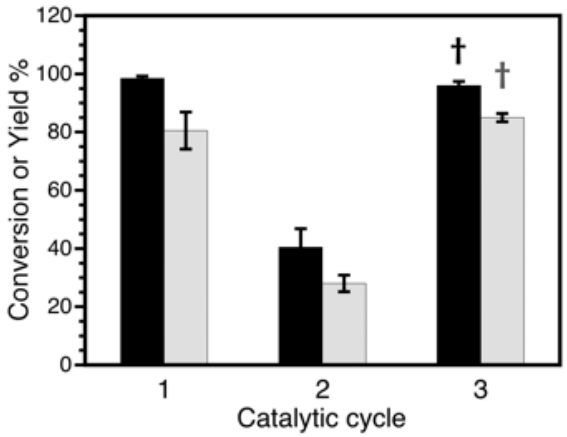

Figure 4.6. Conversions (black) and yields (grey) obtained after 3 catalytic cycles for Sonogashira coupling. Cycle 3 shows the recovery of catalytic activity after THF treatment (†). Compare with cycle 3 in Figure 1A and Supplementary Table S4.10.

In summary, we propose a paradigm shift that calls for reaction rotation in heterogeneous catalysis as a strategy to enhance catalyst longevity. We define this practice (catalytic farming) in the following terms: Target product rotation is the practice of performing a series of dissimilar or different types of catalytic processes using the same catalyst in sequenced reactions. It is done so that the catalysts are not deactivated by a fixed set of reactants. It helps in reducing catalyst deterioration and increases longevity and product yield.

The set of reactions, catalyst, and rotation sequence will depend on the synthetic goals of a given laboratory or organization. Once again, the analogy with agriculture is very enlightening. When 16 farmers in one region were asked to provide their favourite crop rotation strategy, they provided 16 different answers, where some crop rotations make frequent appearances (rye, alfalfa, garlic).[14] Just as in chemistry, there is no perfect rotation sequence, as external parameters must be considered, including the usefulness of the crop or target product, and in our case, consideration that one reaction

may play a key role in maintaining catalyst ("soil") performance. Therefore, different laboratories may create rotation sequences that meet their needs, involving some reactions included mainly for catalyst reactivation, such as the catalyst irradiation in THF in the case above.

EXPERIMENTAL SECTION

Materials

Unless otherwise specified, all chemicals were purchased from Sigma-Aldrich or Fisher Scientific and used without further purification. Titanium dioxide (TiO_2-P25) was purchased from Univar Canada. All solvents were of HPLC grade.

Instrumentation

Transmission electron microscopy (TEM) images were collected on a JEM-2100F FETEM (JEOL) operating at 200 kV. The Pd content of the catalysts was determined by Inductively Coupled Plasma Optical Emission Spectrometry (ICP-OES), using Agilent 5110 ICP-OES instrument. Approximately 10 mg portions were accurately weighed in triplicate and digested with aqua regia. Solutions were further diluted and measured by ICP-OES. The Pd 340.458 nm emission line was used for quantification. The XPS spectra were measured on a Kratos Nova AXIS spectrometer equipped with an Al X-ray source. The XPS data were collected using AlKα radiation at 1486.69 eV (150 W, 15 kV), charge neutralizer and a delay-line detector (DLD) consisting of three multi-channel plates. Binding energies are referred to the C1s peak at 284.8 eV. XPS data was analyzed using CasaXPS software, Version 2.3.15 and all fittings obtained using a Gaussian 30% Laurentian and a Shirley baseline. UV irradiation used for catalyst synthesis was performed in a Luzchem photoreactor equipped with UVA lamps (typically operated with 14 lamps, corresponding to ~0.029 Wcm^{-2} with ~4% spectral contamination. Light-emitting diodes (centered at 368 and 465 nm, respectively) of 10 W from LedEngin and Luzchem LED illuminator (LEDi) equipped with a head of seven powerful blue LEDs (centered at 450 nm) with adjustable intensity at focal point were used as described for the photocatalytic reactions studied. Quantification was carried out in a Perkin Elmer, Claurus Gas Chromatograph coupled to a Flame Ionization Detector

(FID) and a DB-5 column (30 m length, 0.320 mm diameter, 0.25 μm film) using Ar as a carrier gas and t-Butyl benzene as external standard. GC-MS analyses were performed on an Agilent 6890-N Gas Chromatograph with an Agilent 5973 mass selective detector calibrated with acetophenone.

Catalyst synthesis

Palladium nanoparticles (~2wt%) supported on TiO_2 (Pd@TiO_2), were prepared by photodeposition of PdNP onto TiO_2 (P25) and fully characterized as described in our previous report.[8]

Sonogashira C-C coupling

Visible light-induced Sonogashira C-C coupling was performed as described in our previous report.[7] In brief, 15 mg of Pd@TiO_2 were dispersed in 4 mL of HPLC grade methanol (MeOH) in a 10 mL clean tube, then 15 μL of iodobenzene (1 eq., 0.13 mmol), 18 μL of phenylacetylene (1.3 eq., 0.16 mmol) and 35 mg of K_2CO_3 (2 eq., 0.26 mmol), were added. The reaction mixture was purged with Ar for 15 min then irradiated with 1x 465 nm LED set up at 1.6 W cm^{-2} for 5 h (or 7x 450 nm LEDs set up at 2.7 W cm^{-2} for 30 min) under continuous stirring. The solid catalyst was separated by centrifugation. Quantification was done by GC-FID using t-butyl benzene as an external standard (See Supplementary Table S4.7).

Alkene isomerization/hydrogenation

Visible light-induced isomerization (or hydrogenation) of estragole was performed with slight modifications to our previous report.[7] In brief, 15 mg of Pd@TiO_2 were dispersed in 4 mL of HPLC grade MeOH in a clean quartz cuvette, then 25 μL (0.16 mmol) of estragole were added. The reaction mixture was purged with Ar for 15 min and then irradiated with 7 x 450 nm LEDs set up at 2.7 W cm^{-2} for 5 h under continuous stirring (or with 1 x 368 nm LED set up at 0.3 W cm^{-2} for hydrogenation). The progress of the reaction was monitored by GC-MS. The quantification was done by GC-FID using t-butyl benzene as an external standard (See Supplementary Table S4.8).

Ullmann homo-coupling

Light-induced Ullmann homo-coupling of methyl 4-iodobenzoate was carried out based on our recent publication:[6] 20 mg Pd@TiO_2 were dispersed in 4 mL of tetrahydrofuran (THF) in a clean quartz tube, then 26 mg (0.1 mmol, 1 eq.) of methyl-4 iodobenzoate and 65 mg (0.2 mmol, 2 eq.) of Cs_2CO_3 were added. The reaction mixture was purged with Ar for 10 min prior to irradiation. Irradiation sources used: 1x 465 nm LED plus 1x 368 nm LED set up at 1.6 and 0.3 Wcm^{-2}, respectively; or 1x 368 nm LED set up at 0.3 Wcm^{-2}. The progress of the reaction and the quantification were done by GC-FID using t-butyl benzene as an external standard (See Supplementary Table S4.9).

Catalyst recyclability

The catalyst was recovered after each cycle by centrifugation (3500 rpm for 15 min). Once the supernatant was decanted, the catalyst was washed three times with ~6 mL fresh methanol. Each time the catalyst was dispersed *via* sonication and isolated through centrifugation. The recovered clean catalyst was suspended in 4 mL HPLC grade MeOH in a clean tube prior to reuse. Reactant concentrations and irradiation time were kept constant for all the cycles and catalyst losses during the recovery process were considered negligible.

Catalyst recovery treatment

The recovered catalyst from two subsequent cycles of light-induced Sonogashira reaction was separated from the reaction mixture by centrifugation (3500 rpm for 15 min). The catalyst was washed 2 times with ~5 mL fresh MeOH then 2 more times with ~5 mL fresh THF prior to activation. In brief, the recovered Pd@TiO_2 was added to 4 mL THF and 60 mg Cs_2CO_3 into a clean quartz tube, suspended by sonication for 10 min then purged with Ar for 15 min prior to 368/465 nm irradiation for ~ 1h. The activated solid catalyst was separated by centrifugation, washed with MeOH three times prior to use for a new cycle for light-induced Sonogashira coupling reaction. Catalyst reactivation using the benzoin photoinitiator (I-2959) was performed as previously reported.[8]

Catalytic farming

The reaction was scaled up twice to facilitate catalyst recovery and reuse. The catalyst was recovered after each cycle by centrifugation (3500 rpm for 15 min). After each cycle the catalyst was dispersed in fresh clean solvent *via* sonication and isolated through centrifugation for at least 3 times, and finally dried. Reactions were carried out at given conditions (see figure captions).

Turnover Number (TON) and Turnover Frequency (TOF) calculations[15]

Considering that each PdNP has at least one catalytic active site, the TON and TOF are calculated related to the moles of Pd NPs as follows:

$$\text{TON} = \frac{\text{moles of reagent} * \text{yield}}{\text{moles of Pd NP(n)}}$$

Where the moles of PdNPs (n) are calculated as follows:

$$n = \frac{\text{mass of catalyst} * \text{wt\% Pd}}{\text{MW} * \text{number of Pd atoms per NP(N)}}$$

and N is the number of Pd atoms per nanoparticle:

$$N = \frac{\text{Pd NP volume}}{\text{Pd atomic volume}}$$

TOF in h^{-1}

$$\text{TOF} = \frac{\text{TON}}{\text{Time of reaction (h)}}$$

CONCLUSIONS

In this contribution we propose a new approach to extend catalyst lifetimes based on the crop rotation system used in agriculture Rotation practices may become a standard strategy in heterogeneous catalysis, just as they do in organic farming. While this contribution demonstrates the benefits of rotation in catalysis, we also recognize that practical applications in industry will have to meet market demands as a

consideration in reaction rotation. Both represent changes in societal attitudes that recognize and celebrate the use of sustainable practices.

REFERENCES

1. A. Biffis, P. Centomo, A. Del Zotto and M. Zeccal, Pd Metal Catalysts for Cross-Couplings and Related Reactions in the 21st Century: A Critical Review, Chem. Rev., 2018, 118, 2249-2295.
2. Q. Liu, M. D. Xu, J. Zhao, Z. Yang, C. Z. Qi, M. F. Zeng, R. Xia, X. Z. Cao and B. Y. Wang, Microstructure and catalytic performances of chitosan intercalated montmorillonite supported palladium (0) and copper (II) catalysts for Sonogashira reactions, Int. J. Biol. Macromol., 2018, 113, 1308-1315; M. F. Zeng, X. Zhang, L. J. Shao, C. Z. Qi and X. M. Zhang, Highly porous chitosan microspheres supported palladium catalyst for coupling reactions in organic and aqueous solutions, J. Organomet. Chem., 2012, 704, 29-37; Z. P. Chen, E. Vorobyeva, S. Mitchell, E. Fako, M. A. Ortuno, N. Lopez, S. M. Collins, P. A. Midgley, S. Richard, G. Vile and J. Perez-Ramirez, A heterogeneous single-atom palladium catalyst surpassing homogeneous systems for Suzuki coupling, Nat. Nanotechnol., 2018, 13, 702-705.
3. C. M. Friend and B. Xu, Heterogeneous Catalysis: A Central Science for a Sustainable Future, Acc. Chem. Res., 2017, 50, 517-521; W. P. Gao, Z. D. Hood and M. F. Chi, Interfaces in Heterogeneous Catalysts: Advancing Mechanistic Understanding through Atomic-Scale Measurements, Acc. Chem. Res., 2017, 50, 787-795; A. Corma and H. Garcia, Supported gold nanoparticles as catalysts for organic reactions, Chem. Soc. Rev., 2008, 37, 2096-2126; A. Corma, R. Juarez, M. Boronat, F. Sanchez, M. Iglesias and H. Garcia, Gold catalyzes the Sonogashira coupling reaction without the requirement of palladium impurities, Chem. Comm., 2011, 47, 1446-1448.
4. M. Argyle and C. Bartholomew, Heterogeneous Catalyst Deactivation and Regeneration: A Review, Catalysts, 2015, 5, 145-269.
5. A. Akcil, F. Veglio, F. Ferella, M. D. Okudan and A. Tuncuk, A review of metal recovery from spent petroleum catalysts and ash, Waste Manage., 2015, 45, 420-433.
6. N. Marina, A. E. Lanterna and J. C. Scaiano, Expanding the Color Space in the Two-Color Heterogeneous Photocatalysis of Ullmann C–C Coupling Reactions, ACS Catal., 2018, 7593-7597.
7. A. Elhage, A. E. Lanterna and J. C. Scaiano, Light-Induced Sonogashira C-C Coupling under Mild Conditions Using Supported Palladium Nanoparticles, ACS Sust. Chem. Eng., 2018, 6, 1717-1722.
8. A. Elhage, A. E. Lanterna and J. C. Scaiano, Tuneable Photocatalytic Activity of Palladium-decorated TiO_2: Non-hydrogen mediated hydrogenation or isomerization of benzyl-substituted alkenes, ACS Catal., 2017, 7, 250-255.
9. The electronic Rothamsted Documents Archive, http://www.era.rothamsted.ac.uk/, Accessed April, 2018.
10. Crop Rotation on Organic Farms: A Planning Manual, Natural Resource, Agriculture, and Engineering Service, Ithaca, NY, USA, 2009.
11. P. Anastas and N. Eghbali, Green chemistry: principles and practice, Chem. Soc. Rev., 2010, 39, 301-312.
12. S. Sarina, E. Jaatinen, Q. Xiao, Y. M. Huang, P. Christopher, J. C. Zhao and H. Y. Zhu, Photon Energy Threshold in Direct Photocatalysis with Metal Nanoparticles: Key

Evidence from the Action Spectrum of the Reaction, J. Chem. Phys. Lett., 2017, 8, 2526-2534; T. Tana, X. W. Guo, Q. Xiao, Y. M. Huang, S. Sarina, P. Christopher, J. F. Jia, H. S. Wu and H. Y. Zhu, Non-plasmonic metal nanoparticles as visible light photocatalysts for the selective oxidation of aliphatic alcohols with molecular oxygen at near ambient conditions, Chem. Comm., 2016, 52, 11567-11570.

13. K. Koehler-Cole, J. R. Brandle, C. A. Francis, C. A. Shapiro, E. E. Blankenship and P. S. Baenziger, Clover green manure productivity and weed suppression in an organic grain rotation, Renew. Agr. Food. Syst., 2017, 32, 474-483.
14. I. R. Chongtham, G. Bergkvist, C. A. Watson, E. Sandstrom, J. Bengtsson and I. Oborn, Factors influencing crop rotation strategies on organic farms with different time periods since conversion to organic production, Biol. Agric. Hortic., 2017, 33, 14-27.
15. G. K. Hodgson and J. C. Scaiano, Heterogeneous Dual Photoredox-Lewis Acid Catalysis Using a Single Bifunctional Nanomaterial, ACS Catal., 2018, 8, 2914-2922.

4.3 Postprint Version of Supporting Information

Supplementary Table S4.1. Catalytic farming of Pd@TiO_2 by rotation between Ullmann homo-coupling and Sonogashira coupling: up to 6 alternating cycles.

Cycle	Reaction	% Conversion[a]	% Yield[a]			TON[b]	TOF[b] (h^{-1})
			DPA	Ar'-Ar'	Ar'-H		
1	B	97	–	65	32	967	967
2	A	98	83	–	–	2140	4280
3	B	97	–	60	35	893	893
4	A	98	85	–	–	2192	4384
5	B	96	–	56	40	833	833
6	A	65(95)	42(80)	–	–	1083 (2063)	2166 (2063)

Reactions conditions: A- Sonogashira coupling: 15 mg of Pd@TiO_2, 1.3 eq. of phenylacetylene, 0.13 mmol of iodobenzene, 2 eq. of K_2CO_3, 4 mL MeOH, Ar atmosphere. Irradiation: 7x 450 nm LED working at 2.7 Wcm^{-2}. Time: 30 min. Values between brackets correspond to results obtained after 1 h of irradiation. B- Ullman homo-coupling: 20 mg Pd@TiO_2, 0.1 mmol of methyl 4-iodobenzoate, 2 eq. of Cs_2CO_3, 4 mL of THF, Ar atmosphere. Irradiation: 368 nm and 465 nm working at 0.3 and 1.6 Wcm^{-2}, respectively. Time: 1 h. [a] Yields and conversion calculated by GC-FID using *t*-butylbenzene as external standard. [b]Calculation per PdNP based on major product.

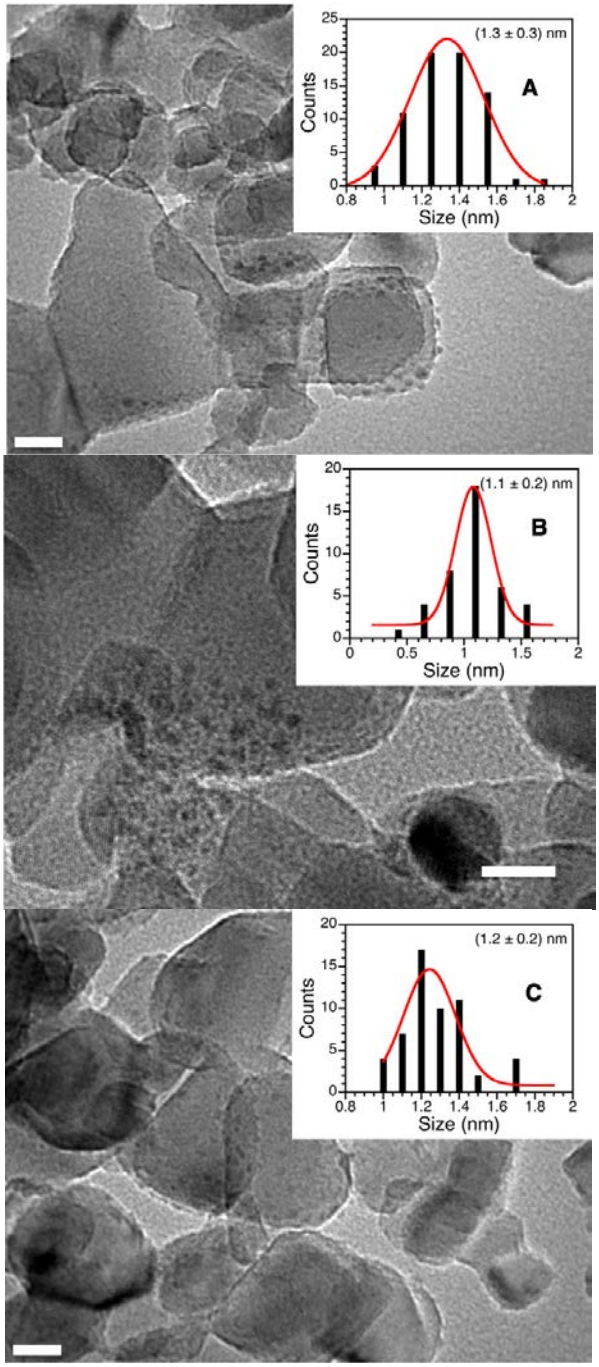

Supplementary Figure S4.1. TEM image of Pd@TiO_2 and particle size distribution (insets) for fresh material (A), after 3 Sonogashira coupling cycles (B) and after 6 catalytic farming cycles (C). Scale bar: 10 nm. Size distribution of Pd nanoparticles supported on TiO_2 obtained by manual counting and sizing of particles identified by TEM.

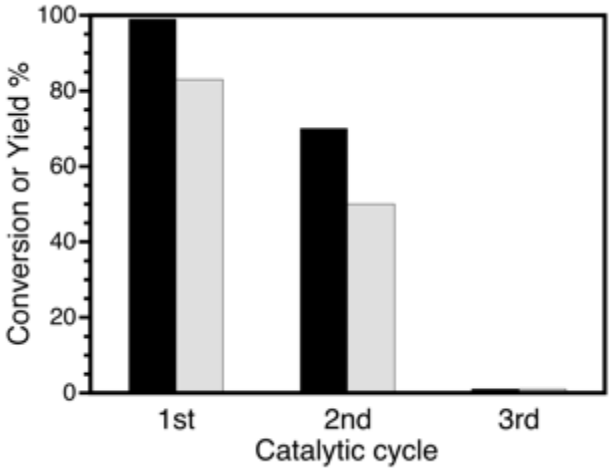

Supplementary Figure S4.2. Conversions and yields obtained after several catalytic cycles of Sonogashira coupling upon 465 nm irradiation at 1.6 W cm^{-2} for 5 h.

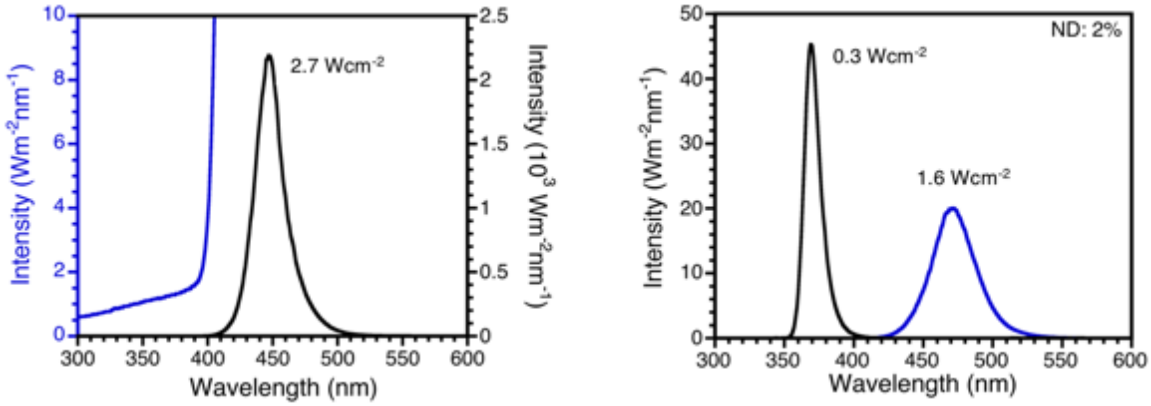

Supplementary Figure S4.3. Emission spectra of light sources used in this work. *Left*: 7x450 nm LED, showing UV contamination in blue. *Right:* 1x365 nm LED (black) and 1x465 nm LED (blue). ND: neutral density filter.

Supplementary Table S4.2 | Catalytic farming of Pd@TiO_2 by rotation between Ullmann homo-coupling and Sonogashira coupling: up to 7 cycles with non-alternating reactions in between.

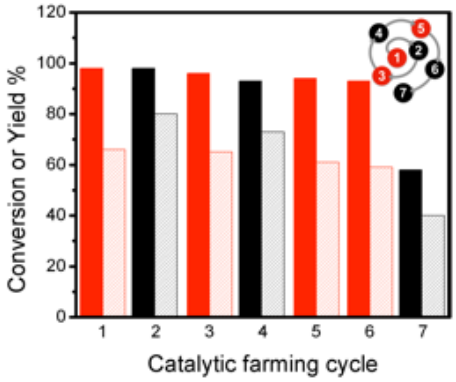

Cycle	Reaction	% Conversion[a]	% Yield[a]			TON[b]	TOF[b] (h^{-1})
			DPA	Ar'-Ar'	Ar'-H		
1	B	98	–	66	29	982	196
2	A	98	80	–	---	2063	413
3	B	96	–	65	31	967	193
4	A	93	73	–	–	1883	377
5	B	94	–	61	33	908	182
6	B	93	–	59	34	878	176
7	A	58 (83)	40(62)	–	–	1032 (1599)	206 (67)

Reactions conditions: A- Sonogashira coupling: 15 mg of Pd@TiO_2, 1.3 eq. of phenylacetylene, 0.13 mmol of iodobenzene, 2 eq. of K_2CO_3, 4 mL MeOH, Ar atmosphere. Irradiation: 465 nm LED working at 1.6 Wcm^{-2}. Time: 5 h. Values between brackets correspond to results obtained after 24 h of irradiation. B- Ullman homo-coupling: 20 mg Pd@TiO_2, 0.1 mmol of methyl 4-iodobenzoate, 2 eq. of Cs_2CO_3, 4 mL of THF, Ar atmosphere. Irradiation: 368 nm LED working at 0.3 Wcm^{-2}. Time: 5 h. [a] Yields and conversion calculated by GC-FID using t-butylbenzene as external standard. [b]Calculation per Pd NP based on major product.

Supplementary Table S4.3. Catalytic farming of Pd@TiO_2 by rotation between alkene isomerization, Ullmann homo-coupling and Sonogashira coupling (scheme 4.1).

Cycle	Reaction	Time (h)	% Conv[a]	% Yield[a]					TON[b]	TOF[b] (h^{-1})
				DPA	Ar'-Ar'	Ar'-H	A	DA		
1	C	5	97	–	–	–	71	25	1831	366
2	A	0.5	ND	ND	–	–	–	–	0	0
3	B	1	96	–	60	36	–	–	893	893
4	B	1	93	–	59	35	–	–	878	878
5	A	0.5 (3)	13(43)	ND(30)	–	–	–	–	0(774)	0(258)
1	B	1	97	–	70	27	–	–	1041	1041
2	C	6	35	–	–	–	25	~10	644	107
3	B	1	95	–	66	29	–	–	982	982
4	A	0.5(1)	74(99)	68(79)	–	–	–	–	1754(2037)	3507(2037)
5	C	6	26	–	–	–	17	~9	438	73
6[c]	C	5(9)	41(80)	–	–	–	~36(60)	ND(19)	928(1547)	186(172)
1	C	5	>99	–	–	–	67	~22	1728	346
2	C	5	98	–	–	–	69	~25	1779	356
3	B	1	96	–	65	33	–	–	967	967
4	B	1	95	–	60	~35	–	–	893	893
5	A	0.5	96	78	–	–	–	–	2011	4023

Reactions conditions: A- Sonogashira coupling: 15 mg of Pd@TiO_2, 1.3 eq. of phenylacetylene, 0.13 mmol of iodobenzene, 2 eq. of K_2CO_3, 4 mL MeOH, Ar atmosphere. Irradiation: 7x 450 nm LED working at 2.7 Wcm^{-2}. B- Ullmann homo-coupling: 20 mg Pd@TiO_2, 0.1 mmol of methyl 4-iodobenzoate, 2 eq. of Cs_2CO_3, 4 mL of THF, Ar atmosphere. Irradiation: 368 nm and 465 nm working at 0.3 and 1.6 Wcm^{-2},

respectively. C- Alkene isomerization: 15 mg of Pd@TiO_2, 0.16 mmol estragole, 4 mL MeOH, Ar atmosphere. Irradiation: 7x 450 nm LED working at 2.7 Wcm^{-2}. [a] Yields and conversion calculated by GC-FID using *t*-butylbenzene as external standard. [b]Calculation per Pd NP based on major product. [c] Catalyst used after reactivation with I-2959 under UVA irradiation for 5h (See ref. {Elhage, 2017 #11}).

Supplementary Table S4.4 | Catalytic farming of Pd@TiO2 by rotation between alkene isomerization and Sonogashira coupling.

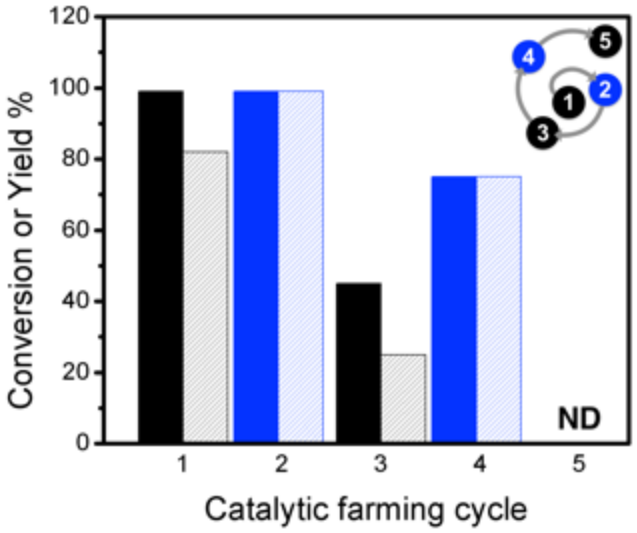

Cycle	Reaction	% Conversion[a]	% Yield[a]		
			DPA	A	DA
1	A	>99	82	–	–
2	C	>99	–	>99	–
3	A	45	25	–	–
4	C	75	–	75	–
5	A	ND	–	–	–

Reactions conditions: A- Sonogashira coupling (black): 15 mg of Pd@TiO_2, 1.3 eq. of phenylacetylene, 0.13 mmol of iodobenzene, 2 eq. of K_2CO_3, 4 mL MeOH, Ar atmosphere. Irradiation: 465 nm LED working at 1.6 Wcm^{-2}. Time: 5h. C- Alkene isomerization (blue): 15 mg of Pd@TiO_2, 0.16 mmol of estragole, Ar atmosphere. Irradiation: 465 nm irradiation at 1.6 Wcm^{-2}. Time: 24 h. [a] Yields and conversion calculated by GC-FID using *t*-butylbenzene as external standard.

Supplementary Table S4.5. Catalytic farming of Pd@TiO2 by rotation between alkene hydrogenation and Sonogashira coupling.

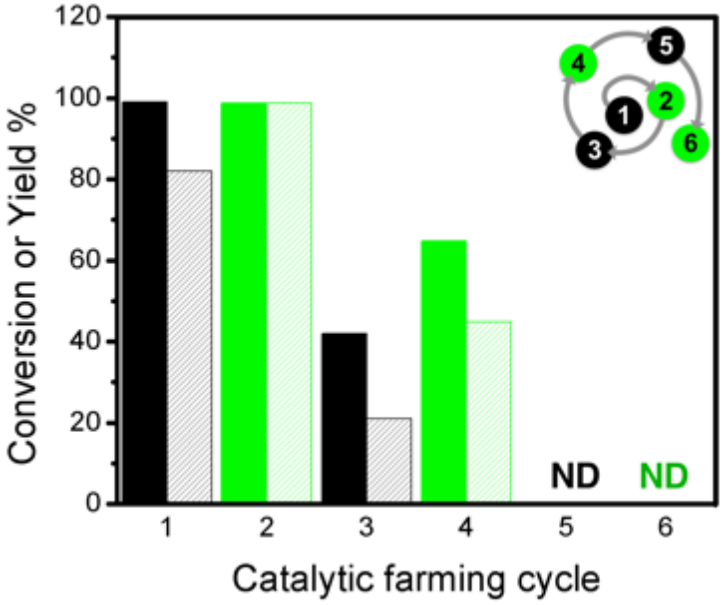

Cycle	Reaction	% Conversion[a]	% Yield[a]		
			DPA	A	DA
1	A	>99	82	–	–
2	D	>99	–	–	>99
3	A	42	21	–	–
4	D	65	–	20	45
5	A	ND	–	–	–
6	D	ND	–	–	–

Reactions conditions: A- Sonogashira coupling (black): 15 mg of Pd@TiO_2, 1.3 eq. of phenylacetylene, 0.13 mmol of iodobenzene, 2 eq. of K_2CO_3, 4 mL MeOH, Ar atmosphere. Irradiation: 465 nm LED working at 1.6 Wcm^{-2}. Time: 5h. D- Alkene hydrogenation (green): 15 mg of Pd@TiO_2, 0.16 mmol of estragole, Ar atmosphere Irradiation: 368 nm irradiation at 0.3 Wcm^{-2}. Time: 4 h. [a] Yields and conversion calculated by GC-FID using *t*-butylbenzene as external standard. ND: nothing detected.

Supplementary Table S4.6. Catalytic farming of Pd@TiO_2 by rotation between alkene hydrogenation, Ullmann reaction and Sonogashira coupling.

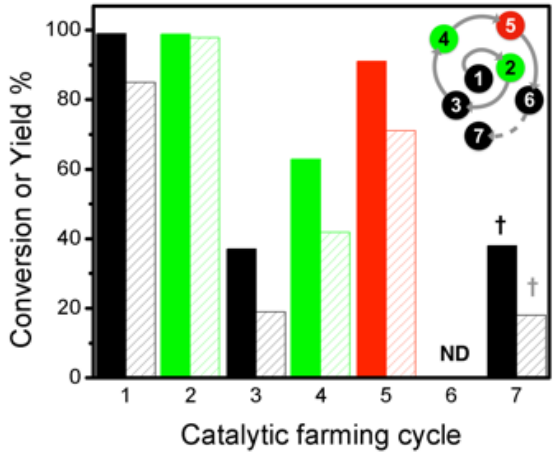

Cycle	Reaction	Time (h)	% Conv[a]	% Yield[a]					TON[b]	TOF[b] (h^{-1})
				DPA	Ar'-Ar'	Ar'-H	A	DA		
1	A	5	99	85	–	–	–	–	2192	438
2	D	4	99	–	–	–	–	98	3110	778
3	A	5	37	19	–	–	–	–	490	98
4	D	4	63	–	–	–	21	42	1333	333
5	B	1	91	–	71	20	–	–	1056	1056
6	A	5	ND	ND	–	–	–	–	0	0
7[c]	A	5	38	18	–	–	–	–	464	93

Reactions conditions: A- Sonogashira coupling (black): 15 mg of Pd@TiO_2, 1.3 eq. of phenylacetylene, 0.13 mmol of iodobenzene, 2 eq. of K_2CO_3, 4 mL MeOH, Ar atmosphere. Irradiation: 465 nm LED working at 1.6 Wcm^{-2}. Time: 5h. B- Ullman homo-coupling (red): 20 mg Pd@TiO_2, 0.1 mmol of methyl 4-iodobenzoate, 2 eq. of Cs_2CO_3, 4 mL of THF, Ar atmosphere. Irradiation: 368 nm and 465 nm working at 0.3 and 1.6 Wcm^{-2}, respectively. Time: 1 h. D- Alkene hydrogenation (green): 15 mg of Pd@TiO_2, 0.16 mmol of estragole, Ar atmosphere Irradiation: 368 nm irradiation at 0.3 Wcm^{-2}. Time: 4 h. [a] Yields and conversion calculated by GC-FID using *t*-butylbenzene as external standard. [b]Calculation per Pd NP based on major product. [c, †] Catalyst used after reactivation with THF treatment under UVA-vis irradiation for 5h. ND: nothing detected.

Supplementary Table S4.7. Kinetics for photocatalytic Sonogashira C-C coupling under different irradiation intensities.

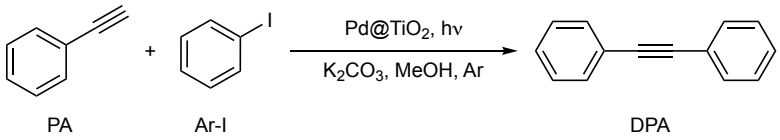

PA Ar-I DPA

	Time (h)	% Conversion[a]	% Yield[a]
465 nm @1.6 Wcm^{-2}	0	0	0
	1	56	46
	2	60	53
	3	64	61
	4.5	77	68
	6	>99	84
450 nm @2.7 Wcm^{-2}	0	0	0
	5	33	29
	10	46	40
	15	67	55
	20	72	60
	30	96	83

Reactions Conditions: 15 mg of Pd@TiO_2, 1.3 eq. of phenylacetylene, 0.13 mmol of iodobenzene, 2 eq. of K_2CO_3, 4 mL MeOH, Ar atmosphere. Irradiation: 1x 465 nm LED working at 1.6 Wcm^{-2} and 7x 450 nm LED working at 2.7 Wcm^{-2}.

Supplementary Table S4.8 | Kinetics for photocatalytic alkene isomerization.

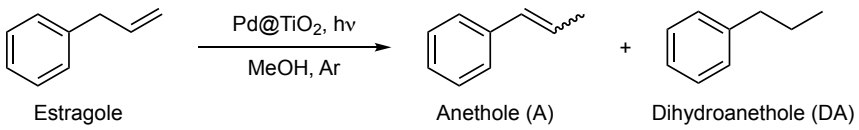

	Time (h)	% Conversion[a]	% A[a]	% DA[a]
450 nm @2.7 Wcm^{-2}	0.5	20	19	ND
	1	36	32	ND
	2	46	40	5
	3	60	44	12
	4	76	53	19
	5	94	70	21
465 nm @1.6 Wcm^{-2}	1	28	27	ND
	3	40	38	ND
	5	51	46	ND
	7	52	51	ND
	9	58	58	ND
	24	<99	94	6

Reactions Conditions: 15 mg of Pd@TiO_2, 1 eq. estragole, 4 mL MeOH, Ar atmosphere. Irradiation: 7x 450 nm LED working at 2.7 Wcm^{-2} or 1x 465 nm LED working at 1.6 Wcm^{-2}. [a] Yields and conversions calculated by GC-FID using *t*-butylbenzene as external standard. Dihydroanethole (DA) is detected as by product due to UV light contamination in the light source.(See Supplementary Figure S4.3)

Supplementary Table S4.9. Kinetics for photocatalytic Ullmann homo-coupling.

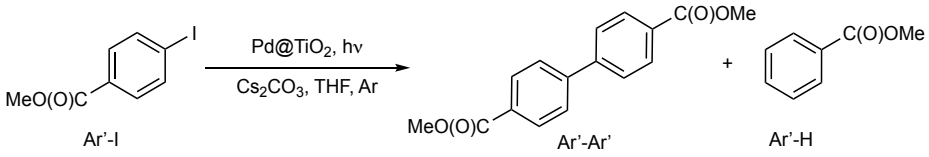

	Time (h)	% Conversion[a]	% Ar'-H[a]	%Ar'-Ar'[a]
368 nm @0.3 Wcm^{-2}	1	36	22	14
	2	60	26	34
	3	69	25	44
	4	86	26	60
	5	96	27	69
368 nm @0.3 Wcm^{-2} 465 nm @1.6 Wcm^{-2}	0.5	61	32	29
	1	95	33	62

Reactions conditions: 20 mg Pd@TiO_2, 0.1 mmol of methyl 4-iodobenzoate, 2 eq. of Cs_2CO_3, 4 mL of THF, Ar atmosphere. [a] Yields and conversions calculated by GC-FID using *t*-butylbenzene as external standard.

Supplementary Table S4.10 | Reusability and recovery of catalytic activity of Pd@TiO_2 towards Sonogashira coupling using Ullmann homo-coupling reaction.

Cycle	% Conversion[a]	% Yield[a]
1	98 ± 1	85 ± 1
2	40 ± 1	35 ± 1
3	ND	ND
4[b]	24(57)	19(37)

Sonogashira reaction as per conditions in Supplementary table S4.7, 450 nmLED working at 2.7 Wcm^{-2}. [a] Yields and conversions calculated by GC-FID using *t*-butylbenzene as external standard. [b] Catalyst was used after one cycle of Ullmann homo-coupling reaction (95 % conversion, 57 % Ar'-Ar', 38 % Ar'-H) as per conditions described in Supplementary table S4.9. ND: None detected.

This manuscript has been adapted from Chem. Sci., **2019**, 10, 1419-1425 with permission, from the Royal Society of Chemistry. Small changes provide consistent formatting and clarity with respect to the overall thesis.

4.4 Accompaniment to Chapter 4

The perpetual issue in the field of heterogeneous catalysis is the loss of catalytic activity and deactivation of the catalyst after repeated reaction. In light of rising demands for greater sustainability, particularly for processes of societal and industrial relevance, extending the lifetime and the performance of the catalyst is consistent with the principles of sustainable green chemistry. This chapter highlighted a new strategy in heterogeneous catalysis to enhance catalyst longevity and product yield by reducing the catalyst deterioration. This practice is achieved by performing a series of dissimilar or different types of catalytic processes using the same catalyst (here $Pd@TiO_2$) in sequenced reactions. One reaction depletes the catalyst whether by blocking the active sites with set of organics materials or by changing the oxidation state of the metal during the reaction while the other catalytic reaction plays a key role in restoring its activity, in particular its oxidation state. Hence the catalysts are not deactivated by a fixed set of reactants. The main complementary factor between the two catalytic transformations is the change in the solvent.

The catalytic farming concept is adopted form the crop rotation methodology employed in agriculture to increase soil fertility and crop yields. In catalysis, rotating through different reactions can be used to extend heterogeneous catalyst lifetimes as well as its selectivity. This strategy shows the benefit of rotations practices in catalysis, which can be extended for practical applications in industry to meet the need of the synthesis goals. It provided a platform for synthesis of valuable target molecules as a tool in reactivating catalysts *in situ*. As per ChemistryWorld report, the consulted catalysis expert Kelsey Stoerzinger −Oregon State University, US− stated: "*You could also think of doing it with a copper catalyst. There are other precious metals that can oxidize or reduce, like iridium or ruthenium, so I think you'd use different reactions, but this could be applicable to a range of catalysts and a different class of reactions*."

Chem. Sci., **2018,** 9, 6844-6852

5. Glass wool: a novel support for heterogeneous catalysis

5.1 Preamble to chapter 5

This Chapter examines the use of glass wool fibers as support for metal and metal oxide nanoparticles. As discussed throughout the previous chapters, heterogeneous catalysts are much easier to separate from the reaction mixture than their homogeneous counterparts and often can easily be reused. Heterogeneous catalysts, such as metal or metal oxide nanoparticles, are usually immobilized on powder-like materials. They are easy to recover after batch reaction but they are not suitable for continuous flow chemistry.

Glass wool offers the advantages of not only being inexpensive −it is available with a variety of surface properties− but also easy to modify in order to provide physical or chemical affinity towards many catalytic species. Grafted metal and/or metal oxide nanoparticles onto glass wool showed that the resulting hybrid materials could catalyze a wide range of reactions, including C–C couplings, dehalogenations and cycloadditions. Although we focused on photocatalytic reactions, heat-driven reactions can be performed as well.

Glass wool is commonly used in household insulation and soundproofing. It has been also used as an attachment surface in some biological studies. However, this is the first time it has been employed as a catalyst support in organic chemistry. It is mainly used to restrict the mobility of active catalyst. This finding provides a platform for future use in flow chemistry systems. These features intensified the impact of this work, thus were highlighted in the news by ChemistryWolrd and ChemistryViews magazines for its important insights.

5.2 Postprint Version of Manuscript

First published in: Chem. Sci.**, 2018,** 9**,** 6844-6852

ABSTRACT

Heterogeneous catalysis presents significant advantages over homogeneous catalysis such as ease separation and reuse of the catalyst. Here we show that a very inexpensive, manageable and widely available material – glass wool – can act as catalyst support for a number of different reactions. Different metal and metal oxide nanoparticles, based on Pd, Co, Cu, Au and Ru, were deposited on glass wool and used as heterogeneous catalysts for a variety of thermal and photochemical organic reactions including reductive de-halogenation of aryl halides, reductions of nitrobenzene, Csp^3-Csp^3 couplings, N-C heterocycloadditions (click chemistry) and Csp-Csp^2 couplings (Sonogashira couplings). The use of glass wool as catalyst support for important organic reactions, particularly C-C couplings, opens the opportunity to develop economical heterogeneous catalysts with excellent potential for flow photochemistry application.

INTRODUCTION

Heterogeneous catalytic processes have several advantages over the equivalent homogeneous ones, specifically, easy catalyst separation, minimal product contamination[1] and the distinct possibility of reuse.[2] Quite frequently these catalysts are in the form of nanometric or micrometric powders decorated with active nanostructures such as metal or metal oxides.[3, 4] Although they are easy to separate after batch reactions, they may not be ideal for flow chemistry, a strategy that enables easy scale up of reactions.[5] In catalysis, the term support is used with a wide range of meanings, from the passive support that simply restricts the mobility of the active catalyst, to cases where the support is an integral part of the catalyst and its performance; frequently, this is the case with semiconductors such as TiO_2.[4, 6, 7] Further, in the case of photocatalysis the absorption and scattering properties of the support are also important. With this in mind, we explored the possibility of using fibrous materials as catalyst supports, as they would be easy to separate after batch reactions and have the potential for flow chemistry

applications where a static catalyst would act on flowing solutions, also facilitating photocatalytic processes. Glass wool (GW) is inexpensive, readily available with a variety of surface properties and easy to modify to provide physical or chemical affinity towards many catalytic materials. Glass wool is widely employed for thermal and noise insulation in homes, appliances and instrumentation. In chemistry, GW is commonly used as filter, packing material in GC columns, purge traps and adsorbent beds,[8] where its normally regarded as a fairly robust inert material towards many chemicals, including good pH tolerance. There are some examples where GW is used as an attachment surface for applications in biology, including bactericidal studies,[9] but its applications in organic chemistry are virtually unexplored. The use of glass fibers and cloths for catalysis was reviewed in 2002;[10] their applications at the time dealt with gas and liquid processes, mostly oxidations, but interestingly recognized that these materials could avoid the technological problems and limitations associated with handling and separation of powders. While this contribution was in preparation, Barelko et al.[11] published a review with the significant technological advances achieved during the last 15 years. Yet, with the exception of a nitro-compound reduction, no applications to organic chemistry were reported, in particular, not a single example on C-C bond formation, a key reaction in organic synthesis and drug-development applications. Some concerns about the inert nature of the glass wool were noted many years ago by Hayes and Macdonald, but no further studies were found in the literature.[12] Apart from these limited examples in catalysis, where high temperature[13] or redox harsh conditions are usually employed,[11] is hard to find GW uses other than the ones mentioned above,[8] largely excluding organic catalysis. There are few studies focused on depositing metals on glass, mostly dedicated to redox reactions,[14] however to the best of our knowledge, no complex organic reactions – such as C-C couplings – have been explored utilizing glass as catalyst support.

In this contribution, we report on a number of metal and metal oxide nanostructures supported on commercially available –sometimes-modified – GW and how they perform on a variety of catalytic processes. We explored individual reactions

emphasizing the use of classic reactions with diverse novel materials. Our work on glass wool was initiated with the assumption that this support would be of the passive type. Notice that the use of these materials extremely facilitates the catalyst separation from the reaction vessel, thus a regular pair of tweezers can be used to remove the GW as shown in Figure 5.1. Further purification by filtration is straightforward.

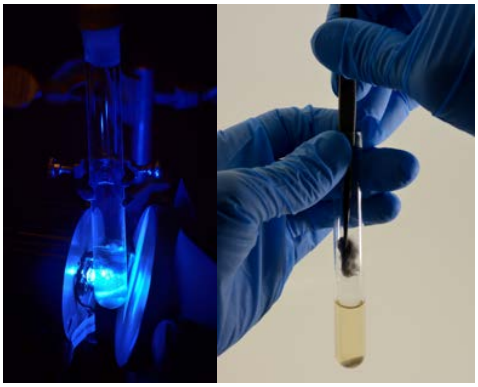

Figure 5.1. Picture showing the reaction setup used under LED irradiation and continuous stirring (left), and the easy removal of the GW material from the reaction vessel utilizing a pair of tweezers (right).

RESULTS AND DISCUSSION

Materials characterization

Two different types of commercial glass wool were used in this work: non-silanized (NGW) and silanized (SGW) glass wool. They were decorated with different metal and metal oxide nanoparticles, namely Au, Pd, Ru, Co and Cu, utilizing photoinduced and chemical methods as described in the Supporting information (SI). The optimal synthetic method was chosen based on the observed catalytic activity and stability of the new materials prepared. Thus, GWs were subjected to different pre-treatments before incorporating the metal/metal oxide nanoparticles in order to efficiently attach the metal to the GW surface. The experimental section summarizes several different trials and the rationale behind the selection of the preferred pre-treatment method. In particular, APTES treatment was selected to add a source of amino groups on the glass surface. These groups not only help to attach metal nanoparticles to the glass surface but can also be used as reducing agents for *in-situ* formation of metal

nanoparticles under dark conditions (See SI).[15] In general, non-silanized and silanized GW show no difference in their catalytic activity. In particular, NGW is preferred in cases were modification with APTES is required. When only acid pre-treatment is used, SGW shows better reactivity (*vide infra*). Figure 5.2 shows the materials before and after different surface modifications.

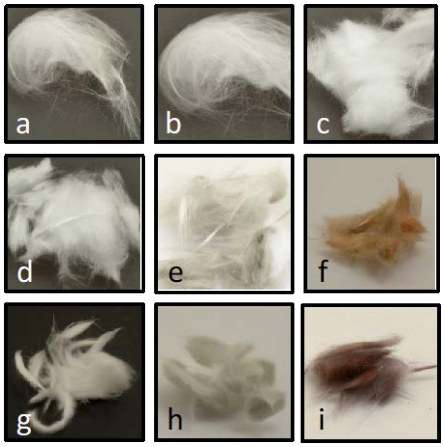

Figure 5.2. Pictures of different materials used in this work: a) pristine SGW, b) pristine NGW, c) HCl-treated SGW, d) APTES-functionalized NGW (NGW*), e) Pd@SGW, f) Cu@NGW, g) Co@SGW, h) Ru@NGW* and i) Au@NGW*.

The microscopic analysis of the GW samples was also performed. As shown in Figure 5.3a, the commercial GW is constituted by glass fibers of about 10 μm diameter. The crystalline structures present together with the fibers correspond to NaCl as determined by a careful EDS analysis of different areas of the image (Figure 5.3b and c). Upon derivatization, the presence of metal or metal oxides nanoparticles can easily be distinguished by SEM. Figure 5.3d and e show the surface of a glass fiber covered by Co_xO_y NPs and the corresponding EDS spectra. The same characterization was performed for each of the different metal-derivatized GWs as shown in Figures S5.5-S5.8.

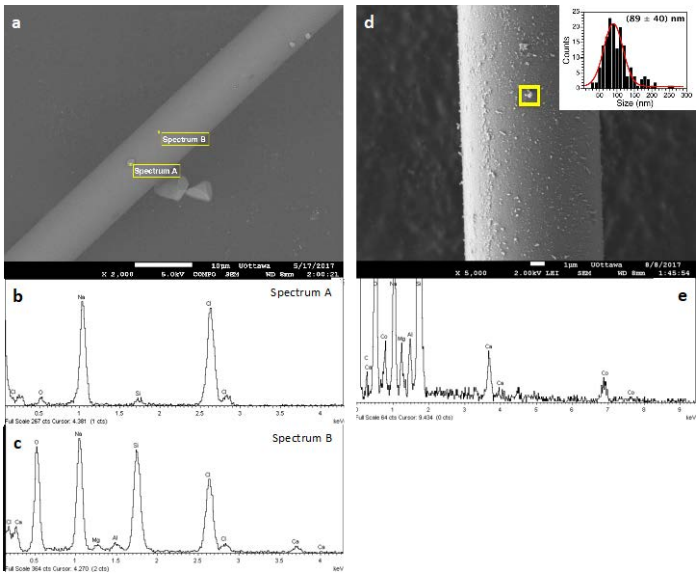

Figure 5.3. SEM images (top) and EDS spectra (bottom) at the marked areas of untreated SGW (a, b, c) and of Co@SGW (d, e). Notice the particulates on the SGW fiber are mostly composed of NaCl. Agglomerated particles were not considered to determine particle size distribution.

The materials were further characterized by ICP-OES, diffuse reflectance (DR) and X-ray photoelectron spectroscopy (XPS). The amount of metal loaded on each material as well as particle size distribution and calculated surface area are reported in Table 5.1. Figure 5.4 *left* shows the absorption profile of SGW before and after Co-derivatization, where slight changes on the absorption of Co@SGW can account for the contribution of Co_xO_y species in the material. The different absorption profiles of other metal-derivatized GWs are presented in figures S5.9-S5.12, where Pd, Au and Ru-derivatized GW show higher absorption in the visible region compared to the non-derivatized GW. XPS deconvolution analyses were performed for each material in order to determine the oxidation state of each metal. Figure 5.4 *right* shows the deconvoluted Co 2p HR-XPS spectrum obtained for Co@SGW, whereas the rest of the materials are described in Figures S5.13-S5.16. Characteristic peaks for Co 2p were fitted using the spin-orbit split constituted by Co $2p_{3/2}$ (781.2 eV) and Co $2p_{1/2}$ (797.7 eV) separated by ~16.5 eV. The corresponding Co (II) satellites (787.4 and 803.5 eV) further proves the presence of Co oxides (Co_xO_y).[16] XPS analysis of the Pd@NGW* exposes a Pd 3d core-level spectrum deconvoluted by using two spin-orbit split Pd $3d_{5/2}$ and Pd $3d_{3/2}$

components centered at 337 eV and 342.4 eV and separated by ~5.4 eV; which more likely corresponds to PdO.[4] In contrast, more reduced Pd species are found in the Pd@SGW material with spin-orbit components at 335 eV and 340.4 eV. The XPS fitting for the Ru 3p in Ru@NGW reveals the presence of two main peaks at 463.1 and 485.5 eV, which according to literature correspond to RuO_2,[17] although other reports suggest a mixture between metallic Ru(0), RuO_2 and $RuO_2 \bullet xH_2O$.[18] In the case of Cu@NGW, the two spin-orbit split Cu $2p_{3/2}$ (934.0 eV) and Cu $2p_{½}$ (953.7 eV) components (Δ~19.7 eV) and the noticeable Cu(II) satellites indicate that CuO[19] is present on this material. Finally, for Au@NGW* the peaks corresponding to Au $4f_{7/2}$ (84.5 eV) and Au $4f_{5/2}$ (88.0 eV) suggest the presence of Au (0). The additional features at lower BE (~ 82 eV) can account for low-coordinated atoms on the Au surface.[20]

Table 5.1. Characterization of the metal content on the metal-derivatized GWs.

Material[a]	Metal amount (wt %)[b]	Particle size (nm)[c]	Surface area (cm^2g^{-1})[d]
Pd@SGW	0.16 ± 0.03	19 ± 8	425
Pd@NGW*	0.54 ± 0.05	22 ± 9	1184
Co@SGW	0.070 ± 0.005	89 ± 40	53
Ru@NGW*	0.030 ± 0.001	63 ± 30	23
Cu@NGW*	1.1 ± 0.2	100 ± 60	737
Au@NGW*	0.9 ± 0.2	23 ± 10	1215

[a]APTES treated GW are denoted with *. [b] By ICP-OES analysis. None of the metals mentioned were detected on NGW*, pristine NGW or pristine SGW. [c]Particle size distributions were calculated without considering agglomerated particles. [d]Metal surface per gram of glass wool; considering the mean diameter of the GW fibers used is 10 µm, GW surface area is approximated to 1820 cm^2g^{-1}.

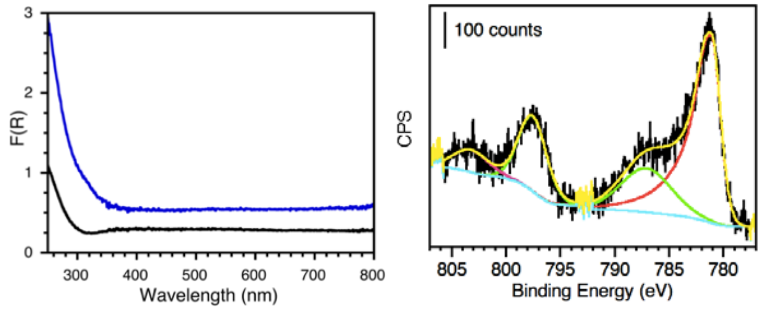

Figure 5.4. *Left*: Diffuse reflectance spectrum of HCl-treated SGW (black) and Co@SGW (blue). *Right:* Deconvoluted Co 2p HR-XPS spectrum for Co@SGW catalyst.

Catalytic activity

In order to determine if these new materials would perform as catalyst we selected different reactions based on some of our previous reports.[4, 6, 7, 21] Scheme 5.1 summarized the reactions tested that were successfully catalyzed utilizing the various new materials.

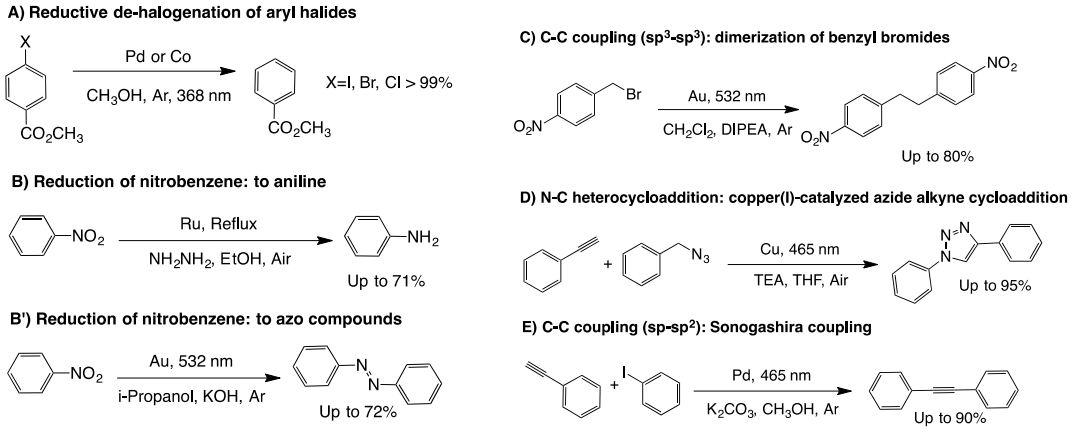

Scheme 5.1. Scope of reactions tested with the modified glass wool composites. Only the reactions that were successfully catalyzed are listed here.

Conditions explored for each reaction vary from thermal control to photo-induced catalysis. Table 5.2 shows a summary of the reactivity of different GW-based materials toward different organic transformation, where the last column shows the Table number and detailed entry for relevant examples. To discuss their activity we divided the following sections according to the organic transformation under study.

Table 5.2. Summary of the best reactivities observed when various GW-based materials are used as catalysts for different organic transformations

Entry	Material[a]	Reaction	% Yield	Table (*entry*)
i	Co@SGW	A) Reductive de-halogenation	>99	3 (*i, v*)
ii	Pd@SGW		>99	3 (ii, vi)
iii	Ru@SGW* (NGW*)	B) Reduction of nitrobenzene to aniline	71	4 (*ii, iv*)
iv	Au@NGW*	B') Reduction of nitrobenzene to azobenzene	72	5 (*ii*)
v	Au@NGW*	C) C-C coupling (sp^3-sp^3)	80	6 (*ii*)
vi	Cu@NGW (NGW*)	D) N-C heterocycloaddition	94	7 (*i*)
vii	Pd@NGW* (SGW*)	E) C-C coupling (sp-sp^2) (Sonogashira)	90	8 (*i*)

[a] The star (*) indicates APTES-treated materials

Reductive de-halogenation of aryl halides

De-halogenation processes are usually dictated by the C-halogen bond strength; thus, C−Cl bonds are harder to break than C-Br bonds and those than C-I bonds, which is usually reflected in harsher reaction conditions to achieve de-halogenation.[22] Recent reports on dehalogenation processes involved the use of either high pressure conditions (H_2, 30 bar),[23] or toxic and expensive iridium complexes.[24] Here we performed photodehalogenation of methyl 4-halogenobenzoates catalyzed by GW-based materials, particularly, Pd@SGW, Co@SGW and SGW. Both Pd- and Co-based NP are known to work as photocatalyst under UV-visible light.[25, 26] The results summarized in Table 5.3 show the reaction in the presence of Co@SGW proceeds under irradiation and can be accelerated under an inert atmosphere. Pd@SGW and SGW show the same reactivity as Co@SGW when methyl 4-iodobenzoate is used. As expected, the reaction slows down moving from iodide to bromide and to chloride reagents. This tendency is more evident with catalysts as Pd@SGW and SGW, whereas Co@SGW have shown exceptional yields, being able to reduce methyl 4-chlorobenzoate within 3 h. Co@SGW showed great reusability; thus, after 3 catalytic cycles >99 % yield of reductive compound was achieved within 4 h of irradiation of methyl 4-chlorobenzoate (table S5.1).

Table 5.3. Light induced reductive dehalogenation catalysed by Co- and Pd-derivatized SGW.

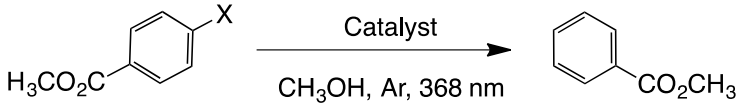

	X (1)[a]	Catalyst	Time (h)	% Yield[b]
i	Br-	Co@SGW	2	>99
ii	Br-	Pd@SGW	2	>99
iii	Br-	SGW	5	>99
ix	Br-	none	5	98
v	Cl-	Co@SGW	3	>99
vi	Cl-	Pd@SGW	20	>99
vii	Cl-	SGW	24	37
viii	Cl-	none	24	36

Reaction conditions: 0.2 mmol of substrate **1**, 0.36 mmol of K_2CO_3, 5 mL methanol, 60 mg catalyst under Ar. [a]When X=I, yield of 99% is reached in the presence of Co@SGW (or SGW) in 15 min of irradiation under Ar or 1 h under air. Only 15 % yield detected after 24 h of reaction in the dark at 47 ºC. [b]Yields were determined by GC-FID using *t*-stilbene as external standard.

Reduction of nitro compounds

The photoreduction of nitrocompounds has been studied as a method to synthesize anilines derivatives under mild conditions.[27] Based on our previous work[15] we decided to test the ability of Ru- and Au-derivatized GW as catalysts for the reduction of nitrobenzene to produce aniline. We used the optimized conditions previously reported for this type of organic transformation[15, 28] (see experimental section). Table 5.4 summarizes the results of the nitrobenzene reduction by Ru-derivatized GWs. We noticed that using NGW* or SGW* as supports show no difference in the catalytic performance of the Ru catalyst. It is worth mentioning that Au-derivatized GW showed no catalytic activity under the same experimental conditions. The reaction kinetics are depicted in Figure S5.3.

Table 5.4. Reduction of nitrobenzene to aniline catalysed by Ru-derivatized GW.

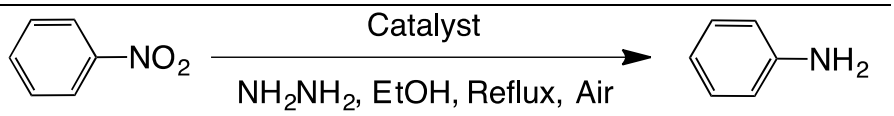

	Catalyst	Time (h)	% Yield[a]
i	Ru@SGW*	24	28
ii	Ru@SGW*	64	71[b]
iii	Ru@NGW*	24	28
iv	Ru@NGW*	64	66[c]
v	NGW*	24	ND
vi	none	24	ND

Reaction conditions: 25 mg of catalyst, 1.5 mmol nitrobenzene, 6 eq hydrazine, 5 mL ethanol. [a]Yields were determined by GC-FID using 1,3,5-trimethoxybenzene as an internal standard. [b]After 4 days 85% of desired product was detected. [c]After 4 days 79% of desired product was detected.

The formation of azo compounds as products of this reaction is also possible. However, their formation under illumination is rarely found as the reductive environment forces the reaction toward the corresponding amine.[29] There are just a few examples where the azo-compounds forms under illumination of AuNP.[28, 30] Here we show that excitation of AuNPs deposited on GW can also catalyze this reaction under green light irradiation for 24 h with moderate yields (Table 5.5). Briefly, the catalyst was mixed together with the nitrocompound in *i*-propanol under inert atmosphere (Ar) in the presence of KOH and irradiated with 532 nm LEDs. The formation of the

azocompound was monitored by UV-Vis spectroscopy (Figure S5.4) following the azobenzene absorption band at ~350 nm. As expected when visible light is utilized only *trans* azobenzene is detected as reaction product.[31]

Table 5.5. Light induced reduction of nitrobenzene to azobenzene catalyzed by Au@NGW*.

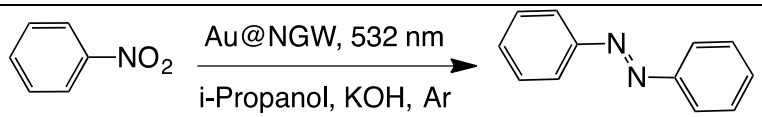

	Catalyst	Time (h)	% Conv[a]	% Yield[a]
i	Au@NGW*	24	68	65
ii	Au@NGW*	48	73	72
iii	Au@NGW*[b]	24	40	35
iv	Au@NGW*[c]	24	ND	ND
v	NGW*	24	ND	ND
vi	none	24	ND	ND

Reaction conditions: 0.3 mmol of substrate, 0.03 mmol of KOH, 5 mL *i*-propanol, 60 mg catalyst under Ar. [a]Conversion and yields were determined by UV-vis spectroscopy. [b]Under dark at 85ºC.[c]Under Air.

Combining the data presented in Tables 5.3 and 5.4 it becomes clear that GW-based catalysts offer an excellent opportunity of product and selectivity control by tuning the metal, its loading and the type of activation used (*i.e.* thermal or photochemical activation).

C-C coupling (sp^3-sp^3)

The reductive dimerization of benzyl bromides can be photoinduced using supported AuNPs and green light excitation.[6] This reaction is known as a radical reaction in which light intensity can lead the selectivity towards the dimer product, thus, higher intensity yields more dimer. Much to our surprise the same reaction proceeds with excellent yields if AuNPs are deposited on GW (Table 5.6). It is worth highlighting that a noticeable product yield is obtained in the absence of catalyst under these irradiation conditions (Entry v,vi, Table 5.6). These have been previously reported as a contribution from the UV contamination on the green light source.[6] The material also shows reasonable reusability (See Table S5.1).

Table 5.6. Light induced reductive dimerization of *p*-nitrobenzyl bromide catalyzed by Au@NGW*.

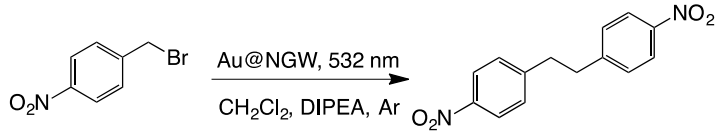

	Catalyst	Time (h)	% Conv[a]	% Yield[b]
i	Au@NGW*	5	77	64
ii	Au@NGW*	7	100	80
iii	Au@NGW*[c]	48	ND	ND
iv	NGW*	24	36	26
v	none[d]	5	-	25
vi	none[d,e]	5	-	ND

Reaction conditions: 0.1 mmol of substrate, 2 eq. of DIPEA, 30 mg of catalyst in 4 mL of CH_2Cl_2. [a]By-product: 4-nitrotoluene. [b]Yields and conversions were calculated by ^{1}H-NMR using caffeine as external standard. [c] Dark reaction at 39°C. [d] From reference.[6] [e]with filter < 500nm.

N-C heterocycloaddition (Click reaction)

We have recently reported on the photocatalyzed click reaction using supported Cu_xO nanoparticles on TiO_2 and Nb_2O_5.[7] The reaction can proceed within 6 h under both UV and visible light. The unexpected reactivity of the material under visible light suggests that the Cu_xO particles play an important light-harvesting role. With this in mind, we decided to test the Cu_xO activity when deposited on GW. The efficiency of the catalyst was compared to the reactivity of a commercial Cu@charcoal catalyst, which is one of the preferred catalysts to perform click chemistry under thermal conditions. As seen in Table 5.7, the new material showed great reactivity and high efficiency under both visible light irradiation or dark conditions at 55°C (same temperature as reached upon illumination). Unfortunately, the catalyst showed poor reusability, probably due to the visible leaching of copper species into the solution.

Table 5.7. Heterogeneous photocatalytic click chemistry catalyzed by Cu@NGW.

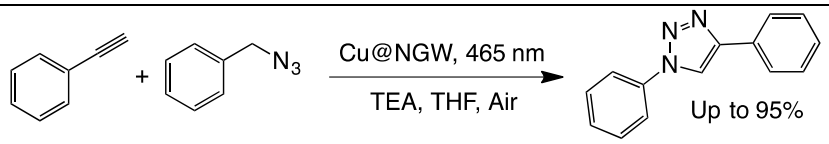

	Catalyst	Condition	Time (h)	% Yield[a,b]
i	Cu@NGW	465 nm, 55 °C	6	92 (95)
ii	Cu@NGW	Dark, 55 °C	6	93 (94)
iii	Cu@NGW	Dark, RT	6	8 (25)
iv	Cu@NGW	Dark, RT	24	75
iv	Cu@Charcoal	Dark, 55°C	6	21
iv	Cu@Charcoal	Dark, 55°C	24	73
v	NGW	Dark, 55°C	6	ND
vi	NGW	Dark, 55°C	24	2[c]

Reactions conditions: 15 mg of catalyst, azide/alkyne/TEA (1:1:1), 6 h under air. [a]Yields were calculated by ^{1}H-NMR analysis in $CDCl_3$ using caffeine as external standard. [b]Values between brackets are yields obtained after 6 h of reaction using supported Cu@NGW*. [c]Mixture of two isomers

C-C coupling (sp-sp^2) (Sonogashira)

One of our recent reports demonstrated that PdNP-decorated materials such as TiO_2, nanodiamonds and Nb_2O_5 can selectively catalyze the cross-coupling of iodobenzene and phenylacetelyne under both reflux and visible light irradiation.[26] Here we show that the same reaction can be catalyzed by the new Pd@SGW* and Pd@NGW* catalysts and selectively lead to the cross-coupling products showing similar activity. Briefly, the selective cross coupling reaction of iodobenzene and phenylacetylene has been studied in methanol as solvent, K_2CO_3 as base and supported PdNPs on activated and/or functionalized surface of GW (Table 5.8). Control reactions in the presence of GW and in the absence of catalyst did not show any product after 24 h. The photocatalyst can be reused at least two times with excellent performance (See Table S1), showing the same reactivity as the previous reported materials.[26]

Table 5.8: Light-induced Sonogashira C-C coupling catalyzed by Pd@GW.

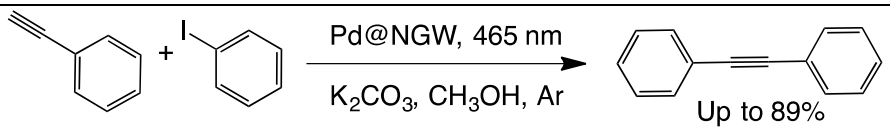

	Catalyst	Time (h)	% Conv	% Yield[a]
i	Pd@NGW*	5	>99(>99)	90 (88)
ii[b]	Pd@NGW*	5	0	ND
ii	NGW*	24	0	ND
iv	none	24	0	ND

Reactions conditions: 1 eq. of Iodobenzene, 1.3 eq. of Phenylacetylene, 2 eq. of K_2CO_3, 4 mL methanol, 60 mg Pd@NGW*. [a]Yields were determined by GC-FID using t-butylbenzene as an external standard. [b]Under dark conditions, reaction was run at 42 °C. Values between brackets are yields obtained after 5 h of reaction using supported Pd@SGW*.

CONCLUSIONS

We show the versatility of the use of glass wool as a very inexpensive, widely available and easy handled material for heterogeneous catalysis. We demonstrate that despite the different nature of the glass wool utilized, the efficacies of at least two commercial materials are similar. We have explored different methods to activate the glass surface in order to better anchor the catalytic species to the material. Also, low surface loadings (ranging from 1 down to 0.07 wt%) with different types of metal or metal oxide nanoparticles were tested, to illustrate how easy to use and reliable these materials are. The materials excel in both thermal and light-induced catalysis in a variety of different organic transformations ranging from reductions to C-C couplings and cyclizations, showing adaptability to different reaction media and conditions. Also important, the material can be easily separated from the reaction mixture eliminating tedious workup. Notice that optimization of the metal loadings could indeed open the door for more exploratory studies of these materials. This is a first effort on the use of GW as a catalytic support for fine organic reactions and more complex and interesting systems can be developed from here. We envision this as a first step towards an easy way to recover heterogeneous catalysts, and to develop catalysts with great flow chemistry potential.

EXPERIMENTAL

General

Unless otherwise specified, all chemicals were purchased from Sigma-Aldrich or Fisher Scientific and used without further purification. Particularly, the following glass wools were used: Non-treated GW (Aldrich catalog #: 20384) and silanized GW (Aldrich catalog #: 20411). Irgacure-2959 (I-2959) was purchase from Ciba.

Scanning electron microscopy (SEM) images were carried out in a JEOL JSM-1600 SE microscope working at an accelerating voltage of 2 kV. X-ray photoelectron spectroscopy (XPS) was recorded using Kratos analytical model Axis Ultra DLD, using monochromatic aluminum Ka X-rays at 140 W. XPS data was analyzed using CasaXPS software, Version 2.3.15. All spectra were calibrated at the C 1s signal at 284.8 eV and fittings obtained using a Gaussian 30% Laurentian and a Shirley baseline. The amount of metal loaded onto the materials was determined by Inductively Coupled Plasma Optical Emission Spectrometry (ICP-OES), using an Agilent Vista Pro ICP Emission Spectrometer. Approximately 10 mg portions were accurately weighed in triplicate and digested with aqua regia. Solutions were further diluted and measured by ICP-OES. The following emission lines were used for quantification when applicable: Pd 229.65 nm, Au 267.59 nm, Cu 327.00 nm, Co 228.00 nm, Ru 245.55 nm. Diffuse reflectance measurements were carried out in Agilent Cary 7000 UV-Vis-NIR Universal Measurement Spectrophotometer coupled with an Agilent praying Mantis accessory. UV-Vis spectroscopy was carried out in an Agilent Cary 60 UV-Vis Spectrophotometer.

UV irradiation used for catalyst synthesis was performed in a Luzchem photoreactor equipped with UVA bulbs (typically operated with 14 bulbs, corresponding to ~0.029 W/cm^2 (with ~ 4% spectral contamination). Light-emitting diodes (LEDs) of 10 W from LedEngin were used for photocatalytic reactions in the visible region (centered at 465 and 532 nm, respectively) and in the UV region (centered at 368 nm), Figure S5.1.

Quantification was carried out in a Perkin Elmer, Claurus Gas Chromatograph coupled to a Flame Ionization Detector (FID) and using a DB-5 column (30 m length, 0.320 mm diameter, 0.25 μm film), Helium as a carrier gas and t-butyl benzene as external standard. GC-MS analyses were performed on an Agilent 6890-N Gas Chromatograph with an Agilent 5973 mass selective detector calibrated with acetophenone. All ^{1}H NMR spectra were recorded on a Bruker AVANCE 400 spectrometer expressing the chemical shifts in ppm relative to the H-signal of tetramethylsilane (TMS).

Catalyst Preparation

Glass wool pre-treatments

Two types of glass wool were used for this work: silanized glass wool (SGW) and non-silanized glass wool (NGW). The materials were used as received or treated by different methods described in the SI.

Metal decoration

Metal or metal oxide nanoparticles were grafted on activated GW surface using different thermal and photochemical methods. The photochemical method is based on a previously described protocol[32] to synthesize metal NP utilizing Irgacure 2959 (I-2959) as photoinitiator. I-2959 can undergo Norrish Type I cleavage upon UVA excitation, generating the corresponding acetyl and ketyl radicals. The latter have been described as strong reducing agents capable of reducing different metals cations (M^{n+}) into the resultant metal (M^{0}) as shown in scheme S5.1. In general, 500 mg of activated GW (SGW or NGW) and the corresponding amount of metal precursor were mixed together in 200 mL of Milli-Q water and sonicated. 10 mL of ethanolic solution of I-2959 are added and irradiated under UVA for ~1h. Detailed synthetic methodologies are described in the SI.

Although some metals are in the form of metal oxides upon deposition on the GW surface, we will refer to all materials as M@GW. In many cases metal oxide

nanoparticles are formed spontaneously following ambient exposure of metal nanoparticles.

Catalytic reactions

Reductive dehalogenation

60 mg of catalyst (Co@SGW, Pd@SGW or SGW) were dispersed in 5 mL of methanol in a clean quartz tube, then 0.2 mmol of methyl 4-halobenzoate and 0.36 mmol of K_2CO_3 were added. The reaction mixture was purged with Ar for 10 min then irradiated with 368 nm LED light source working at 0.4 Wcm^{-2}. The solid catalyst was separated by filtration. Quantification of the product was done by GC-FID using *t*-stilbene as external standard. Time of irradiation varies depending on the aryl halides.

Nitrobenzene reductions

Aniline formation:

Using Ru@NGW or Ru@SGW**. 25 mg of catalyst were placed in a centrifuged tube together with 1.5 mL of nitrobenzene (1 M), 1.7 mL of EtOH, 0.3 mL internal standard 1,3,5-trimethoxy benzene (0.5M) and 1.5 mL NH2NH2 solution (6M). The tube was tightly closed and immersed in oil bath at 78 °C under constant stirring. Aliquots of 15 µL were taken from reaction mixture, diluted with 1.5 mL of ethylacetate prior to GC-FID quantification.

*Using Au@NGW**. 60 mg of Au@NGW* were dispersed in 5mL of EtOH in a clean dry round bottom flask then 1 mmol of nitrobenzene and 5 mmol of hydrazine were added. The resulting mixture was heated up to 78 °C under continuous stirring. The progress of the reaction was monitored by UV-visible spectroscopy. No reaction was detected under these conditions.

Azobenzene formation:

60 mg of Au@NGW* (or Ru@NGW) were dispersed in 5 mL of i-propanol in a clean glass tube and then 0.03 mmol of KOH and 0.3 mmol of nitrobenzene were added.

The resulting mixture was sonicated for 5 min prior to irradiation using a 532 nm LED. The solid catalyst was removed by filtration and quantification was done by UV-visible spectroscopy (Figure S5.4). Notice that no reaction was detected under these conditions when Ru@NGW was tested as catalyst.

Isomerization/hydrogenation of estragole

Thermal-induced isomerization:

50 mg of Ru@NGW* (or Ru@SGW*) were dispersed in 8 mL of i-propanol by sonication ca. for 5 min in a clean round bottom flask, then 25 μL (0.16 mmol) of reactant were added. The reaction mixture was heated up to 85 ºC (solvent boiling point) under air with continuous stirring for 24 hours. The progress of the reaction was monitored by GC-FID. The solid catalyst was separated by filtration and crude product was obtained after solvent evaporation. Quantification was done by GC-FID.

Light-induced isomerization or hydrogenation:

60 mg of Pd@NGW*(or Pd@SGW) were dispersed in 4 mL of methanol in a clean glass tube, then 0.14 mmol of estragole were added. The reaction mixture was purged with argon for 15 min then irradiated with 465 nm LED (368 nm LED for hydrogenation) for 24 hours at room temperature. The progress of the reaction was monitored by GC-FID. The solid catalyst was separated by filtration; crude product was obtained after solvent evaporation. Quantification was done either by ^{1}H-NMR or by GC-FID.

Unfortunately, no reaction was detected under neither of these conditions.

C-C coupling (sp-sp^2)

Thermal-induced Sonogashira C-C coupling:

60 mg of Pd@NGW* (Pd@SGW or Ru@NGW) were dispersed in 4 mL of methanol by sonication for about 5 min in a clean round bottom flask. Then 0.12 mmol of iodobenzene, 0.16 mmol of phenylacetylene and 0.24 mmol of K_2CO_3 were added.

The reaction mixture was purged with Ar and heated up to 42 °C (temperature of reaction mixture under blue LED irradiation) with continuous stirring for 5 hours. The solid catalyst was separated by filtration and crude product was obtained after solvent evaporation. Quantification was done by GC-FID.

Light-induced Sonogashira C-C coupling:

60 mg of Pd@NGW* (or Ru@NGW) were dispersed in 4 mL of methanol in a 10 mL clean glass tube, then 0.12 mmol of Iodobenzene, 0.16 mmol of phenylacetylene and 0.24 mmol of K_2CO_3 were added. The reaction mixture was purged with Ar for 15 min then irradiated with 465 nm LED light source set up at 1 W/cm^2 for 5 hours. The solid catalyst was separated by filtration and crude product was obtained after solvent evaporation. Quantification was done by GC-FID. Control experiments were carried out as mentioned above. Notice that no reaction was detected under these conditions when using Ru@NGW as catalyst; only Pd@NGW* was effective.

N-C heterocycloaddition

We followed a previously reported protocol.[7] Briefly, 15 mg of Cu@NGW (or Cu@NGW*) were dispersed in 1.5 mL of THF in a quartz test tube and mixed with the azide (0.5 mmol), alkyne (0.5 mmol), and amine (0.5 mmol). The reaction mixture was stirred and irradiated with 465 nm LED at room temperature and under air for 6 h. The solid catalyst was separated by filtration and the pure product was obtained after vacuum evaporation. Yields calculated by ^{1}H NMR in $CDCl_3$.

Control experiments were performed under dark conditions at room temperature or at 55°C (Maximum temperature reached upon illumination) under air.

C-C coupling (sp^3-sp^3): dimerization of benzyl bromides

We followed a previously reported protocol.[7] Briefly, 30 mg of Au@NGW* were dispersed in 4 mL of dichloromethane DCM in a glass test tube then 0.1 mmol of 4-nitrobenzylbromide and 0.2 mmol of diisopropyl ethylamine (DIPEA) were added. The resulting mixture was purged with argon for 15 minutes prior to 532 nm LED

irradiation with a 4xLED system each working at 0.56 W/cm^2. The solid catalyst was separated by filtration and the product was obtained after vacuum evaporation. Yields and conversions were calculated by ^{1}H NMR in $CDCl_3$ using caffeine as external standard. Control experiments were carried out as mentioned above.

Catalyst Recyclability

Co@SGW, Pd@NGW* and Au@NGW* catalysts were tested for potential reusability in the direct, selective and efficient reductive dehalogenation, Sonogashira coupling and 4-nitrobenzyl bromide dimerization respectively, using the conditions described above within at least two reusability cycles. The catalyst was removed from the reaction mixture by filtration, washed twice with methanol and 3 times with water, then dried in the oven at 100 °C overnight prior to reuse (Table S5.1).

REFERENCES

1. I. W. Davies, L. Matty, D. L. Hughes and P. J. Reider, Are heterogeneous catalysts precursors to homogeneous catalysts?, J. Am. Chem. Soc., 2001, 123, 10139-10140.
2. R. Schlçgl, Heterogeneous Catalysis, Angew. Chem. Int. Ed., 2015, 54, 3465 – 3520.
3. W. C. Conner and J. L. Falconer, Spillover in Heterogeneous Catalysis, Chem. Rev., 1995, 95, 759-788.
4. A. Elhage, A. E. Lanterna and J. C. Scaiano, Tuneable photocatalytic activity of Palladium-decorated TiO_2: non-hydrogen mediated hydrogenation or isomerization of benzyl-substituted alkenes, ACS Catal., 2017, 7, 250-255.
5. D. Cambie, C. Bottecchia, N. J. W. Straathof, V. Hessel and T. Noel, Applications of Continuous-Flow Photochemistry in Organic Synthesis, Material Science, and Water Treatment, Chem. Rev., 2016, 116, 10276-10341.
6. A. E. Lanterna, A. Elhage and J. C. Scaiano, Heterogeneous photocatalytic C-C coupling: mechanism of plasmon-mediated reductive dimerization of benzyl bromides by supported gold nanoparticles, Catal. Sci. Technol., 2015, 5, 4336-4340.
7. B. Wang, J. Durantini, J. Nie, A. E. Lanterna and J. C. Scaiano, Heterogeneous Photocatalytic Click Chemistry, J. Am. Chem. Soc., 2016, 138, 13127-13130.
8. Sigma-Aldrich, Glass Wool, http://www.sigmaaldrich.com/catalog/product/supelco/20411?lang=en&region=CA, Accessed September, 2017.
9. B. Steyn, M. C. Oosthuizen, R. MacDonald, J. Theron and V. S. Brozel, The use of glass wool as an attachment surface for studying phenotypic changes in Pseudomonas aeruginosa biofilms by two-dimensional gel electrophoresis, J. Proteomics., 2001, 1, 871-879; M. Nisnevitch, M. Kolog-Gulco, D. Trombka, B. S. Green and M. A. Firer, Immobilization of antibodies onto glass wool, J. Chromatogr. B, 2000, 738, 217-223.
10. Y. Matatov-Meytal and M. Sheintuch, Catalytic fibers and cloths, Appl. Catal., A, 2002, 231, 1-16.

11. V. V. Barelko, M. V. Kuznetsov, V. G. Dorokhov and I. Parkin, Glass-Fiber Woven Catalysts as Alternative Catalytic Materials for Various Industries. A Review, Russ. J. Phys. Chem. B, 2017, 11, 606-617.
12. R. W. Macdonald and K. E. Hayes, Glass Wool as an Oxidation Catalyst, J. Chem. Soc. Chem. Comm., 1972, 1030.
13. G. K. Ramaswamy, A. Somasundaram, B. K. Kuppuswamy and M. Velayudham, Glass Wool Catalysed Regioselective Isomerization of Styrene Oxides, J. Chin. Chem. Soc., 2013, 60, 97-102.
14. H. T. Yang, Z. P. Fang, X. Y. Fu and L. F. Tong, A novel glass fiber-supported platinum catalyst for self-healing polymer composites: Structure and reactivity, Chinese J. Catal., 2007, 28, 947-952; B. S. Bal'zhinimaev, A. P. Suknev, Y. K. Gulyaeva and E. V. Kovalyov, Silicate Fiberglass Catalysts: From Science to Technology, Catal. Ind., 2015, 7, 267-274; L. G. Simonova, V. V. Barelko, A. V. Toktarev, A. F. Chernyshov, V. A. Chumachenko and B. S. Bal'zhinimaev, Catalysts based on fiberglass support: IV. Platinum catalysts based on fiberglass support in oxidation of hydrocarbons (propane and n-butane) and sulfur dioxide, Kinet. Catal., 2002, 43, 61-66.
15. A. I. Carrillo, K. G. Stamplecoskie, M. L. Marin and J. C. Scaiano, 'From the mole to the molecule': ruthenium catalyzed nitroarene reduction studied with 'bench', high-throughput and single molecule fluorescence techniques, Catal. Sci. Technol., 2014, 4, 1989-1996.
16. B. H. R. Suryanto, X. Y. Lu, H. M. Chan and C. Zhao, Controlled electrodeposition of cobalt oxides from protic ionic liquids for electrocatalytic water oxidation, RSC Adv., 2013, 3, 20936-20942.
17. D. J. Morgan, Resolving ruthenium: XPS studies of common ruthenium materials, Surf. Interface Anal., 2015, 47, 1072-1079.
18. K. C. Park, I. Y. Jang, W. Wongwiriyapan, S. Morimoto, Y. J. Kim, Y. C. Jung, T. Toya and M. Endo, Carbon-supported Pt–Ru nanoparticles prepared in glyoxylate-reduction system promoting precursor–support interaction, J. Mater. Chem., 2010, 20, 5345; C. Bock, C. Paquet, M. Couillard, G. A. Botton and B. R. MacDougall, Size-selected synthesis of PtRu nano-catalysts: Reaction and size control mechanism, J. Am. Chem. Soc., 2004, 126, 8028-8037.
19. J. P. Espinos, J. Morales, A. Barranco, A. Caballero, J. P. Holgado and A. R. Gonzalez-Elipe, Interface effects for Cu, CuO, and Cu_2O deposited on SiO_2 and ZrO_2. XPS determination of the valence state of copper in Cu/SiO_2 and Cu/ZrO_2 catalysts, J. Phys. Chem. B, 2002, 106, 6921-6929.
20. A. Y. Klyushin, T. C. R. Rocha, M. Havecker, A. Knop-Gericke and R. Schlogl, A near ambient pressure XPS study of Au oxidation, Phys. Chem. Chem. Phys., 2014, 16, 7881-7886.
21. C. S. Higman, A. E. Lanterna, M. L. Marin, J. C. Scaiano and D. E. Fogg, Catalyst Decomposition during Olefin Metathesis Yields Isomerization-Active Ruthenium Nanoparticles, ChemCatChem, 2016, 8, 2446-2449.
22. R. B. Bedford, C. S. J. Cazin and D. Holder, Coord. Chem. Rev., 2004, 248, 2283-2321; CRC Handbook of Chemistry and Physics, Taylor and Francis Group: Boca Raton, FL, 2007.
23. B. Sahoo, A. E. Surkus, M. M. Pohl, J. Radnik, M. Schneider, S. Bachmann, M. Scalone, K. Junge and M. Belle, A Biomass-Derived Non-Noble Cobalt Catalyst for Selective Hydrodehalogenation of Alkyl and (Hetero)Aryl Halides, Angew. Chem. Int. Ed., 2017, 129, 11394-11399.

24. J. J. Devery, J. D. Nguyen, C. Dai and C. R. J. Stephenson, Light-Mediated Reductive Debromination of Unactivated Alkyl and Aryl Bromides, ACS Catal., 2016, 6, 5962−5967.
25. L. B. Liao, Q. H. Zhang, Z. H. Su, Z. Z. Zhao, Y. N. Wang, Y. Li, X. X. Lu, D. G. Wei, G. Y. Feng, Q. K. Yu, X. J. Cai, J. M. Zhao, Z. F. Ren, H. Fang, F. Robles-Hernandez, S. Baldelli and J. M. Bao, Efficient solar water-splitting using a nanocrystalline CoO photocatalyst, Nat. Nanotechnol., 2014, 9, 69-73; A. S. Hainer, J. S. Hodgins, V. Sandre, M. Vallieres, A. E. Lanterna and J. C. Scaiano, Photocatalytic Hydrogen Generation Using Metal-Decorated TiO_2: Sacrificial Donors vs True Water Splitting, ACS Energy Lett., 2018, 3, 542-545; A. Elhage, A. E. Lanterna and J. C. Scaiano, Tunable Photocatalytic Activity of Palladium-Decorated TiO_2: Non Hydrogen-Mediated Hydrogenation or Isomerization of BenzylSubstituted Alkenes, ACS Catal, 2017, 7, 250-255.
26. A. Elhage, A. E. Lanterna and J. C. Scaiano, Light-Induced Sonogashira C–C Coupling under Mild Conditions Using Supported Palladium Nanoparticles, ACS Sustainable Chem. Eng., 2018, DOI: 10.1021/acssuschemeng.1027b02992.
27. P. Roy, A. P. Periasamy, C. T. Liang and H. T. Chang, Synthesis of Graphene-ZnO-Au Nanocomposites for Efficient Photocatalytic Reduction of Nitrobenzene, Environ. Sci. Technol., 2013, 47, 6688-6695; B. W. Zhou, J. L. Song, H. C. Zhou, L. Q. Wu, T. B. Wu, Z. M. Liu and B. X. Han, Light-driven integration of the reduction of nitrobenzene to aniline and the transformation of glycerol into valuable chemicals in water, RSC Adv., 2015, 5, 36347-36352.
28. H. Y. Zhu, X. B. Ke, X. Z. Yang, S. Sarina and H. W. Liu, Reduction of Nitroaromatic Compounds on Supported Gold Nanoparticles by Visible and Ultraviolet Light, Angew. Chem. Int. Ed., 2010, 49, 9657-9661.
29. K. Selvam, H. Sakamoto, Y. Shiraishi and T. Hirai, Photocatalytic secondary amine synthesis from azobenzenes and alcohols on TiO_2 loaded with Pd nanoparticles, New. J. Chem., 2015, 39, 2856-2860.
30. S. Sarina, E. R. Waclawik and H. Y. Zhu, Photocatalysis on supported gold and silver nanoparticles under ultraviolet and visible light irradiation, Green. Chem., 2013, 15, 1814-1833; L. B. Wang, X. Q. Pan, Y. Zhao, Y. Chen, W. Zhang, Y. F. Tu, Z. B. Zhang, J. Zhu, N. C. Zhou and X. L. Zhu, A Straightforward Protocol for the Highly Efficient Preparation of Main-Chain Azo Polymers Directly from Bisnitroaromatic Compounds by the Photocatalytic Process, Macromol., 2015, 48, 1289-1295.
31. H. M. D. Bandara and S. C. Burdette, Photoisomerization in different classes of azobenzene, Chem. Soc. Rev., 2012, 41, 1809-1825.
32. K. L. McGilvray, M. R. Decan, D. Wang and J. C. Scaiano, Facile photochemical synthesis of unprotected aqueous gold nanoparticles, J. Am. Chem. Soc., 2006, 128, 15980-15981.

5.3 Postprint Version of Supporting Information

EXPERIMENTAL DETAILS

Instrumentation

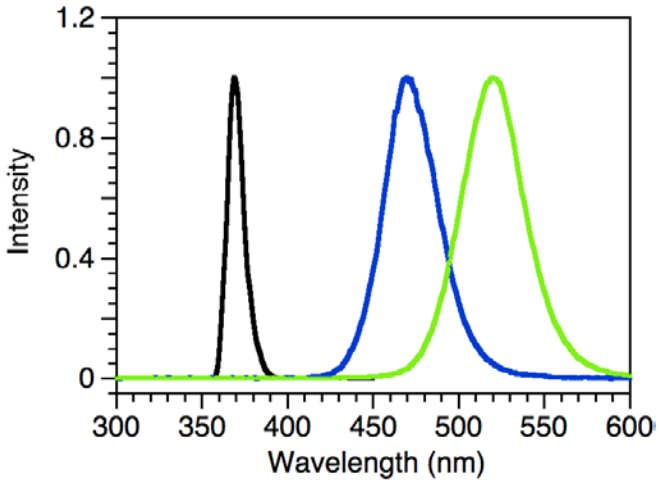

Figure S5.1. Normalized emission spectra of the LEDs used in this work: 368 nm (black), 465 nm (blue) and 532 nm (green).

Catalyst Preparation

Glass wool pre-treatments:

Activation using harsh acid-conditions

Surface activation of SGW was performed using HCl 6M solution, sodium hydroxide NaOH 6M, MeOH:HCl solution[1] and piranha solution[2]. In order to determine the best activation method, the materials were subjected to AuNPs loading. This metal was selected as the formation of AuNP on the GW surface would turn the off-white color of GW into purple/pink when the particles are successfully anchored to the surface, thus giving an easy way to determine the metal modification. Among the different activation processes only two seemed to successfully attach AuNPs to the surface (pink color, see Figure 5.2i in MS), these are the treatments with HCl or NaOH. However, the last one changes drastically the mechanical properties of the GW, which after treatment

becomes harder and brittle, converting the fibers in a fine powder. For this reason, only the treatment with HCl was considered for further work. Briefly, the SGW was soaked for 3 days in a 6M HCl solution and then recovered by filtration, washed several times with pure water until pH ~6 is reached. The resulting material was dried in the oven at 100°C overnight prior to further functionalization.

Activation using (3-Aminopropyl)triethoxysilane (APTES)

Both, the HCl-treated SGW and NGW surfaces were further modified by the addition of APTES. The APTES-amino groups are believed to facilitate the formation of siloxane bonds with surface Si-OH.[3] Briefly, APTES was grafted by immersing the NGW (or SGW) in a solution of 1% concentration of APTES in HPLC grade toluene and heating at 110 °C overnight to allow monolayer coverage.[4] After cooling down to room temperature, the mixture was stirred for 6 hours and then washed with toluene (3x) and acetone (3x) in order to remove weakly bonded silane molecules and hydrolyzes residual alkoxy linkages in the silanized layer. The resulting material was dried in the oven at 100°C overnight prior to metal decoration. We will refer with an asterisk all GW subjected to APTES modification (*i.e.*, GW*).

Metal decoration:

Thermal methods

Ru@NGW and Ru@SGW*:* Ru supported on NGW activated with APTES (NGW*) was prepared as follows: 500 mg of NGW* and 50 mg of $RuCl_3 \bullet xH_2O$ (enough for 3% Ru@NGW*, w/w%) were dispersed in 50 mL of Milli-Q water. The resulting mixture was stirred overnight in a fumehood prior to filtration and then washed with Milli-Q water at least five times to remove unreacted species. The resulting material was dried in an oven overnight at 100°C. The light grey fibers were characterized by SEM, XPS, ICP-EOS and EDS. Same protocol was followed for Ru supported on APTES-treated SGW (SGW*).

*Pd@NGW**. Palladium supported on NGW activated with APTES was prepared using the protocol described for the synthesis of Ru@NGW. The material was prepared aiming for 2% Pd@NGW*, w/w%. The resulting brownish fibers were characterized by SEM, XPS, ICP-EOS and DRS.

Photochemical methods

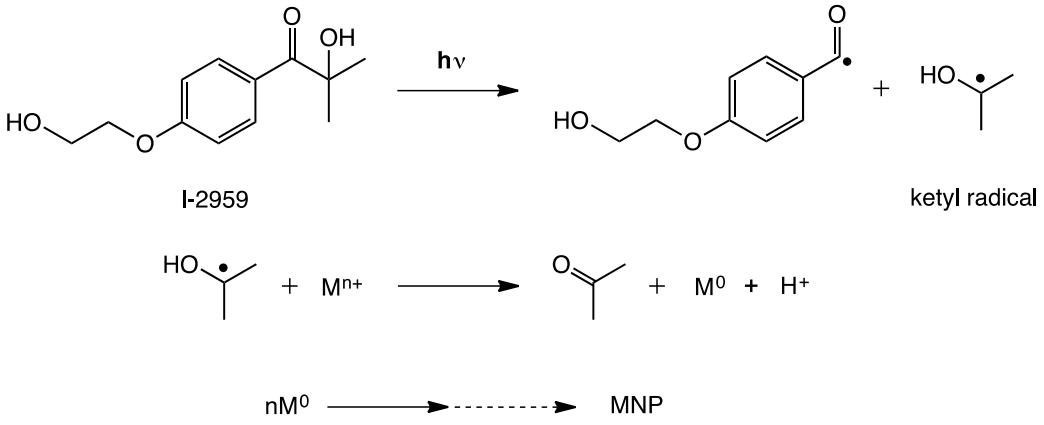

Scheme S5.1. Norrish Type I cleavage of the benzoin I-2959 forming ketyl radicals that subsequently can reduce metal cations into the corresponding metal species.

Synthesis of Pd@SGW. Palladium supported on SGW was prepared by photodeposition of $PdCl_2$ onto the SGW. In brief, 500 mg of activated SGW and $PdCl_2$ (22 mg, for 3% Pd@SGW, w/w%) were dispersed in 200 mL of Milli-Q water and sonicated for 15 min. Next, 24 mg of the I-2959 in 10 mL of EtOH 99% were added as a photo-initiator, the resulting mixture was purged with Ar for 15 min then irradiated in a Luzchem photoreactor equipped with 14 UVA bulbs for 1 h under vigorous stirring. The brownish/grey fibers were filtered and washed with Milli-Q water at least five times to remove unreacted $PdCl_2$ and dried in the oven overnight at 100°C. The resulting dark gray fibers were characterized by SEM, XPS, ICP-EOS and DRS.

Synthesis of Co@SGW. Cobalt supported on SGW was prepared by photodeposition of $CoCl_2$ onto HCl-treated SGW using the same procedure as for Pd@SGW utilizing enough Co precursor to obtain 3 % Co@SGW, w/w%. The resulting light gray fibers were characterized by SEM, XPS, ICP-EOS and DRS.

Synthesis of Cu@NGW. Copper supported on pristine NGW and on NGW* was prepared by photodeposition of $CuCl_2.2H_2O$ (enough amount for 5% Cu@GW w/w%) onto NGW (or NGW*) using the same procedure explained above for Pd@SGW. The resulting brownish/redish fibers were characterized by SEM, XPS, ICP-EOS and DRS.

*Synthesis of Au@NGW***.** Gold supported on NGW* was prepared by photodeposition of $HAuCl_4$ (for 3% Au@NGW*, w/w%) onto NGW*. The resulting purple fibers were characterized by SEM, XPS, ICP-EOS and DRS.

Catalytic reactions

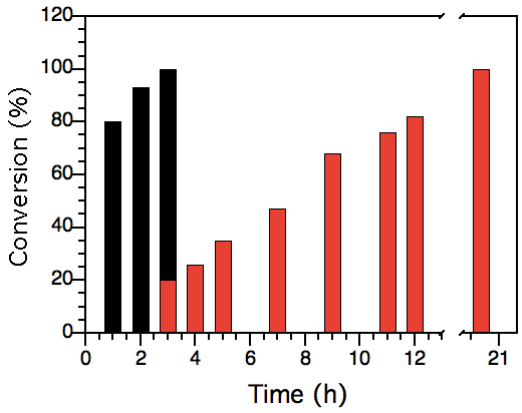

Figure S5.2. Photoreductive dehalogenation of 4-chloromethylbenzoate catalyzed by Co@SGW (Black) and Pd@SGW (red) under conditions described in Table 5.2.

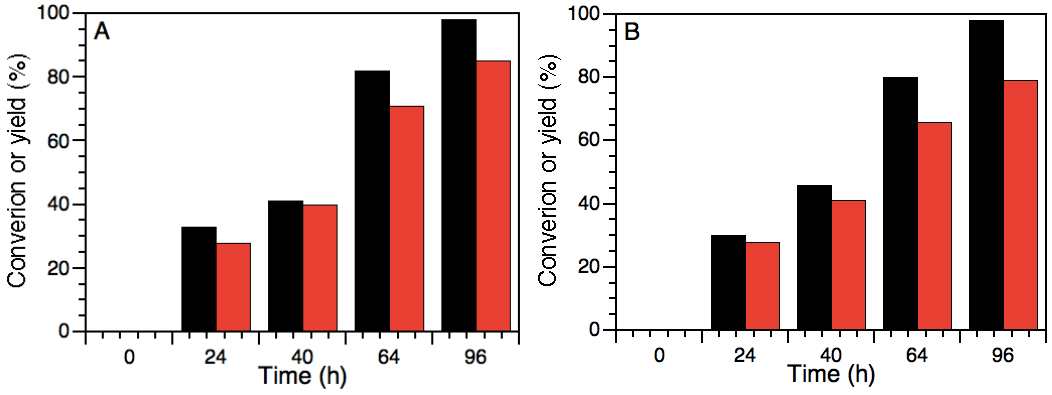

Figure S5.3. Kinetics of Reduction of nitrobenzene to aniline catalysed by (A) Ru@SGW* and (B) Ru@NGW*. Conversion (black) and yield (red).

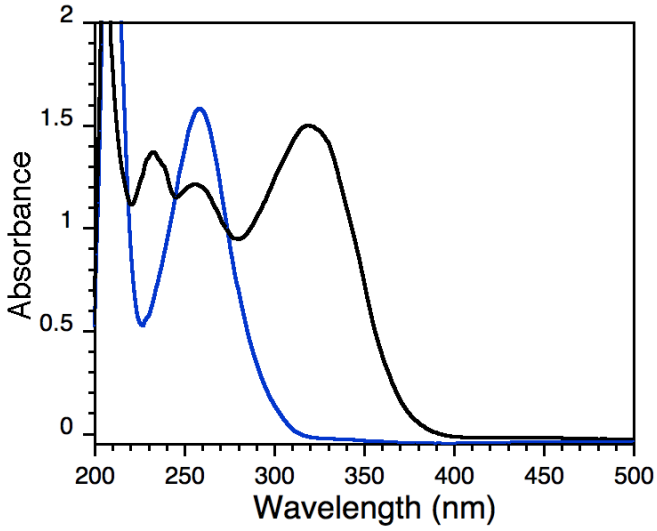

Figure S5.4. Photoreduction of nitrobenzene toward azobenzene catalyzed by Au@NGW* under conditions described in table 5.5, entry i. Absorption spectra of reaction mixture before (blue) and after 24 h of irradiation (black).

Table S5.1. Catalyst reusability

Reaction	Catalyst	Cycle	Time (h)	% Conv	%Yield	Apparent rate (M h^{-1})
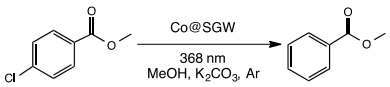	Co@SGW	1	3	100	>99	>13.3
		2	3	100	>99	>13.3
		3	3	75	75	10.0
		3[a]	4	100	>99	>10.0
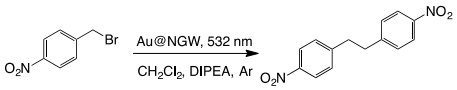	Au@NGW*	1	5	77	64	3.9
		1	7	100	80	>3.6
		2	5	58	43	2.9
		2[b]	24	82	66	0.9
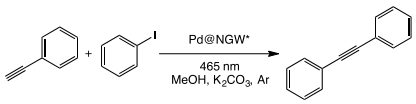	Pd@NGW*	1	5	100	90	6.0
		2	5	90	68	5.4
		2[c]	7	100	87	>4.3

[a] Remaining Co loading = (0.0276 ± 0.0004)%. [b] Remaining Au loading = (0.592 ± 0.007)%; Au particle size = (35 ± 12) nm. [c] Remaining Pd loading = (0.369 ± 0.007)%; Pd particle size = (28 ± 10) nm.

CHARACTERIZATION OF THE CATALYSTS

Electron microscopy characterization

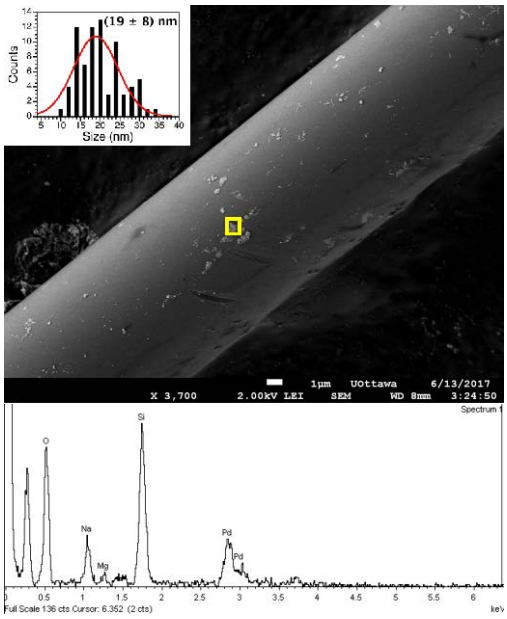

Figure S5.5. SEM image and particle size distribution (*top*) and EDS spectrum of the squared area (*bottom*) of Pd@SGW. Notice that agglomerated particles were not considered to determine particle size distribution.

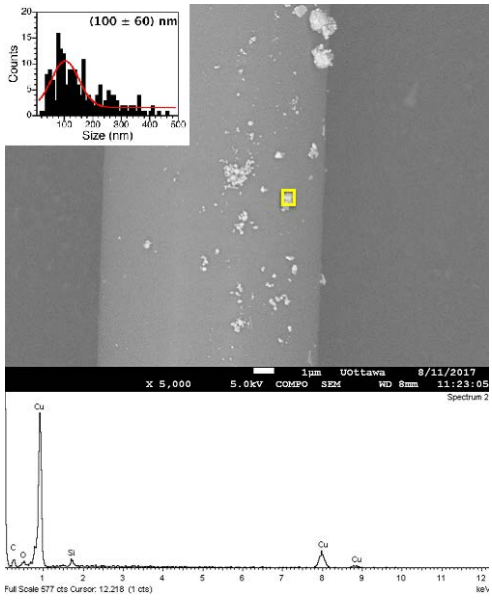

Figure S5.6. SEM image and particle size distribution (*top*) and EDS spectrum of the squared area (*bottom*) of Cu@NGW. Notice that agglomerated particles were not considered to determine particle size distribution.

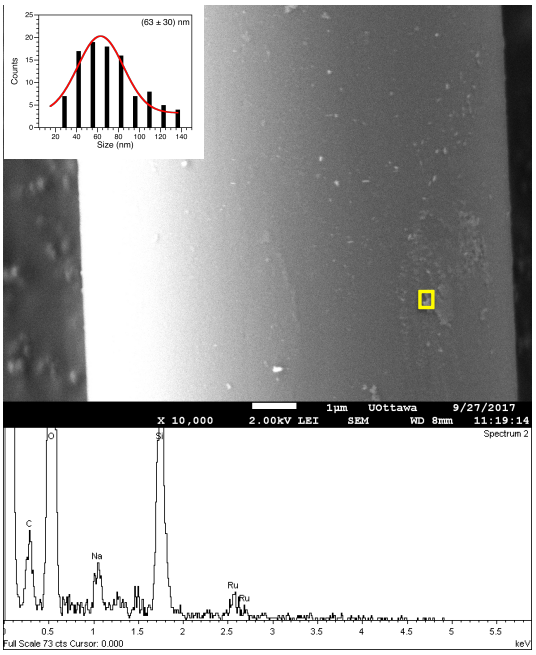

Figure S5.7. SEM image and particle size distribution (*top*) and EDS spectrum of the squared area (*bottom*) of Ru@NGW*. Notice that agglomerated particles were not considered to determine particle size distribution.

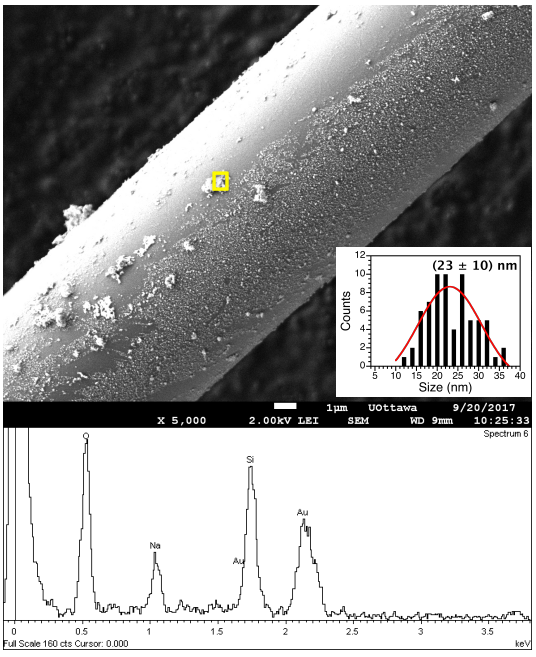

Figure S5.8. SEM image and particle size distribution (*top*) and EDS spectrum of the squared area (*bottom*) of Au@NGW*. Notice that agglomerated particles were not considered to determine particle size distribution.

Diffuse reflectance spectroscopy

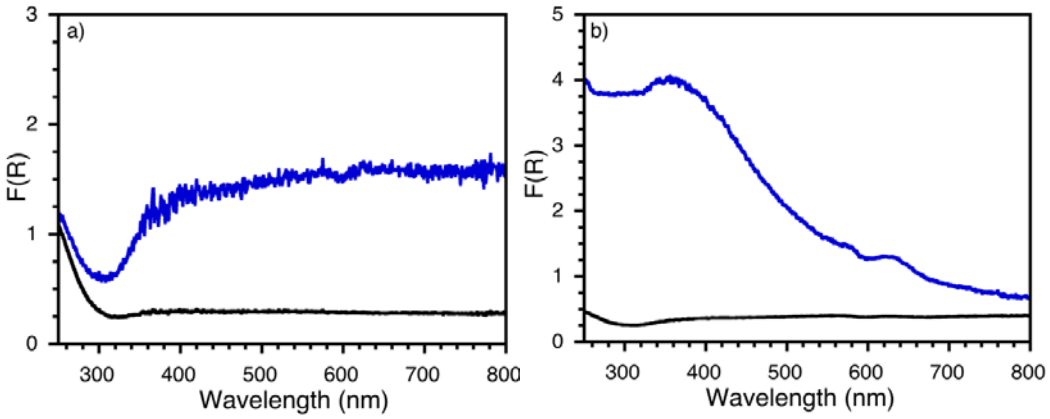

Figure S5.9. a) Diffuse reflectance spectra for HCl-treated SGW (black) and for Pd@SGW (blue) and b) for NGW* (black) and for Pd@NGW* (blue).

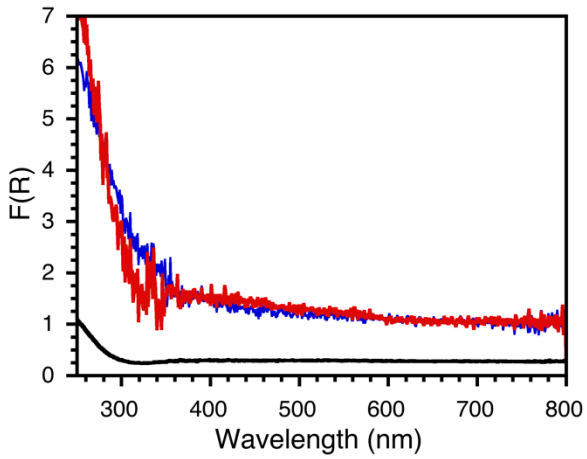

Figure S5.10. Diffuse reflectance spectrum of treated NGW* (black), Cu@NGW* (blue) and Cu@NGW (red).

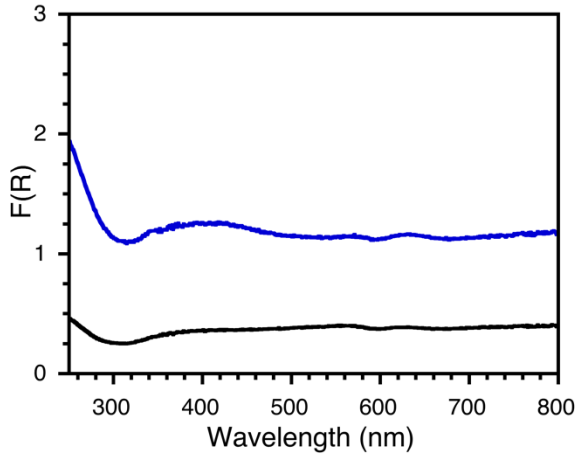

Figure S5.11. Diffuse reflectance spectrum of treated NGW* (black) and Ru@NGW* (blue)

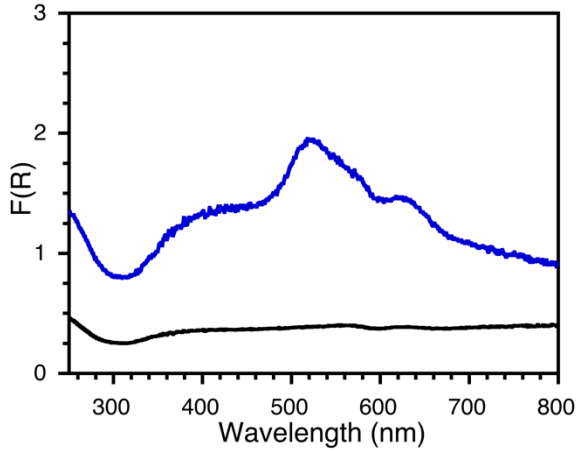

Figure S5.12. Diffuse reflectance spectrum of treated NGW* (black) and Au@NGW* (blue)

X-ray Photoelectron Spectroscopy

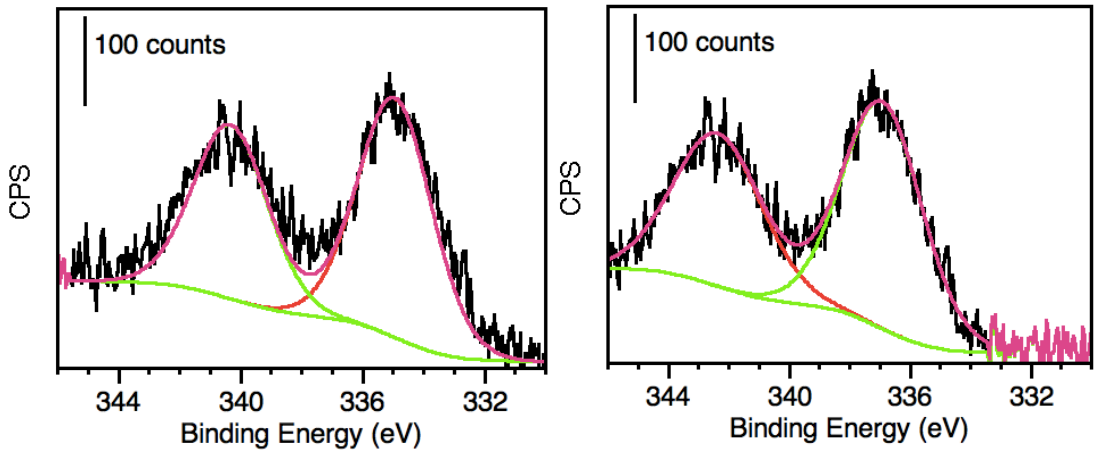

Figure S5.13. Deconvoluted Pd 3d HR-XPS spectrum for Pd@SGW (*left*) and Pd@NGW* (*right*) catalysts.

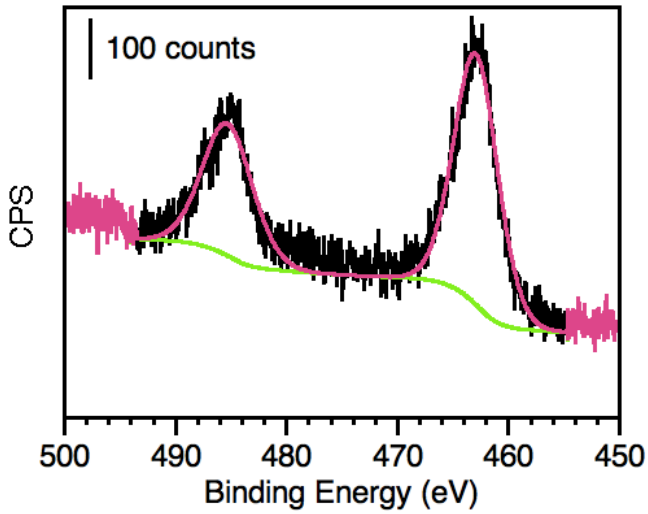

Figure S5.14. Deconvoluted Ru 3p HR-XPS spectrum for Ru@NGW* catalyst.

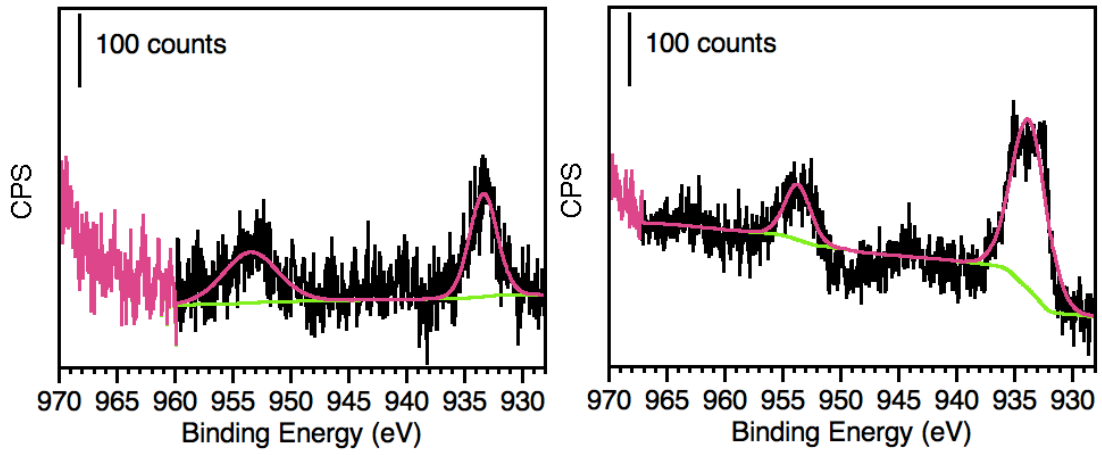

Figure S5.15. Deconvoluted Cu 2p HR-XPS spectrum for Cu@NGW (*left*) and Cu@NGW* (*right*).

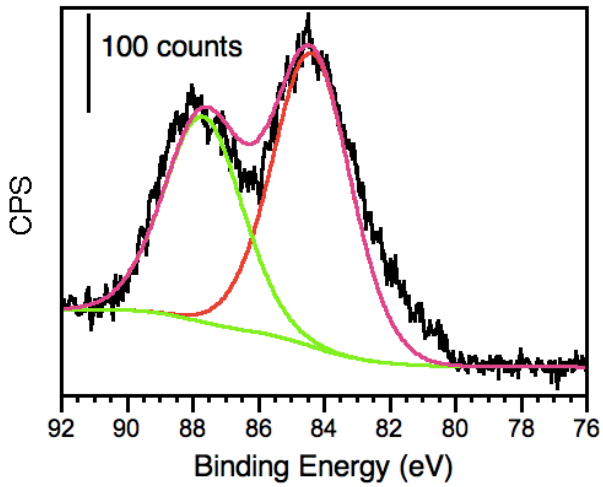

Figure S5.16. Deconvoluted Au 4f HR-XPS spectrum for Au@NGW* catalyst.

REFERENCES

1. J. J. Cras, C. A. Rowe-Taitt, D. A. Nivens and F. S. Ligler, Comparison of chemical cleaning methods of glass in preparation for silanization, Biosens. Bioelectron., 1999, 14, 683-688.
2. N. Aissaoui, L. Bergaoui, J. Landoulsi, J. F. Lambert and S. Boujday, Silane layers on silicon surfaces: mechanism of interaction, stability, and influence on protein adsorption, Langmuir., 2012, 28, 656-665.
3. L. R. Chamberlain, L. D. Durfee, P. E. Fanwick, L. Kobriger, S. L. Latesky, A. K. McMullen, I. P. Rothwell, K. Folting, J. C. Huffman, W. E. Streib and R. Wang,

Synthesis, structure and spectroscopic properties of early transition metal .eta.2-iminoacyl complexes containing aryl oxide ligation, J. Am. Chem. Soc., 1987, 109, 390-402; S. K. Vashist, E. Lam, S. Hrapovic, K. B. Male and J. H. T. Luong, Immobilization of Antibodies and Enzymes on 3‑Aminopropyltriethoxysilane-Functionalized Bioanalytical Platforms for Biosensors and Diagnostics, Chem. Rev., 2014, 114, 11083−11130.

4. E. T. B. Vandenberg, L.; Liedberg, B.; Uvdal, K.; and R. E. Erlandsson, H.; Lundström, I. J, Structure of 3-aminopropyl triethoxy silane on silicon oxide, J. Colloid. Interface Sci., 1991, 147, 103-118.

This manuscript has been adapted from Chem. Sci**.**, **2018,** 9,6844-6852 with permission, from the Royal Chemical Society. Small changes to the original manuscript provide consistent formatting and clarity with respect to the overall thesis.

5.4 Accompaniment to Chapter 5

We implemented a novel fibrous support for heterogeneous photocatalysis. Glass wool fiber is an inexpensive and widely available material with different surface properties that can be easily modified prior to metal or metal oxide nanoparticle grafting. Metal decoration of glass wool surface was performed using either photochemical or thermal approaches. The resulting hybrids materials are robust and mechanically stable, they excel in both thermal and light-induced catalysis in a variety of different organic transformations ranging from reductions to C-C couplings and cycloadditions. Our main goal when performing this line of research was to develop a fibrous catalyst, easy to recover from batch reaction with great potential towards continuous flow chemistry applications. Chapter 6 describes in details the application of glass wool and glass filters as catalyst supports in continuous flow heterogeneous photocatalysis.

6. Scalable Strategies for Continuous Flow Heterogeneous Photocatalysis

6.1 Preamble to Chapter 6

Continuous flow chemistry has gained lots of interest in industries and research laboratories. The main advantages of continuous flow chemistry are enhanced mixing and heat transfer. However, the drawback of widely used microflow reactor is that solid catalyst in powder form would clog the miniaturized flow devices. Therefore, immobilization of catalysts by a fibrous or filament-type support is of significant importance in this field. The fibrous support offers the benefits of being easily packed in the flow reactor, recovered after reaction by using a pair of tweezers, and mainly used to restrict the mobility of active catalyst. Hence, our approach presented in chapter 6 to heterogeneous flow-photocatalysis is based on using glass fibers as a support to immobilize the nanocatalysts (*i.e.* PdNP) that will stay in place while reactants are flowing. Glass fibers are robust, mechanically stable and easy to recovery after reaction. As test reactions for the flow system, we used the Sonogashira C-C coupling reaction (C-C bond coupling is a key reaction in organic synthesis) and the dehalogenation of iodoarenes. This chapter describes the use of a prototype flow reactor with moderately large cells enabling simple catalyst replacement and cell reassembly. Likewise, this new flow system (flow reactor and catalysts) is expected to facilitate scale-up to production levels.

6.2 Postprint Version of submitted Manuscript

ABSTRACT

The Sonogashira C-C coupling reaction and the dehalogenation of iodoarenes have been used as test reactions to evaluate the use of fibrous catalyst for heterogeneous flow photocatalysis in a moderately large volume flow assembly. The approach circumvents the surface limitations intrinsic to derivatization of the flow channel surface by using catalysts that are robust and mechanically stable, while at the same time having excellent light transmission properties. The use of relatively large flow cells enabling simple catalyst replacement and cell reassembly is expected to facilitate scale-up to production levels. The catalysts tested are based on palladium-decorated glass wool, already utilized in earlier work, as well as a new support consisting of fibrous glass filters, which shows good mechanical stability.

INTRODUCTION

Flow chemistry has been used for decades in the production of commodities, such as petroleum-derived products (e.g., processes such as fluid catalytic cracking) and over the last 20 years as an important tool for liquid phase reactions and to scale up organic reactions at the bench level. Flow catalytic applications in photochemistry are moderately developed for systems in which the homogeneous catalyst flows with the sample, which in most cases means homogeneous catalysis. [1] The use of heterogeneous photo-catalysts in continuous-flow is not trivial,[1] that is reflected in the small number of papers in literature on this subject, one of them dealing with organic synthesis[2] and a few others with environmental remediation mostly related to water treatment. [3] While flow systems are relatively easy to scale up, those dealing with microliter volume may present some challenges for water treatment or pollutant degradation, as at a minimum multiliter scales will be needed. Further, in photochemical systems any scale up will require major surface incrementation, as stacking photoreactors may pose a challenge

for the irradiation efficiency. The majority of flow heterogeneous photocatalysis experiments involve fixing the catalyst to the interior channel surfaces, either by some attachment mechanism, or by direct reaction of the channel material to generate the catalyst.

Our approach to heterogeneous flow photocatalysis is based on the development of catalysts that are either fibrous, filament or highly porous solids constructed of materials that will stay in place while liquid is flowing, and that –at least at the macroscale– are constructed from light transmitting materials. In this contribution, we used two types of glass wool, one of them as a fibrous material, essentially the same type used for house insulation, and the other a semi-rigid filter constructed of compressed glass fibers. Both are readily available commercial materials. Our prototype flow reactor was designed by Luzchem Research, Inc, and consists of four chambers, each one with a volume of about 9 mL. The relatively large volume that poses some challenges at this stage is expected to facilitate scale-up as we reach production levels. This study concentrates on relatively large volume laboratory systems, mechanically robust heterogeneous catalysts that are not part, or chemically attached to the reactor walls, and reactor chambers that are easy to dismantle and reassemble for cleaning or catalyst replacement purposes. We believe that these characteristics are essential for the utilization of flow systems for heterogeneous catalysis in organic chemistry and for water remediation applications.

We have recently reported that palladium nanoparticles on glass wool can photocatalyze Sonogashira couplings in high yields and can be reused.[4] The macroscopic nature of the glass wool makes it easy to be loaded into and recovered from the reaction vessel. The use of amine-functionalized glass wool as a catalyst support is also attractive because it is chemically and photolytically inert, thermally stable, flexible to fit within vessels of various shapes and sizes, and inexpensive. In other words, having flexible, shape-adopting catalysts is highly desirable for flow heterogeneous photocatalysis. In previous analytical studies, our reactions were carried out in small sample tubes where optical path-lengths were short providing excellent mixing and well

distributed light penetration. In contrast, scaling up photosynthetic reactions using conventional hardware require larger reaction vessels and higher reagent concentrations that lead to the irradiation of a smaller fraction of the vessel volume. Even with vigorous stirring this can lead to extensive product irradiation, poor quantum yields, and more side products. Further, if one wants to use nanometric fibrous materials, vigorous stirring is a sure path to catalyst fragmentation and unlikely reusability. Large-scale flow reactions offer several advantages over traditional batch protocols including improved efficiency, scalability, and heat and mass transfer.[5, 6, 7] Several studies show that microreactor technology provides the most efficient and selective flow photochemistry, and scaling up is sometimes achieved not through reactor size but the number of microreactors running in parallel.[7, 8] Nevertheless, this can require a substantial investment in hardware, expertise, and technology to develop microreactors that incorporate specific catalysts. Another goal of the current study is to develop simple but efficient photoreactors that can be readily assembled in a typical synthetic chemistry laboratory and the development and validation of new heterogeneous photocatalysts suitable for flow applications. While there have been many studies focused on homogeneous and heterogeneous metal catalysts in flow systems,[5, 8, 9] limited examples in heterogeneous photocatalysis under continuous flow can be found in the literature.[10, 11]

Based on our expertise of developing heterogeneous photocatalysts for batch systems,[12, 13, 14] we selected Pd-based catalysts and two different reactions to carry out the current study. Sonogashira coupling between iodobenzene and phenylacetylene, and reductive dehalogenation of methyl 4-iodobenzoate (Scheme 6.1) were chosen to investigate the photocatalytic activity of Pd nanoparticles (PdNP) deposited on glass wool (GW) and glass filters (GF) using the flow reactor illustrated in Figure 6.1.

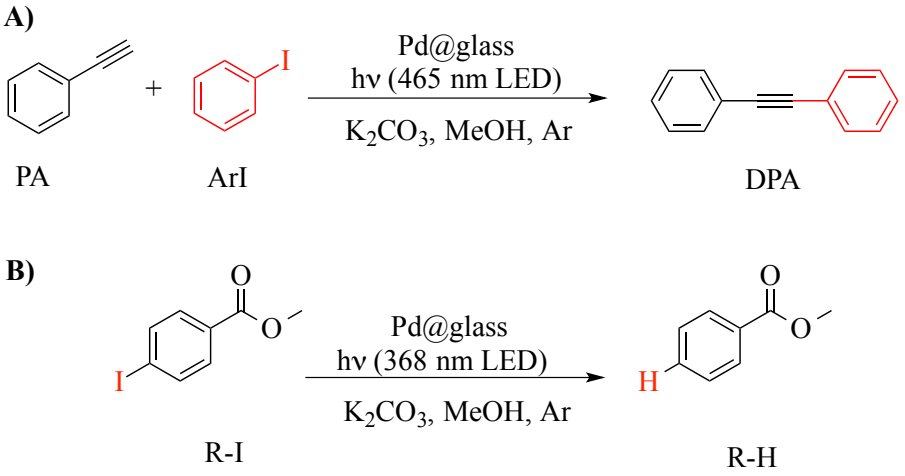

Scheme 6.1. Model reactions used for the continuous flow system using heterogeneous photocatalysts. A) Light-induced Sonogashira coupling between phenylacetylene (PA) and iodobenzene (ArI) for the quantitatively formation of diphenylacetylene (DPA). B) Light-induced reductive dehalogenation of methyl 4-iodobenzoate (R-I) to yield methylbenzoate (RH).

Experimental

Materials

Unless otherwise specified, all chemicals were purchased from Sigma-Aldrich or Fisher Scientific and used without further purification. Irgacure-2959 (I-2959) was a generous gift from BASF. For the glass materials used as supports, glass wool was purchased from Sigma Aldrich, while glass filters, Type A/E 47 mm, (P/N 61631 from Pall Life Sciences) were purchased from Filtros Anoia SA.

Instrumentation

Scanning electron microscopy (SEM) images were obtained with a JEOL JSM-1600 SE microscope working at an accelerating voltage of 2 kV. Transmission electron microscopy (TEM) images were acquired using the JEOL JEM-2100F FETEM operating at 200 kV. Both techniques are coupled to energy dispersive x-ray spectroscopy (EDS) that allows for identification of the elemental composition of materials. X-ray photoelectron spectroscopy (XPS) data were obtained using a Kratos Nova AXIS spectrometer equipped with an Al X-ray source (AlKα radiation at 1486.69 eV, 150 W, 15 kV), a charge neutralizer, and a three multi-channel plate delay-line

detector. The C 1s peak at 284.8 eV was the binding energy used as reference. XPS data were analyzed using CasaXPS software Version 2.3.15, and the spectra were fitted using a Gaussian 30% Laurentian with a Shirley baseline. The amount of palladium loaded onto the glass material was determined by Inductively Coupled Plasma Optical Emission Spectrometry (ICP-OES) using an Agilent 5110 ICP-OES measuring the Pd 340.458 nm emission line. Samples were prepared in triplicate by weighing approximately 10 mg of catalyst followed by digestion with aqua regia. Diffuse reflectance spectroscopy was carried out in an Agilent Cary 7000 UV-Vis-NIR Universal Measurement Spectrophotometer coupled to an Agilent Praying Mantis accessory.

Photoproduct yields were determined by gas chromatography using a Perkin Elmer Clarus Gas Chromatograph (DB-5 column, 30 m length, 0.320 mm diameter, 0.25 μm film) coupled to a Flame Ionization Detector (GC-FID) with helium carrier gas and *t*-butylbenzene as an external standard.

Light-emitting diodes (LEDs) of 10 W from Led Engin were used for photocatalytic reactions in the visible region (centered at 465 nm) and in the UV region (centered at 368 nm), Figure S6.1.

Catalyst Preparation

Details of the preparation of the palladium nanoparticles (PdNP) deposited on GW have been reported recently.[4] Both GW and GF were activated with 3-aminopropyltriethoxysilane (APTES), prior to the deposition of the PdNP. Briefly, APTES was grafted by immersing the GW or GF in a 1% APTES solution in HPLC grade toluene and refluxing overnight to allow monolayer coverage.[15] After cooling to room temperature, the mixtures were washed with toluene (3x), acetone (3x) and water (3x) to remove weakly bonded silanes and to hydrolyze residual alkoxy linkages in the silanized layer. The resulting materials were dried in the oven at 100°C overnight prior to metal decoration. PdNP were deposited using two different methodologies: 1) thermal method under dark conditions, to afford Pd@GW^{D} or Pd@GF^{D}, and 2) photochemical

method to furnish Pd@GW^{L} or Pd@GF^{L}. Materials labelled as Pd@GW are the same type as published earlier,[4] while those labeled Pd@GF are new catalysts. Although some palladium on the glass surface is in the form of metal oxide, we will refer to all materials as Pd@GW or Pd@GF.

1-Thermal method (preparation of Pd@GW^{D} and Pd@GF^{D}). Activated GW (500 mg) and PdCl2 (18 mg) were stirred in 100 mL of Milli-Q water for two days. After filtration, the GW was washed with 100 mL of Milli-Q water at least five times and dried overnight at 100 °C. Light brown fibers (Pd@GWD) were characterized by SEM, XPS, ICP-EOS and DRS as previously reported.4 The same protocol (without stirring) was followed for the preparation of Pd@GFD. The resulting dark brown glass filters were characterized by TEM, XPS, ICP-EOS and DRS.

2-Photochemical method (preparation of Pd@GW^{L} and Pd@GF^{L})**.** Activated GW (1g) and $PdCl_2$ (36 mg) were sonicated in 200 mL of Milli-Q water for 15 min, then 10 mL of an ethanolic solution of I-2959 (3 eq.) were added, and the mixture was irradiated 2 h in a Luzchem photoreactor equipped with 14 UVA lamps (typically ~0.029 W/cm^2 with ~4% spectral contamination). The grey fibers were filtered and washed with 100 mL of Milli-Q water at least five times to remove unreacted $PdCl_2$ and dried in the oven overnight at 100 °C. The resulting dark grey fibers were characterized by SEM, XPS, ICP-EOS and DRS. The same protocol was followed (without stirring) for the synthesis of Pd@GF^{L}. The resulting dark grey glass filters were characterized by TEM, XPS, ICP-EOS and DRS.

Sample Preparation for TEM Imaging

In a clean and dry mortar, ~10 mg of the photocatalyst were grinded then suspended in ~ 5 mL of ethanol and sonicated for 10-15 min. One to two drops of the supernatant were deposited on carbon-coated copper grid and left to dry at room temperature prior to imaging.

Flow Reactor Construction

The flow system was designed by Luzchem Research, Inc (Ottawa, Canada) and provided as a prototype. It consisted of a 4”x 4” square Teflon block with four round cells (1/3” deep by 3/2” wide, 38 mL total) connected serially and terminated by Luer Joints at the first and last cell (Figure 6.1); an aluminium frame (5”x5”) completed the assembly. Cell volumes were minimized as needed by partially filling with 3.6 cm diameter glass discs. The reactor face was polished on flat surface with 320-grit sandpaper and sealed with Teflon tape to a 100 mm square by 9.5 mm thick glass window. Commercial 3/8” glass plate obtained from a local vendor was used in the interest of making the reactor construction economically accessible for other research groups. The reactor was connected in a closed loop with Teflon tubing (Cole-Parmer PTFE Tubing, 1/16"ID x 1/8"OD, # RK-06605-27) to a reservoir (usually a septum-sealed graduated cylinder) and a Masterflex peristaltic pump (6” x 3/16“ ID Masterflex platinum-cured silicone tubing, L/S 15, Item # RK-96410-15).

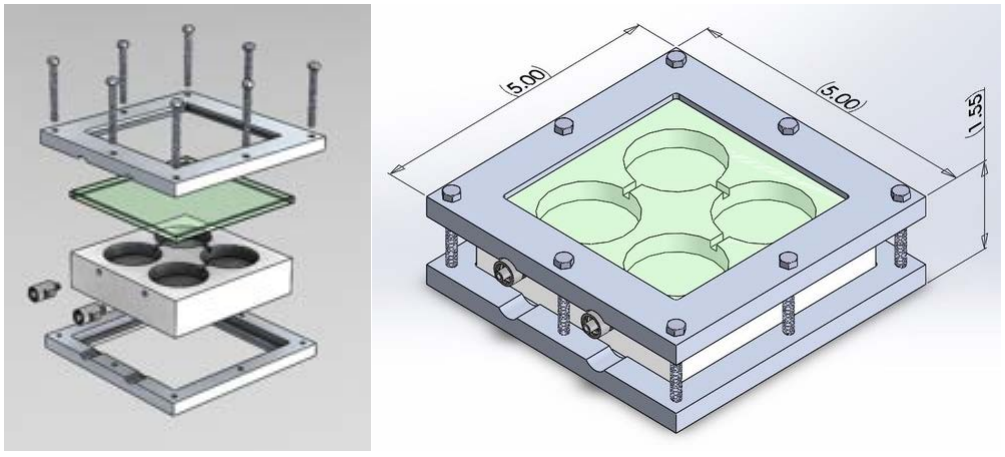

Figure 6.1. Teflon flow reactor with Inlet/outlet connections (Luer joints). Dimensions: 4”x 4” square Teflon block with four round cells (1/3” deep by 3/2” wide, 38 mL total. Drawing courtesy from Luzchem Research Inc.

Catalytic Reactions

All solutions were purged at least 15 min with Argon during preparation and continuously during reaction.

Sonogashira coupling. Details of light-induced Sonogashira coupling have been described previously.[4] Preliminary studies to investigate the effect of flow were carried out with catalyst in a septum-sealed test tube connected to a reservoir. Irradiated solution was sampled from the test tube before and after circulation with the reservoir. Thermal and light induced coupling were compared with catalyst loaded in two flow reactor cells (Figure S6.2). The flow reactor was irradiated with two 465 nm LED (Figure S6.2) with a flow rate of 10 mL min^{-1} to maintain temperature at 60 ^{o}C. The same setup was used for the thermal-induced Sonogashira coupling where the reactor was heated to the same temperature with a hot plate and temperature controlled by the flow rate of 9-12 mL min^{-1}. Control experiments were carried out with GF and in the absence of catalyst as mentioned above.

Reductive Dehalogenation. Light-induced reductive dehalogenation described in a previous report was modified for flow experiments.[4] Fresh Pd@GW was loaded into two cells (100 mg each). The flow rate was 9 mL min^{-1} (*ca*. 30 s residence time) as each reactor cell was irradiated with a 368 nm LED (0.33-0.4 Wcm^{-2}).

Results and Discussion

Catalyst Preparation and Characterization

The APTES treatment of GW and GF provides amine groups on the glass surface that can promote the PdNP attachment.[16] PdNP decoration of the APTES-functionalized glass supports was achieved by two different methods. The thermal methodology relies on the use of the amino groups from APTES to reduce the palladium ions to afford the $Pd@GW^{D}$ and $Pd@GF^{D}$. The photochemical method involves the use of a photoinitiator (I-2959) and UVA light to generate ketyl radicals, strong reducing agents that can easily reduce Pd^{2+} into Pd^{0} then generate PdNP as shown in Scheme 6.2, to furnish the $Pd@GW^{L}$ and $Pd@GF^{L}$.

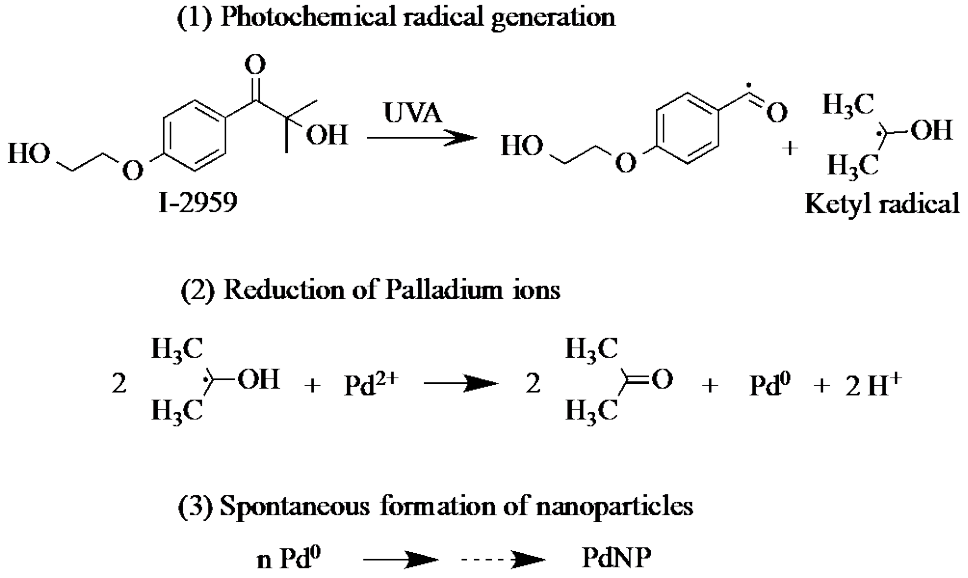

Scheme 6.2. Norrish Type I cleavage of the benzoin I-2959 forming ketyl radicals that subsequently can reduce Pd cations into the corresponding metal species.

The decorated glass fibers were subjected to different characterization techniques. UV-Vis spectroscopy analysis of the materials revealed a broad absorption band in the visible region for the derivatized glass supports, which is attributed to the presence of PdNP (Figures S6.3-S6.4). Electron microscopy images indicate the GW fibers are ~10 μm diameter while the GF fibers are between 100 and 160 nm (Figure S6.5-S6.9). The TEM images also reveal that the fibers are uniformly cylindrical with relatively smooth surfaces, and a simple geometrical calculation indicates the GF fibers surface area per gram is 60-100 times that of GW fibers. TEM imaging of the PdNP derivatized glass materials show the presence of PdNP that were further confirmed by EDS analysis (SI and Figure 6.2). The particle size distribution was determined by manual counting and sizing of particles identifiable by TEM, and are reported in Table 6.1 together with the amount of Pd loaded on each glass support determined by ICP-EOS. XPS spectra of the APTES functionalized glass supports reveal the presence of nitrogen on the surface of treated material (*cf.* Figures S6.10 and S6.11). Analyzing the Pd 3d binding energy region (Figure 6.3), HR-XPS spectrum suggests that a mixture of Pd^0 and PdO species is present in the Pd@GF^L. Interestingly, after use in the light-induced Sonogashira coupling reaction (vide infra) more reduced Pd species

are found in the material, suggesting a change in the oxidation state of the catalyst after reaction, as previously proposed.[12, 17] Similar results are observed for the other Pd-decorated glass supports (Figures S6.12-S6.13).

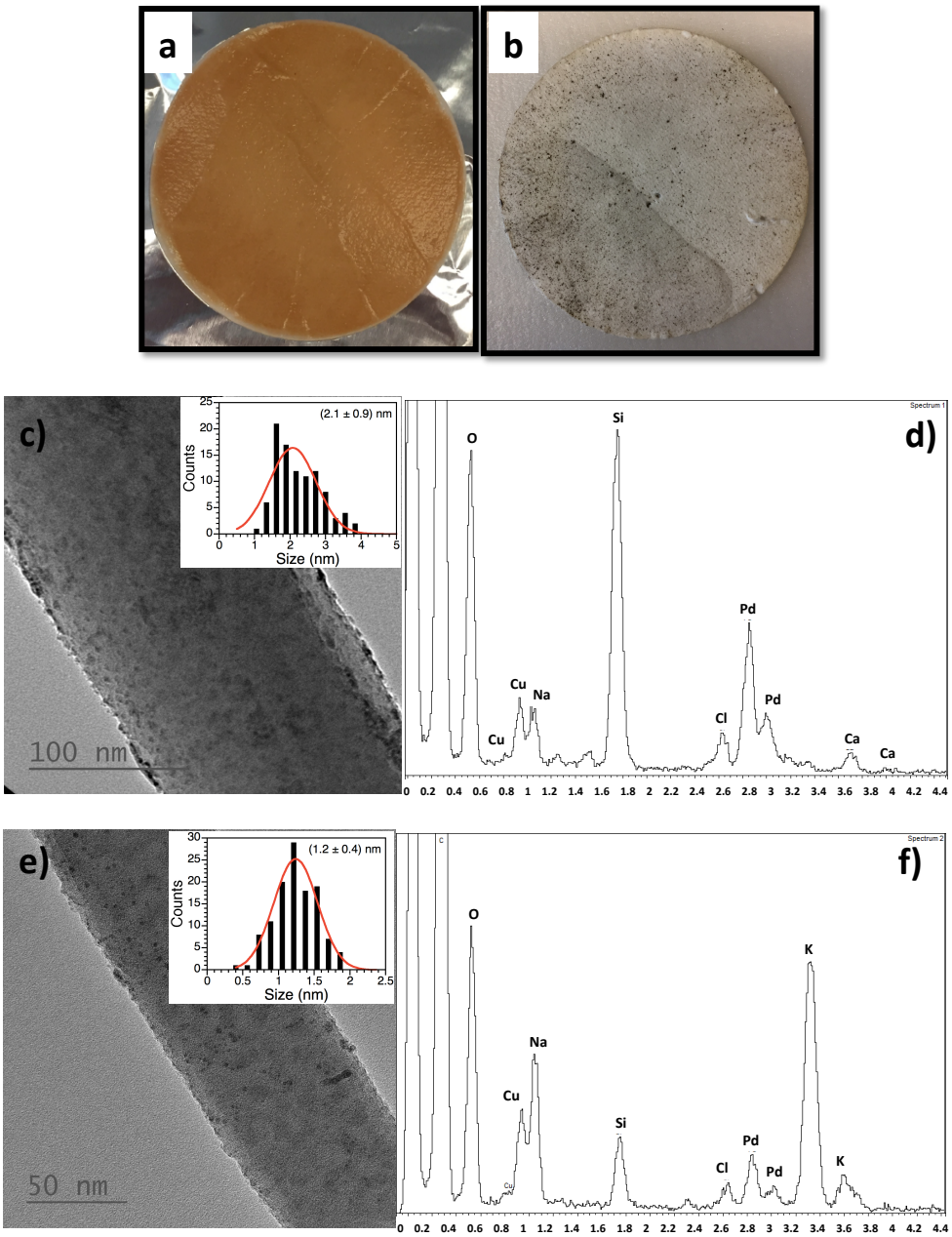

Figure 6.2. a) Thermal-deposition of PdNP on activated GF (Pd@GF^{D}). b) Photo-deposition of PdNP on activated GF (Pd@GF^{L}). TEM images and corresponding EDS spectra of Pd@GF^{D} (c-d) and Pd@GF^{L} (e-f). Particle average size (2.1 ± 0.9) nm and (1.2 ± 0.4) nm, respectively.

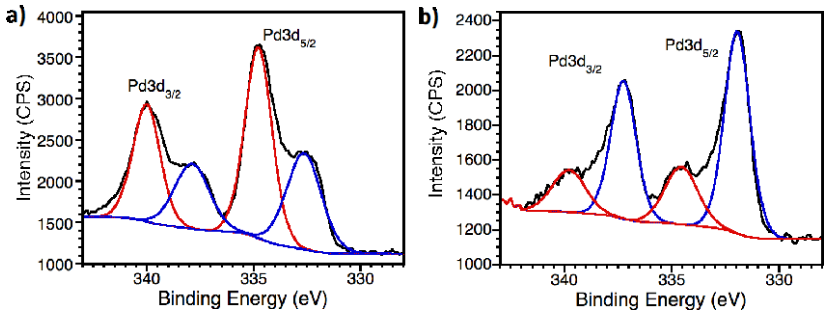

Figure 6.3. a) Pd 3d HR-XPS spectrum of Pd@GF^{L}: Pd 3d core-level spectrum deconvoluted by using two spin-orbit split Pd $3d_{5/2}$ and Pd $3d_{3/2}$ components centered at 334.5 eV and 339.9 eV and separated by ~5.4 eV; attributed to PdO. A considerable contribution of more reduced Pd species are also found on the material (components at 332.4 eV and 337.8 eV). b) Pd 3d HR-XPS spectrum of Pd@GF^{L} after use in the light-induced Sonogashira reaction showing higher concentration of more reduced Pd species.

Table 6.1. Characterization of palladium content on the metal-derivatized glass supports

Catalyst	% Pd loading (wt%)[a]	Particle size (nm)[b]
Pd@GW^{D}	4.8 ± 0.2	4.6 ±1.8
Pd@GW^{L}	3.4 ± 0.2	1.4 ± 0.5
Pd@GF^{D}	4.8 ± 0.2	2.1 ± 0.9
Pd@GF^{L}	4.8 ± 0.5	1.2 ± 0.8

[a]By ICP-OES analysis. [b]From TEM imaging.

Sonogashira coupling

Initial studies on the Sonogashira coupling (Scheme 6.1A) reaction were focused on inspecting the Pd@GW^{D} performance under static conditions to be sure the flow assembly (pump, tubing, and reactor components) did not measurably affect the reaction. A septum-sealed test tube, charged with Pd@GW^{D} and 9 mL of reaction solution was connected by Teflon tubing to a pump and a reservoir (graduated cylinder) containing another 21 mL of solution. Teflon tubing extended to the bottom of the test tube, used to deliver and return the solution from and to the reservoir. LED beams were aimed at the catalyst from opposite sides of the test tube. A 62% yield (based on 9 mL sample in the tube) was obtained without flow during the first hour of irradiation with a single 465 nm LED. Analysis after thoroughly mixing the reservoir with the test tube solutions resulted in a 19% yield consistent with the dilution to 30 mL volume (Figure 6.4 *left*, Table S6.1).

Under the same conditions with flow during the second hour, the additional yield of 16 % was nearly the same as the first hour (35% total) with a recirculation of the solution in the reactor nearly five times per hour. Increasing the light intensity with a second LED did not increase significantly the rate of product formation. After 4 h of visible light irradiation, a ~55% yield of desired product was detected. The results in Figure 6.4 (*left*) show that the catalyst functions in the tube reactor and is compatible with the flow assembly. Starting with fresh solution, the catalyst was washed and reused in a second experiment under the same flow conditions with two LEDs and reached 33% yield of coupling product after 9.5 h of irradiation suggesting significant catalyst deterioration (Figure 6.4, *right*). Note the catalytic process is centered exclusively on the Pd nanoparticles to selectively favour the Sonogashira coupling and the support is catalytically inactive.[4, 12] Catalyst deterioration or poisoning is not uncommon in heterogeneous catalysis; this is an important reason why flow systems of scalable heterogeneous catalysis must include easy catalyst replacement as an essential design consideration.

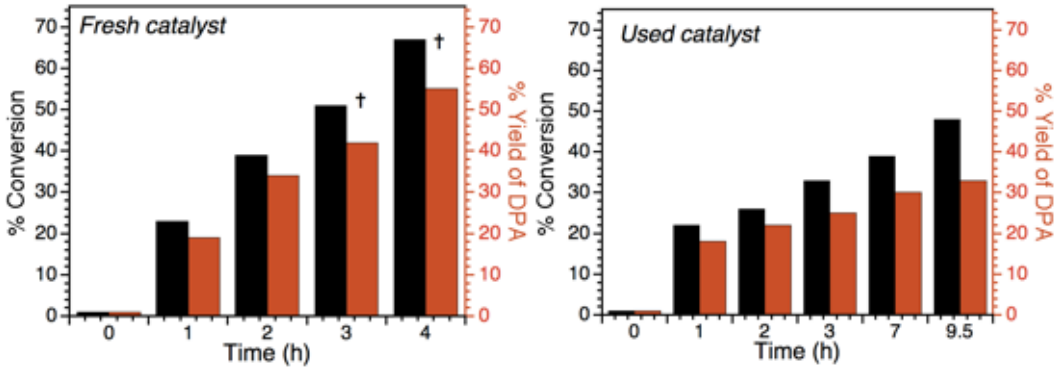

Figure 6.4. Effect of flow and catalyst reusability during Sonogashira coupling using Pd decorated glass wool catalyst in test tube reactor. Pd@GW^{D} (155.7 mg) in a test tube, 0.45 mmol of Ar-I, 0.6 mmol of PA, 0.9 mmol of K_2CO_3, 30 mL HPLC methanol under Argon. *Left:* Fresh catalyst: One 465 nm LED working at 1.6 W.cm^{-2}. No flow in the 1st hour with 9 mL in reactor tube and 21 mL in reservoir. Flow at 2.4 mL min^{-1} from 2nd hour, †two 465 nm LED's. *Right*: Reusability test: used catalyst, 30 mL fresh solution, 2.4 mL min^{-1}, two 465 nm LED's. Numerical tabulation in Table S6.1.

The next study compares the performance of the Teflon reactor (Figure 6.1) with the test tube reactor for Sonogashira coupling. The Luzchem prototype Teflon reactor

volume was reduced to about 12 mL as described in the Experimental section, and the conditions (concentrations, volume, flow, and lamps) are the same as in Figure 6.4 but with nearly twice as much catalyst (290 mg Pd@GW^{D}) layered evenly in two reactor cells above glass spacers. Analysis of the sample after 24 h of reaction show a 55% yield (67% conversion, Figure S6.14), nearly the same result obtained using the test tube reactor for 4 h and less amount of catalyst. While the light intensities for the two LEDs are the same for the test tube and Teflon reactor experiments, the configuration of the Teflon reactor with respect to incident light is not optimized for absorbing all the light since catalyst it was spread evenly over a wide area and the LED light is focused in a small rounded area. Consequently, loading the flow compartment of the photoreactor with big amount of catalyst (~ 290 mg) does not enhance the reaction rate. The optimum amount of catalyst need it in each compartment of the Teflon reactor is between 100 and 150 mg for better light penetration and efficiency (*vide infra*). It is well known that the photocatalytic Sonogashira coupling by PdNP can compete with thermal catalysis,[18, 19] and considering that light absorption can significantly heat the Teflon reactor. We decided to test the contribution of heat, for that the Teflon reactor −loaded with Pd@GW^{L} (no LED irradiation) − was heated, and Sonogashira coupling was evaluated (Figure 6.5, grey bars). After 4 h of heating, only ~23 % of coupling product was detected. Simultaneous light and thermal induced Sonogashira coupling with fresh catalyst at the same temperature was likewise determined using the hot plate to supplement LED heating (Figure S6.2, *right*). The improvement due to light irradiation was determined by subtracting the extent of product formation in the dark (thermal conditions) from the overall yield of DPA obtained when the system was irradiated and heated (Figure 6.5). After 4 h of LED irradiation a ~70 % yield of coupling product was detected, the relative contributions of light and thermal processes to the hetero-coupling product formation is shown in Figure 6.5. In four hours, the photocatalysis (44% yield) appears to be 60% more productive than the thermal catalysis, as it was previously demonstrated.[18, 20]

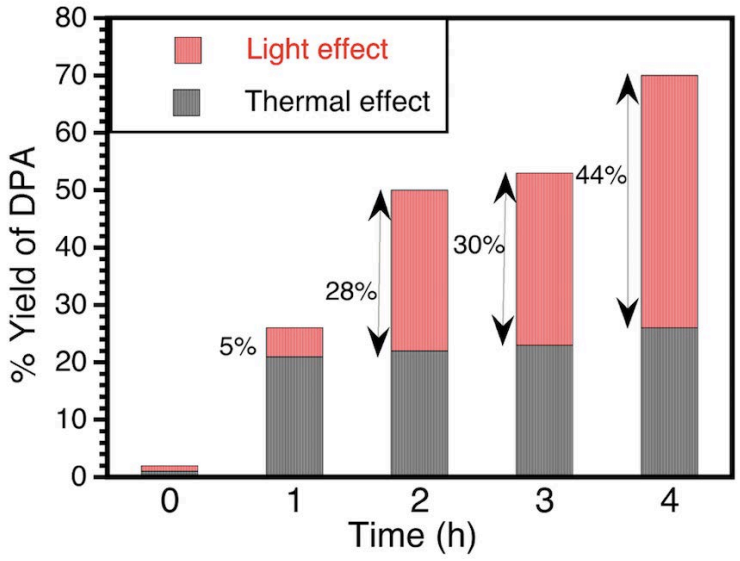

Figure 6.5. Photochemical and thermal contributions to the Sonogashira coupling catalyzed by Pd@GW^{L} under continuous flow in Teflon reactor. The percentage numbers show the photocatalytic contribution. Thermal reaction: Pd@GW^{L} in two cells (100 mg each), 0.82 mmol of iodobenzene, 1.34 mmol of phenylacetylene, and 2.24 mmol of K_2CO_3 in 30 mL MeOH, ~60°C, flowing at 11 mL min^{-1}. The surface temperature recorded with an IR thermometer was 60 °C. Thermal and photo reaction: Pd@GW^{L} in two cells (109.3 and 112.2 mg), 0.80 mmol Ar-I, 1.35 mmol PA, 2.26 mmol K_2CO_3 in 30 mL MeOH, 59°C, 10 mL min^{-1}, two 465 nm LED at 1.6 W cm^{-2}. Numerical tabulation in Table S6.3.

In addition to the greater surface area per gram, palladium-decorated GF are attractive for ease of manipulating into specific shapes and being mechanically "well behaved" by maintaining shape while loading in a reactor cell. Both Pd@GF^{D} and Pd@GF^{L} (Figure 6.2, a and b) were tested for light-induced Sonogashira coupling under continuous flow. Good yields were obtained in 24 h for both filters (Table 6.2). The greater yield after 24h for Pd@GF^{L} (Entry iv, Table 6.2) compare to Pd@GF^{D} (Entry iii, Table 6.2) may be due in part to the different PdNP size distribution. TEM images (Figure 6.2) show that the particle size (~ 2.1 nm) of Pd@GF^{D} was slightly larger than those found by the photochemical deposition on GF (~ 1.2 nm), also agglomeration of NP were observed for Pd@GF^{D} (not shown). This is probably due in part to the deposition time; up to 48h is needed for thermal preparation compare to 2h for the photochemical preparation. The yields are low at 5-6 h compared to Pd@GW^{L} experiments (Figure 6.5). It is important to note that particle size and surface bonding

may play an important role in determining the catalytic activity.[21] Additionally, the dense fibre packing of the filter may influence the exchange and residence time at protected locations in the material. Control experiments using the support GF (without PdNP) and in absence of catalyst were performed. No conversion was observed after 24h of visible light irradiation (Entry i and ii, Table 6.2).

Reductive Dehalogenation

The versatility of Pd@GF photocatalysts in the Teflon reactor was demonstrated with a large-scale dehalogenation of methyl 4-iodobenzoate (Scheme 6.1B). Since the dehalogenation of aryl halides process is dictated by the carbon-halogen bond strength, in some cases reductive dehalogenation requires harsh reactions conditions (H_2, 30 bar), or toxic metal complexes.[22] Here we use continuous flow photoreductive dehalogenation of methyl 4-iodobenzoate under very mild conditions as previously reported.[4] PdNP is known to work as photocatalyst under UV-visible light.[12, 14] It should be noted that the same reaction does not occur thermally. Thus within 6 h, a 87% yield of methyl benzoate was obtained from 0.82 mmol methyl 4-iodobenzoate using two flow compartments with Pd@GF^L (two cells, 100 mg each) and two UV LEDs (Entry v, Table 6.2). The light induced reductive dehalogenation was scaled up by a factor of six again using two UV LEDs but with Pd@GW^L as catalyst (two cells, 100 mg each) with 59% (~0.4 g) and 93% (~0.6 g) yields of desired product for 6 h and 9 h irradiation, respectively (Figure 6.6).

Table 6.2. Sonogashira coupling and reductive dehalogenation photocatalyzed by PdNP@GF.

Entry	Reaction	Catalyst	Time (h)	% Conversion[a]	% Yield[a]
i	Sonogashira	none	24	ND	ND
ii	Sonogashira	GF	24	ND	ND
iii	Sonogashira	Pd@GF^{D}	24	~65	~58
iv	Sonogashira	Pd@GF^{L}	24	~85	~73
v	Dehalogenation	Pd@GF^{L}	6	~99	~87

[a]Conversion and yield determined by GC-FID **Reactions conditions**: Entry 1. Pd@GF^{D} in two cells (140 mg total), 0.81 mmol Ar-I, 2.6 mmol PA, 2.2 mmol K_2CO_3 in 30mL of MeOH, 38 °C, two 465 nm LED at 1.6 W.cm^{-2} Entry 2. Pd@GF^{L} in two cells (150 mg total), 0.80 mmol Ar-I, 2.4 mmol PA, 2.3 mmol K_2CO_3 in 30mL of MeOH, 43 °C, two 465 nm LED at 1.6 W.cm^{-2} Entry 3. Pd@GF^{L} in two cells (100 mg each), 0.82 mmol methyl 4-iodobenzoate, and 2.24 mmol of K_2CO_3 in 30 mL MeOH, flow 7 mL/min at 28 °C, two 368 nm LED working at 0.40 W.cm^{-2}. ND: nothing detected

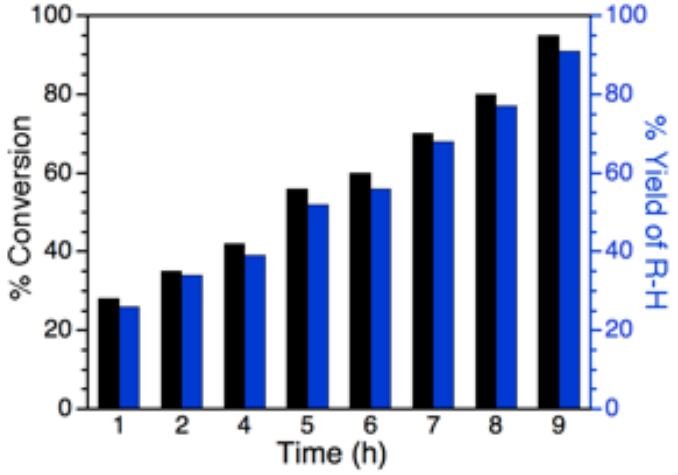

Figure 6.6. Large-scale photocatalytic reductive dehalogenation of methyl-4 iodobenzoate by Pd@GW^{L} versus time under continuous flow. Black bars: % Conversion. Blue bars: % Yield of methylbenzoate. Reaction conditions. Pd@GW^{L} in two cells (100 mg each), 5.0 mmol methyl 4-iodobenzoate and 20.5 mmol K_2CO_3 in 200 mL MeOH, 27 °C, 12.5 mL/min, two 368 nm LED at 0.4 W cm^{-2}. Numerical tabulation in Table S6.4

CONCLUSIONS

In this report we demonstrate the versatility of a simple and easy way to use Teflon photoreactor to evaluate the use of widely available glass fibers as suitable supports for heterogeneous flow photocatalysis. Further, flow systems that can be easily disassembled and reassembled are critical design features required for future scale up of

flow heterogeneous photocatalysis The new flow system (flow reactor and catalysts) is efficient in both thermal and light-induced catalysis for two different types of organics transformations: Sonogashira C-C coupling and reductive dehalogenation. We envision this as a first step toward future flow studies and the design of new robust photocatalysts.

REFERENCES

‡

1. D. Cambie, C. Bottecchia, N. J. W. Straathof, V. Hessel and T. Noel, Applications of Continuous-Flow Photochemistry in Organic Synthesis, Material Science, and Water Treatment, Chem. Rev., 2016, 116, 10276-10341.
2. N. Ishigami, H. Ago, Y. Motoyama, M. Takasaki, M. Shinagawa, K. Takahashi, T. Ikuta and M. Tsuji, Microreactor utilizing a vertically-aligned carbon nanotube array grown inside the channels, Chem. Commun., 2007, 1626-1628.
3. Q. Zhang, Q. H. Zhang, H. Z. Wang and Y. G. Li, A high efficiency microreactor with Pt/ZnO nanorod arrays on the inner wall for photodegradation of phenol, J. Hazard. Mater., 2013, 254, 318-324; M. Krivec, K. Zagar, L. Suhadolnik, M. Ceh and G. Drazic, Highly Efficient TiO_2-Based Microreactor for Photocatalytic Applications, ACS Appl. Mater. Inter., 2013, 5, 9088-9094; N. Wang, F. Tan, L. Wan, M. Wu and X. Zhang, Microfluidic reactors for visible-light photocatalytic water purification assisted with thermolysis, Biomicrofluidics, 2014, 8, 054122.
4. A. Elhage, B. Wang, N. Marina, M. L. Marin, M. Cruz, A. E. Lanterna and J. C. Scaiano, Glass wool: a novel support for heterogeneous catalysis, Chem Sci, 2018, 9, 6844-6852.
5. D. C. Crowley, D. Lynch and A. R. Maguire, Copper-mediated, heterogeneous, enantioselective intramolecular Buchner reactions of alpha-diazoketones using continuous flow processing, J. Org. Chem., 2018, 83, 3794-3805.
6. V. Sans and L. Cronin, Towards dial-a-molecule by integrating continuous flow, analytics and self-optimisation, Chem. Soc. Rev., 2016, 45, 2032-2043.
7. T. Noel, Y. H. Su and V. Hessel, Beyond Organometallic Flow Chemistry: The Principles Behind the Use of Continuous-Flow Reactors for Synthesis, Organometal. Chem., 2016, 57, 1-41.
8. I. Rossetti and M. Compagnoni, Chemical reaction engineering, process design and scale-up issues at the frontier of synthesis: Flow chemistry, Chem. Eng. J., 2016, 296, 56-70.
9. R. Munirathinam, J. Huskens and W. Verboom, Supported Catalysis in Continuous-Flow Microreactors, Adv. Synth. Catal., 2015, 357, 1093-1123; T. Wirth, Microreactors in Organic Chemistry and Catalysis, Wiley-VCH, Weinheim, Germany, 2013.
10. J. Chakraborty, I. Nath and F. Verpoort, Dataset on the development of palladium nanoparticle decorated colloidal porous organic polymer for photocatalytic Suzuki coupling, Data Brief., 2018, 21, 1157-1165; M. T. Yilleng, E. C. Gimba, G. I. Ndukwe, I. M. Bugaje, D. W. Rooney and H. G. Manyar, Batch to continuous photocatalytic degradation of phenol using TiO_2 and Au-Pd nanoparticles supported on TiO_2, J. Environ. Eng., 2018, 6, 6382-6389; J. W. Pickering, V. R. Bhethanabotla and J. N. Kuhn, Plasmonic photocatalytic reactor design: Use of multilayered films for improved organic degradation rates in a recirculating flow reactor, Chem. Eng. J., 2017, 314, 11-18; M. J. Munoz-Batista, D. Rodriguez-Padron, A. R. Puente-Santiago, A. Kubacka, R. Luque and M. Fernandez-Garcia, Sunlight-Driven Hydrogen Production Using an

Annular Flow Photoreactor and g-C_3N_4-Based Catalysts, Chemphotochem., 2018, 2, 870-877.

11. J. Chakraborty, I. Nath and F. Verpoort, Pd-nanoparticle decorated azobenzene based colloidal porous organic polymer for visible and natural sunlight induced Mott-Schottky junction mediated instantaneous Suzuki coupling, Chem. Eng. J., 2019, 358, 580-588; D. Sun, S. Jang, S. J. Yim, L. Ye and D. P. Kim, Metal Doped Core-Shell Metal-Organic Frameworks@Covalent Organic Frameworks (MOFs@COFs) Hybrids as a Novel Photocatalytic Platform, Adv. Funct. Mater., 2018, 28; S. Kumar, A. G. Fedorov and J. L. Gole, Photodegradation of ethylene using visible light responsive surfaces prepared from titania nanoparticle slurries, Appl. Catal. B-Environ., 2005, 57, 93-107.
12. A. Elhage, A. E. Lanterna and J. C. Scaiano, Light-Induced Sonogashira C-C Coupling under Mild Conditions Using Supported Palladium Nanoparticles, ACS Sustain. Chem. Eng., 2018, 6, 1717-1722.
13. B. Wang, J. Durantini, J. Nie, A. E. Lanterna and J. C. Scaiano, Heterogeneous Photocatalytic Click Chemistry, J. Am. Chem. Soc., 2016, 138, 13127-13130.
14. A. Elhage, A. E. Lanterna and J. C. Scaiano, Tunable Photocatalytic Activity of Palladium-Decorated TiO_2: Non-Hydrogen-Mediated Hydrogenation or Isomerization of Benzyl-Substituted Alkenes, ACS Catal., 2017, 7, 250-255.
15. E. T. B. Vandenberg, L.; Liedberg, B.; Uvdal, K.; and R. E. Erlandsson, H.; Lundström, I. J, Structure of 3-aminopropyl triethoxy silane on silicon oxide, J. Colloid. Interface Sci., 1991, 147, 103-118.
16. S. K. Vashist, E. Lam, S. Hrapovic, K. B. Male and J. H. T. Luong, Immobilization of Antibodies and Enzymes on 3‑Aminopropyltriethoxysilane-Functionalized Bioanalytical Platforms for Biosensors and Diagnostics, Chem. Rev., 2014, 114, 11083−11130; L. R. Chamberlain, L. D. Durfee, P. E. Fanwick, L. Kobriger, S. L. Latesky, A. K. McMullen, I. P. Rothwell, K. Folting, J. C. Huffman, W. E. Streib and R. Wang, Synthesis, structure and spectroscopic properties of early transition metal .eta.2-iminoacyl complexes containing aryl oxide ligation, J. Am. Chem. Soc., 1987, 109, 390-402.
17. A. Elhage, A. E. Lanterna and J. C. Scaiano, Catalytic farming: reaction rotation extends catalyst performance, Chem. Sci., 2019, 10, 1419-1425.
18. Q. Xiao, S. Sarina, A. X. Bo, J. F. Jia, H. W. Liu, D. P. Arnold, Y. M. Huang, H. S. Wu and H. Y. Zhu, Visible Light-Driven Cross-Coupling Reactions at Lower Temperatures Using a Photocatalyst of Palladium and Gold Alloy Nanoparticles, ACS Catal., 2014, 4, 1725-1734.
19. R. Ciriminna, V. Pandarus, G. Gingras, F. Beland, P. D. Cara and M. Pagliaro, Heterogeneous Sonogashira Coupling over Nanostructured SiliaCat Pd(0), ACS Sustain. Chem. Eng., 2013, 1, 57-61.
20. S. Sarina, H. Zhu, E. Jaatinen, Q. Xiao, H. Liu, J. Jia, C. Chen and J. Zhao, Enhancing catalytic performance of palladium in gold and palladium alloy nanoparticles for organic synthesis reactions through visible light irradiation at ambient temperatures, J. Am. Chem. Soc., 2013, 135, 5793-5801.
21. G. C. Bond, The Origins of Particle-Size Effects in Heterogeneous Catalysis, Surf. Sci., 1985, 156, 966-981.
22. J. J. Devery, J. D. Nguyen, C. Dai and C. R. J. Stephenson, Light-Mediated Reductive Debromination of Unactivated Alkyl and Aryl Bromides, ACS Catal., 2016, 6, 5962−5967; B. Sahoo, A. E. Surkus, M. M. Pohl, J. Radnik, M. Schneider, S. Bachmann, M. Scalone, K. Junge and M. Belle, A Biomass-Derived Non-Noble Cobalt Catalyst for

Selective Hydrodehalogenation of Alkyl and (Hetero)Aryl Halides, Angew. Chem. Int. Ed., 2017, 129, 11394-11399.

6.3 Postprint Version of Supporting Information

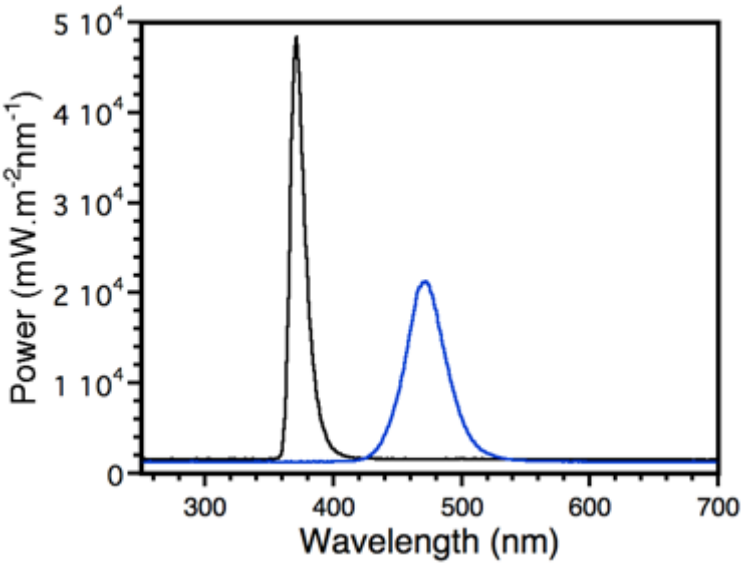

Figure S6.1. Emission spectra of the light sources used in this work: LED centred at 368 nm (black line) and LED centred at 465 nm (blue line).

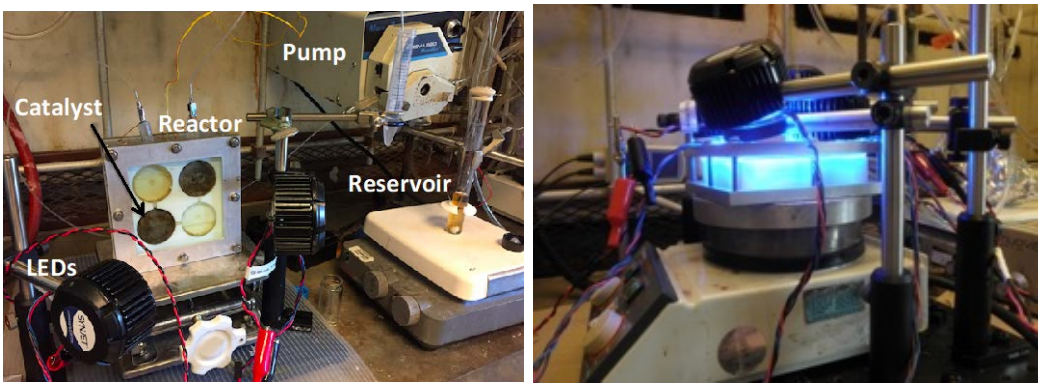

Figure S6.2. *Left*: flow reactor containing Pd@GW packed into two cells with other components for circulations and irradiation. *Right:* typical arrangement of hot plate, light sources, and flow reactor for irradiation during photo-thermal catalysis.

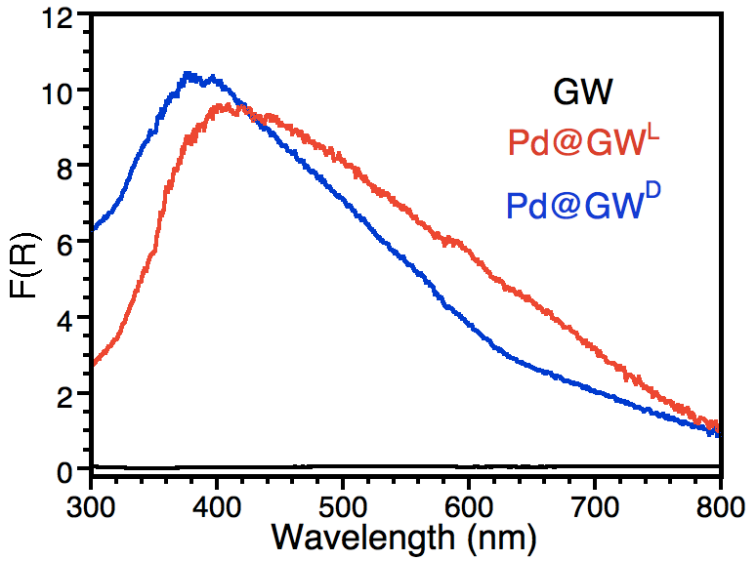

Figure S6.3. Diffuse reflectance spectra of GW (black), Pd@GW^{D} (blue) and Pd@GW^{L} (red).

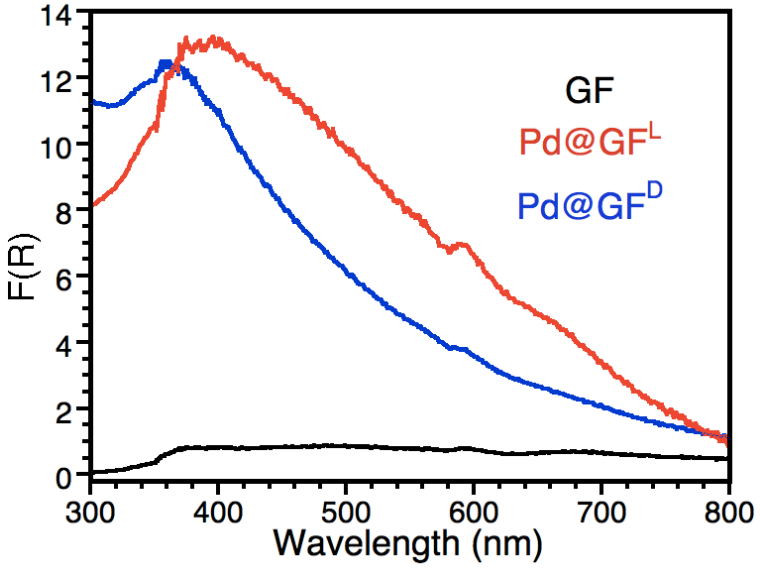

Figure S6.4. Diffuse reflectance spectra of GF (black), Pd@GF^{D} (blue) and Pd@GF^{L} (red).

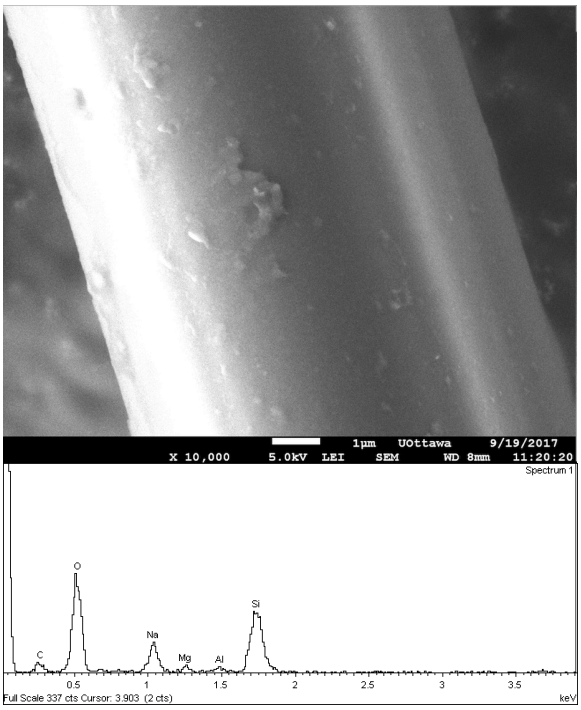

Figure S6.5. SEM image (*top*) and EDS spectrum (*bottom*) of GW functionalized with APTES.

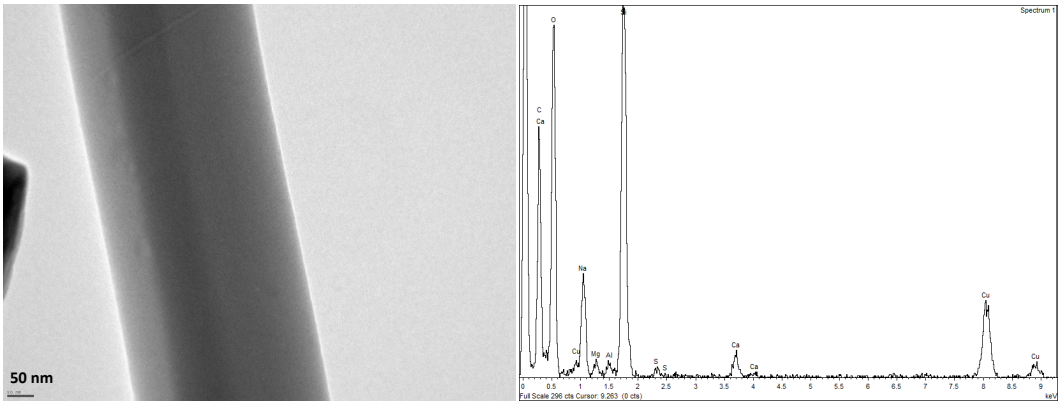

Figure S6.6. TEM image (*left*) and EDS spectrum (*right*) of pristine GF.

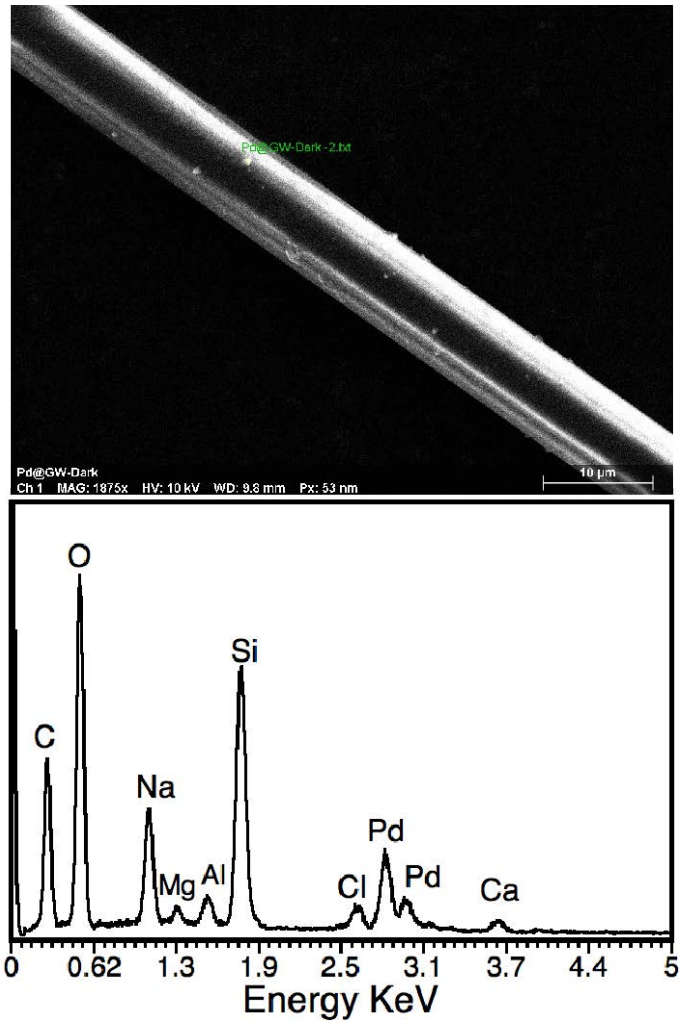

Figure S6.7. SEM image (*top*) and EDS spectrum (*bottom*) of Pd@GW^{D}

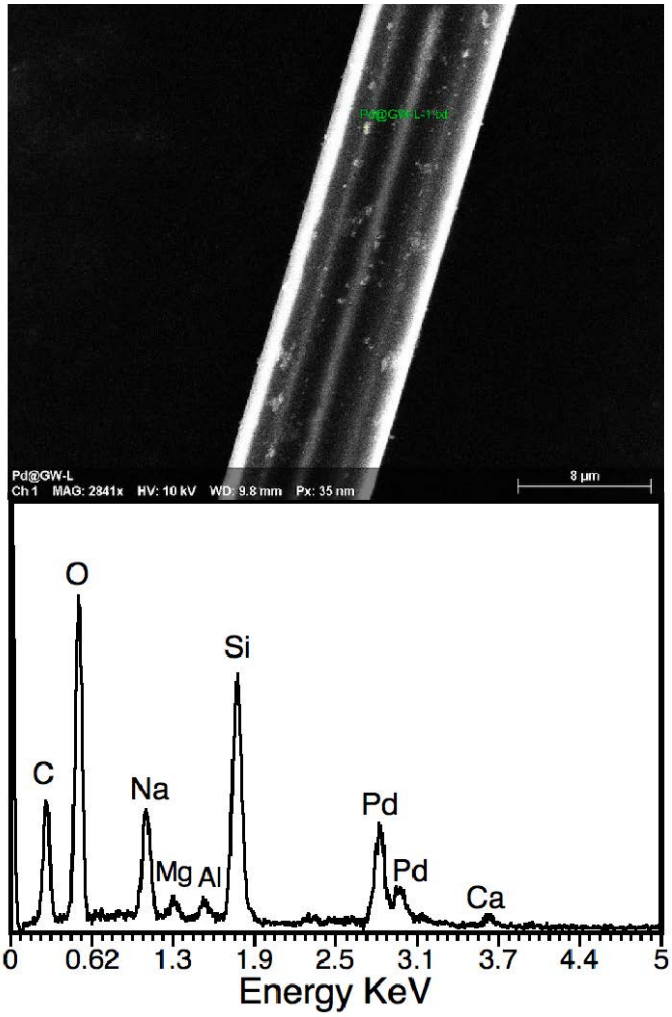

Figure S6.8. SEM image (*top*) and EDS spectrum (*bottom*) of Pd@GW^{L}.

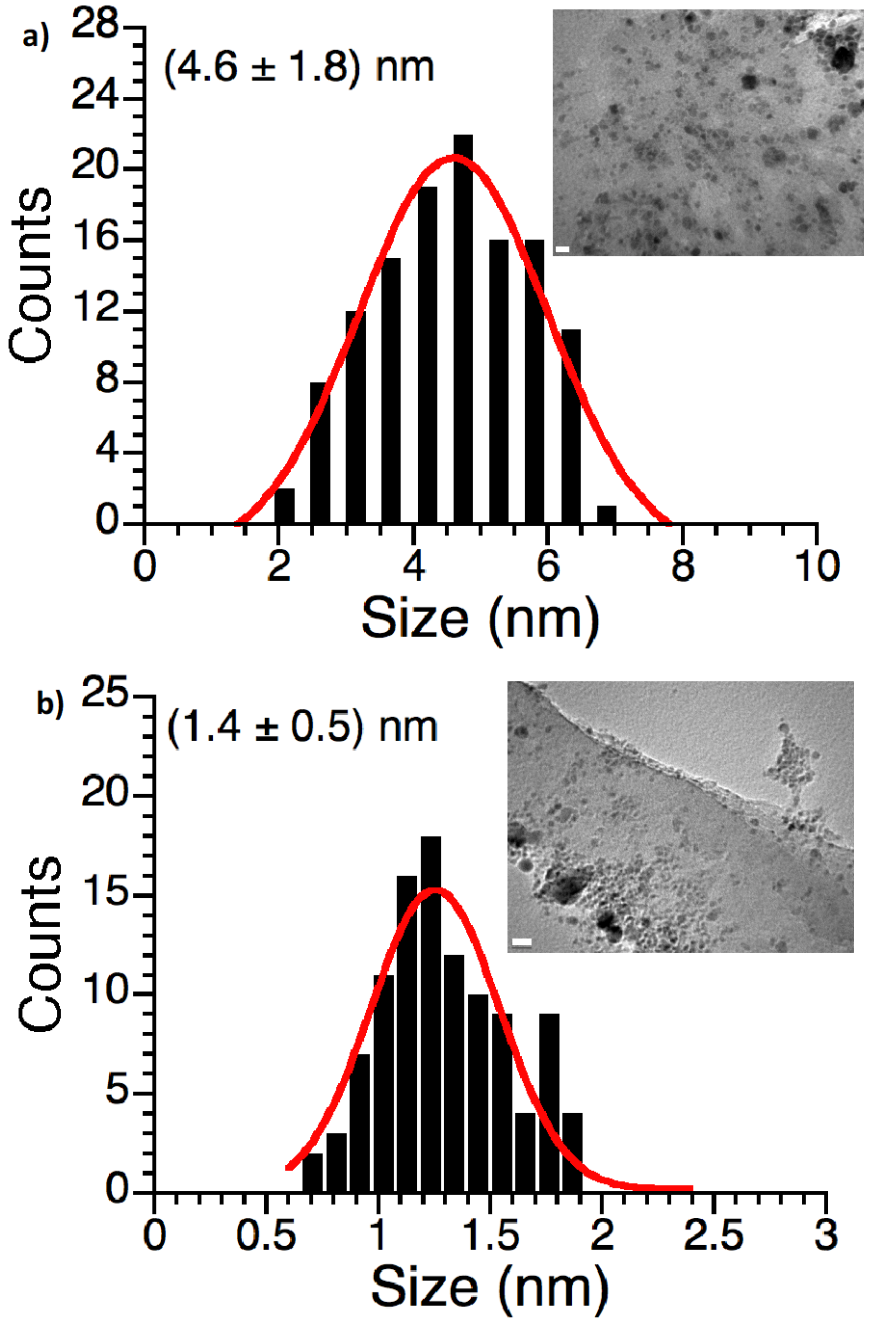

Figure S6.9. Pd particle size distribution for (a) Pd@GW^{D} (mean particle size: 4.6 nm, scale bar 20 nm), and (b) Pd@GW^{L} (mean particle size: 1.4 nm, scale bar 10 nm).

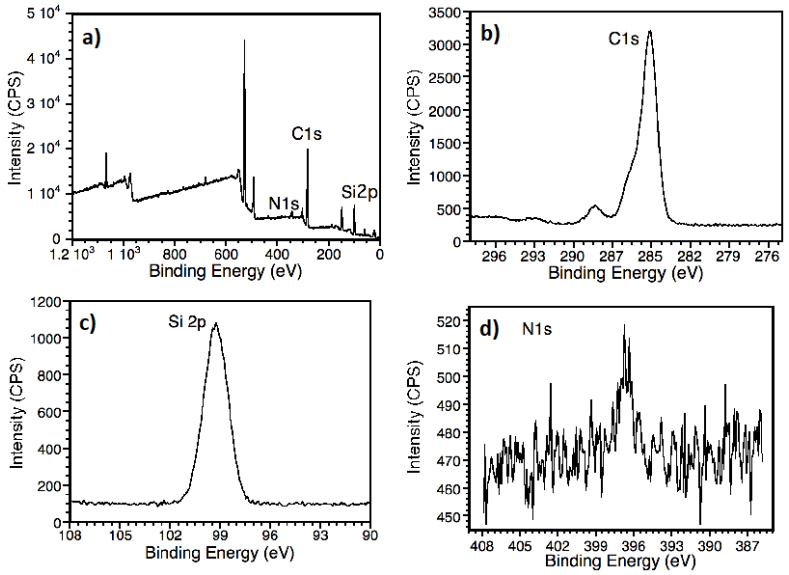

Figure S6.10. XPS survey (a) and HR-XPS spectra for (b) C1s BE region, (c) Si 2p BE region and (d) N 1s BE region for pristine GW.

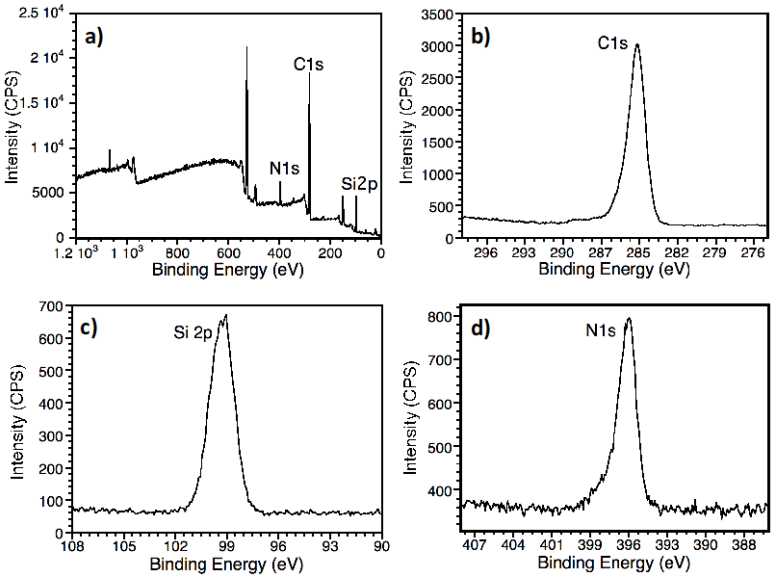

Figure S6.11. XPS survey (a) and HR-XPS spectra for (b) C1s BE region, (c) Si 2p BE region and (d) N 1s BE region for APTES functionalized GW.

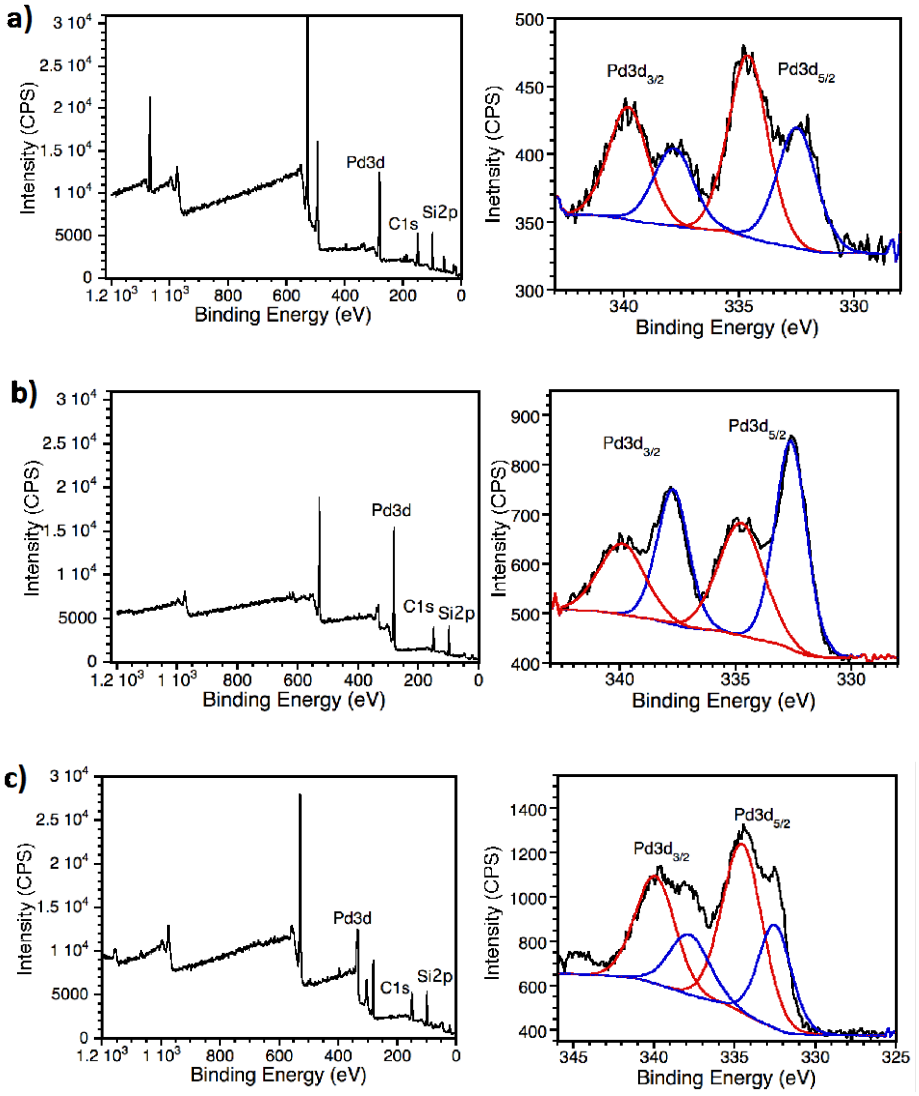

Figure S6.12. XPS survey and deconvoluted Pd 3d HR-XPS spectra of Pd@GW^{L} a) before use, b) after use in the thermal-induced Sonogashira reaction and c) after use in the photo-induced Sonogashira reaction catalyst.

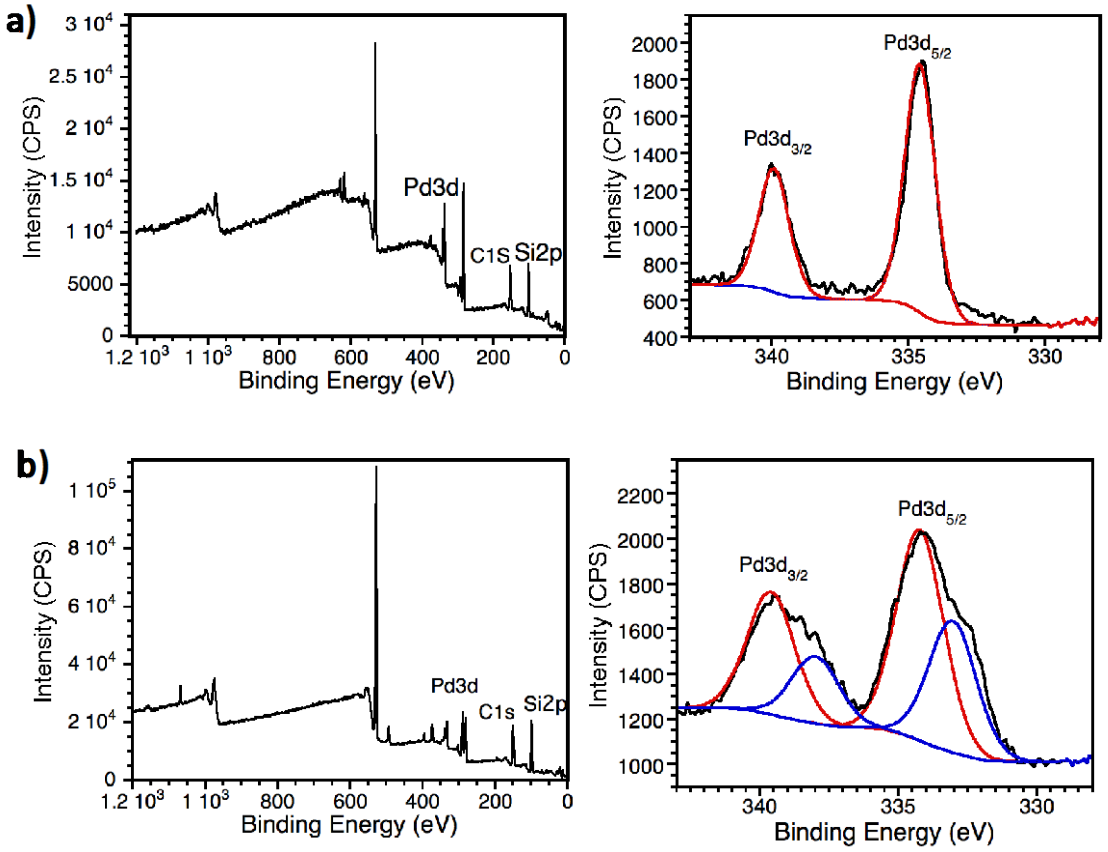

Figure S6.13. XPS survey and deconvoluted Pd 3d HR-XPS spectra of a) Pd@GW^{D} and b) Pd@GF^{D}.

Table S6.1. Test of flow and catalyst reusability for photocatalytic Sonogashira coupling by Pd@GW^{D} as catalyst in test tube reactor.

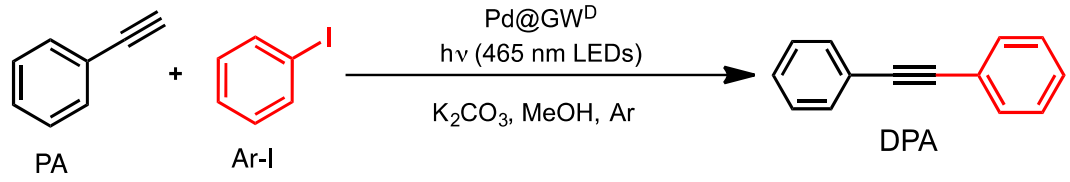

Entry	Time (h)	% Conversion[a]	% Yield[a]
1st cycle: Fresh Catalyst			
i[b]	1	23	19
ii[c]	2	39	34
iii[d]	3	51	42
iv[d]	4	67	55
2nd cycle: Used catalyst			
i	1	22	18
ii	2	26	22
iii	3	33	25
iv	7	39	30
v	9.5	48	33

Reactions conditions: 1st cycle: Pd@GW^{D} (155.7 mg) in a test tube, 0.45 mmol of Ar-I, 0.58 mmol of PA, 0.96 mmol of K_2CO_3, 30 mL HPLC methanol under Argon, 2nd cycle: 155.7 mg of Pd@GW^{D}, 0.45 mmol of Ar-I, 0.60 mmol of PA, 0.9 mmol of K_2CO_3, 30 mL HPLC methanol, [a]Conversions and yields were determined by GC-FID using an external standard based on 30 mL solution. [b]Without flow using one 465nm LED. [c]With flow using one 465 nm LED. [d]With flow using two 465 nm LED.

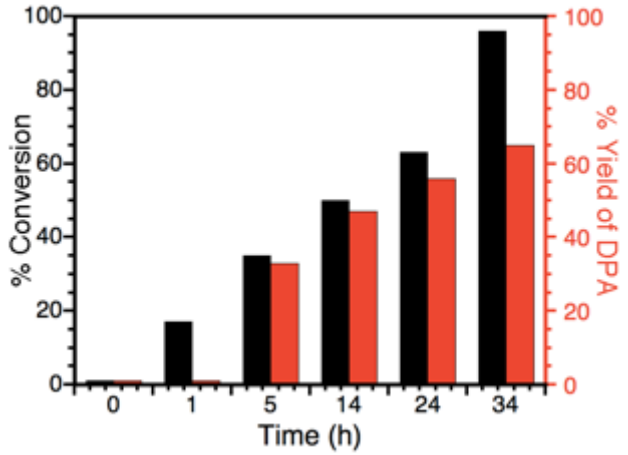

Figure S6.14. Yield versus time plot for the photocatalytic Sonogashira coupling using Pd@GW^{D}. Reactions conditions: 290 mg of Pd@GW^{D} in each of two cells, 0.45 mmol of Ar-I, 0.59 mmol of PA, 0.98 mmol of K_2CO_3, and 30 mL of MeOH under Argon. Visible light irradiation with 2x465 nm LED working at 1.6 W.cm^{-2}, flow 0.6 mLmin^{-1}. Numerical tabulation in **Table S6.2**.

Table S6.2. Photocatalytic Sonogashira coupling by Pd@GW^{D} as catalyst versus time in flow reactor.

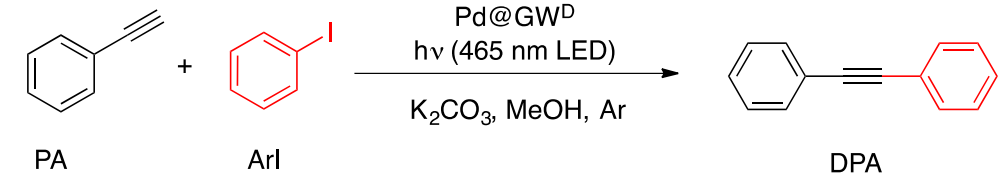

Entry	Time (h)	% Conversion[a]	% Yield of R-H[a]
i	1	17	ND
ii	5	35	33
iii	14	50	47
iv	24	63	56
v	34	~99	65

Reactions conditions: as per Figure S6.14. ND: nothing detected.

Table S6.3. Thermal effect vs light effect on the catalytic activity of Pd@GW^{L} for Sonogashira coupling under continuous flow

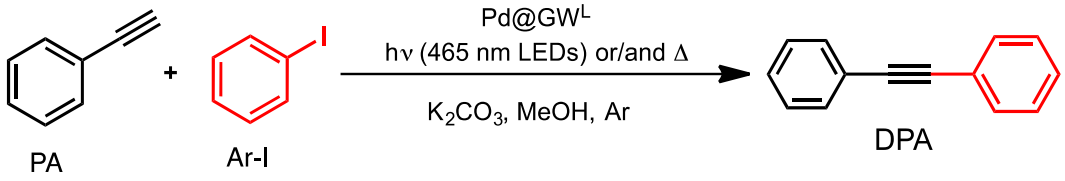

Entry	Time (h)	% Conversion[a]	% Yield[a]	Light contribution
Thermal-induced Sonogashira coupling				
i	1	25	21	ND
ii	2	29	22	ND
iii	3	35	23	ND
iv	4	38	26	ND
Thermal and light-induced Sonogashira coupling				
i	1	42	26	5
ii	2	58	50	28
iii	3	65	54	33
iv	4	82	68	44

Reactions conditions: Thermal-induced reactions: 0.82 mmol of iodobenzene, 1.34 mmol of phenylacetylene, and 2.24 mmol of K_2CO_3 in 30 mL MeOH at 65°C, 9.6 mL/min. Light-induced reactions: Pd@GW^{L} in Teflon reactor, two cells (109.3 and 112.2 mg), 0.80 mmol Ar-I, 1.35 mmol PA, 2.26 mmol K_2CO_3, 30 mL MeOH at 57-65°C, 9.6 mL/min, two 465 nm LED at 1.6 W cm^{-2}. [a]Conversions and yields were determined by GC-FID.

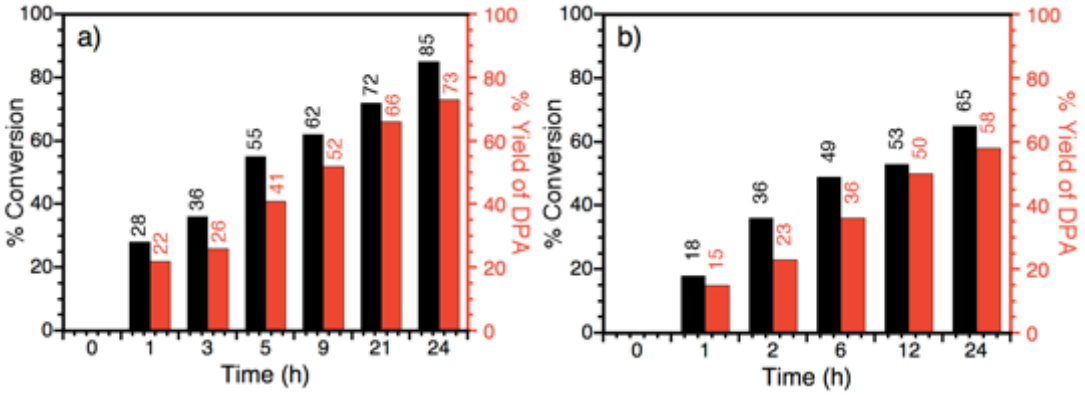

Figure S6.15. Photocatalytic Sonogashira coupling using PdNP@GF vs time. Conversion and yield under continuous flow with Pd@GF^{L} (a) Pd@GF^{D} (b). Reaction conditions: a) 150 mg Pd@GF^{L} total in two cells, 0.81 mmol Ar-I, 2.6 mmol PA, 2.2 mmol K_2CO_3 in 30mL of MeOH, 38 °C, two 465 nm LED at 1.6 W.cm^{-2} **b)** 140 mg Pd@GF^{D} total in two cells, 0.80 mmol Ar-I, 2.4 mmol PA, 2.3 mmol K_2CO_3 in 30mL of MeOH, 43 °C, two 465 nm LED at 1.6 W.cm^{-2}.

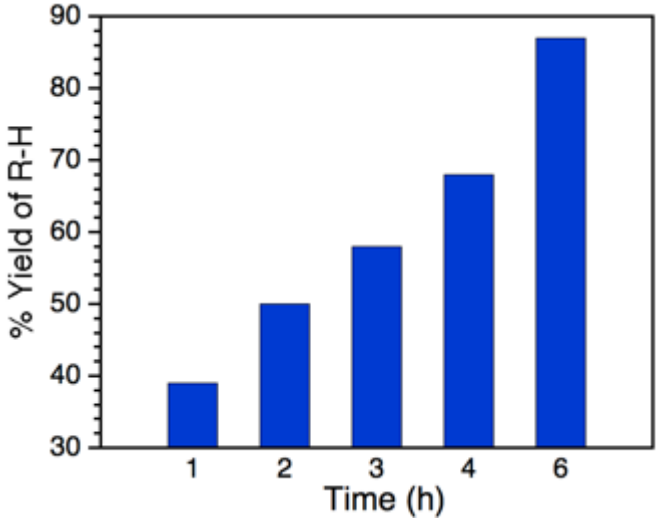

Figure S6.16. Light induced reductive dehalogenation by Pd@GF^{L} vs time. Reaction conditions: 100 mg Pd@GF^{L} in each of two cells, 0.82 mmol methyl 4-iodobenzoate, and 2.24 mmol of K_2CO_3 in 30 mL MeOH, flow 7 mL/min at 28 °C, two 368 nm LED working at 0.40 W.cm^{-2}.

Table S6.4. Large scale photocatalytic reductive dehalogenation of methyl 4-iodoebenzoate by Pd@GW^{L} vs time under continuous flow.

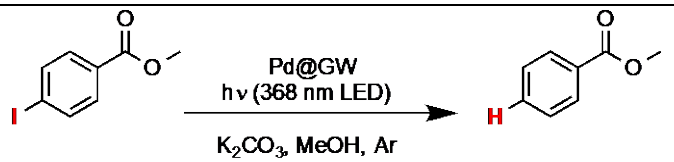

R-I R-H

Entry	Time (h)	% Conversion[a]	% Yield of R-H[a]
i	1	28	26
ii	2	35	34
iii	4	42	39
iv	5	56	52
v	6	60	56
vi	7	70	68
vii	8	80	77
viii	9	95	91

Reactions conditions: 100 mg Pd@GWL in each of two cells, 5.0 mmol methyl 4-iodobenzoate, 20.5 mmol K_2CO_3, 200 mL MeOH, 12.5 mL/min, two 368 nm LED at 0.40 W cm^{-2}, 27 ºC. [a]Conversions and yields were determined by GC-FID.

6.4 Accompaniment to Chapter 6

This final chapter in the iterative design of supported PdNP for heterogeneous photocatalysis represents the culmination of the doctoral work presented in this thesis. Building upon experimental results and insights from previous investigations to ultimately design efficient, selective, and reusable heterogeneous catalytic system for various organic reactions along with a suitable system for continuous flow photochemistry to achieve the primary objective of this doctoral research plan.

The heterogeneous flow system presented in this chapter is based on using robust and mechanically stable catalyst, PdNP decorated glass fibers that is efficient in both thermal and light-induced catalysis for two different types of organics transformations: Sonogashira C-C coupling and reductive dehalogenation. Indeed, this is a first step toward future studies where suitable system could be designed for various catalytic transformations, for low temperature heterogeneous photocatalysis with high flow or a heat exchanger. The understanding of the catalytic mechanisms leads to additional insight on how best to elevate the nanomaterial further.

7. Conclusions and Future directions

7.1 Summary and Conclusions

In all parts of this dissertation, the theme is centered on strategies to the design and application of nanomaterials in heterogeneous photocatalysis. The applied research presented in this doctoral thesis make a significant contribution toward an innovative methodology in reactivating heterogeneous catalyst as well as development of novel catalyst support for a wide varieties of organics transformations ever reported.

Development of a visible light responsive heterogeneous catalyst Pd decorated TiO_2 as an alternative to the homogeneous catalyst −based on Pd complexes, to catalyze photoredox transformations under mild conditions, described in Chapter 2, offer the advantage of being easily recovered from the reaction mixture, either by filtration or by centrifugation. They also present the advantages of being reusable in several catalytic cycles with good efficiency. We decided to employ heterogeneous semiconductor particles like TiO_2, as photocatalyst functionalized with PdNP. As discussed throughout this dissertation, the multifunctional Titanium dioxide supported palladium nanoparticles proved to be versatile, tuneable, and efficient for different types of organic transformations application in heterogeneous catalysis under mild conditions. Pd@TiO_2 show different reactivity when irradiated with different light sources and thus, the preferred outcome can be tuned by the correct selection of wavelengths to which a single material is exposed. Irradiating the support, here TiO_2, with UV light leads to either alkenes hydrogenation in alcoholic suspension under H_2 source free at room temperature and under atmospheric pressure or to Ullmann homocoupling, C-C coupling of aryl iodides in THF as a solvent. On the other hand, irradiating PdNP with visible light leads to alkenes isomerization in alcoholic suspension under H_2-free conditions at room temperature or to Sonogashira coupling, cross coupling between alkyne and aryl iodides. Chapter 2 and 3 describe the photocatalytic activity of Pd@TiO_2 under different

light irradiation sources. Thus, production of target valuable molecules can be tuned by the right selection of wavelength to either afford alkene hydrogenation, alkene isomerization or C-C coupling product at room temperature.

The successful implementation of reaction rotation approach to extend the lifetime and selectivity of heterogeneous catalyst after several catalytic cycles is described in Chapter 4. Although, the advantages of heterogeneous systems over their homogeneous counterparts are related to the ease of separation and reusability of the catalysts, the deactivation of heterogeneous catalysts after first catalytic cycles is an abundant problem. Chapter 4 carries forward the concept of heterogeneous catalyst recovery and reusability, by incorporating sustainable recovery methodology. We developed an innovative approach labeled "*Catalytic farming*" based on alternating different photocatalytic reactions to extend Pd@TiO_2, lifetime as well as preserving its selectivity and efficiency. In general, the regeneration of heterogeneous catalysts involves the use of expensive procedures such as high temperature or oxygen or hydrogen sources. Similar to farmers maintaining nutrient levels in their fields by rotating through different crops each season, we employed the same strategy in catalysis as agriculture. One catalytic process depletes the catalyst surface while other type of catalytic process in the following catalytic cycle restores its catalytic activity by regenerating its oxidation state. This strategy is not only limited to the systems we have studied, indeed it can be extended to different catalytic systems as long as the catalyst can be employed for more than one catalytic reaction.

Finally, the development of novel support −glass wool fibers as support for metal or metal oxide nanoparticles− for heterogeneous catalysis is described in Chapter 5. As discussed throughout this dissertation**,** catalysts on a solid support are much easier to separate from the reaction mixture than homogeneous catalysts and often can easily be reused. Although powder-like heterogeneous catalysts are easy to recover after batch reaction but they are not suitable for continuous flow chemistry. Glass fibers offer the advantages of not only being easy to modify their surface in order to provide physical or chemical affinity towards many catalytic materials, they are also easy to recover from

batch reaction. Grafted metal and/or metal oxide nanoparticles onto glass wool showed that the resulting hybrid materials could promote a wide range of reactions, including carbon–carbon couplings, dehalogenations and cycloadditions. In particular, we focused on photocatalytic reactions, although they also performed some heat-driven reactions. Glass fibers are mainly used to restrict the mobility of active catalyst. From here, more complex and interesting heterogeneous systems can be developed with excellent potential for flow photochemistry application. In this context, this methodology has been successfully implemented in continuous flow conditions using palladium nanomaterials decorated glass fibers as a catalyst. Chapter 6 describes in details the development of a flow system −flow reactor and catalysts− for two light driven test reactions: Sonogashira C-C coupling and reductive dehalogenation.

7.2 Future Directions and Outlook

The work presented in this thesis demonstrates that both semiconductors and glass fibers can be employed as support whether in active or passive form for alternatives heterogeneous catalyst, PdNP. While Pd@TiO_2 appear quite promising when light source is used to tune the catalytic process outcome. In this regard, both PdNP and TiO_2 support play an important role in the catalytic process. Thus, the selection of light wavelength and intensity can be served to tune the reaction outcome. Expanding the current line of research to similar bifunctional catalytic nanomaterials based upon other noble metal nanoparticle namely the plasmonic metal nanoparticles would be another avenue to consider. Au nanoparticles (AuNP) exhibit a strong absorption in the visible region. The fact of incorporation Pd into AuNP at TiO_2 surface may lead to more advanced photocatalytic activity of the bimetallic NP for various reactions. The advantages of having photocatalyst consisting of plasmonic metal (Au) and metal with an intrinsic catalytic ability (Pd) are:

a- Expanding the range of reactions that can be catalyzed using low intensity visible light irradiation.

b- Further to light excitation, the electronic heterogeneity at the bimetallic NP surface, electron-rich sites (Au) and slightly positively charged sites (Pd), promotes the interaction between NP sites and both electrophilic or nucleophilic reactant molecules.

Consequently, the scopes of the coupling reaction can be extended to include other types of visible light driven transformations; C-C coupling between alkyl halides and terminal alkene, aryl halides and terminal alkynes/alkenes, hydroamination of alkynes, and many more. Moreover, strategies based on tuning the light excitation by using multi-wavelengths sources may also lead to the discovery of new synthetic routes.

It would be also ideal to implement Microscopy tools like single molecule fluorescence microscopy for mechanistic insights of the behaviour of the nanocatalysts in order to interpret and improve the overall reactivity of the organic transformations. Single molecule microscopy is an effective tool for studying surface reactivity of heterogeneous catalyst at the nanoscale using fluorescent probes. Additionally, preforming AFM-Raman spectroscopy measurement might help identifying actives sites of supported nanoparticles in real time. The facts of studying the catalytic processes in real time facilitate research on a much larger scale or redesign of the catalyst for better efficiency and higher longevity.

7.3 Claims to Original Research

- The first report of tuneable photocatalytic activity of palladium nanoparticles/ titanium dioxide by just switching the light sources.

- Development of heterogeneous photocatalytic system employing supported PdNP for Sonogashira coupling reaction under mild conditions.

- The first report on reactivating and extending heterogeneous catalyst lifetime, $Pd@TiO_2$, by alternating catalytic reactions.

- The first report on using glass wool as novel support for metal nanoparticles and its application in different organic transformations.

- Development of continuous flow heterogeneous photocatalysis system using glass fibers as catalyst support.